STABILIZATION AND CARBONIZATION STUDIES OF POLYACRYLONITRILE/CARBON NANOTUBE COMPOSITE FIBERS

A Dissertation
Presented to
The Academic Faculty

by

Yaodong Liu

In Partial Fulfillment
of the Requirements for the Degree
Doctor of Philosophy in the
School of Polymer, Textile and Fiber Engineering

Georgia Institute of Technology
DECEMBER 2010

STABILIZATION AND CARBONIZATION STUDIES OF POLYACRYLONITRILE/CARBON NANOTUBE COMPOSITE FIBERS

Approved by:

Dr. Satish Kumar, Advisor
School of Materials Science and Engineering
Georgia Institute of Technology

Dr. Meisha L. Shofner
School of Materials Science and Engineering
Georgia Institute of Technology

Dr. Anselm Griffin
School of Materials Science and Engineering
Georgia Institute of Technology

Dr. Samuel Graham
Woodruff School of Mechanical Engineering
Georgia Institute of Technology

Dr. Donggang Yao
School of Materials Science and Engineering
Georgia Institute of Technology

Date Approved: October 29, 2010

ACKNOWLEDGEMENTS

The writing of this dissertation has been one of the most significant academic challenges that I faced and completed. Without the support, guidance, encouragement and patience of the following people; this study would have been impossible to complete. I wish to show my deepest gratitude to them.

I would like to gratefully and sincerely thank Dr. Satish Kumar for his guidance, encouragement, understanding and patience during my graduate studies at Georgia Tech. He gave me invaluable advices and support during all the stages of my research. He encouraged me, not only to grow as an experimentalist, but also as an independent thinker. I learned a lot from him not just ideals but also attitude and style. Not just what, but try to know why and how. For everything you've done for me, Dr. Kumar, I thank you.

I would like to thank my committee members, Dr. Anselm Griffin, Dr. Meisha L. Shofner, Dr. Donggang Yao, and Dr. Samuel Graham for their support, and advice.

I would like to thank Dr. Han Gi Chae for his great help and advice; Dr. Marilyn Minus for assistance with the X-ray diffraction and help with my presentation and fiber spinning; Young Ho Choi for assistance with XRD and fiber spinning; Dr. Sudhakar Jagannathan for surface area measurement; Dr. Prabhakar Gulgunje, Dr. M. G. Kamath, Laura Lanier for comments on my thesis; Ericka Ford, Dr. Rahul Jain, Dr. Asif Rasheed, Dr. Shanju Zhang, Dr. Dhriti Nepal, Dr. Kishor Gupta and all other members of our group for help during my research and thesis writing.

Finally, I would like to express my appreciation to my parents and my wife, Dr. Fengying Zhang, for their long-standing encouragement, support and sacrifice.

TABLE OF CONTENTS

LIST OF TABLES

LIST OF FIGURES

SUMMARY

Carbon fibers contain more than 90 wt. % carbon. They have low density, high specific strength and modulus, and good temperature and chemical resistance. Therefore, they are important candidate as reinforcement materials. Carbon fiber is made by pyrolysing precursor polymers. Polyacrylonitrile (PAN) which has been used as precursor to produce high strength carbon fiber is used as precursor in this study. The theoretical tensile strength of carbon fibers can reach over 100 GPa. Currently, the best commercial carbon fibers reach only 7.5 GPa. To make good quality carbon fiber and to narrow the gap between theoretical values and currently achieved experimental properties, the entire manufacturing process including fiber spinning, stabilization and carbonization, needs to be improved optimized. In this dissertation, the stabilization processes of gel-spun PAN/carbon nanotubes (CNTs) composite fibers are studied.

PAN/CNT (1 wt. % CNT) composite fibers are spun by dry-jet gel-spinning. Three types of CNTs with different number of walls and varying catalyst content are used as additives. The effect of different types of CNTs on the properties of the stabilized fibers was compared. It is found that the CNTs with the highest surface area shows the best reinforcement efficiency on the tensile modulus, and reduces the formation of β-amino nitrile. The residual catalyst in the range of 1 to 4 wt. % shows little effect on the mechanical properties of the stabilized fibers.

Stabilization involves complex chemical reactions, including cyclization, oxidation, dehydration, and cross-linking. These complex reactions are separated by using different gas environments during stabilization. The cross-linking reaction has the

highest activation energy among all stabilization reactions, and requires a temperature higher than 300 ^{o}C to be completed. The effect of applied tension on the stabilized fiber properties are investigated, and it is found that higher tension leads to better properties for the stabilized fiber, including higher Young's modulus, higher orientation, less formation of β-amino nitrile, and less shrinkage.

The relationship between stabilization conditions and the mechanical properties of the carbonized fiber is investigated, and the methods to identify optimum stabilization conditions are proposed. It is observed that the highest tension should be applied during both stabilization and carbonization, and the mechanical properties of the resulting carbon fibers are increased if fibers are further stabilized at a temperature of ~ 320 ^{o}C to improve the cross-linking degree as compared with the fibers only stabilized at 255 ^{o}C. The optimum stabilization time depends on both the stabilization temperature and on the applied tension. A new characterization method by monitoring the dynamic mechanical properties, while stabilization is in progress is used to narrow down the range of the optimum stabilization time. Also, the effect of carbonization temperature on the ultimate carbon fiber properties is studied in the batch process carbonization. Preliminary studies are carried out to find the relationship between the structure and properties of precursor fibers and the tensile strength of carbon fibers, including mechanical properties and co-monomers of precursor fibers.

CHAPTER 1

INTRODUCTION

Carbon, with an atomic number of six, has four electrons in its outermost orbital that can form covalent bonds. These covalent bonds can be single, double or even triple bonds, which makes various and distinct allotropes of carbon. Although some carbon materials, such as diamond and graphite, are very familiar to us, carbon still surprises us with its new forms. The bucky ball [1], C_{60}, was found in 1985, and carbon nanotubes (CNTs) [2] were recognized in 1991. It would not be surprising if new forms of carbons are found in the future. Hither to now, carbon shows all kinds of spatial forms in its allotropes: 3-dimensional diamond, 2-dimensional graphite, 1-dimensional CNTs and 0-dimensional bulky ball; each form shows distinct properties.

1.1 Carbon fibers and manufacturing process

1.1.1 Carbon fibers

Carbon fibers [3-5] contain more than 90 % carbon by weight, and normally have a tensile strength of 2-7 GPa, compressive strength (1-3 GPa), modulus (200-900 GPa), density (1.75-2.18 g/cm^3), and good corrosion and temperature resistance. For their excellent properties, carbon fibers are mainly used as high-performance reinforcement materials. The main applications of carbon fibers (word market) include:

1. Sport equipments (~ 20 %) - normally low property carbon fibers are used in this application.

2. Industrial applications (~ 70 %) - such as structural engineering, wind generator blades, pressure vessels, medical instruments, automobile bodies. The usage of carbon fibers in general engineering requires cost constraints, high production rate requirements, while generally less critical performance is needed.

3. Aerospace (~ 10 %) - these applications are driven by the maximum performance and fuel efficiency, the cost becomes the secondary factor. Spacecrafts use carbon fibers as shell materials, as they have excellent heat tolerance and could bear the intensive heat generated during atmospheric re-entry.

The worldwide production of carbon fibers was 45,000 tons in 2009, and is expected to increase by more than 10 % per year in the next decade.

1.1.2 Carbon fiber history

Carbon fibers are made from the pyrolysis of precursor fibers. In the late of 1870s, carbon fiber was first commercial used as light bulb filaments by carbonizing cellulose based materials such as natural bamboo and cotton at high temperature in non-oxidative environment. The prepared carbon fibers had good temperature resistance and could endure extensive heat of incandescence; however the mechanical properties of these carbon fibers were very poor. The practical uses of carbon fibers as reinforcement materials only began in the late 1950s, wherein synthetic rayon was used as precursor [6] and the mechanical properties of the resulting carbon fibers were greatly improved (modulus ~ 50 GPa, and strength ~ 1 GPa). In 1960s, polyacrylonitrile (PAN) was processed to manufacture carbon fibers. PAN-based carbon fiber has a yield ~50 %, which is much higher than that of rayon-based carbon fiber; also, PAN is easier to process in comparison with rayon. Today, no carbon fiber in united state is made from

rayon. In 1970s, petroleum pitch was used to make high modulus carbon fibers. However, processes to purify and spin pitch into fibers are expensive; also, the compressive strength of the pitch-based carbon fibers is much lower than PAN-based carbon fibers. Now, more than 90 % of commercial carbon fibers are made from PAN precursors. PAN-based fibers are recognized as the most important precursor to produce the high strength carbon fibers, and are used in the studies in this dissertation.

The benefits of carbon fibers are obvious. As compared with steel, the density of carbon fibers is up to four times lower, while their strength is much higher. Carbon fibers and their composite materials [4] can provide excellent structural properties as well as light weight. For example, the new generation of Boeing planes uses more and more carbon fiber composites to replace metal. In December 2009, the Boeing 787 dreamliner which used extensive carbon-fiber composites, ~ 33 tons for each plane, made its first flight. Automotive industry also uses carbon fibers to reduce the weight of vehicle and thereby improve its fuel efficiency. For high performance race cars, such as NASCAR and Formula One, carbon fiber composite is used as body material, which not only reduces the weight of cars, but also improves driver safety. In summary, due to variety of applications of carbon fibers, it is considered to be one of the most important inventions of the 20^{th} century. Theoretically, the carbon fibers can reach a high strength of 70 GPa; however, the best carbon fibers available today possesses strength of 7 GPa, which is only ~ 10 % of the theoretical strength. Therefore more effort is required to narrow this gap between the current experimental tensile strength and the theoretical value.

1.1.3 Carbon fiber manufacturing process

Carbon fibers are made by pyrolysing precursor fibers [3, 7]. During the conversion from PAN precursor to carbon fibers, the heat treatment protocol is crucially important [8] for the properties of the resulting carbon fibers. In general, heat treatment of PAN precursor can be divided into three stages by processing temperatures and gas environments.

1.1.3.1. Oxidative stabilization.

The temperature range of this step is from 200 to 400 ^{o}C, and an oxidative gas, typically air, is used as the environment. During stabilization, PAN precursor forms ladder polymer that can withstand higher temperature and increases carbon yield. This step is the focus of this dissertation.

1.1.3.2. Carbonization.

The temperature range of carbonization is from 900 to 1600 ^{o}C in an inert atmosphere. The ladder polymer formed during stabilization further cross-links and forms a turbo-static carbon structure. Non-carbon atoms are released and the final carbon content is over 90 % after carbonization. Usually, nitrogen gas can be used up to 2000 ^{o}C and argon is used above this temperature, since carbon may react with nitrogen to from cyanogens at this high temperature.

1.1.3.3. Graphitization

The temperature range of graphitization is from 1800 to 3000 ^{o}C in an inert atmosphere. This step further improves the orientation of basel planes and forms graphite-like structure. The stiffness of fibers can be greatly improved by this step.

1.1.3.4. Surface treatment

All the commercial carbon fibers are given a surface treatment to improve the inter-laminar shear strength between carbon fibers and matrix by enhancing their adhesion and bonding. Oxidation (gas-phase, liquid-phase, and catalytic), non-oxidation (deposition of active carbons and grafting) and plasma treatments are commonly used; however the exact knack of these treatments is still a trade secret.

1.2 Stabilization of PAN-based precursor fibers

Stabilization is one of the most important steps [9-11] and strongly affect the properties of the resulting carbon fibers. After stabilization, fibers can endure higher temperature and carbon yield can be improved. Optimization of this process is very important for the properties of the resulting carbon fibers, whereas non-optimized stabilization will lead to more carbon loss during carbonization and poor properties of the carbonized fibers.

In stabilization, complex chemical reactions occur, such as cyclization, oxidation, dehydration, and cross-linking. Stabilization is a time consuming process, as it takes 1 to 24 hours to complete. Since stabilization reactions are exothermal, and PAN polymer is not a good thermal conductive medium, extreme care needs to be taken to avoid local over-heating, which will lead to uneven stabilization, and form defects in the carbon fiber. Researchers have tried many other gases besides air, such as hydrogen chloride (HCl) [12] and sulfur dioxide (SO_2) [13], to facilitate the stabilization and reduce the consumption time. However, these gases are corrosive, and the process will need special instruments. The studies in this dissertation use air as stabilization environment. For stabilizations in inert atmospheres, studies [7] have shown that these stabilized fibers

possessed much worse mechanical properties, along with poor carbon yield for carbonization, compared with fibers stabilized in air. To better understand the stabilization process of PAN-based fibers, the chemical and physical structure of PAN precursor fibers is introduced, followed by the studies of the chemical reactions and physical changes that occur during stabilization.

1.2.1 Structure of PAN fibers

The chemical structure and commonly accepted physical structure of PAN molecules are shown in Figure 1.1. Because of the dipole repulsion between intra-nitrile groups, the molecules tend to form a rod-like helical structure.

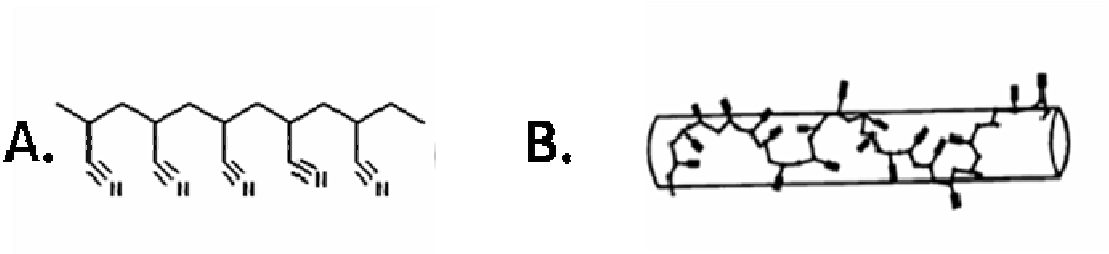

Figure 1.1 Schematic figure of PAN molecule. A: chemical structure; B: conformation – typical helical structure.

Wide angle X-ray diffraction (WAXD) is the most common method used to study the physical structures of materials [14]. For PAN fibers, WAXD normally shows two obvious equatorial diffraction peaks at *d*-spacing of around 0.53 and 0.30 nm [15]. In meridional scan, only weak diffuse diffraction peak was observed. PAN is reported to pack in hexagonal or orthorhombic geometry [16] as shown in Figure 1.2. The ratio of a over b for hexagonal packaging is $3^{1/2}$, and can be either larger or less than $3^{1/2}$ for orthorhombic packaging.

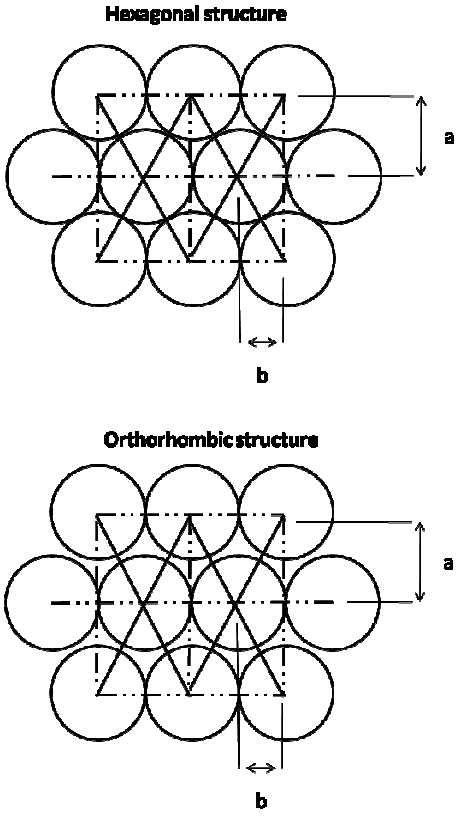

Figure 1.2 Illustrations of hexagonal and orthorhombic packing of PAN molecules.

From the ratio of two major equatorial peaks, the ratio of a-axis/b-axis can be calculated to determine the feasible packing model in a given fiber. The diameter of the rod-like structure was found to increase with increase in temperature [17]. The typical diameter is 0.6054 nm at 25 ^{o}C and this increased to 0.6346 nm at 240 ^{o}C. The thermal expansion coefficient of the rod's diameter is linear with temperature, with a transition occuring at glass transition (T_g) temperature. PAN has different stereo-regularities, such as atacticity and isotacticity. WAXD studies showed that the packing of chains along the fiber axis is independent of the stereo-regularity [17]. The conformation of PAN molecules shows obvious differences in the meridional scan, where peaks at ~ 36.3^{o} and ~ 40^{o} are assigned to planar zigzag and helical sequences, respectively [18].

Two theories have been proposed to illustrate the crystal structure of PAN fibers based on its WAXD patterns: para-crystal [16] and two-phase structure [19,20]. The para-crystal theory describes PAN structures with ideal crystal positions and position derivations, thus, it can describe all XRD patterns from perfect crystals to totally amorphous materials, like gas. The two phase structure theory proposes that PAN structures contain both crystal regions (ordered) and amorphous regions (disordered). The morphological model of PAN is shown in Figure 1.3.

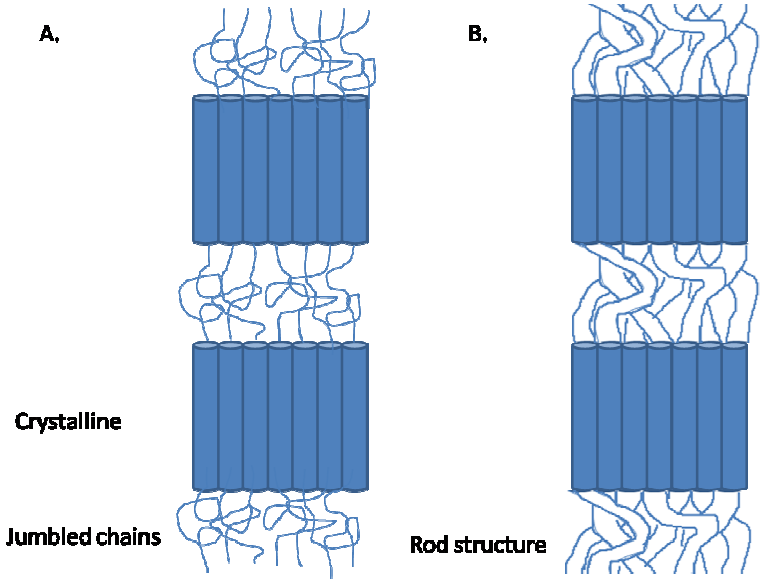

Figure 1.3 Models of PAN fibers consist of two phases - amorphous and crystal regions.

Unlike common flexible polymers, such as polyethylene (PE) and polypropylene (PP), whose molecules can easily fold and form folded chain structures, PAN molecules are much more rigid; therefore, it is difficult to form folded chain structures in PAN. PAN structure is normally considered to be laterally ordered with no order along the fiber-axis. Differential scanning calorimeter (DSC) experiments with very fast heating

rates (60 ~ 120 ^{o}C/min) show the melting peak of PAN crystals [21] to be between 320 to 360 ^{o}C.

The possibility of dipolar interactions between intermolecular nitrile groups in amorphous regions is lower than that in crystalline regions. Two models were proposed for molecular arrangement in amorphous regions. Warner et al. [19-20] supposed the randomly jumbled chain structures shown in Figure 1.3A, and Gupta et al. [19-20] suggested the randomly aligned rods structure shown in Figure 1.3B. No further structural evidence was reported, we do not know about which model is correct. High resolution transmission electron microscopy (HR-TEM) results indicated the existence of amorphous and crystalline regions in PAN precursor fiber [22]. Since for most conditions not much difference exists, both models are acceptable. It is believed that the stabilization reactions are initiated in the amorphous regions, and then diffuse into the crystalline regions.

1.2.2 Stabilization chemistry

The stabilization reactions in PAN fibers have been studied for over 50 years. To a certain degree, there are agreements among these studies; however, for the detailed stabilization reactions, no direct evidence or definitive mechanisms have been reported and verified. In this part, commonly accepted findings of stabilization reactions are introduced.

1.2.2.1 Cyclization reaction

The cyclization reaction is the most important reaction during stabilization. During cyclization, the nitrile groups in precursor fibers form a stable ladder polymer with adjacent groups. This ladder polymer withstands higher temperatures and improves

carbon yield. The reaction is exothermic, and previous studies [7] show that it is of first order. The reactions make the fiber structure more dense and stiffer; additionally, subsequently color change can be observed. For PAN fibers, color changes from slight yellow to yellow to brown to golden brown and finally to black. The reaction of cyclization is considered to be the formation of the conjugated carbon nitrogen double bond structure from the triple bond structure [23]. The cyclization reactions can be initiated by several sources [24]: impurities, acid co-monomers, chain end groups, α-hydrogen atoms to the nitrile, ketonitrile formed by hydrolysis, and so on. The reaction is shown in Figure 1.4. Chen [25] found that cyclization with formation of ladder polymer was non-stereo-specific; this means that no matter whether the PAN polymer is iso-tactic or syndio-tactic, the cyclization reaction would not be affected.

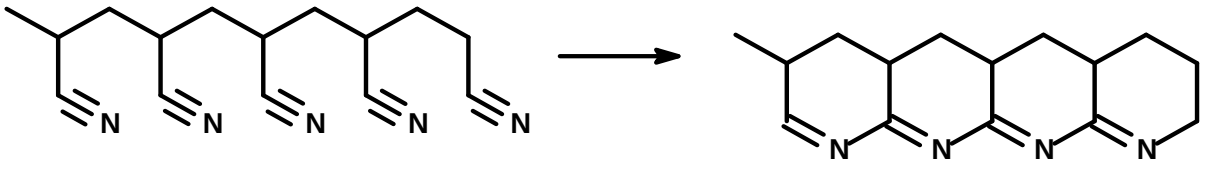

Figure 1.4 Cyclization reactions of nitrile bands. [23]

1.2.2.2. Oxidation reaction

The oxidation reaction takes place when PAN fibers are stabilized in an oxidative atmosphere. When stabilized in an inert atmosphere, the resulting fibers possess lower thermal stability. After oxidation, fiber can withstand higher temperature and has better thermal stability [26]. Oxygen content in well stabilized PAN fibers is around 8 wt. %. There exist many assumptions for oxidized structures, such as ketonic oxygen on

cyclized PAN [27], nitrone structure [28], and cyclization with epoxide bridges [29]. The most commonly accepted model is ketonic structure. The ketonic structure will form after elimination of water from oxidized structure. This structure typically shows a deep shoulder in the IR spectrum at around 1900 cm^{-1}. One of the proposed oxidation reaction is shown in Figure 1.5.

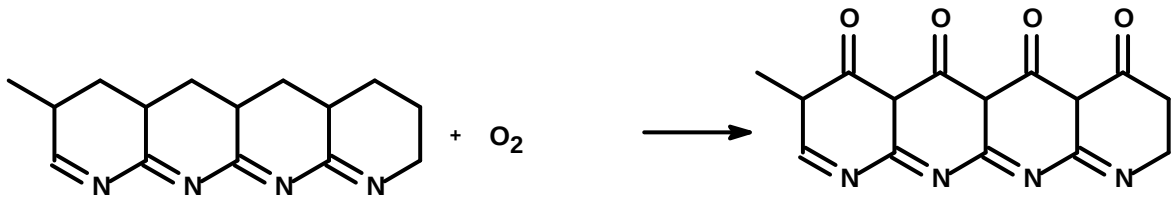

Figure 1.5 Oxidation reaction and formed ketonic structure. [27]

Watt and Johnson et al. [27] studied the stabilization of fibers made from two types of PAN polymers: homo-polymer and copolymer with acid monomers. After thermal treatment at 230 ^{o}C for 6 hours, the copolymer PAN fibers adsorbed much more oxygen than homo-polymer, and stabilization was diffusion limited. By comparison, stabilization was reaction limited in homo-polymer PAN fibers. However, if both fibers were pre-treated in vacuum at 230 ^{o}C for 6 hours and then re-treated at 230 ^{o}C in air, no difference in oxygen absorbance and color changes was found. Watt et al. concluded that the primary reaction caused by heating was cyclization and cyclized ladder polymer was the prerequisite for oxidation reaction. Fitzer and Muller [7] found that during oxidation, the oxygen can also initiate cyclization.

1.2.2.3. Dehydration reactions

Gas chromatography (GC) was used to monitor the by-products released in stabilization; it was found that water was produced during dehydration [32] and C=C double bonds were formed. The dehydration must happen after the oxidation and will not happen in an inert atmosphere. Oxidation happens after cyclization, and dehydration happens after oxidation; however, it is impossible to completely separate the dehydration and oxidation reactions. The formation of C=C double bonds improves thermal stability and reduces chain scission during further carbonization. The schematics of the reactions are shown in Figure 1.6 [7].

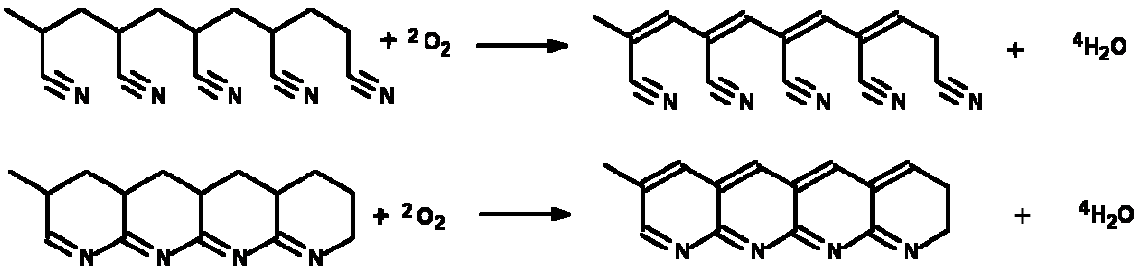

Figure 1.6 Dehydration reactions for PAN and ladder polymer. [7]

1.2.2.4. Intermolecular cross-linking reaction

Azomethine cross-linking arises due to proton being abstracted from a chain by the nitrile nitrogen from an adjacent chain [23]. The schematic is shown in Figure 1.7. The cyclization may be inter or intra-moleculer. Cyclization does not occur along the whole chain, and the cyclized segment length is typically around 3 ~ 5 nitrile groups. The transfer reaction may occur leading to the propagation cross-linking [30] as shown in Figure 1.8.

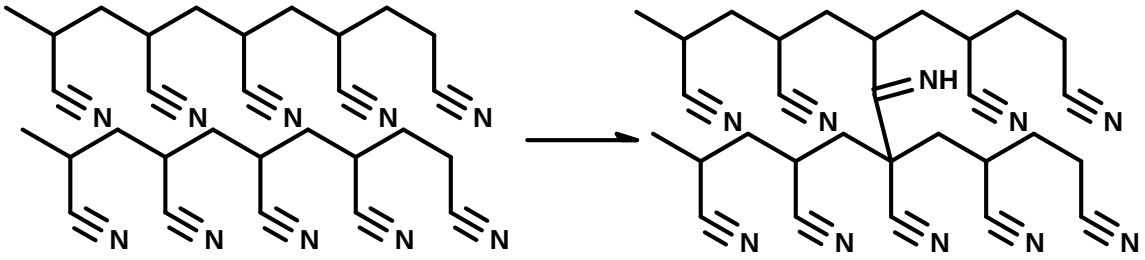

Figure1.7 Azomethine cross-linking reaction. [23]

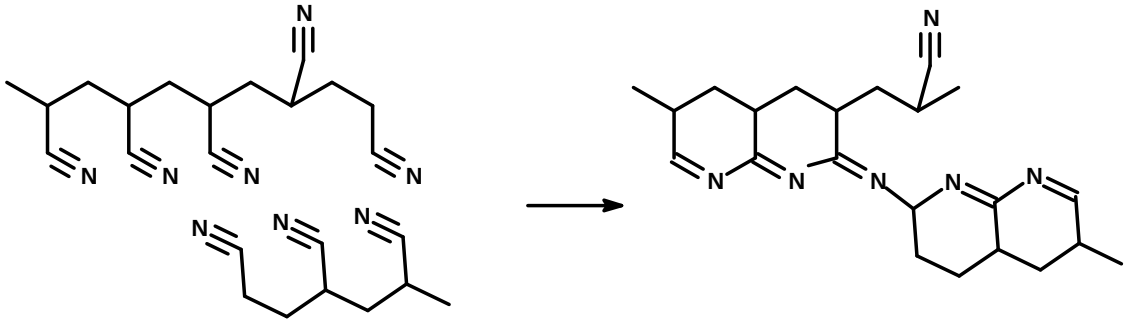

Figure 1.8 Propagation cross-linking reaction. [30]

1.2.2.5 Chemical structure in stabilized PAN fibers

The air-stabilized PAN structure was proposed by Morita by using X-ray photoelectron spectroscopy (XPS) [31]. By analyzing fine spectra of N_{1s}, O_{1s}, and C_{1s} XPS peaks of stabilized fibers, the formed chemical structures were proposed as shown in Figure 1.9, and their relative concentrations were calculated from the peak fitting results. Now, this proposed chemical structure of stabilized PAN fibers is widely accepted.

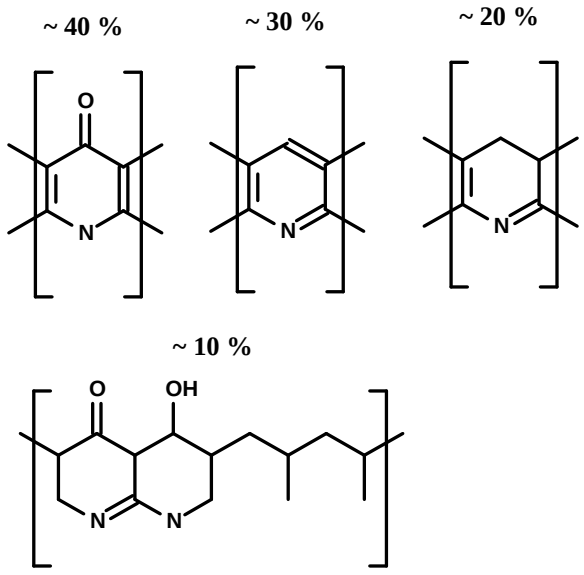

Figure 1.9 Chemical structure groups in PAN fibers stabilized in air.

1.2.2.6 Volatile by-products during stabilization

During the stabilization of PAN fibers in air, some volatile by-products were released and detected by GC [32]. The gas evolution is shown in Figure 1.10.

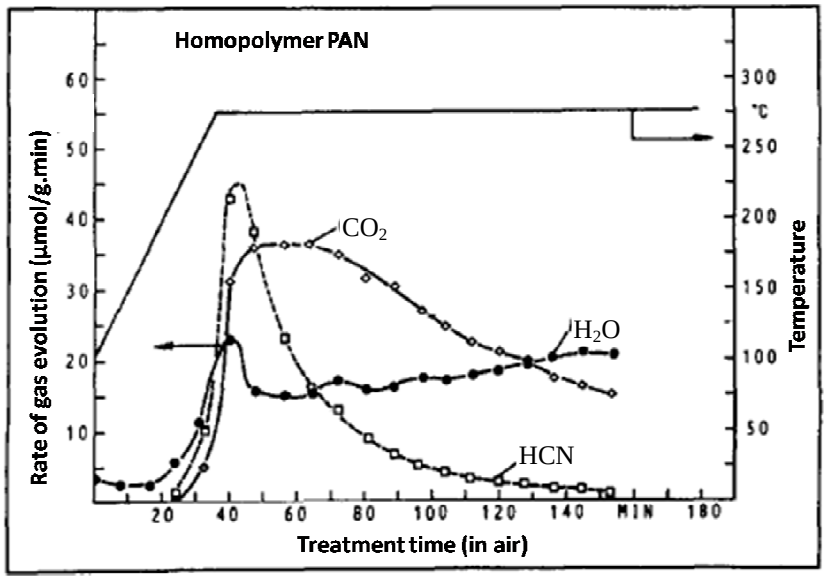

Figure 1.10 Gas evolutions during stabilization of homo-polymer PAN in air. [32]

HCN forms during cyclization, and CO_2 and H_2O form during oxidation, dehydration and cross-linking. The release of HCN mostly happens in the early stage of stabilization, while the release of CO_2 and H_2O took a much longer time indicating that the stabilization of homo-polymer PAN is limited by oxygen diffusion. In summary, the overall mechanism of stabilization chemistry is shown in Figure 1.11.

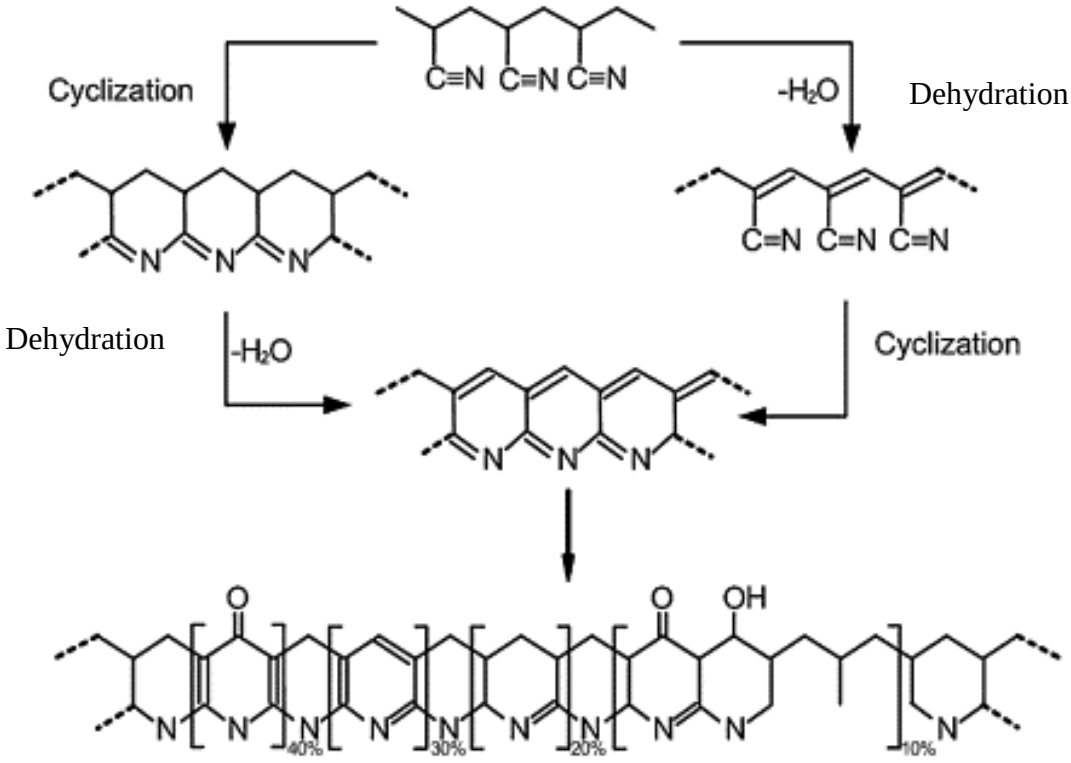

Figure 1.11 Reaction mechanisms of PAN stabilization. [32]

1.2.3 Methods to estimate stabilization reactions

During stabilization, complex physical and chemical changes occur. Many methods have been proposed to estimate the degree of stabilization by monitoring the changes of the chemical or correlated physical properties, and some of them are briefly discussed here.

1.2.3.1 Infrared spectroscopy (IR)

The chemical structure evolution during stabilization can be monitored by IR spectra [33-38]. The nitrile band C≡N has a strong absorption peak at ~ 2240 cm^{-1}. During stabilization, nitrile group is converted to the cyclized structure, and this IR peak weakens. Also, new bonds C=C, C=N are formed and show new absorbance peak at ~ 1600 cm^{-1}. If all nitrile groups cyclize, the nitrile peak will totally disappear; however, a small amount of nitrile groups always exists after stabilization, because cyclization happens randomly, and some nitrile groups are isolated and hard to react. The intensity of the nitrile band can be used as a stabilization index [37]. Li et al. [33] suggested that the peak intensity ratio of the double bond over the nitrile band can also be used as stabilization index.

1.2.3.2 WAXD

Since PAN molecules are converted to cyclized polymer during stabilization, the diffraction peak of PAN crystals will disappear [11, 34-35, 39-40], and simultaneously, formed aromatic polymer showed a broad diffraction peak at $2\theta=25.5^{o}$. An aromatic index is defined as the intensity ratio of the aromatic peak over the sum of the aromatic peak and the PAN (200),(110) diffraction peaks [11].The intensity of the PAN (200), (110) diffraction peak is also suggested to be used as stabilization index [39].

1.2.3.3 Shrinkage

Length change is one of the major physical changes that occur during stabilization. Figure 1.12 shows a typical length change of PAN fibers during the heating up process in air.

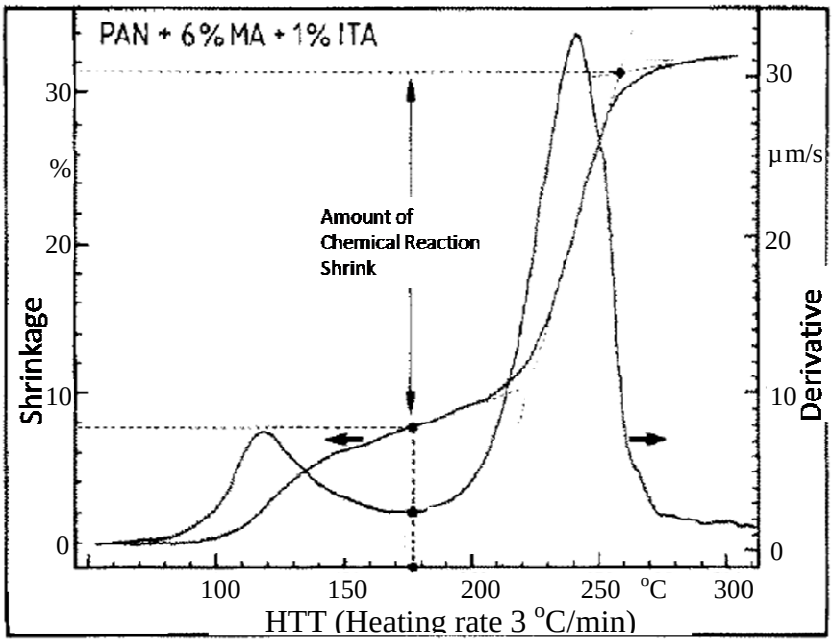

Figure 1.12 Typical shrinkage curves during stabilization (without tension). [32]

The shrinkage can be divided into entropic part and chemical part, which can be separated based on the derivation of the shrinkage curve (Figure 1.12). The entropic shrinkage is caused by the retraction of stretched polymer chains, and the chemical shrinkage is due to the formation of denser structures after chemical reactions. Entropic shrinkage represents only physical changes and is independent of the heating rate. While chemical shrinkage increased with increasing heating rate. For heating rate lower than 5 ^{o}C/min, no obvious difference was found. A correlation between chemical shrinkage and the kinetics of the chemical reactions has been proposed by Johannis and Hou et al. [41, 42]. By curve fitting isothermal chemical shrinkage, the activation energy of cyclization can be calculated. The difference in activation energy results calculated by the shrinkage and the DSC methods is less than 2 %.

1.2.3.4 Stress

If fibers are stabilized at constant length, entropic and chemical stress will develop. During isothermal stabilization at different temperatures, the maximum entropic stress did not change; but the maximum chemical stress slightly increased with a decrease in temperature [43]. The chemical stress increased faster at higher temperature. For fibers stabilized at a constant temperature, higher oxygen content made reaction stress increase faster and lowered the saturated reaction stress. The behavior of shrinkage stress strongly depends on conditions of oxidation. Ogawa et al. used the ratio of the stress at 180 °C in cooling to that at the temperature at which cooling started to evaluate the degree of modification in chemical structure by oxidation [43]. Also, Liu et al. observed that the temperatures that chemical stress began and the temperature at which the stress reached the maximum value had good correlation with starting point of DSC exothermic peak and the peak temperature [44], respectively.

1.2.3.5 DSC

Stabilization reactions are exothermic and can be monitored by DSC [45, 46]. The area under the exothermal peak can be used to estimate the degree of conversion of stabilization reactions. Also, the peak position [7, 32, 33] and shape [46] could be used to calculate the reaction activation energy of cyclization.

1.2.3.6 Other methods

During stabilization, density increases. For completely stabilized PAN fibers, the density is close to 1.6 g/cm^3, whereas density of the precursor fiber is less than 1.2 g/cm^3. Therefore, it is possible to use density as an index of stabilization [10]. Since fibers

absorbed oxygen during stabilization, some researchers suggested that stabilization can be estimated by oxygen content in the stabilized fibers.

1.2.4 Effect of co-monomer

Precursor fibers are manufactured from homo-polymer PAN, as well as co-polymer PAN. The most commonly used co-monomers are itaconic acid (IA) and methacrylic acid (MAA). The typical DSC curves of homo-polymer and co-polymer PAN precursor fibers are shown in Figure 1.13.

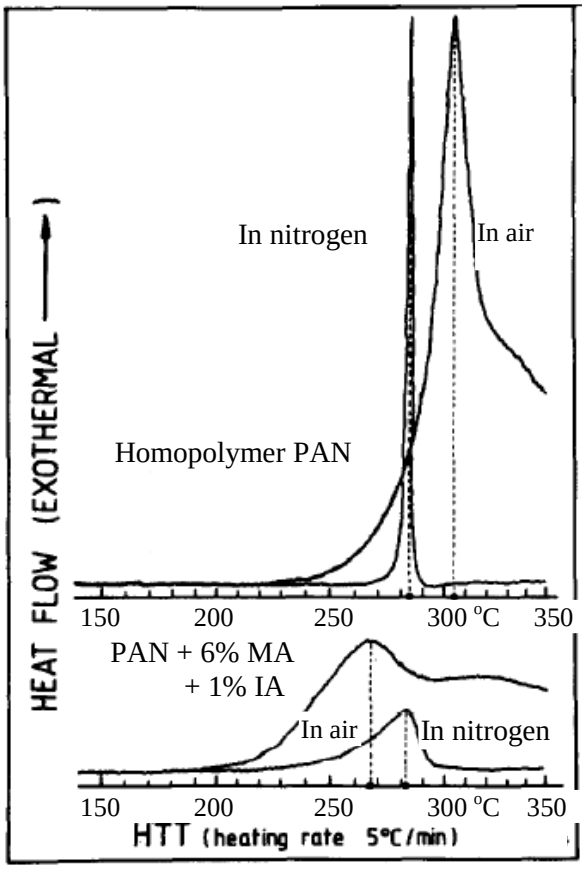

Figure 1.13 Typical DSC curves of homo-polymer and Acid copolymer PAN stabilized in air and nitrogen at a heating rate of 5 ^{o}C/min. [32]

From Figure 1.13, it can be seen that the addition of co-monomer significantly lowers the cyclizaton temperature and makes the exothermic peak much broader. The lower reaction temperature will require less energy consumption and will speed up the stabilization. A broader exothermic peak means a lower heat releasing rate, and, therefore, less possibility of local overheating. Fitzer et al. found that the addition of co-monomer lowered the reaction activation energy and acted as a catalyst or initiator [7]. The stabilization reaction rate strongly depends on the chemical structure of co-monomers [47]. The content and type of co-monomers affected both entropic and chemical shrinkages; compared with homo-polymer, higher content of co-monomer increased both kinds of shrinkages and lowered the starting temperature of chemical shrinkage. Although MAA and IA are the most commonly adopted co-monomers, there is no conclusion reported in the literature as to which type of co-monomer, and in what quantity, is the best for producing good carbon fibers.

1.2.5 Other studies on stabilization

1.2.5.1 Reaction temperature and activation energy

Stabilization involves complex reactions. It is very difficult to determine the optimum stabilization temperature; also, the reaction activation energy of each individual reaction is very hard to get for overlapped reactions. For the relationship of temperature and stabilization reactions, Mathur et al. [48] stabilized PAN fibers at a higher temperature in air, and found a new DSC exothermal peak at around 350 ^{o}C shown in Figure 1.14.

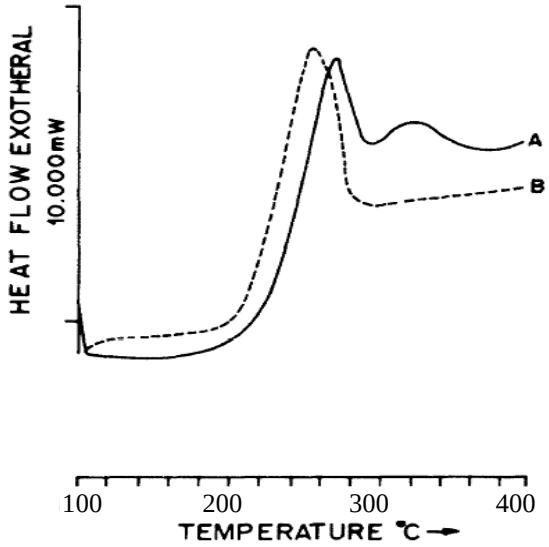

Figure 1.14 DSC curves of courtelle PAN (6 % MA) fibers at a heating rate of 5 ^{o}C/min, a. in air; b: in nitrogen. [48]

The first exothermal peak was caused by cyclization. For the fibers stabilized at higher temperature, they observed an increase in both strength and modulus of stabilized fibers [49]. IR [48] analysis proved that the exothermic peak in the DSC curve at ~ 350 ^{o}C was due to certain intermolecular cross-linking. The same reaction led to the increase in both strength and modulus of the stabilized fibers. The strength of carbonized fibers at 1000 ^{o}C after stabilized to the extent of the second exothermic peak was 2.4 GPa, 28 % higher than the carbon fiber from stabilized only up to the first peak, 1.88 GPa. Ouyang et al. [33,50] also found similar phenomena during DSC analysis, but they ascribed the exothermic peak at higher temperature to oxidation reaction. The apparent activation energy (E_a) of the stabilization reactions was determined by the Kissinger method and by the Ozawa method. The activation energy of the later exothermic peak was ~ 13 % higher than that of the former exothermic peak.

1.2.5.2 Mechanical properties of stabilized fibers

During stabilization, the tensile strength of PAN-based fibers decreases [51] rapidly in the beginning and then gradually with increase in stabilization time. The behavior of strength of stabilized fibers in air is similar to the intake of oxygen, which is very rapid in the beginning and becomes slow with time, as well as the conversion of C≡N to C=N.

With increase in stabilization time, it is found that the tensile strength of the resulting carbon fibers increases rapidly at first and then sharply decreases. After long stabilization time, the tensile strength decreases gradually [51].

1.2.5.3 Effect of tension during stabilization

During thermal treatment, tension needs to be applied to the fibers to reduce the chain relaxation in order to maintain the highly oriented structure obtained in precursor fibers [9, 52-55]. Mechanical properties of stabilized fibers improve with increase in applied tension. Both entropic and chemical shrinkages reduced significantly with higher applied tension [56]. High tension can even stretch the fibers; however, if the tension is too high, fibers will break [57]. Entropic shrinkage first occurs above the glass transition temperature; then, while temperature is further increased, fibers become plasticized. Under high tension, fibers can even be drawn during this stage.

Wu et al. [58] studied the effect of tension on the mechanical properties of the resulting carbon fibers and found that the tension at low temperatures led to a greater increase of the tensile strength than the tension at high temperatures, due to that the structure is fixed by cross-linking at high temperatures.

1.2.5.4 Effect of stabilization temperature

Stabilization reactions normally happen in the temperature range of 200 – 400 ^{o}C. Proper selection of stabilization temperatures and its profile are important to obtain good quality carbon fibers. Normally, the temperature profile can be divided into isothermal, continuously heating, step-wise, or their mixtures [32]. The heating rate [32, 59] also affects the properties of stabilized and carbonized fibers. Many researchers [35-36, 48, 60-61] have studied structural changes of PAN precursor fibers during different temperature stages; however, the optimum temperature profile for stabilization remains unclear at this stage.

1.2.5.5 Structure of stabilized PAN fibers

Yu et al. [62] studied the micro-structure of fibers during stabilization by high resolution transmission electron microscopy (HRTEM) and observed formation of nanocrystallites and two kinds of amorphous structures: onion-like and maze-like. During stabilization, changes happen earlier in onion-like amorphous regions than in the ordered structures. It was concluded that fine crystallites and homogeneous structures are important to produce high performance carbon fibers. Additionally, during the stabilization, Ji et al. [63] found that during the very initial stage, crystal size and orientation increased and subsequently decreased.

1.2.5.6 Other studies

Yu et al. [64] studied effects of the PAN precursor fibers on stabilization and found that the crystallinity of precursor fibers influences stabilization significantly; they concluded that higher content co-monomer and lower crystallinity can initiate reactions at a lower temperature, which is important to obtain the uniform microstructure of carbon

fibers. Mathematic models of stabilization and heat transfer have been proposed by Dunham [65] and Grove et al. [66]. Suresh et al. [67] used dynamic mechanical analyzer (DMA) to probe the visco-elastic properties during thermal stabilization and studied the effect of co-monomers. The same method [68,69] has been used to monitor the curing process of thermally set epoxy, which suggested that it may be used to detect the end of chemical reactions. Paiva et al. [70] tried to stabilize PAN fibers using ultra-violet radiation. Thus, it appears that researchers have worked very broadly on the stabilization of PAN-based fibers.

In summary, although there is some consensus on the general structure of PAN precursor fibers, the exact structure is still unknown. The chemical reactions that occur during stabilization are so complex that many mechanisms are still under research. For stabilization, several factors exist that affect the final properties of stabilized fibers, such as atmosphere, temperature, stress, co-monomers, and heating rate. Hither to now, no suitable mathematical model has been provided to explain the effect of all processing conditions or even that of just one factor. The only method to optimize the stabilization process is to test carbonized fiber with a series of conditions to determine which condition is the best one; however, this approach is very time and labor consuming. Overall, many questions and challenges remain in this field.

1.3 Carbon nanotubes reinforced PAN-based carbon fibers

1.3.1 Carbon nanotubes (CNTs)

CNTs, especially single wall carbon nanotubes, have extraordinary mechanical, electrical and thermal properties. It is expected that the properties of materials can be

greatly improved when reinforced with CNTs. CNTs can be divided into single wall CNTs (SWNT), double wall CNTs (DWNT), and multi wall CNTs (MWNT), as well as metallic and semi-conductive CNTs. Among them, SWNTs have the best mechanical properties. SWNTs usually have a diameter from 0.8 to 4 nm, tensile modulus around 1 TPa, and strength of > 100 GPa. These excellent properties make CNTs great reinforcement materials for polymers to enhance stiffness, strength, and toughness.

1.3.2 Effect of CNTs on properties of PAN precursor fibers

Since CNTs have excellent mechanical properties and have been found to improve the mechanical properties of many materials, can they be used to enhance the properties of PAN precursor fibers and the resulting carbon fibers? Chae et al. have shown that all types of CNTs including SWNT, DWNT, MWNT, as well as vapor growth carbon nanofibers (VGCNF) can improve the tensile and dynamic mechanical properties of PAN fibers [71]. With well dispersed SWNT in PAN fibers [72], addition of as little as 1 wt. % SWNT strongly enhances its strength and modulus from 0.9 to 1.07 GPa and from 22.1 to 28.7 GPa, respectively.

Also, the presence of CNTs affects the arrangement of adjacent PAN molecules. In the meridional scan [72], addition of SWNTs shifts the peak position to lower 2θ value. The PAN meridional peak can be deconvoluted into two peaks at $2\theta = 36^{o}$ and 40^{o}, which have been ascribed to be planar zigzag and helical sequences [18], respectively. The lower meridional peak position in the composite fibers means that more planar zigzag structure exists in comparison with control PAN fibers.

In dynamic mechanical testing, the addition of CNTs lowered the magnitude of tan(δ) and shifted tan(δ) peak position to a higher temperature [72]. The calculated

activation energy of the composite fibers showed significantly higher value, 809 kJ/mol, than that of the control PAN fibers, which is around 544 kJ/mol. Also, the storage modulus of composite fibers was higher than that of the control fibers. In summary, the addition of CNTs in PAN fibers strongly affects the structure and properties of the PAN chains in the CNT vicinity.

1.3.3 Effect of CNTs on stabilized and carbonized fibers

Studies [73, 74] show that the addition of CNT affects the PAN stabilization reactions, leads to highly ordered carbonized structure and greatly improves the tensile properties of the resulting carbon fibers. After stabilization, the chemical structure of the nitrile groups in the stabilized PAN fiber was found to be affected by the addition of CNTs as shown in Figure 1.15. The nitrile absorbance in IR spectra can be de-convoluted into three types of nitrile groups including unreacted nitrile, β-amino nitrile, and conjugated nitrile. After stabilization, a significantly higher content of conjugated nitrile and a considerably lower content of β-amino nitrile were observed when SWNT (1 wt. %) is added into PAN precursor fibers. β-amino nitrile is supposed to be formed due to termination of cyclization and chain scission. Thus, the lower fraction of β-amino nitrile means the lower possibility of chain scission and fewer defects in the carbon fibers; as a result, the mechanical properties of the carbon fibers will be improved.

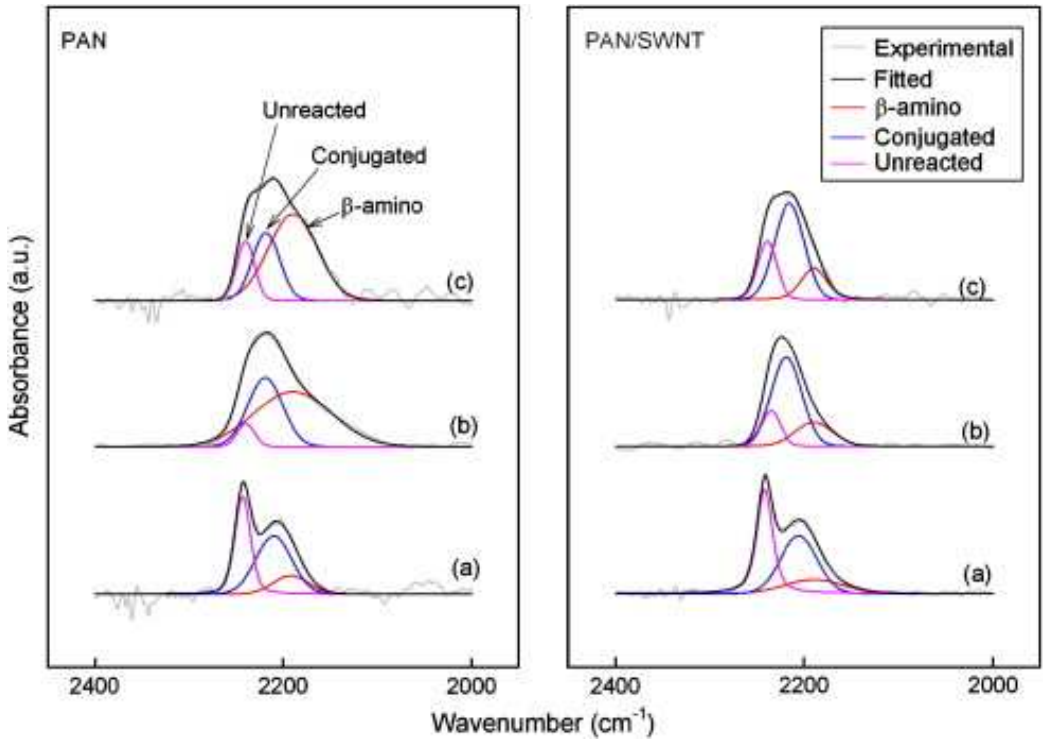

Figure 1.15 Nitrile band fitting results of IR spectra of stabilized PAN and PAN/CNT composite fibers. (a) stabilized in TGA at 285 ^{o}C for 30 min in air, (b) stabilized in furnace at 0.006 N/tex stress, and (c) stabilized in furnace at 0.025 N/tex in air. [74]

In XRD patterns, the azimuthal scan at a typical diffraction peak is related to the orientation of the diffraction planes. The azimuthal scan of the formed ladder structure in the stabilized composite fibers is found to be much sharper in comparison with the stabilized PAN fibers, and can not be fitted by single curve which works well for the stabilized PAN fibers [73]. Therefore, two curves were fitting in the composite samples, one of these was a low intensity narrow peak and the second peak was much broader with high intensity. This result indicates that a small portion of highly ordered ladder structure was induced by the addition of CNTs. Additionally, same phenomenon can be observed in the carbonized fibers as well.

Composite carbon fibers showed fibrillar fracture structure, whereas control carbon fibers showed non-fibrillar glassy fracture [74]. The fibrillar structure was further observed by HRTEM, and a highly ordered structure was observed in the vicinity of CNTs. The Raman spectra of the carbonized PAN/SWNT fiber showed a distinct graphitic G-band peak, and confirmed the formation of graphite-like structure in the vicinity of the CNTs. The G-band intensity increased with increasing applied stress, which confirmed stress induced graphitization. In PAN-based carbon fiber, graphitic structure is observed only when carbonized fibers are further graphitizated at temperatures over 2500 ^{o}C. However, with the addition of CNTs, graphite-like structure can be formed at a relative low carbonization temperature of 1100 ^{o}C. Tensile modulus and strength of the carbonized fibers [74] were as high as 250 N/tex and 1.8 N/tex for the composite fibers and 168 N/tex and 1.1 N/tex for the control PAN based carbon fibers, respectively. The addition of only 1 wt. % CNTs enhanced the carbon fiber modulus by 49 % and strength by 64 %.

1.4 Thesis objectives

This thesis has the following objectives:

1. To compare the effect of different types of CNTs on stabilization.
2. To study stabilization reaction kinetics in PAN/CNT fibers.
3. To study the effect of stress, temperature, and stabilization time on stabilized and carbonized fibers and find the optimum stabilization conditions for PAN/CNT composite fibers.
4. To study the effect of precursor fiber properties and that of the co-monomer on the structure and properties of the resulting carbon fibers.

1.5 References

[1] Kroto HW, Heath JR, O'Brien SC, Curl RF, Smalley RE. C60: Buck minster fullerene. Nature. 1985;318(6042):162-3.

[2] Iijima S. Helical microtubules of graphitic carbon. Nature. 1991;354(6348):56-8.

[3] Minus ML, Kumar S. The processing, properties, and structure of carbon fibers. JOM. 2005;57(2):52-8.

[4] Chand S. Carbon fibers for composites. Journal of Materials Science. 2000;35(6): 1303-13.

[5] Fitzer E. Pan-based carbon fibers--present state and trend of the technology from the viewpoint of possibilities and limits to influence and to control the fiber properties by the process parameters. Carbon. 1989;27(5):621-45.

[6] Paluch E.A. Outbreaks of carbon disulfide poisoning in rayon staple fiber plants in poland. Journal of Industrial Hygiene and Toxicology. 1948;30(1):37-42.

[7] Fitzer E, Müller DJ. The influence of oxygen on the chemical reactions during stabilization of pan as carbon fiber precursor. Carbon. 1975;13(1):63-9.

[8] Rahaman MSA, Ismail AF, Mustafa A. A review of heat treatment on polyacrylonitrile fiber. Polymer Degradation and Stability. 2007;92(8):1421-32.

[9] Clarke AJ, Bailey JE. Oxidation of Acrylic Fibres for Carbon Fibre Formation. Nature. 1973;243(5403):146-50.

[10] Gupta A, Harrison IR. New aspects in the oxidative stabilization of pan-based carbon fibers. Carbon. 1996;34(11):1427-45.

[11] Ko TH, Ting HY, Lin CH. Thermal stabilization of polyacrylonitrile fibers. Journal of Applied Polymer Science. 1988;35(3):631-40.

[12] Didchenko R, Amata, Charles D. Rapid stabilization of polyacrylonitrile fibers prior to carbonization. 1976. US Patent 3954947.

[13] Weber C, Altenhofen U, Zahn H. Basic studies on the stability of filtration fabrics1. The effect of sulfur-dioxide and nitrogen-oxides on polyacrylonitrile. Text Res J. 1988;58(9):507-14.

[14] Colvin BG, Storr P. The crystal structure of polyacrylonitrile. European Polymer Journal. 1974;10(4):337-40.

[15] Bashir Z. Cocrystallization of solvents with polymers - The x-ray diffraction beheavior of solvent-containing and solvent-free polyacrylonitrile. Journal of Polymer Science Part B-Polymer Physics. 1994;32(6):1115-28.

[16] Lindenmeyer PH, Hosemann R. Application of theory of paracrystals to crystal structure analysis of polyacrylonitrile. J Appl Phys. 1963;34(1):42-9.

[17] Bashir Z, Rastogi S. The explanation of the increase in slope at the Tg in the plot of d-spacing versus temperature in polyacrylonitrile. J Macromol Sci-Phys. 2005;B44(4):611-7.

[18] Sawai D, Yamane A, Kameda T, Kanamoto T, Ito M, Yamazaki H, et al. Uniaxial Drawing of Isotactic Poly(acrylonitrile): Development of Oriented Structure and Tensile Properties. Macromolecules. 1999;32(17):5622-30.

[19] Warner SB, Uhlmann DR, Peebles LH. Oxidative stabilization of acrylic fibers .3. morphology of polyacrylonitrile. Journal of Materials Science. 1979;14(8):1893-900.

[20] Gupta AK, Singhal RP. Effect of co-polymerization and heat-treatment on the structure and x-ray-diffraction of polyacrylonitrile. Journal of Polymer Science Part B-Polymer Physics. 1983;21(11):2243-62.

[21] Dunn P, Ennis BC. Thermal analysis of polyacrylonitrile .1. melting of polyacrylonitrile. Journal of Applied Polymer Science. 1970;14(7):1795-9.

[22] Bai YJ, Wang CG, Lun N, Wang Y-X, Yu M-J, Zhu B. HRTEM microstructures of PAN precursor fibers. Carbon. 2006;44(9):1773-8.

[23] Josef S. Discoloration effect in acrylonitrile polymers. Journal of Polymer Science. 1958;28(117):438-9.

[24] Lafdi K, Bonnamy S, Oberlin A. Mechanism of anisotropy occurrence in a pitch precursor of carbon-fibers .1. pitches-a and pitches-b. Carbon. 1991;29(7):831-47.

[25] Chen SS, Herms J, Peebles LH, Uhlmann DR. Oxidative stabilization of acrylic fibers .5. the decoloration reaction. Journal of Materials Science. 1981;16(6):1490-510.

[26] Rangarajan P, Bhanu VA, Godshall D, Wilkes GL, McGrath JE, Baird DG. Dynamic oscillatory shear properties of potentially melt processable high acrylonitrile terpolymers. Polymer. 2002;43(9):2699-709.

[27] Watt W, Johnson W. Mechanism of oxidization of polyacrylonitrile fibers. Nature. 1975;257(5523):210-2.

[28] Peebles LH, Brandrup J. A Chemical means of distinguishing between conjugated bonds. Makromolekulare Chemie. 1966;98(NOV):189-94.

[29] Standage AE, Matkowsk.Rd. Thermal oxidation of polyacrylonitrile. European Polymer Journal. 1971;7(7):775-82.

[30] Henrici-Olivé G, Olivé S. Molecular interactions and macroscopic properties of polyacrylonitrile and model substances. 1979, p. 123-52.

[31] Lavin JG. Chemical-reactions in the stabilization of mesophase pitch-based carbon-fiber. Carbon. 1992;30(3):351-7.

[32] Fitzer E, Frohs W, Heine M. Optimization of stabilization and carbonization treatment of PAN fibres and structural characterization of the resulting carbon fibres. Carbon. 1986;24(4):387-95.

[33] Ouyang Q, Cheng L, Wang H, Li K. Mechanism and kinetics of the stabilization reactions of itaconic acid-modified polyacrylonitrile. Polymer Degradation and Stability. 2008;93(8):1415-21.

[34] Jing M, Wang CG, Wang Q, Bai YJ, Zhu B. Chemical structure evolution and mechanism during pre-carbonization of PAN-based stabilized fiber in the temperature range of 350-600^{o}C. Polymer Degradation and Stability. 2007;92(9):1737-42.

[35] Jing M, Wang CG, Bai YJ, Zhu B, Wang YX. Effect of temperatures in the rearmost stabilization zone on structure and properties of PAN-based oxidized fibers. Polymer Bulletin. 2007;58(3):541-51.

[36] Dalton S, Heatley F, Budd PM. Thermal stabilization of polyacrylonitrile fibres. Polymer. 1999;40(20):5531-43.

[37] Zhu Y, Wilding MA, Mukhopadhyay SK. Estimation, using infrared spectroscopy, of the cyclization of poly(acrylonitrile) during the stabilization stage of carbon fibre production. Journal of Materials Science. 1996;31(14):3831-7.

[38] Shimada I, Takahagi T, Fukuhara M, Morita K, Ishitani A. FT-IR study of the stabilization reaction of polyacrylonitrile in the production of carbon fibers. Journal of Polymer Science Part A: Polymer Chemistry. 1986;24(8):1989-95.

[39] Yu MJ, Bai YJ, Wang CG, Xu Y, Guo PZ. A new method for the evaluation of stabilization index of polyacrylonitrile fibers. Materials Letters. 2007;61(11-12):2292-4.

[40] Yu MJ, Wang CG, Bai YJ, Wang YX, Wang QF, Liu HZ. Combined effect of processing parameters on thermal stabilization of PAN fibers. Polymer Bulletin. 2006;57(4):525-33.

[41] Johannis Simitzis SS. Correlation of chemical shrinkage of polyacrylonitrile fibres with kinetics of cyclization. Polymer International. 2008;57(1):99-105.

[42] Hou Y, Sun T, Wang H, Wu D. A new method for the kinetic study of cyclization reaction during stabilization of polyacrylonitrile fibers. Journal of Materials Science. 2008;43(14):4910-4.

[43] Ogawa H, Saito K. Oxidation behavior of polyacrylonitrile fibers evaluated by new stabilization index. Carbon. 1995;33(6):783-8.

[44] Liu J, Wang L, Zhang WX, Li J, Liang JY. Relationships between thermal stress and the thermo-chemical reaction of PAN fibers during thermal stabilization. New Carbon Mater. 2005;20(4):343-9.

[45] Kakida H, Tashiro K, Kobayashi M. Mechanism and kinetics of stabilization reaction of polyacrylonitrile and related copolymers .1. Relationship between

isothermal DSC thermogram and FT/IR spectral change of an acrylonitrile methacrylic acid copolymer. Polym J. 1996;28(1):30-4.

[46] Devasia R, Reghunadhan CP, Sivadasan NP, Katherine BK, Ninan KN. Cyclization reaction in poly(acrylonitrile/itaconic acid) copolymer: An isothermal differential scanning calorimetry kinetic study. Journal of Applied Polymer Science. 2003;88(4):915-20.

[47] Coleman MM, Sivy GT. Fourier transform ir studies of the degradation of polyacrylonitrile copolymers - I: Introduction and comparative rates of the degradation of three copolymers below 200°c and under reduced pressure. Carbon. 1981;19(2):123-6.

[48] Mittal J, Bahl OP, Mathur RB, Sandle NK. IR studies of PAN fibres thermally stabilized at elevated temperatures. Carbon. 1994;32(6):1133-6.

[49] Mathur RB, Bahl OP, Mittal J. A new approach to thermal stabilisation of PAN fibres. Carbon. 1992;30(4):657-63.

[50] Ouyang Q, Cheng L, Wang HJ, Li KX. DSC study of stabilization reactions in poly(acrylo-nitrile-co-itaconic acid) with peak-resolving method. Journal of Thermal Analysis and Calorimetry. 2008;94(1):85-8.

[51] Bahl OP, Manocha LM. Characterization of oxidised pan fibres. Carbon. 1974;12(4):417-23.

[52] Edie DD. The effect of processing on the structure and properties of carbon fibers. Carbon. 1998;36(4):345-62.

[53] Yu MJ, Wang CG, Bai YJ, Wang YX, Zhu B. Evolution of tension during the thermal stabilization of polyacrylonitrile fibers under different parameters. Journal of Applied Polymer Science. 2006;102(6):5500-6.

[54] Wu GP, Lu CX, Ling LC, Hao AM, He F. Influence of tension on the oxidative stabilization process of polyacrylonitrile fibers. Journal of Applied Polymer Science. 2005;96(4):1029-34.

[55] Deurbergue A, Oberlin A. Stabilization and carbonization of pan-based carbon fibers as related to mechanical properties. Carbon. 1991;29(4-5):621-8.

[56] Bahl OP, Manocha LM. Shrinkage behaviour of polyacrylonitrile during thermal treatment. Angewandte Makromolekulare Chemie. 1975;48(1):145-59.

[57] Layden GK. Tensile response of polyacrylonitrile fibers during air heating. Journal of Applied Polymer Science. 1971;15(7):1709-15.

[58] Wu GP, Lu CX, Ling LC, Hai AM, He F. Influence of tension on the oxidative stabilization process of polyacrylonitrile fibers. Journal of Applied Polymer Science 2005; 96(4): 1029-1034.

[59] Hou YP, Sun TQ, Wang HJ, Wu D. Effect of heating rate on the chemical reaction during stabilization of polyacrylonitrile fibers. Text Res J. 2008;78(9):806-11.

[60] Yan X, Wang CG. High-temperature DSC study of polyacrylonitrile precursors during their conversion to carbon fibers. Journal of Applied Polymer Science. 2007;106(3):1787-92.

[61] Zhang WX, Li J, Wang G. Evolution of structure and properties of PAN precursors during their conversion to carbon fibers. Carbon. 2003;41(14):2805-12.

[62] Yu M, Wang C, Bai Y, Zhu B, Ji M, Xu Y. Microstructural evolution in polyacrylonitrile fibers during oxidative stabilization. Journal of Polymer Science Part B: Polymer Physics. 2008;46(7):759-65.

[63] Ji MX, Wang CG, Bai YJ, Yu MJ, Wang YX. Structural evolution of polyacrylonitrile precursor fibers during preoxidation and carbonization. Polymer Bulletin. 2007;59(4):527-36.

[64] Yu MJ, Wang CG, Bai YJ, Wang YX, Xu Y. Influence of precursor properties on the thermal stabilization of polyacrylonitrile fibers. Polymer Bulletin. 2006;57(5):757-63.

[65] Dunham MG, Edie DD. Model of stabilization for pan-based carbon fiber precursor bundles. Carbon. 1992;30(3):435-50.

[66] Grove Iii DA, Abhiraman AS. A mathematical model of solid-state thermo-oxidative stabilization of acrylic fibers. Carbon. 1992;30(3):451-7.

[67] Suresh KI, Thomas KS, Rao BS, Nair CPR. Viscoelastic properties of polyacrylonitrile terpolymers during thermo-oxidative stabilization (cyclization). Polymers for Advanced Technologies. 2008;19(7):831-7.

[68] Ramis X, Cadenato A, Morancho JM, Salla JM. Curing of a thermosetting powder coating by means of DMTA, TMA and DSC. Polymer. 2003;44(7):2067-79.

[69] Cadenato A, Salla JM, Ramis X, Morancho JM, Marroyo LM, Martin JL. Determination of gel and vitrification times of thermoset curing process by means of TMA, DMTA and DSC techniques - TTT diagram. John Wiley & Sons Ltd; p. 269-79.

[70] Paiva MC, Kotasthane P, Edie DD, Ogale AA. UV stabilization route for melt-processible PAN-based carbon fibers. Carbon. 2003;41(7):1399-409.

[71] Chae HG, Sreekumar TV, Uchida T, Kumar S. A comparison of reinforcement efficiency of various types of carbon nanotubes in polyacrylonitrile fiber. Polymer. 2005;46(24):10925-35.

[72] Chae HG, Minus ML, Kumar S. Oriented and exfoliated single wall carbon nanotubes in polyacrylonitrile. Polymer. 2006;47(10):3494-504.

[73] Chae HG, Choi YH, Minus ML, Kumar S. Carbon nanotube reinforced small diameter polyacrylonitrile based carbon fiber. Composites Science and Technology. 2009;69(3-4):406-13.

[74] Chae HG, Minus ML, Rasheed A, Kumar S. Stabilization and carbonization of gel spun polyacrylonitrile/single wall carbon nanotube composite fibers. Polymer. 2007;48(13):3781-9.

CHAPTER 2

EFFECT OF ADDITION OF DIFFERENT TYPES OF CARBON NANOTUBES ON STABILIZATION

In this chapter, chemical, structural and mechanical property evolutions during the thermal stabilization were studied, and the effect of CNTs on stabilization was explored. Three types of CNTs with different wall numbers and catalyst contents were used to enhance PAN precursor fibers, and their effect on stabilization was compared. This study will help to better understand the effect of different types of CNTs on stabilization, to choose appropriate type of CNTs, and to optimize the stabilization conditions.

2.1 Experimental

2.1.1 Materials

The PAN used in this study is a homo-polymer (M_w ~ 250,000 g/mol), supplied by Japan Exlan Company. Before using, PAN powder was dried in vacuum at 100^{o}C for 2 days. Dimethyformamide (DMF, DX 1730-2), purchased from EMD Company, was dried by molecular sieve (~ 10 g for 4L) for over 2 days before use. Molecular Sieves (4Å, beads, 8-12 meshes, Batch# 08908AH) were obtained from Aldrich Company. Methanol (> 99.8 %) was obtained from BDH Company.

CNTs were purchased from Unidym, Inc. CNTs with lot numbers XO122UA, XO437UA, and XB928, and having catalyst residues of 1.2 wt. %, 1.2 wt. %, and 4 wt. %, were named as CNT1, CNT2, and CNT3, respectively. For CNT1 and CNT2, the process parameters were altered and led to the changes of diameters and wall numbers.

2.1.2 Characterization

Raman spectra were conducted on Holoprobe Research 785 Raman microscope (Kaiser Optical system) using 785 nm excitation laser in VV mode (polarizer and analyzer are parallel to each other). WAXD patterns were obtained by Rigaku micromax-002 (Cu K_α radiation) using Rigaku R-axis IV++ detector. Surface area of CNTs powder was measured by Micromeritics' ASAP 2020 accelerated surface area and porosimetry analyzer. Infrared spectra (IR) were collected using infrared microscope (Spectrum One, Perkin Elmer) with a resolution of 2 cm^{-1} and 256 scans. Peakfit software (Seasolve software Inc. v4.12) was used for peak fitting of IR spectra. The mechanical properties of single fiber were tested on RSA III solids analyzer (Rheometric Scientific Co.) at a gauge length of 25 mm and crosshead speed of 0.25 mm/s. Statistic analysis method described in appendix B is used and the confidence level of at least 95 % is used as the criterion for distinguishing between the two or more data sets. Fiber morphologies were observed using scanning electron microscope (SEM, 1530, Leo Electron Microscopy Ltd.) at an operating voltage of 10 kV on gold coated samples. The shrinkage and stress-temperature curves were recorded by thermal mechanical analyzer (TMA, Q-400, TA Instrument). Stabilization was carried out in a box furnace (Lindberg, 51668-HR, Blue M Electric).

The Raman spectra of all three kinds of CNT powders showed no RBM band (150 ~ 300 cm^{-1}), which indicated that the CNTs did not contain single-wall CNTs. WAXD was used to estimate the average numbers of walls in each of the CNTs. The WAXD patterns and integrated curves are shown in Figure 2.1. The crystallite size (XS) can be estimated from the breadth of the diffraction peak using the Scherrer's equation. The WAXD peak of the walls in MWNTs is around *d* spacing=0.34 nm, and its breadth can

be used to estimate the average number of walls. CNT2 and CNT3 have similar average numbers of walls, about 6, and CNT1 has the least average number of walls, around 4.

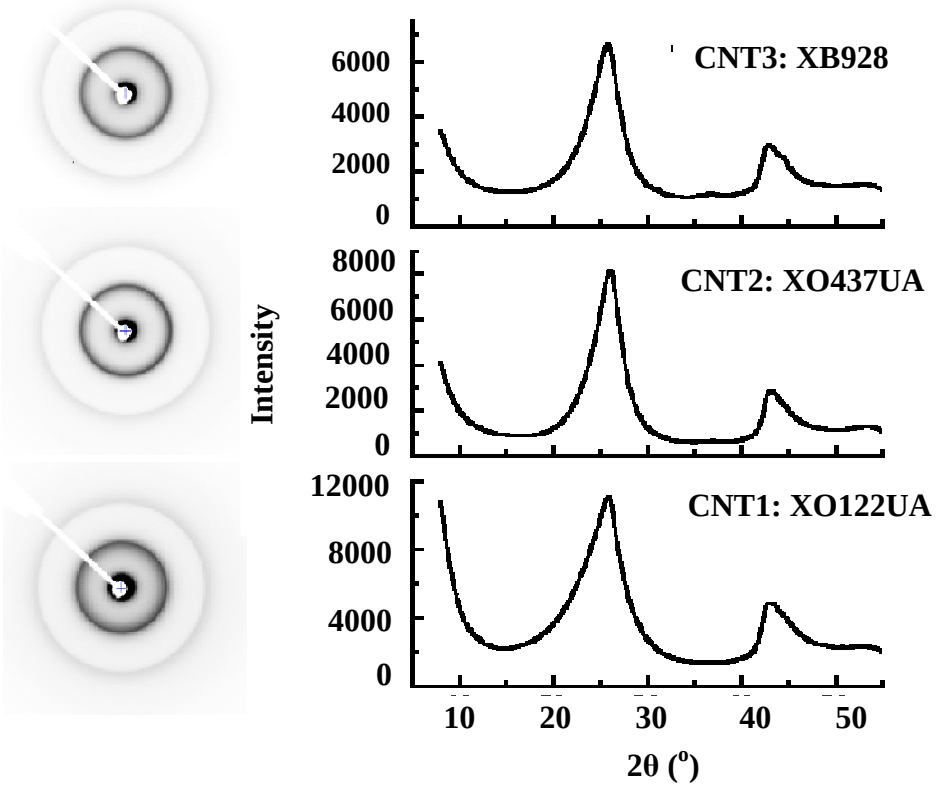

Figure 2.1 WAXD patterns and integrated curves of CNTs powders.

One of the important properties of CNTs is their high surface area; for typical SWNT, the surface area can reach 1300 m^2/g. To compare the differences of CNT1, CNT2 and CNT3, surface area was measured using the nitrogen gas absorbance method. The pore size distributions and BET surface area of the three CNTs obtained by gas absorbance are plotted in Figure 2.2. The surface area in CNT2 and CNT3 is similar whereas that in CNT1 is the largest.

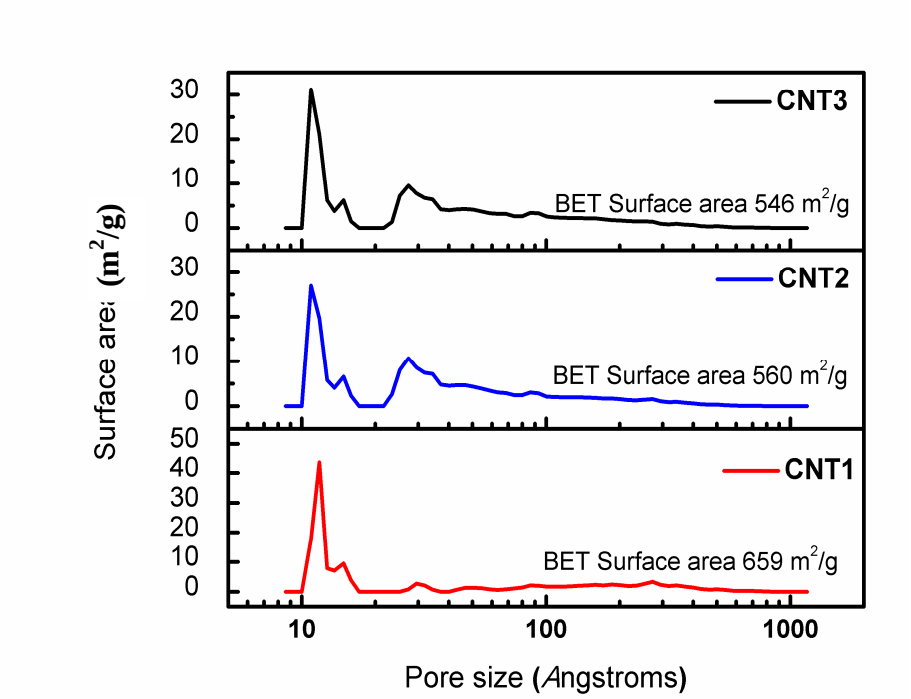

Figure 2.2 Surface area and pore size distributions of CNT1, CNT2 and CNT3.

2.1.3 Fiber Spinning

2.1.3.1 Spinning solution preparation

14.85 g dried PAN powder was dissolved in 140 ml DMF at 80 ^{o}C. To ensure good dispersion of CNTs, CNTs were first dispersed in DMF at a concentration of 42.8 mg/L and were sonicated in a bath sonicator for 24 hr. Optically homogeneous dispersion of CNT was obtained. CNT/DMF dispersion was poured into the PAN solution. Excess amount of DMF was evaporated under vacuum at 100 ^{o}C to obtain 15 g solid (PAN and CNT) /100ml DMF solution.

2.1.3.2 Dry-jet gel-spinning

The solution was spun through a 120 μm diameter single hole spinneret at 110 ^{o}C into a methanol bath maintained at a temperature lower than - 60 ^{o}C with an air gap of about 4 cm. Linear jet velocity and take up speed were 27.2 and 82 m/min, respectively; thus, the as-spun draw ratio was 3. After spinning, collected fibers were immediately immersed in methanol bath (cooled by dry ice) for 2 days to ensure gelation. As-spun fibers were hot drawn at 160 ^{o}C in glycerol bath at a draw ratio of 4.5. The cumulated draw ratio was 13.5. Ethanol was used to wash the fibers to remove the residual glycerol; then, washed fibers were dried at 50 ^{o}C under vacuum for 3 days.

2.1.4 Stabilization

For oxidative stabilization, fibers were kept inside the box furnace. A constant force was applied by a pair of iron clamps. During stabilization, the furnace chamber was continuously purged with air at a flow rate of 20 SCFH. The furnace was calibrated by a temperature sensor; the detected position and calibration curve are shown in Figure 2.3.

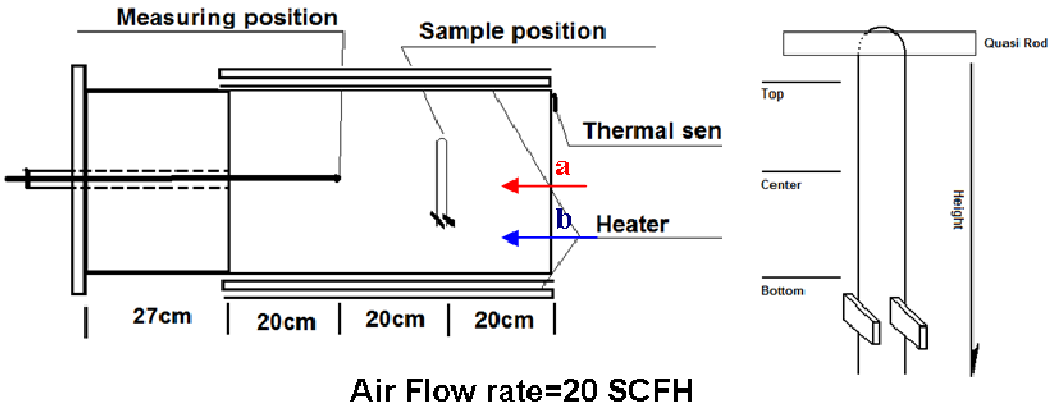

Figure 2.3 Position of temperature probe in the box furnace.

The temperatures at two different positions were detected by the temperature probe under an air flow at 20 SCFH. Position A was close to the fiber samples, and position B was close to the bottom of furnace. The relationship between the measured temperatures and the setting temperatures was plotted in Figure 2.4. Reported temperatures are measured temperatures shown in Figure 2.4.

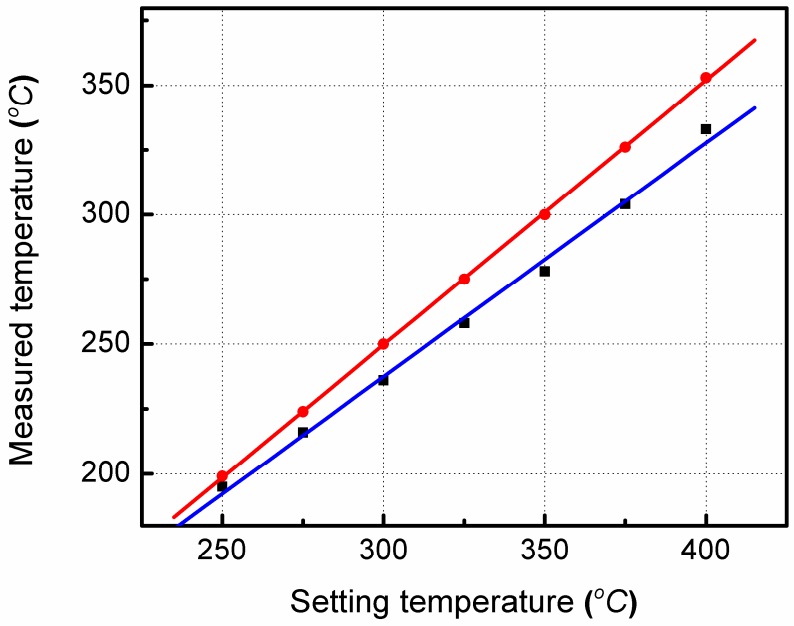

Figure 2.4 Calibrated temperatures of box furnace by temperature probe. Solid circle: position a; solid square: position b shown in Figure 2.3.

Comparing the temperatures of position A and B, the difference is about 10 ^{o}C. The large difference will significantly affect the stabilization reactions and lead to non-uniform properties of the stabilized fibers. Hence, the temperature of position A was used as the actual temperature, as position A was very close to the fiber samples. Stabilized samples were collected at different stabilization stages as shown in Figure 2.5. The stabilization time is defined as the isothermal time at the final temperature. In the

experiments, the fibers were stabilized at 234 ^{o}C and 267 ^{o}C for various times with constant tension (20 MPa) applied by clamps.

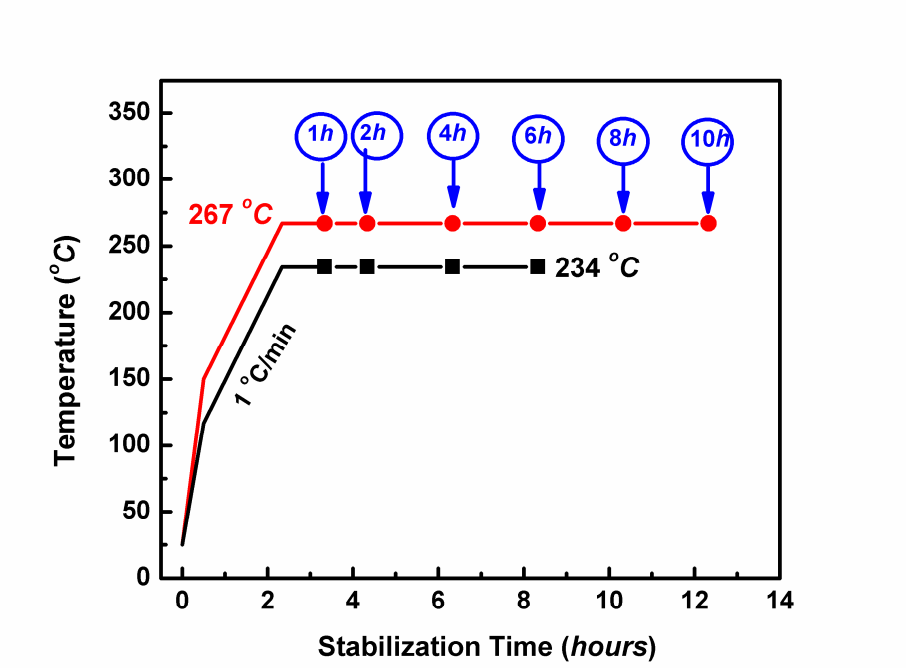

Figure 2.5 Stabilization process and samples collection points.

2.2 Results and Discussion

2.2.1 Effect of addition of CNTs on precursor fibers

2.2.1.1 Tensile properties of precursor fibers

Assuming that the diameter of fiber was uniform, the length and weight of the fibers were measured. The fiber density and diameter were calculated by the volume fractions of PAN and CNTs as shown in Table 2.1.

Table 2.1 Diameter of precursor fibers.

	Control PAN	PAN/CNT1	PAN/CNT2	PAN/CNT3
Length (m)	27	25	29	15
Weight (mg)	2.77±0.04	2.15±0.04	3.30±0.03	1.44±0.03
Diameter (μm)	10.4	9.6	11.1	10.2

For tensile tests, 16 filaments were tested for each sample, the typical stress-strain curves of all the types of precursor fibers are shown in Figure 2.6 and the results are summarized in Table 2.2. The reinforcement efficiency of CNT was calculated by comparing the Young's modulus of the composite fiber and the control PAN fiber. In precursor fibers, addition of CNT2 and CNT3 shows similar reinforcement efficiencies, whereas addition of CNT1 shows the best reinforcement efficiency. The porosity tests (Figure 2.2) show that CNT2 and CNT3 have BET surface areas of 560 m^2/g and 546 m^2/g respectively, which are lower than that for CNT1, which has a BET surface area of 659 m^2/g. The ratio of the surface areas of CNT1/CNT2/CNT3 is 1.21/1.02/1.00 and reinforcement efficiencies ratio of the three CNTs is 1.31/1.00/1.00. This shows that CNTs reinforcement efficiency increases with increasing CNT surface area. The surface area of CNTs is proportional to the interfacial area of well dispersed CNTs in the PAN matrix, and affects the load transfer from the matrix to the CNTs. This is consistent with other reports [1-3] and suggests that the reinforcement efficiency of CNT correlates positively with CNT interfacial area.

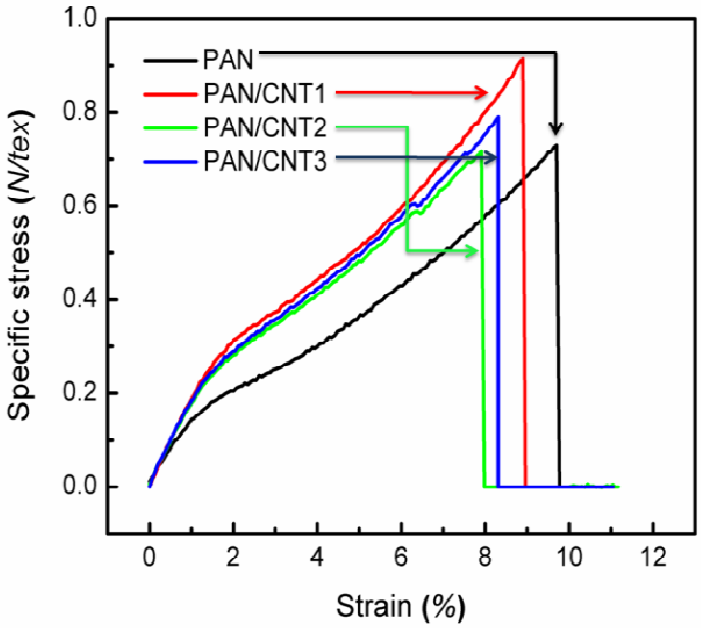

Figure 2.6 Typical stress-strain curves of precursor fibers.

Table 2.2 Tensile properties of precursor fibers.

	PAN	PAN/CNT1	PAN/CNT2	PAN/CNT3
Tensile modulus (N/tex)	14.1±1.4	16.3±2.5	15.8±2.7	15.8±2.1
Tensile strength (N/tex)	0.68±0.10	0.86±0.06	0.70±0.04	0.76±0.06
Strain to failure (%)	9.5±1.0	8.7±0.7	7.7±0.3	8.4±0.7
Reinforcement* (N/tex)	--	239	188	186

Note: *The reinforcement efficiency of CNT was calculated by $\frac{YM_{Composite} - YM_{Control} \cdot f_w(PAN)}{f_w(CNT)}$ (YM: Young's modulus (N/tex), f_w: Weight fraction (wt %)). Tex: linear density of fibers which is defined as the mass in gram per 1000 meter of fibers.

2.2.1.2 Dynamic mechanical analysis (DMA)

Due to the sensitivity of the instrument, DMA was performed on a bundle of fibers containing 100 filaments. Before DMA testing, fibers were dried in vacuum oven for over two days at 50 ^{o}C to remove absorbed moisture. Sample gauge length was 25 mm, pre-strain was 0.5 % (linear region), and vibration strain was 0.2 %. The DMA tests

were performed in the temperature range of -100 to 200 ^{o}C at a heating rate of 1 ^{o}C/min. Nitrogen was used as the environment. Typical DMA curves are shown in Figure 2.7.

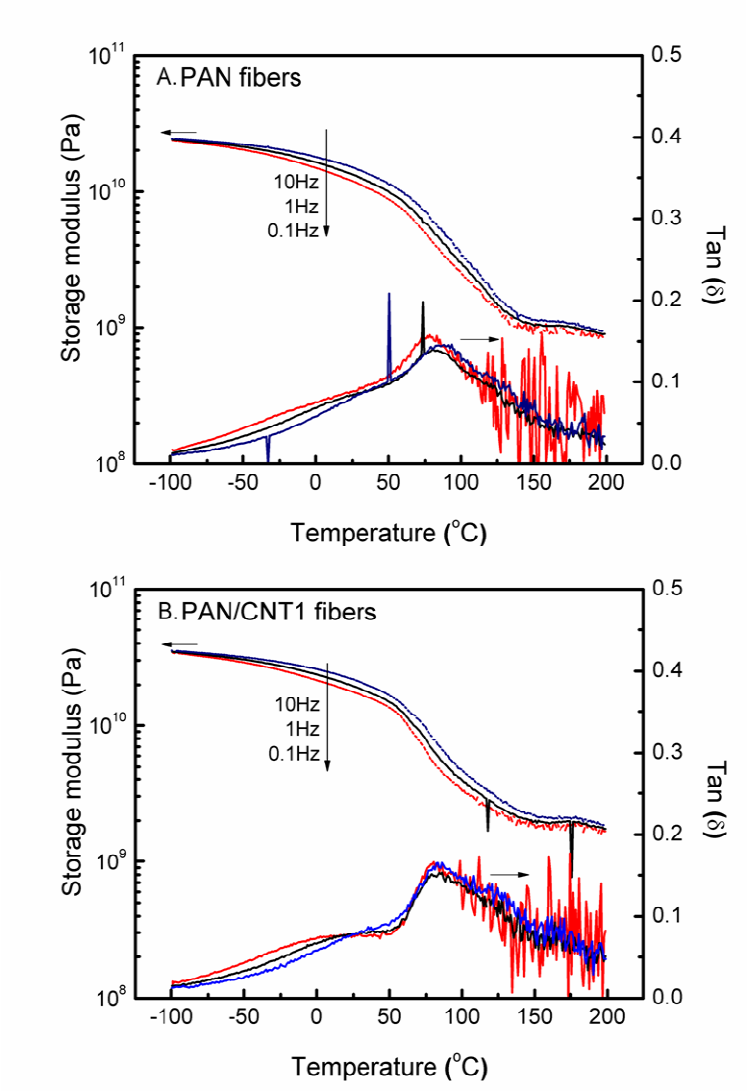

Figure 2.7 Typical DMA curves of PAN and PAN/CNT1 composite fibers tested under 0.1, 1 and 10 Hz.

The observed glass transition temperature (tan(δ) peak temperature) depended on the test frequency, $\ln(F) = \ln(A) - \frac{E_a}{RT}$, where, F is frequency, T is temperature, and E_a

is activation energy. By plotting the natural logarithm of frequency versus *1/T* (Figure 2.8), the slope can be used to calculate the activation energy. The composite fibers have a much higher activation energy of glass transition than that in the control PAN fibers.

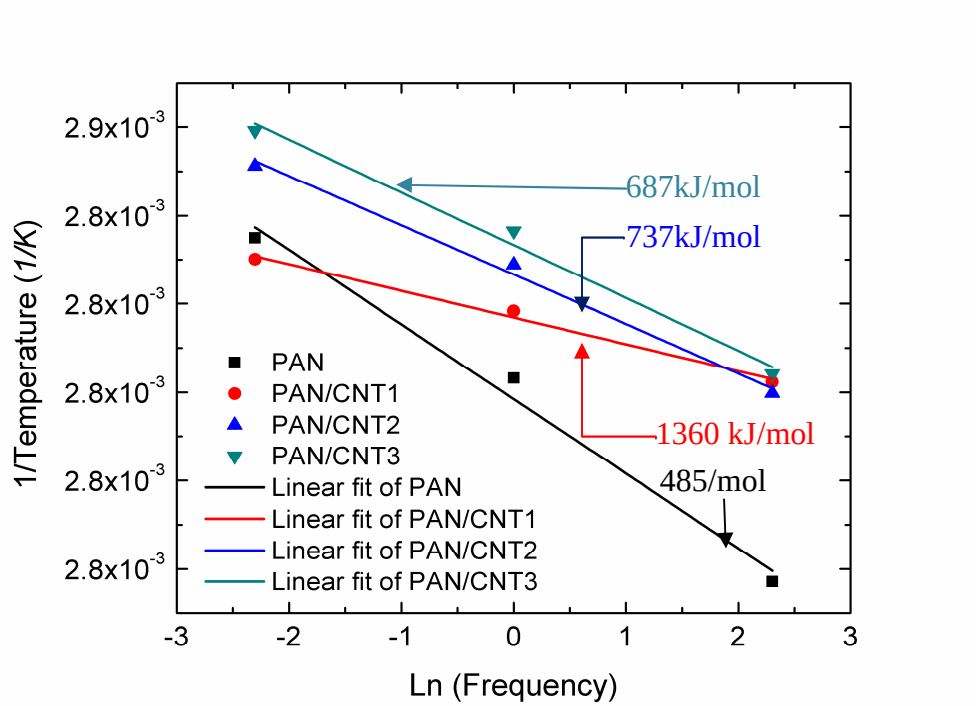

Figure 2.8 Arrhenius plots of PAN and PAN/CNT fibers. Calculated activation energy is given adjacent to each of the linear fits.

Comparing different types of CNTs, addition of CNT1 makes the chain segment hardest to move around. The enhancement in the elastic modulus of PAN/CNT1 (PAN/CNT2) over that in control PAN fibers was calculated and plotted in Figure 2.9.

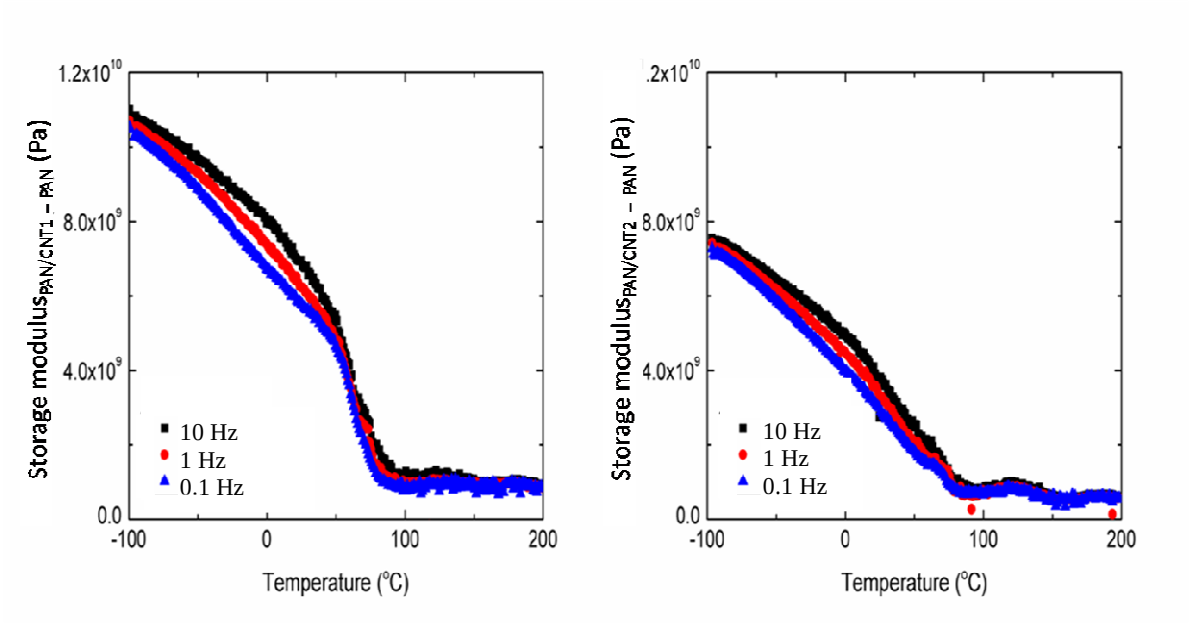

Figure 2.9 Reinforcement of storage modulus by the addition of CNTs as a function of temperature.

It can be observed that CNT1 showed better reinforcement on storage modulus than CNT2. CNT1 has smaller diameter than CNT2; therefore, for the same weight fraction of CNTs, the interfacial area of PAN and CNT1 will be larger than that of PAN and CNT2, leading to better interaction between CNT and PAN matrix. Enhancement of CNTs on storage modulus reduced with increasing temperature and dropped quickly beyond glass transition temperature. Chenyu [4] simulated the reinforcement and adhesion of CNTs in polyethylene and showed a similar trend for the reinforcement of Young's modulus as a function of temperature. An absorbed polymer layer with higher density as compared with bulky polymer was found in the vicinity of CNTs. The density of the absorbed layer decreases with increasing temperature, leading to the decrease of the interfacial van der Waals energy; thus, the reinforcement of the modulus decreases with increasing temperature. When temperature is higher than glass transition

temperature, the system becomes viscous or liquid-like, and the Young's modulus dramatically decreases.

Figure 2.10 shows the difference of storage modulus of fibers consisting different CNTs. Although the CNT1 better reinforces the storage modulus of PAN fibers than the CNT2, the difference in elastic modulus reduces to ~ 0.1 GPa beyond glass transition. When temperature is above T_g, the PAN chain segments gain mobility and the PAN becomes rubbery.

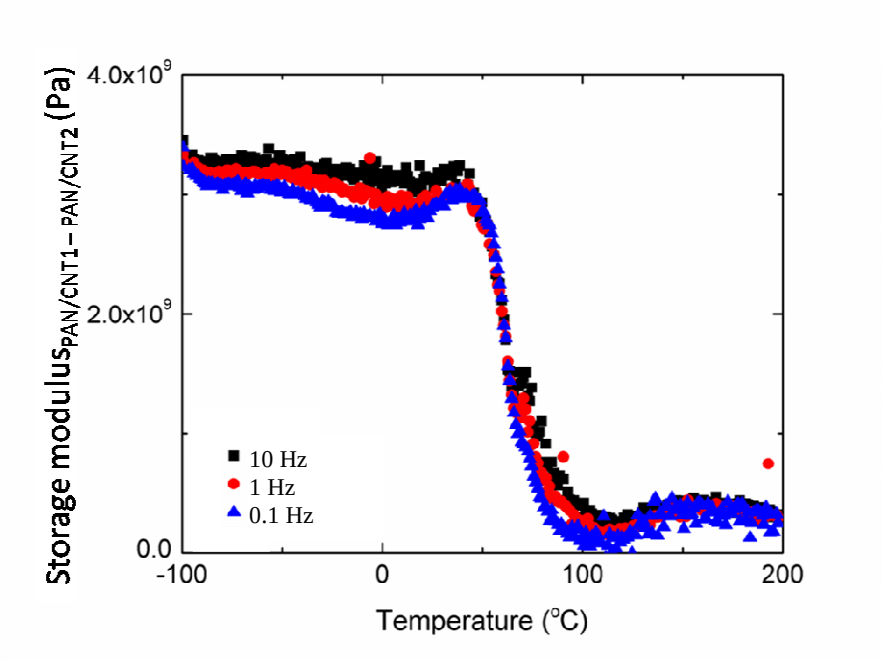

Figure 2.10 Difference between storage modulus by the addition of CNT1 and CNT2.

2.2.1.3 Orientation of PAN and CNTs

For WAXD testing, a fiber bundle containing multi-filaments was aligned perpendicular to the incident X-ray beam; the 2-D diffraction pattern was recorded by a

film detector. Figure 2.11 shows the typical diffraction pattern and integrated curve of PAN precursor fibers.

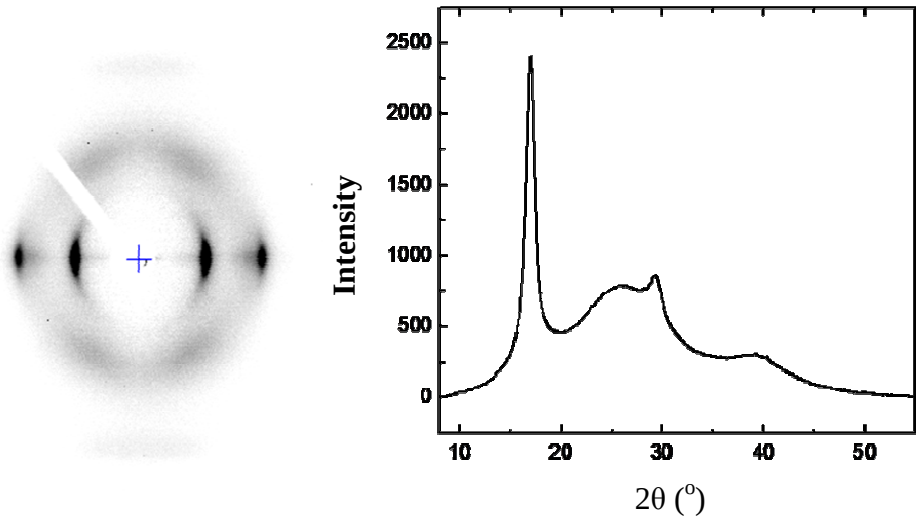

Figure 2.11 2-D XRD pattern and integrated curve of PAN precursor fibers.

The characteristic equatorial diffraction peak at $2\theta=16.9^{o}$ is due to planes (110), (200) in PAN crystal structure. In the diffraction pattern shown in Figure 2.11, PAN (110), (200) planes show the strongest diffraction along the equatorial direction and the weakest diffraction along the meridional direction. The spatial distribution of diffraction is related to the orientation of PAN crystals. The Herman's orientation factor of PAN crystals can be calculated by the following equations from azimuthal curves of (100), (210) diffraction peak shown in Figure 2.12. $\left\langle \cos^2 \chi \right\rangle = \dfrac{\int_{-\pi/2}^{\pi/2} I(\chi)\cos^2(\chi)\sin\chi d\chi}{\int_{-\pi/2}^{\pi/2} I(\chi)\sin\chi d\chi}$,

$f = \frac{3\langle \cos^2 \chi \rangle - 1}{2}$, where, χ is off axis angle, *I* is diffraction intensity, and *f* is Herman's orientation factor.

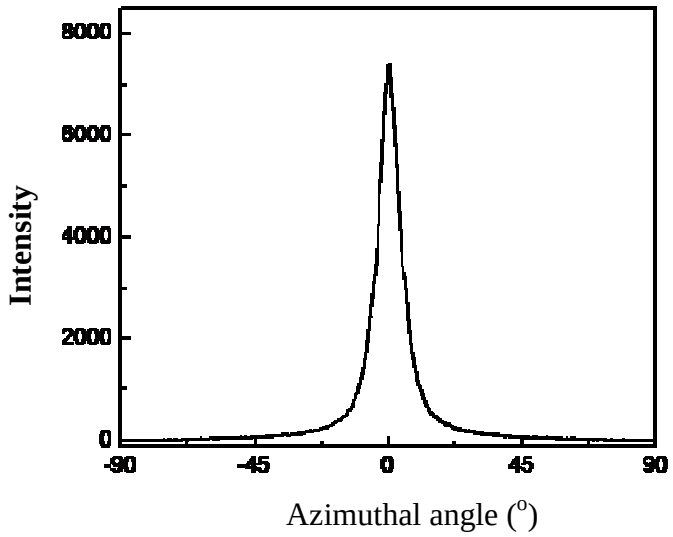

Figure 2.12 Azimuthal scan of (110), (200) diffraction peak of PAN fibers.

The orientation of CNTs was calculated from the graphitic *G* band in the Raman spectra. A series of *G* band intensities at various polar angles were collected. Extreme care was taken to collect spectra at the same sample area. The fitting equation is $I_{Fiber}^{VV}(\phi) \propto \left(\cos^4 \phi - \frac{6}{7}\cos^2 \phi + \frac{3}{35} \right) \langle P_4(\cos\chi) \rangle + \left(\frac{6}{7}\cos^2 \phi - \frac{2}{7} \right) \langle P_2(\cos\chi) \rangle + \frac{1}{5}$, where I is intensity of *G* band, φ is polar angle, and $P_2(\cos\chi)$ is hernman's orientation factor [5]. The fitting curves are shown in Figure 2.13, and the calculated orientation factors of PAN crystal and CNTs are listed in Table 2.3.

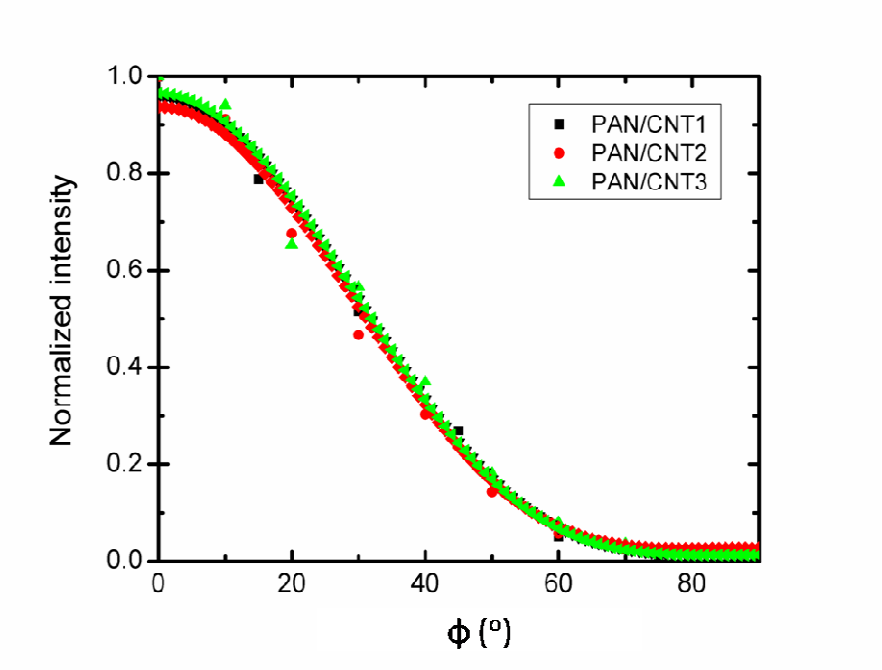

Figure 2.13 Normalized Raman *G* band intensity versus polar angle φ with fitting curves.

Table 2.3 Calculated Herman's orientation factors of precursor fibers.

	PAN	**PAN/CNT1**	**PAN/CNT2**	**PAN/CNT3**
f_{PAN}	0.890	0.896	0.892	0.889
f_{CNTs}	--	0.934	0.901	0.942

2.2.1.4 DMF dissolving test of solvent resistance

A small quantity of fiber samples (~ 2 mg) were put in ~100 ml DMF solvent with the solvent temperature maintained at 100 ^{o}C. PAN fibers are totally dissolved in less than 5 min, whereas, in the case of composite fibers, there were some small fragments left in the bottom even after 30 minutes. This observation indicates that the addition of CNTs significantly improves the solvent resistance of PAN fibers.

2.2.2 Effect of addition of CNTs on stabilization

2.2.2.1 DMF boiling test of stabilized fibers

Stabilized fibers were soaked in boiling DMF for 6 hr to remove under-stabilized or decomposed PAN molecules. Fiber surfaces of the PAN/CNT1 composite fibers and stabilized fibers after DMF boiling test are shown in Figure 2.14. For fibers stabilized at 267 ^{o}C for 1 hr, PAN fibers were totally dissolved in few minutes; whereas, some small fragments were left on the bottom for PAN/CNT1 fibers. The color of solution became yellowish brown. For fibers stabilized for 2 hr after the DMF boiling test (Figure 2.14B), rough surfaces were observed, which are possibly caused by the dissolving of under-stabilized polymer. Fibers stabilized for 4 hr or longer remained mostly after the DMF boiling test, and the fiber surface was relatively smooth (Figure 2.14C). Additionally, the color of the DMF after the boiling test became lighter and lighter with the increase of stabilization time of the PAN and PAN/CNT fibers, which indicated that solvent resistance of the stabilized fibers improved with increasing stabilization time.

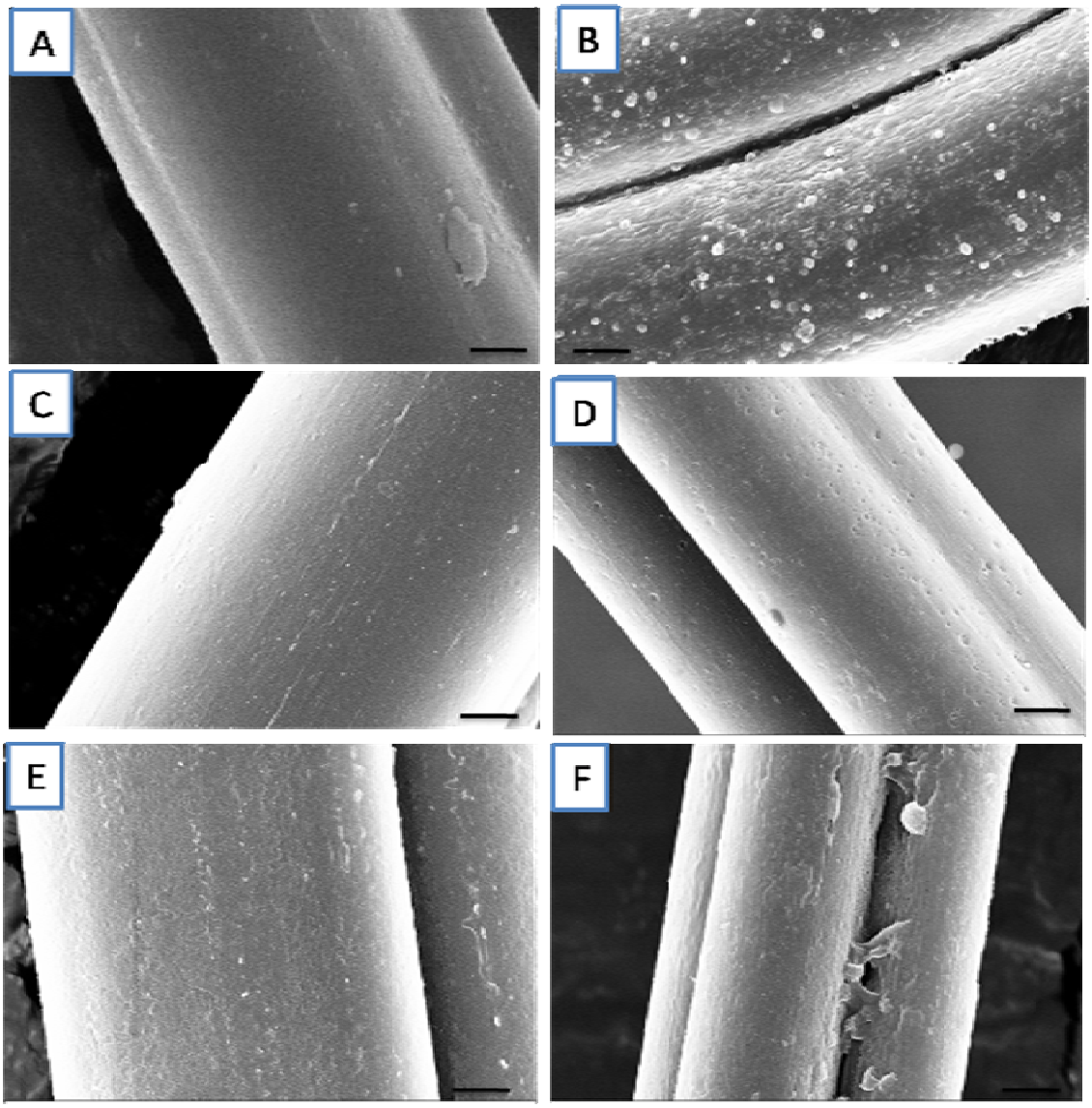

Figure 2.14 SEM images of PAN/CNT1 precursor fiber (A) and stabilized fibers (B-F: stabilized at 267 ^{o}C for 2hr, 4 hr, 6 hr, 8 hr and 10 hr) after DMF boiling test. Scale Bar: 1 µm.

The cross-sections of the stabilized PAN fibers are shown in Figure 2.15. The cross-section was prepared by cutting the fibers with a sharp blade.

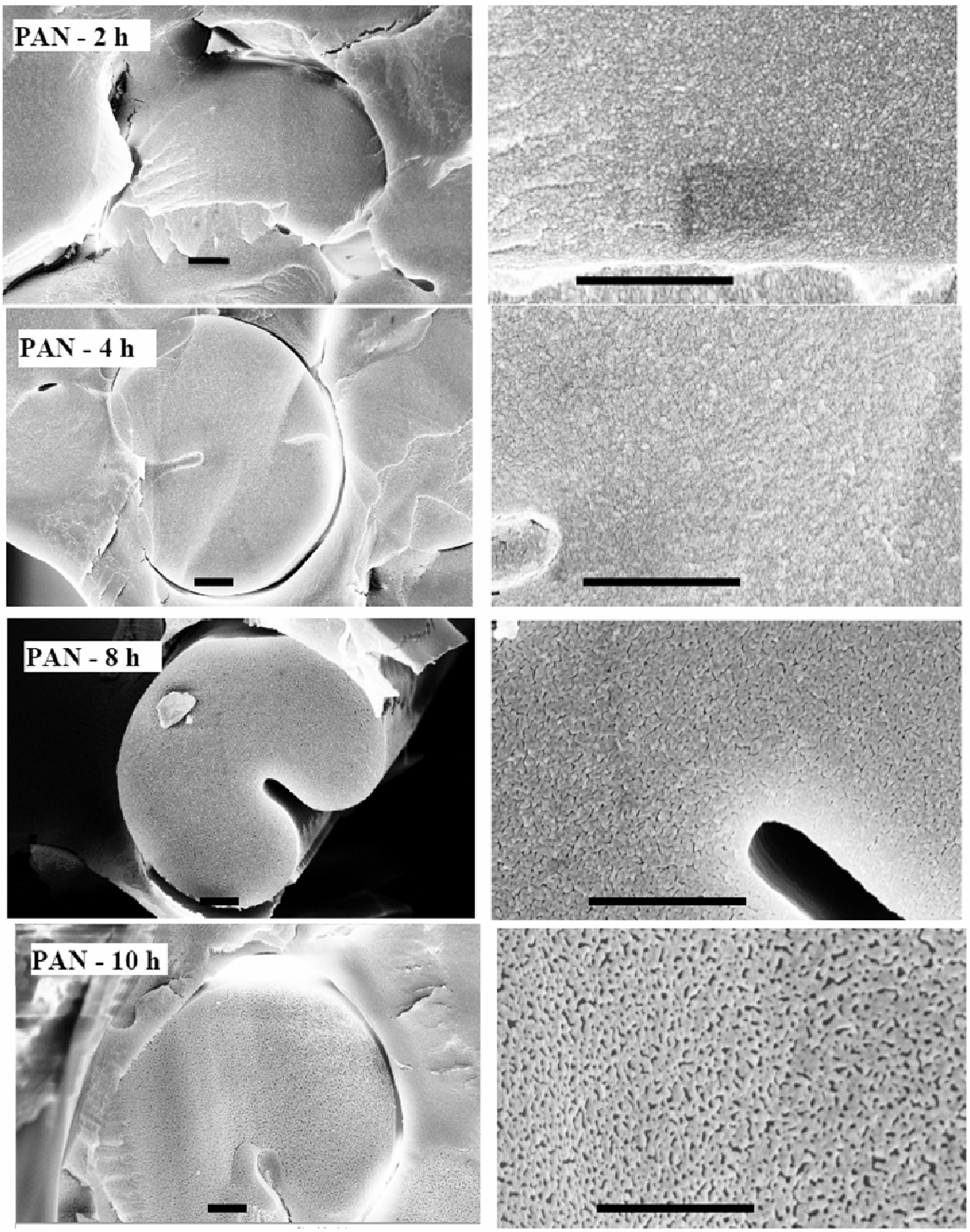

Figure 2.15 SEM images of cross sections of stabilized PAN fibers after boiling in DMF for 6 hr. Matrix surrounding the fibers on the left is the embedding resin. Times indicated in the figures on the left are stabilization time at 267 ^{o}C. All scale bars: 2 μm.

After the DMF boiling test, the cross-section for PAN fibers stabilization at 267 ^{o}C for 2 hr shows even features. After stabilization for 6 hr, tiny pores with diameters in the range of tens of nanometers appeared in the fiber cross-section, and their dimension increased with increasing stabilization time, which indicates over-stabilization, this reopens the cyclized PAN structure and causes decomposition. The over-stabilized polymer could be removed in boiling DMF. The method of observing the cross-sections of stabilized fibers after dipping them in boiling DMF may be used to roughly judge the optimum stabilization time. For PAN fibers, 10 hr at 267 ^{o}C appears to be too long and causes over-stabilization.

Cross-sections of PAN/CNT1 composite fibers after DMF boiling test are shown in Figure 2.16. For PAN/CNT1composite fibers, except for tiny pores caused by pulling out of CNT bundles, no more pores caused are found on the cross-sections for fiber over-stabilized, which may be attributed to the benefit of the addition of CNTs.

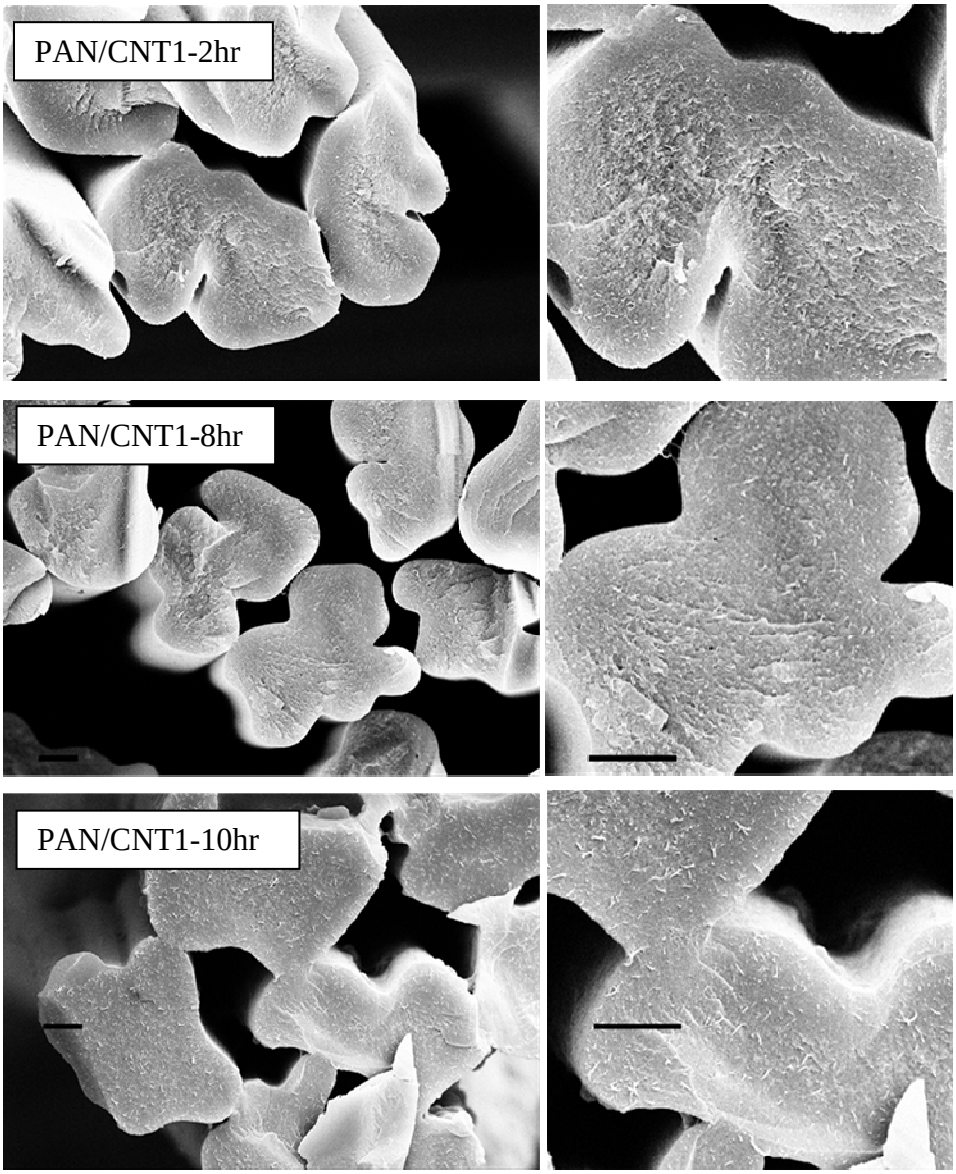

Figure 2.16 SEM images of cross sections of stabilized PAN/CNT1 fibers after boiling in DMF for 6 hr. Times indicated in the figures on the left are stabilization time at 267 ^{o}C. All scale bars: 2 μm.

2.2.2.2 Chemical structure of stabilized fibers

The chemical structure of stabilized fibers was characterized using FTIR. IR spectra of control PAN and PAN/CNT1 fibers stabilized at 267 ^{o}C for various times are shown in Figure 2.17. In the FTIR spectra of precursor fibers, the peak at 1673 cm^{-1} is assigned to C=O which is due to residual DMF, the 2242 cm^{-1} band belongs to C≡N

groups, and the 2938 cm^{-1} and 1456 cm^{-1} bands are assigned to CH_2 [6]. During stabilization, the peak at ~ 1600 and ~ 1620 cm^{-1} is caused by the formation of C=C and C=N. A shoulder at ~ 1740 cm^{-1} is assigned to the carbonyl group formation due to oxidation. The peak intensity at ~ 801 cm^{-1} which belongs to C=C-H increases during stabilization. For fibers stabilized at 267 ^oC for 6 hr, the C-H_2 peak at 2938 cm^{-1} becomes very weak, and the C≡N peak position shifts to a lower wave-number.

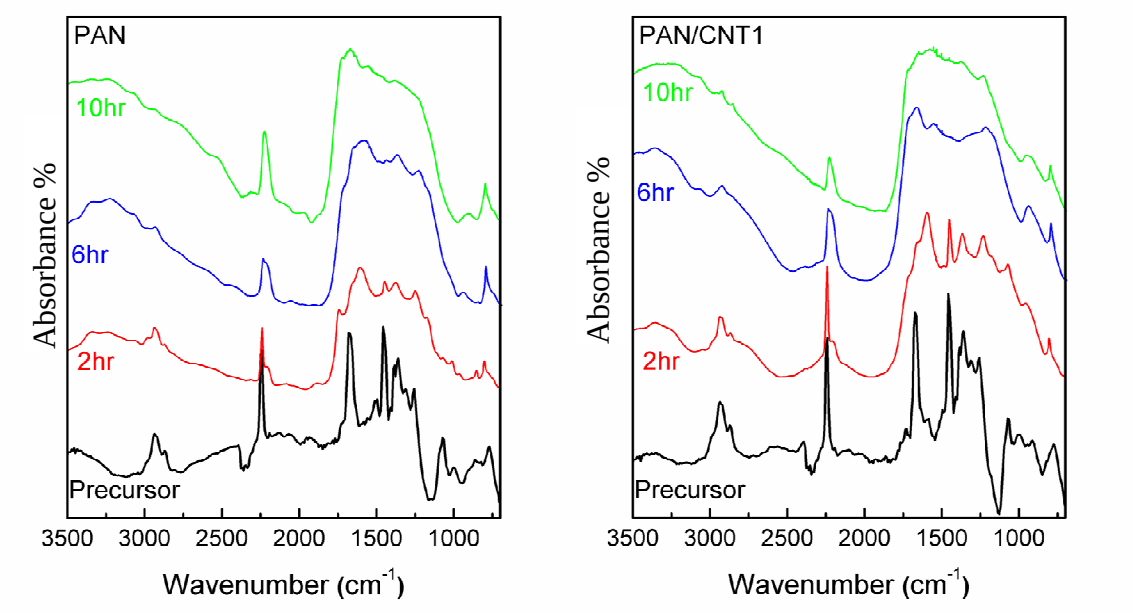

Figure 2.17 FT-IR spectra of control PAN and PAN/CNT1 (99/1) precursor and stabilized fibers. Stabilization carried out at 267 ^oC under a tension of 20 MPa.

The peaks in the range of 2180 ~ 2260 cm^{-1} are assigned to three kinds of nitrile groups (Figure 2.18): the un-reacted nitrile group at ~ 2242 cm^{-1}, conjugated nitrile at ~ 2220 cm^{-1}, and β-amino nitrile at ~ 2194 cm^{-1} [7-14]. Mole fractions of different groups can be calculated by the peak fitting method. Figure 2.19 shows the examples of nitrile band curve fitting. Peak positions were fixed at 2194 $cm^{-1}$for β-amino nitrile, 2242 for

un-reacted nitrile, and 2220 for conjugated nitrile, respectively, while peak width and intensity were adjusted to get the best fit.

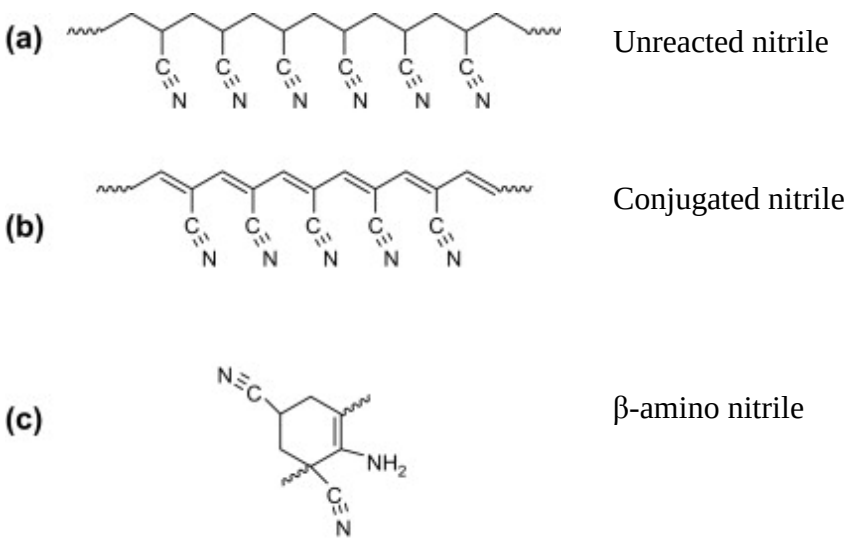

Figure 2.18 Chemical structures of nitrile groups of stabilized fibers. [7]

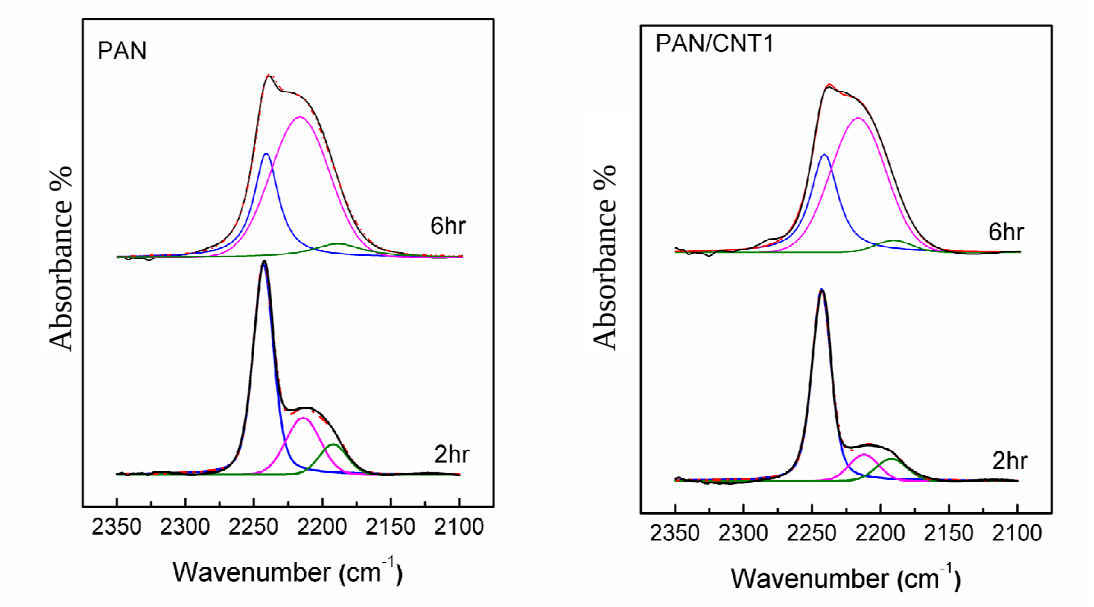

Figure 2.19 Nitrile band peak fitting of IR spectra of PAN and PAN/CNT1 fibers. Stabilization was carried out at 267 ^{o}C under a tension of 20 MPa.

From the results of nitrile band peak fitting, approximate mole percentages of conjugated nitrile (ϕ_c) and β-amino (ϕ_a) nitrile were calculated by equations, $\phi_c = \frac{Area_{2220}}{Area_{2242} + Area_{2220} + Area_{2194}} \cdot 100\%$ and $\phi_a = \frac{Area_{2194}}{Area_{2242} + Area_{2220} + Area_{2194}} \cdot 100\%$, and the results are listed in Table 2.4.; where, Area is the area of the corresponding fitted nitrile peak.

Table 2.4 Fraction of conjugated nitrile and β-amino nitrile in PAN and PAN/CNT composite fibers stabilized under a tension of 20 MPa at 267 ^{o}C for various times.

Time (hr)	PAN			PAN/CNT1			PAN/CNT2			PAN/CNT3		
	ϕ_c (%)	ϕ_a (%)	$\frac{\phi_c}{\phi_a}$	ϕ_c (%)	ϕ_a (%)	$\frac{\phi_c}{\phi_a}$	ϕ_c (%)	ϕ_a (%)	$\frac{\phi_c}{\phi_a}$	ϕ_c (%)	ϕ_a (%)	$\frac{\phi_c}{\phi_a}$
1	17	6	2.9	19	5	3.8	21	6	3.5	15	4	3.7
2	39	8	4.9	36	6	6.0	46	8	5.8	30	5	6.0
4	57	10	5.7	62	8	7.7	68	9	7.4	63	9	7.0
6	66	10	6.6	66	8	8.2	72	9	8.0	71	9	7.9
8	74	11	6.8	70	8	8.8	73	10	7.3	70	10	7.0
10	72	12	6.0	71	10	7.1	71	10	7.1	71	12	5.9

Note: φ_c: Mole fraction of conjugated nitrile. φ_a*:* Mole fraction of β-amino nitrile. Fractions are calculated from nitrile peak fitting curves as shown in Figure 2.20.

Previous study [7] has shown that the addition of CNTs lowers the fraction of formed β-amino nitrile in the stabilized fiber. The present experiments also show similar behavior. Among different types of CNTs, the smallest diameter tube, CNT1, which has the highest surface area, reduces the formation of β-amino nitrile more than other kind of CNTs. The β-amino nitrile is formed by the termination of the cyclization reaction [14]. Less β-amino nitrile means less possibility of chain scission in stabilized fibers, and therefore improved properties of carbon fibers. The ratio of ϕ_c / ϕ_a is proportional to the average unit number of conjugated nitrile segments. From Table 2.5, it is found that the

ratio first increases with increase in stabilization time and then decreased after a prolonged stabilization time. The highest mole ratio of ϕ_c / ϕ_a for the stabilized PAN is 6.8, which is lower than the corresponding values for PAN/CNT composite fibers, which are 8.8, 8.0, and 7.9 for PAN/CNT1, PAN/CNT2, and PAN/CNT3 composite fibers, respectively. The higher ratio means longer conjugated nitrile segment. The time that the ϕ_c / ϕ_a ratio reaches the maximum value is the optimum stabilization time. The fibers stabilized for optimum time will have the optimum chemical structure. Beyond a certain stabilization time, the ratio decreases due to over-stabilization.

2.2.2.3 Orientation and crystalline structure

WAXD patterns and integrated scans of stabilized PAN/CNT1 composite fibers are shown in Figure 2.20. The diffraction peaks at $2\theta=16.7^o$ and 29.3^o correspond to the (200), (110) and (310), (020) planes of PAN crystals, respectively. The intensity of these peaks decreases with increasing stabilization time. The diminishing of the PAN (200), (110) peak can also be used to determine the degree of stabilization [15]. The increase of peak intensity at $2\theta \sim 25.7^o$ can be attributed to the formation of the ladder polymer. Azimuthal scans at $2\theta \sim 25.7^o$ for precursor and stabilized PAN and PAN/CNT1 fibers are shown in Figure 2.21.

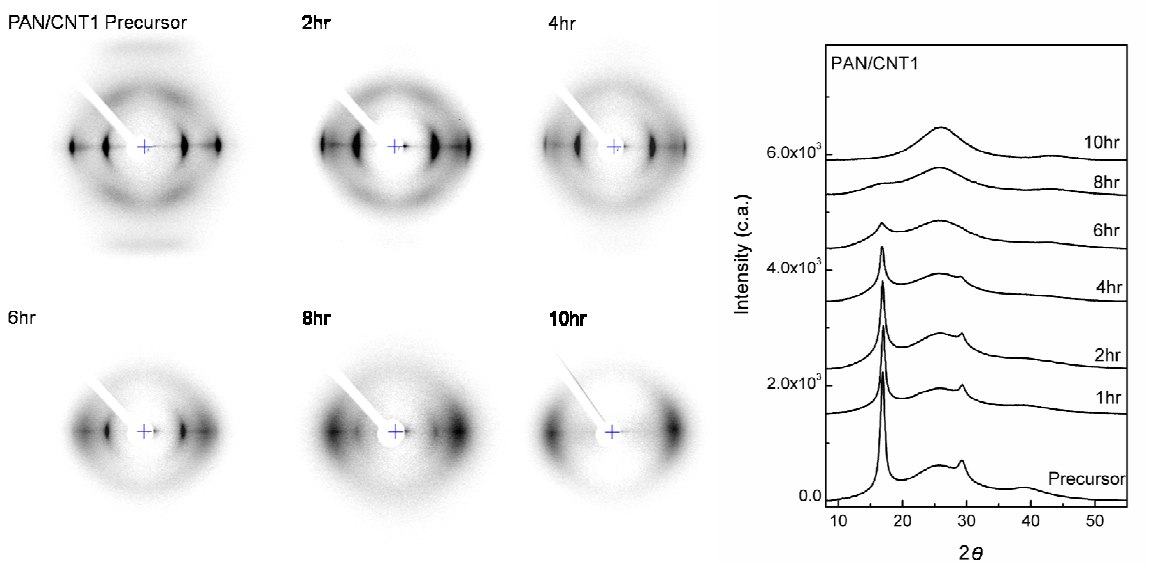

Figure 2.20 2D X-ray diffraction patterns and integrated scans of PAN/CNT1 composite fibers stabilized at 267 °C for various times under a tension of 20 MPa.

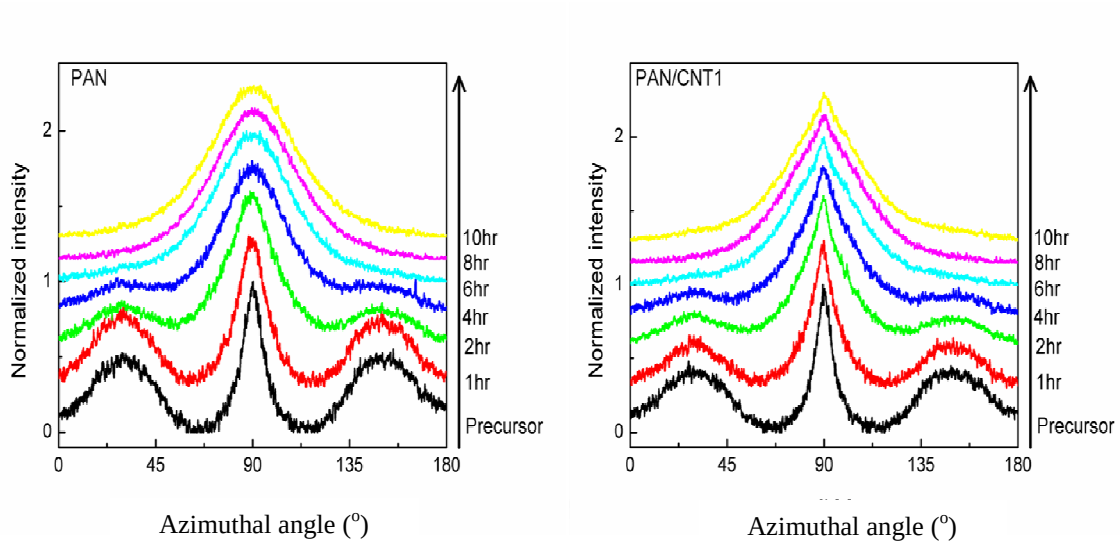

Figure 2.21 - Azimuthal scans of PAN (A) and PAN/CNT1 composite fibers (B) at 2θ=25.7°. Fibers were stabilized at 267 °C for various times under a tension of 20 MPa.

Herman's orientation factors of ladder polymer calculated from azimuthal scans, also the crystal sizes and orientation factors of the stabilized fibers calculated from WAXD data are listed in Table 2.5.

Table 2.5 Crystal size and Herman's orientation factors of PAN and PAN/CNT composite fibers stabilized under a tension of 20 MPa at different temperatures.

Stabilization time (hr)	Control PAN				PAN/CNT1			
	234 °C	at 267 °C			234 °C	267 °C		
	XS* (nm)	XS (nm)	f_{PAN}	$f_{ladder-polymer}$	XS (nm)	XS (nm)	f_{PAN}	$f_{ladder-polymer}$
0	9.2	9.2	0.89	--	11.4	11.4	0.90	--
1	15.0	17.5	0.88	--	15.5	14.7	0.87	--
2	14.8	13.2	0.84	0.46	16.9	13.7	0.84	0.48
4	16.8	11.5	0.80	0.51	15.7	13.6	0.81	0.56
6	14.9	4.0	0.67	0.61	14.6	5.7	0.74	0.64
8	--	1.2	0.53	0.64	--	1.9	0.57	0.67
10	--	--	--	0.62	--	--	--	0.63
	PAN/CNT2				PAN/CNT3			
0	9.3	9.3	0.89	--	9.1	9.1	0.89	--
1	14.5	13.6	0.85	--	14.8	17.4	0.88	--
2	14.9	10.8	0.83	0.51	15.4	11.7	0.85	0.50
4	15.3	4.25	0.65	0.62	14.7	6.1	0.65	0.62
6	12.1	1.6	0.54	0.66	13.2	2.9	0.63	0.66
8	--	1.3	--	0.65	--	1.7	--	0.65
10	--	--	--	0.64	--	--	--	0.65

Note: * XS: PAN crystallite size, calculated by the width of (200), (110) peak using Scherrer equation. *f*: Herman's orientation factor; for PAN crystal, it is calculated from Azimuthal scan of PAN (200), (110) planes; for ladder polymer in stabilized fibers, it is calculated from Azimuthal scan at $2\theta=25.7^{o}$.

PAN and PAN/CNT1 fibers were heated from room temperature to 200 °C at a heating rate of 5 °C/min, then quickly quenched to room temperature. Fiber length was held constant during thermal treatment. The crystal size, crystallinity, and orientation before and after heat treatment are listed in Table 2.6. It becomes clear that after heat treatment the crystallinity slightly decreases. The crystal size increases to as high as 140 % after treatment. The peak of the PAN (200), (110) planes slightly shifts to a lower 2θ value, and the ratio of the two distinct PAN diffraction peaks comes closer to the theoretical value (1.732), indicating that more perfect hexagonal packing forms after heat treatment. Crystallinity did not increase, in fact, it slightly decreased, while crystal size

significantly increased; this may be caused by the merging of adjacent crystallized domains to form more perfect and larger crystals.

Table 2.6 XRD data of PAN and PAN/CNT1 fibers after thermal treatment.

Treatment	Sample	Crystallinity (%)	L_c (*nm*)	f_{PAN}	$2\theta_{(110,200)}$	Ratio
Before	PAN	53	9.2	0.89	16.98	1.718
	PAN/CNT1	57	11.4	0.89	16.87	1.725
After	PAN	49	13.6	0.88	16.94	1.727
	PAN/CNT1	50	14.7	0.87	16.78	1.733

Note: L_c: PAN crystal size; f_{PAN}: Herman's orientation factor; ratio= $d_{(110)}/ d_{(310)}$.

In the very early stage of stabilization, PAN crystal size increased as high as 150 % of the crystal size. Similar phenomenon was reported by Yu et al. [16]. Orientation of stabilized ladder polymer initially increased with increasing stabilization time, reached a maximum value, and then decreased: the decrease maybe due to over-stabilization. The transition point indicates that fibers are optimally stabilized.

The temperature strongly affected the reaction rate in stabilization as can be seen from the decrease in crystal size. When fibers were stabilized at 234 ^{o}C, PAN crystal size began to decrease only after 4 hr of stabilization; whereas stabilized at 267 ^{o}C, crystal size began to decrease after 1 hr and finally totally disappears after 8 to 10 hr of stabilization. For PAN/CNT1 fiber, the IR data in Table 2.4 indicates that over 60 % nitrile groups (from amorphous and crystalline regions) reacted after fibers were stabilized at 267 ^{o}C for 4 hr. In comparison, Table 2.5 shows that PAN crystal size only slightly decreases from 14.7 nm after 1 hr to 13.6 nm after 4 hr stabilization at 267 ^{o}C. These results indicate that cyclization reactions mainly occur in amorphous regions in the early stabilization stage. When stabilized over 4 hr, PAN crystal size decreases rapidly,

which suggests that the stabilization reaction in crystal regions has a time lag compared to the reactions in the amorphous regions. It is believed that stabilization is initiated in the amorphous regions and then diffuses into crystals [17, 18]. Devasia et al. [8] also found a slowing of the reaction rate in the late stabilization stage by studying the absorbance of the nitrile band in IR spectra. When cyclized structure is formed in stabilization, the helical chain of PAN needs to be unwound to form a planar structure. PAN molecular conformation can be more easily changed in the amorphous regions than in the crystalline regions. Also, stabilization involves complex reactions, including cyclization, oxidation, dehydration, and cross-linking. Oxygen is an important reactant in the stabilization reactions. It participates in the oxidation reaction, leads to further dehydration, and may also initiate cyclization [19]. Oxygen diffuses more easily in the amorphous regions than in the crystalline regions. Thus, it is reasonable to state that the stabilization in amorphous regions will be much faster than that in the crystalline regions. Comparing the ratio of ϕ_c / ϕ_a in Table 2.4 and Herman's orientation factor in Table 2.5, they show the same transition time. The ratio of ϕ_c / ϕ_a increases with increase of stabilization time, then decreases due to over-stabilization. Since stabilization reactions are initiated from amorphous regions and then diffuse into the crystalline regions, these results indicate that stabilized polymer in crystallized regions has a higher ϕ_c / ϕ_a ratio than that in the amorphous regions. The positions of the PAN (200), (110) peak and the meridional peak are shown in Figure 2.22. The peak position of PAN (200), (110) planes in equatorial scan shifts to a lower 2θ value, suggesting that PAN crystals begin to lose order during stabilization. The meridional peak shifts from ~ 39^o to ~ 43.3^o after stabilization.

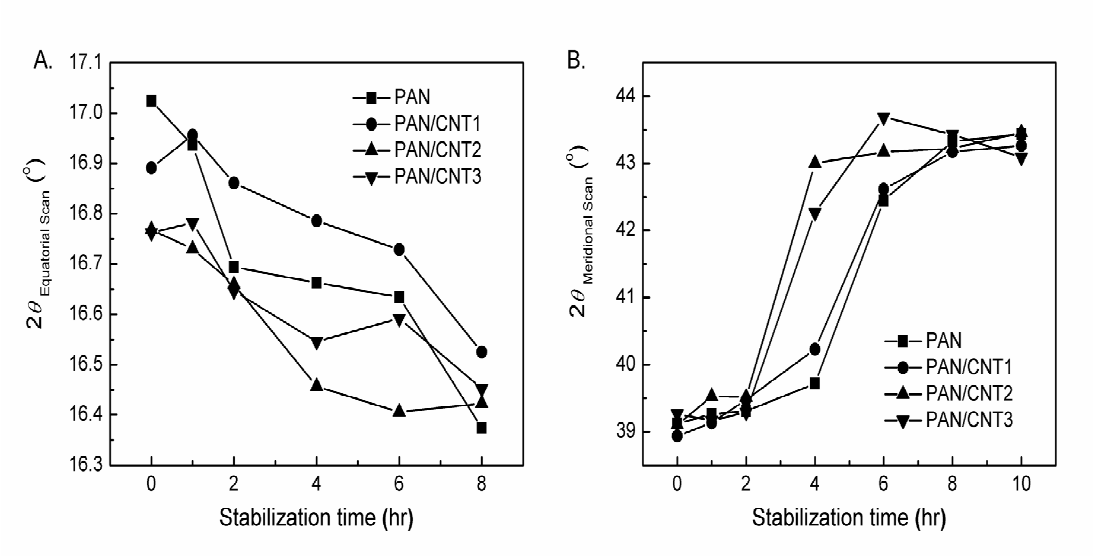

Figure 2.22 Changes in XRD Peak positions of PAN and PAN/CNT composite fibers after stabilization at 267 ^{o}C under a stress of 20 MPa. A. PAN (200), (110) peak in equatorial scan; B. meridional scan peak.

2.2.2.4 Shrinkage behavior

The shrinkage behavior of the stabilized fibers was monitored by TMA (Figure 2.23). The temperature profile and applied tension were set to be exactly the same as in the stabilization experiments conducted in the box furnace. The occurrence of entropic shrinkage and chemical shrinkage is mentioned in chapter 1. Under high tension, a drawing stage can be found between these shrinkages. However, due to the complexity of the stabilization reaction, these different kinds of shrinkages may overlap and cannot be completely separated. Here, the derivative of shrinkage is used to divide these three types of shrinkages.

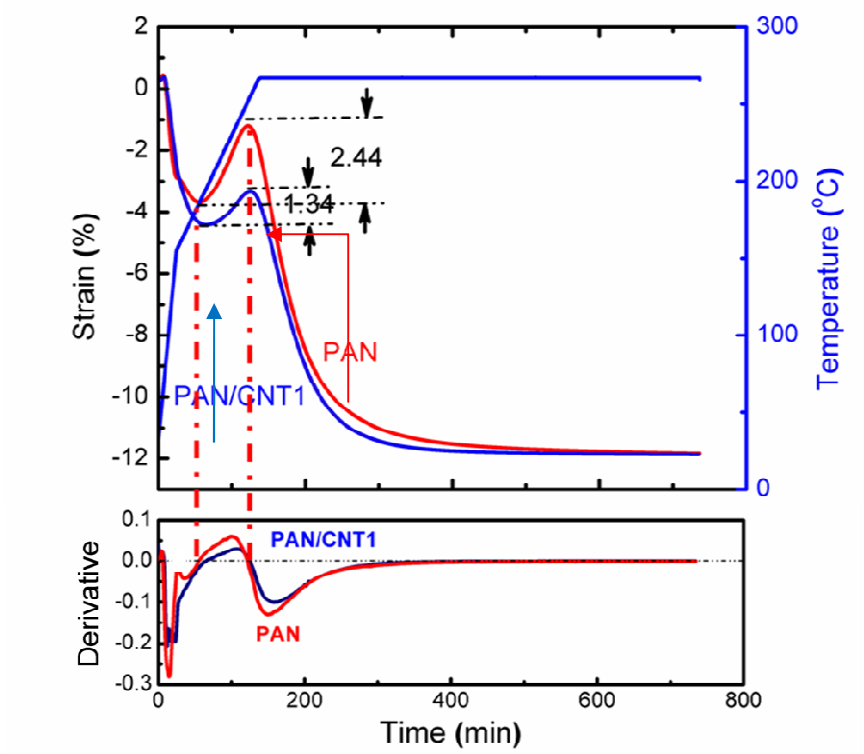

Figure 2.23 Length change and its derivative for PAN and PAN/CNT1 composite fibers during stabilization under a tension of 20MPa in air. Stabilization temperature followed the temperature profile shown in Figure 2.5, and fiber length changes were monitored by TMA. Negative value means shrinkage, and positive value means elongation.

Although the final shrinkages of the PAN and PAN/CNT1 fibers were comparable, the control PAN fiber was drawn more, 2.44 %, than the PAN/CNT1 fiber, 1.34 %. The entropic shrinkage of the composite fibers is larger than that of the control fibers, because the PAN fibers are more stretchable than the composite fibers. This suggests that the CNT reinforced fiber has higher modulus even above T_g as expected [3] and is harder to be stretched. Under a low tension at 4 MPa (Figure 2.24), no drawing occurred, and PAN fibers had a larger entropic shrinkage than the PAN/CNT1 composite fiber.

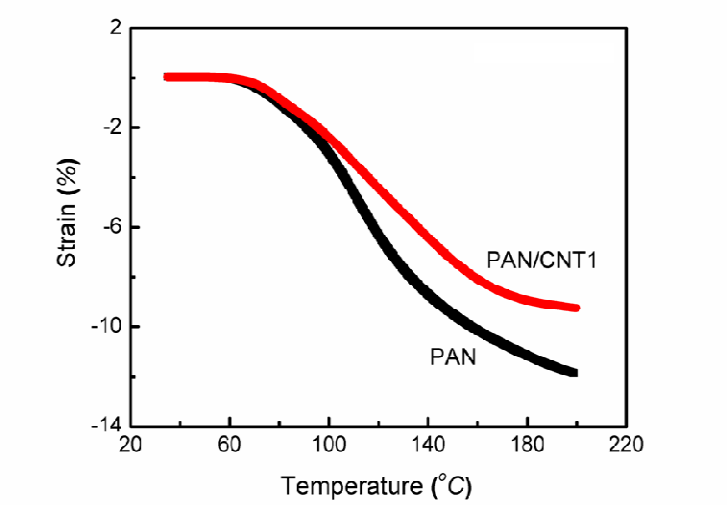

Figure 2.24 Entropic shrinkage curves of PAN and PAN/CNT1 fibers at a tension of 4 MPa in air. Heating rate is 5 ^{o}C/min.

Under a tension of 20 MPa, fibers were stabilized in air at various temperatures; the shrinkage curves are shown in Figure 2.25. Higher temperature reduces the chemical shrinkage for both PAN and PAN/CNT1 composite fibers. Kim et al. [21] and Bahl et al. [22] have reported similar results for homo-polymer and copolymer PAN fibers. During cyclization, PAN molecules are converted into denser ladder polymer, along with the increase in density and shrinkage of length. When the stabilization temperature is increased, the cyclization reaction becomes much faster; the low diffusion rate of oxygen will limit further oxidation, dehydration, and cross-linking reactions, leading to the decrease of chemical shrinkage.

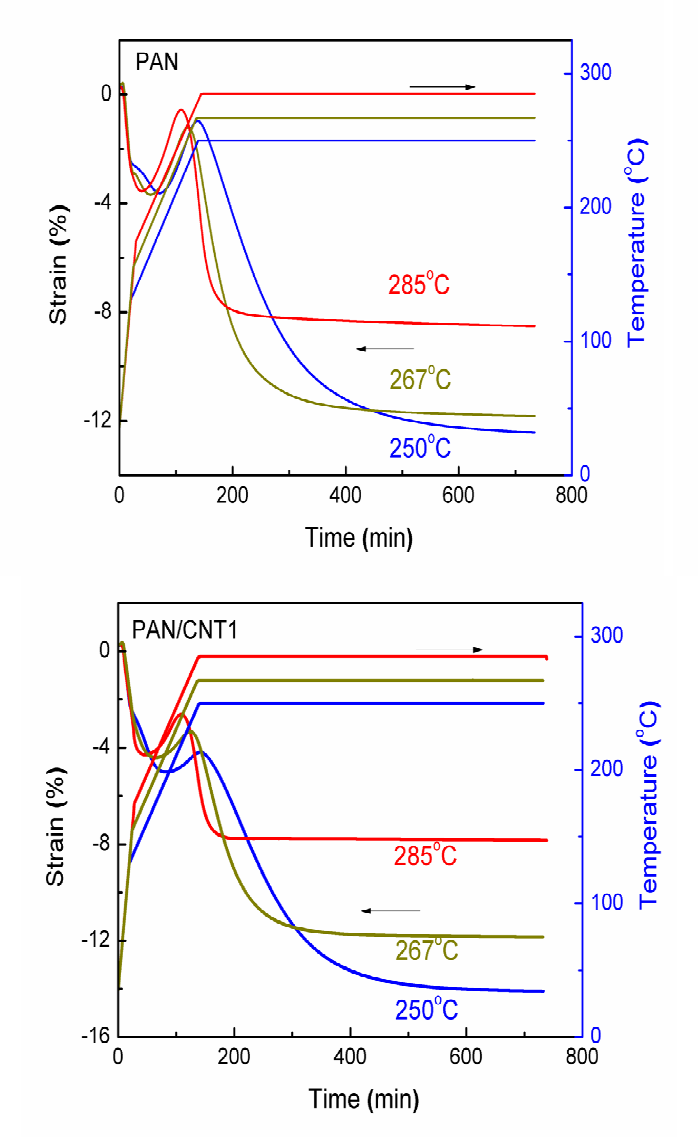

Figure 2.25 Shrinkage curves of PAN and PAN/CNT1 fibers stabilized at various temperatures under a tension of 20 MPa in air.

2.2.2.5 Tensile properties

Table 2.7 shows the tensile properties of the stabilized fibers. In PAN/CNT fibers, the elongation at break increased at low stabilization times. For fully stabilized fibers, the elongation at break shows significant decrease compared to that of the precursor fibers. After stabilization at 267 ^{o}C for 10 hr, the specific strength of all fibers decreased

significantly to about 0.2 N/tex, as compared to the tensile strength of precursor fiber, which is ~ 0.8 N/tex. The specific modulus of fully stabilized fibers shows obvious improvement with the addition of CNTs. The reinforcement efficiencies of modulus for CNT1, CNT2, and CNT3 were 309 N/tex, 279 N/tex, and 239 N/tex, respectively, which is higher than their reinforce efficiencies in the precursor fibers. Similar to the results in precursor fibers, CNT1, which had the highest surface area to mass ratio, shows the best reinforcement efficiency in the stabilized fibers.

Table 2.7 Tensile properties of PAN and PAN/CNT composite fibers stabilized under a tension of 20 MPa at 267 ^{o}C for various duration times.

Stabilization time (hr)	Control PAN			PAN/CNT1 (99/1)		
	S* (N/tex)	M** (N/tex)	ε_b***	S (N/tex)	M (N/tex)	ε_b
0	0.73±0.11	15.0±1.5	9.5±1.0	0.92±0.07	17.5±2.7	8.6±0.6
1	0.44±0.09	13.5±1.7	9.1±2.0	0.44±0.06	15.2±1.6	7.7±1.0
2	0.38±0.05	12.3±1.4	9.2±1.4	0.40±0.04	15.1±1.9	10.0±1.0
4	0.19±0.03	8.6±1.1	6.4±1.9	0.35±0.05	12.9±1.9	9.3±0.7
6	0.22±0.03	9.0±1.0	8.1±2.3	0.22±0.04	11.4±1.9	6.1±1.8
8	0.19±0.02	8.7±0.9	6.1±1.2	0.19±0.02	11.7±2.1	4.4±0.9
10	0.18±0.01	8.4±0.8	6.4±1.6	0.18±0.02	11.5±2.4	3.2±1.4
	PAN/CNT2 (99/1)			PAN/CNT3 (99/1)		
0	0.75±0.04	16.9±2.9	7.7±0.3	0.81±0.06	16.9±2.3	8.3±0.6
1	0.48±0.09	14.9±1.8	8.3±1.0	0.54±0.10	15.5±1.8	8.7±0.8
2	0.42±0.06	14.3±2.1	9.8±1.3	0.43±0.10	14.0±2.6	9.0±1.3
4	0.29±0.05	11.2±2.3	9.0±1.2	0.34±0.07	11.4±2.8	9.8±1.3
6	0.25±0.04	11.4±2.8	6.0±1.2	0.26±0.04	11.0±1.4	8.0±1.2
8	0.22±0.03	11.2±1.9	4.6±0.9	0.24±0.05	10.8±2.4	6.9±1.2
10	0.21±0.03	10.8±3.0	4.3±1.0	0.20±0.03	10.3±2.2	5.7±1.0

Note: * Specific strength, ** specific Young's modulus, and *** elongation at break. tex: mass of 1000 meters length of fiber in grams.

Detecting the end of stabilization is very important for the production of high quality carbon fibers, since both under-stabilization and over-stabilization lead to low mechanical property carbon fibers. For the fibers stabilized at 267 ^{o}C, WAXD and IR

show the same optimum time for stabilization. The optimum stabilization time at 267 ^{o}C for PAN, PAN/CNT1, PAN/CNT2, and PAN/CNT3 in this study is around 6–8 hr. However, this can be only verified upon further carbonization. Correlation between stabilized structure and the properties of the resulting carbon fibers needs to be studied to obtain the optimally stabilized PAN or PAN/CNT fibers.

2.2.3 Effect of applied tension on stabilized fibers

In this section, the stabilization time at 267 ^{o}C was fixed at 8 hr and the effect of applied stress on stabilized fibers is discussed. Applied tension values during the stabilization process were 2.1 MPa, 10 MPa, 15 MPa, and 22 MPa. The tensile properties of stabilized fibers are listed in Table 2.8. Higher tension applied during stabilization improves tensile properties of stabilized fibers. When applied tension is increased from 15 MPa to 22 MPa, the elongation at break of the stabilized PAN fibers increases from 5.0 % to 8.2 %. Under the same tension, CNT reinforced PAN fibers show better tensile strength and modulus than PAN fibers. Table 2.9 shows that higher applied tension will reduce the formation of β-amino nitrile in stabilized fibers.

Table 2.8 Tensile properties of stabilized PAN and PAN/CNT1 fibers.

Applied tension (MPa)	PAN			PAN/CNT1		
	S (N/tex)	M (N/tex)	ε_b (%)	S (N/tex)	M (N/tex)	ε_b (%)
2.1	0.14±0.02	5.0±1.1	6.0±2.2	0.17±0.01	7.6±0.8	6.6±1.6
10	0.15±0.01	6.4±1.6	5.8±1.4	0.16±0.02	9.0±0.8	4.7±1.2
15	0.15±0.02	7.2±1.2	5.0±1.4	0.17±0.03	9.9±1.5	5.0±0.9
22	0.20±0.03	8.6±1.2	8.2±1.5	0.21±0.02	10.5±1.4	7.5±1.4

Note: S: specific strength; M: specific Young's modulus; ε_b: elongation at break.

Table 2.9 Nitrile band fitting data of PAN and PAN/CNT1 fibers stabilized at 267 ^{o}C for 8 hr under various tensions.

Applied tension (MPa)	PAN			PAN/CNT1		
	ϕ_c (%)	ϕ_a (%)	$\frac{\phi_c}{\phi_a}$	ϕ_c (%)	ϕ_a (%)	$\frac{\phi_c}{\phi_a}$
2.1	18	60	3.3	12	67	5.4
10	14	70	5.0	12	68	5.6
15	13	66	5.1	10	67	6.5
22	10	74	7.3	8	71	9.0

Note: ϕ_c: Mole fraction of conjugated nitrile. ϕ_a: Mole fraction of β-amino nitrile. Ratio=Mole fraction of conjugated nitrile (ϕ_c) over β-amino (ϕ_a) nitrile.

Figure 2.26 shows the azimuthal scans of stabilized PAN and PAN/CNT1 fibers under a tension of 22 MPa. Stabilized composite fibers show a much sharper peak than the stabilized PAN fibers, which is attributed to the formation of highly oriented stabilized PAN structure in the vicinity of CNTs [20]. The azimuthal scans of stabilized PAN/CNT1 fibers were deconvoluted using the two peaks fitting method [20] to obtain the molecular orientation of highly ordered regions. Herman's orientation factors of separated phases are calculated and are listed in Table 2.10. Higher tension applied during stabilization improved the orientation of the ladder polymers. In composite fibers, the highly oriented phase has an orientation factor over 0.9. Also, the addition of CNTs improves the orientation of the surrounding matrix in comparison with the stabilized PAN fibers.

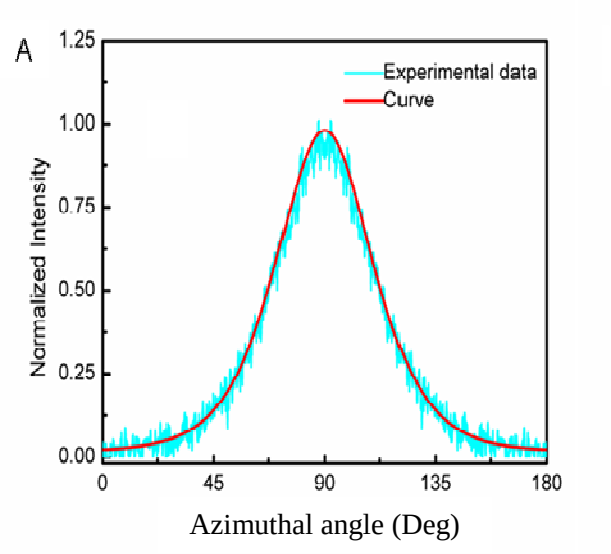

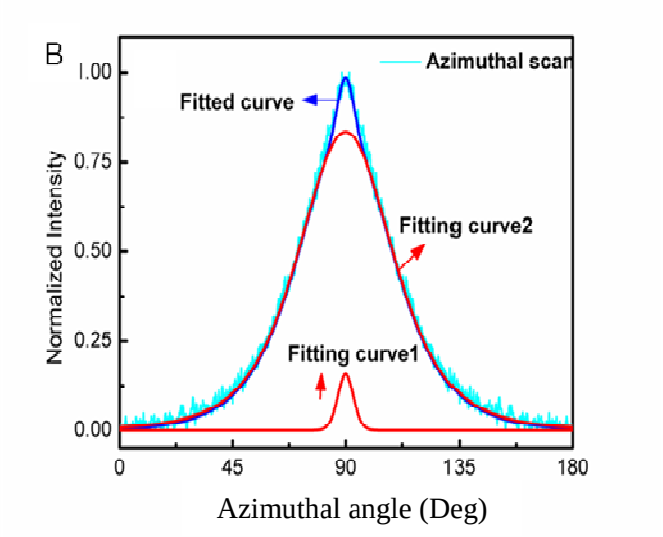

Figure 2.26 Azimuthal scans of ladder polymer at 2θ=25.7^{o} for fibers stabilized at 267 ^{o}C for 8 hr under a stress of 22 MPa. A: Stabilized PAN fibers; B: Stabilized PAN/CNT1 composite fiber. Azimuthal scan of stabilized composite fibers was deconvoluted into a highly ordered region (Fitting curve 1) and surrounding matrix (Fitting curve 2).

Table 2.10 Herman's orientation factors of stabilized PAN and PAN/CNT1 fibers.

Applied Stress (MPa)	PAN	PAN/CNT1		
		Overall curve	Curve 1	Curve 2
2.1	0.54	0.60	0.97	0.59
10	0.58	0.61	0.96	0.61
15	0.61	0.62	0.91	0.62
22	0.63	0.66	0.99	0.65

Note: * For PAN/CNT1 fibers, Azimuthal scan is deconvoluted into a highly ordered region (Fitting curve 1) and surrounding matrix (Fitting curve 2).

Fiber shrinkage under various stresses was monitored in TMA and is shown in Figure 2.27. Shrinkage is very sensitive to applied stress and was greatly reduced if higher stress was applied. Shrinkage is separated into three parts: entropic shrinkage, stretching (only under high stress), and chemical shrinkage.

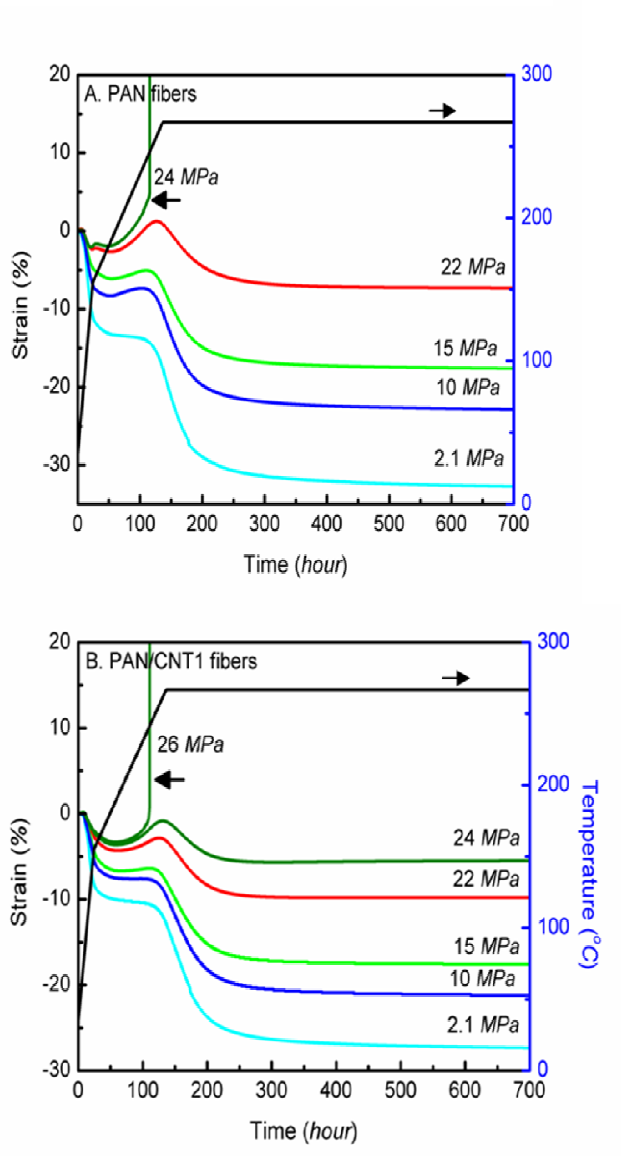

Figure 2.27 Shrinkage curves of PAN and PAN/CNT1 fibers stabilized under various stresses. A. PAN fibers; B. PAN/CNT1 composite fibers. The arrows toward left indicate breakage of fibers.

The detailed shrinkage values were calculated from Figure 2.27 and are listed in Table 2.11. For fibers stabilized with very low tension of 2.1 MPa, the final shrinkages for PAN fibers exceeded 30 %. Addition of CNTs reduces both entropic and chemical shrinkage. Correspondingly, stretching of composite fibers was less than that of the PAN fibers. It can be also found that the addition of CNTs improves the maximum tension that can be applied during stabilization; the maximum tensions of PAN and PAN/CNT1 fibers are 22 MPa and 24 MPa, respectively. While tension is increased from 22 to 24 MPa, the total shrinkage of PAN/CNT1 fibers reduces from 9.7 to 5.8 %.

Table 2.11 Shrinkage values from plots shown in Figure 2.27.

Applied Stress (MPa)	PAN			PAN/CNT1		
	$S_{Entropic}$ (%)	$S_{Stretch}$ (%)	$S_{Chemical}$ (%)	$S_{Entropic}$ (%)	$S_{Stretch}$ (%)	$S_{Chemical}$ (%)
2.1	-13.6	0	-18.8	-9.9	0	-17.0
10	-8.5	1.1	-15.4	-7.4	0	-13.5
15	-5.9	1.2	-12.7	-6.7	0.4	-11.0
22	-2.8	4.1	-8.2	-4.1	1.2	-6.8
24		Break		-3.3	2.5	-5.0
26		--			Break	

Note: S: Strain. Negative value indicates shrinkage, and positive value indicates elongation.

In summary, these results suggest that higher stress will benefit chemical structure and mechanical properties of the stabilized fibers. For stabilization, the maximum stress without breaking the fibers should be applied. Most fiber breakage during stabilization occured when temperature was around 200 ^{o}C. In this temperature range, fibers became plasticized, resulting in breakage at tension values. To further improve the properties of stabilized fibers, tension should be varied in different temperature regions.

2.2.4 Other effect of addition of CNTs on stabilization

2.2.4.1Effect of addition of CNTs on exothermic behavior of stabilization reaction

To compare the effect of different kinds of CNTs on stabilization, fibers with approximately the same diameter (around 10 μm) were used. The DSC curves are shown in Figure 2.28 and the data is listed in Table 2.12.

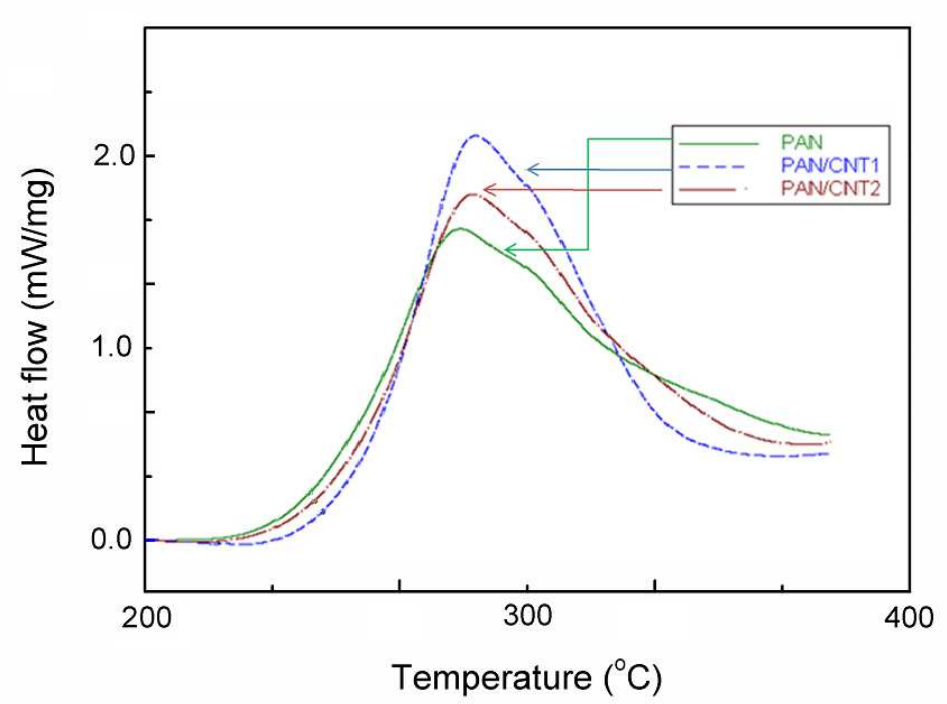

Figure 2.28 DSC exotherm of PAN, PAN/CNT1 and PAN/CNT2 composite fibers. Air flow rate is 50 ml/min, and heating rate is 1 ^{o}C/min.

Table 2.12 DSC data of PAN, PAN/CNT1, and PAN/CNT2 composite fibers in air.

Sample	Peak Temp (^{o}C)	$\Delta H_{Stabilization}$ (J/g)	Start Temp (^{o}C)	End Temp (^{o}C)	Diameter (μm)
PAN	281	5959	219	380	10.4
PAN/CNT1	286	6611	229	365	9.6
PAN/CNT2	285	6166	221	372	11.1

In composite fibers, the onset and peak position shifts to higher temperatures as compared to the control PAN. PAN/CNT1 fibers shows the highest peak temperature. This seems reasonable as CNT1 has the highest surface area/mass ratio and more PAN molecules will be affected in comparison with that affected by CNT2 at the same weight fraction. The DMA analysis discussed in Chapter 1 shows that the activation energy of T_g and the elastic modulus increases with the addition of CNTs. The addition of CNT restricts and reduces the polymer mobility of the chain in its vicinity regions, which makes composite fibers much stiffer and more difficult to stretch in comparison with the control PAN fibers. Since stabilization reactions are believed to initialize in amorphous regions, reduced chain mobility by the addition of CNTs will retard the initiation of cyclization and shift the starting point of exothermic peak to higher temperature. The integrated heat work of composite fibers is higher than that of control PAN fibers; also, it is to be noted that the exothermic peak becomes narrower with the addition of CNTs. Heat of reaction may be affected by two factors: 1. types of reactions; 2. reaction degree. The IR results of the stabilized fibers show that the addition of CNTs leads to the formation of more conjugated nitrile groups and less β-amino nitrile. Also, the difference in diameter affects oxygen diffusion, an important reactant; therefore, it will affect the exothermic behavior. To explore the effect of fiber diameter, larger diameter fibers were used for test. The fibers were made from the same PAN polymer. For composite fibers, 1 wt. % SWNTs were added. Fibers were spun by a spinneret (Diameter = 250 μm) with an as-spun draw ratio of 3.2, and hot draw ratio of 13. The diameters of fibers are around 20 microns. The DSC curves of PAN and PAN/SWNT fibers are shown in Figure 2.29. The integrated heat work of PAN and PAN/SWNT fibers are 2864 J/g and 3423 J/g,

respectively. The addition of SWNT increases the integrated exothermic area. Additionally, it can be found that under the same heating rate, the heat work of the larger diameter fibers (20 μm) is much lower than that of the smaller diameter fibers (10 μm).

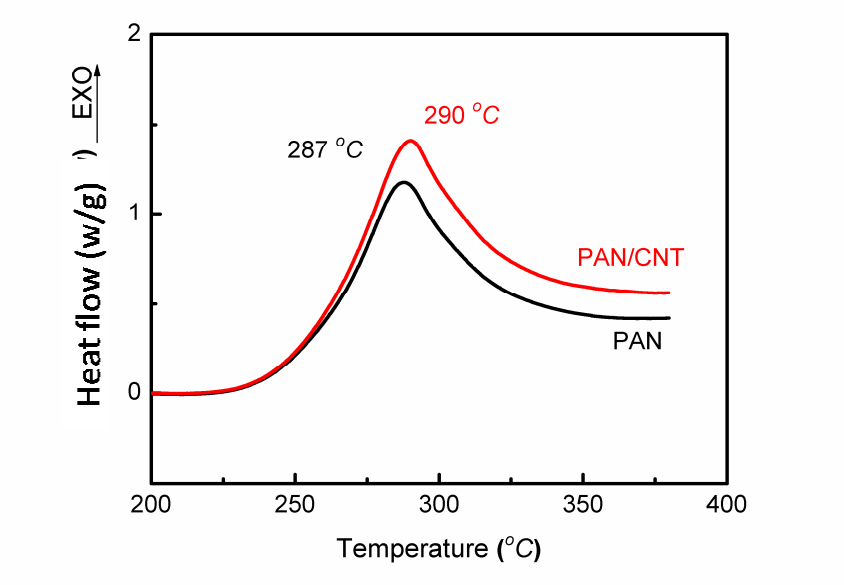

Figure 2.29 DSC curves of PAN and PAN/SWNT fibers with a diameter of 20 μm. Air flow rate is 50 ml/min, and heating rate is 1 °C/min.

Among the several kinds of stabilization reactions, oxidation is the most exothermic. The cross-sectional area of the larger diameter fibers (20 μm) will be 4 times as large as that of the smaller diameter fibers (~10 μm). Thus, the oxygen diffusion will take a much longer time in the larger diameter fibers. Since the same heating rate was used in the DSC experiments, the oxidation reaction of the larger diameter fibers may not have been completed as in the smaller diameter fiber, due to longer diffusion time. This explains the less exothermic heat evolved in the larger diameter fibers. PAN/MWNT composite fibers with different draw ratios were also compared. The same PAN polymer

and MWNT content of 1 wt % was used. The DSC curves are shown in Figure 2.30, and the data is listed in Table 2.13.

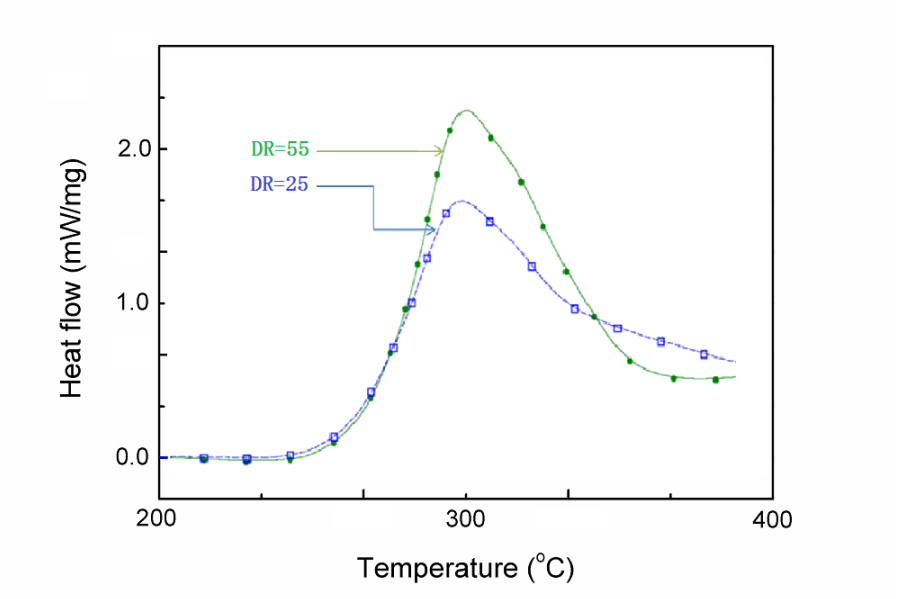

Figure 2.30 DSC curves of PAN/MWNT fibers with different draw ratios (DR). Air flow rate is 50 ml/min, and DSC heating rate is 1 °C/min.

Table 2.13 DSC data of PAN/MWNTs with different draw ratios.

Samples	Peak (°C)	ΔH Stabilization (J/g)	Start Temp (°C)	End Temp (°C)	D (μm)
PAN	281.6	5959	219	380	10.4
PAN/MWNT*	283.5	5292	221	380	15.5
PAN/MWNT**	285.3	6567	223	364	10.5

Note: *Draw ratio=25; ** Draw ratio=55, D: Diameter.

For fibers with similar diameter, the addition of MWNT increases the integrated heat work and narrows the exothermic peak. For PAN/MWNT fibers with a lower draw ratio, the fiber diameter is larger, and the heat evolved is lower. For fibers with comparable diameters, the addition of CNTs increases heat evolved in stabilization

reactions. The cause of the increase, whether it is the different reactions, as shown in IR spectra, change of oxygen diffusion rate, or both, needs further investigation. The above set of experiments lead to the conclusion that the elevated exothermic peak temperature is caused by restricted chain mobility after the addition of CNTs; higher heat evolved in stabilization and narrower peak breadth are caused by different cyclization reactions with the addition of CNTs, as well the possible changes of gas diffusion rate.

2.2.4.2 Effect of addition of CNTs on shrinkage and stress

The thermal shrinkage and thermal stress of fibers during stabilization were monitored in TMA. Two types of studies were performed: constant length and constant force. The stress value is calculated from the diameter of the precursor fibers. Due to the limitation of instrument, a fiber bundle containing 16 filaments was used. Some preliminary thermal shrinkage behavior of PAN and PAN/CNT1 fibers has been discussed in section 2.2.3. In this section, the effect of the addition of CNTs on shrinkage and stress evolution during stabilization is investigated in greater detail. The shrinkage curves of PAN and PAN/CNT1 fibers under a tension of 20 MPa in air are shown in Figure 2.31. PAN fibers are easier to be drawn than PAN/CNT1 fibers. At beginning, the addition of CNTs reduces the entropic shrinkage; then, the stretching of PAN fibers caused a cross-point of shrinkages when temperature is ~ 160 ^{o}C. In the late stabilization stage, the length of stabilized PAN fibers continuously decreased, whereas that of stabilized composite fiber remains unchanged.

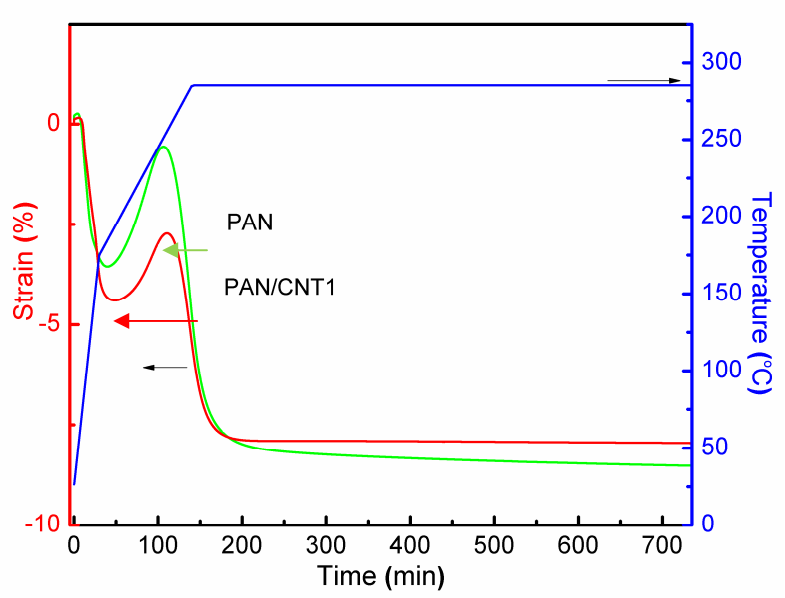

Figure 2.31 Shrinkage curves of PAN and PAN/CNT1 composite fibers under a tension of 20MPa in air. Negative value indicates shrinkage of length; Positive value indicates elongation.

The stress development during stabilization was studied by using constant length mode in TMA. Figure 2.32 showed the stress curves of PAN and PAN/CNT1 fibers during the stabilization with a pre-strain of 0.3%, 0.4% and 0.5%. Three stress peaks show in the curves, including preloading stress caused by pre-strain, entropic stress caused by the retraction of stretched chains, and chemical stress caused by stabilization reaction . The pre-strain has no effect on the stress during stabilization process, although pre-stress shows large difference. The detailed results are listed in Table 2.14. The addition of CNT does not affect the trends of stress evolutions during the stabilization process; however, it increases the starting temperature of entropic and chemical stress, which is similar to DSC results. Also, it can be observed that the control PAN shows much higher entropic stress, higher chemical stress, and higher residual stress than that in the PAN/CNT1 composite fiber. During fiber spinning, the PAN and PAN/CNT1 fibers

were drawn under exactly same conditions, and possess similar crystalline orientations; it will be expected the PAN chains will be stretched at the same degree in both fibers. However the maximum entropic stress and chemical stress in CNT1 fibers are lower than that in the control PAN fibers. It suggests that the addition of CNTs may withstand more stress.

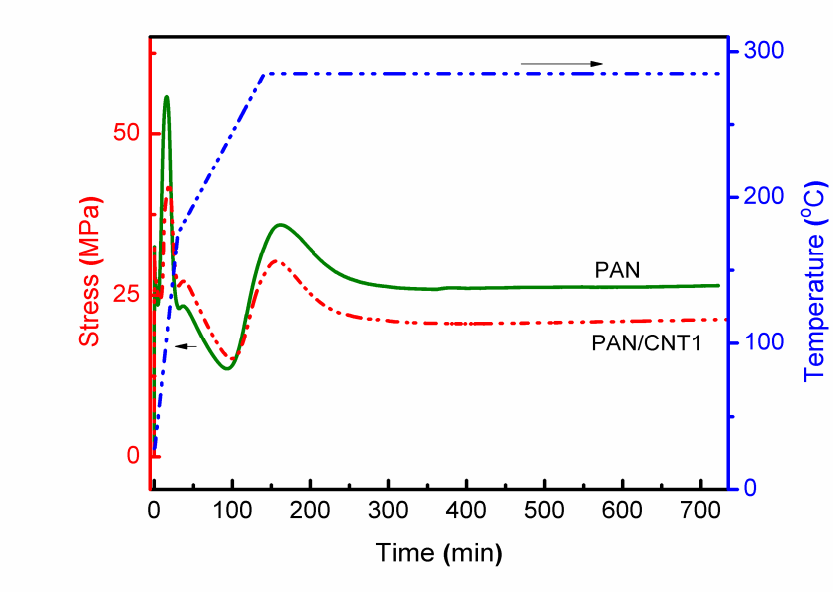

Figure 2.32 Thermal stress curves of PAN and PAN/CNT1 composite fibers in constant length mode.

Table 2.14 Stress changes of PAN and PAN/CNT1 fibers in constant length mode during stabilization in air.

		PAN	**PAN/CNT1**
Entropic stress	Start temperature (°C)	47 ~ 56	62 ~ 72
	Peak temperature (°C)	98 ~ 109	121 ~ 125
	Peak stress (MPa)	55 ~ 61	39 ~ 41
Reaction stress	Start temperature (°C)	234 ~ 239	244 ~ 248
	Peak stress (MPa)	35 ~ 39	29 ~ 31
	Residual stress (MPa)	~ 26	~ 21

The fiber with higher draw ratio usually possesses better mechanical properties, what is the effect of draw ratio on shrinkage behavior of composite fibers will be discussed here. The shrinkage curves of PAN/MWNT (1 wt. %) composite fibers with various draw ratios are shown in Figure 2.33. Fibers with draw ratio of 35, 45 and 55 show close entropic shrinkage, which may due to the amorphous chains are highly oriented under high draw ratios. These results indicate that the extension degrees of stretched amorphous PAN chains are similar for all fibers. The fibers with the lowest draw ratio (DR=25) can be easily stretched under a tension of 20 MPa and a significant length increase can be observed. The fiber with higher draw ratio shows larger chemical shrinkage.

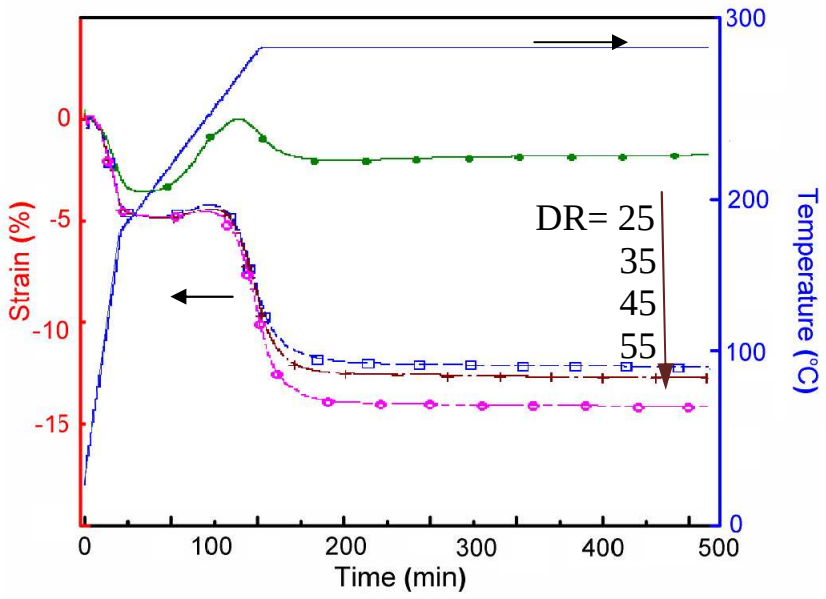

Figure 2.33 Thermal shrinkage behaviors of PAN/MWNT (1 wt. %) composite fibers with different draw ratios (DR). Constant tension is 20MPa.

PAN/MWNT fibers with different draw ratios of 25, 35, 45 and 55, have diameters of 15.5, 13.1, 11.7 and 10.5 μm, respectively. The difference in diameter causes different oxygen diffusion behavior, leads to different chemical reactions and is possible to affect the chemical shrinkage. Stress curves of PAN/MWNTs fibers with different drawn ratios are shown in Figure 2.34. A pre-strain (0.3 %) was applied, and the fiber length was kept constant during testing.

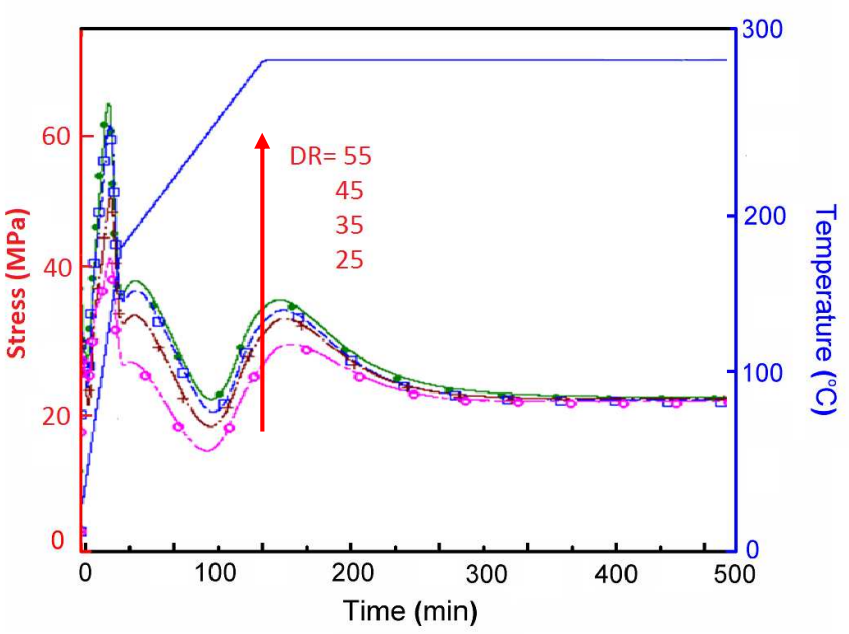

Figure 2.34 Stress curves of PAN/MWNTs composite fibers during stabilization in air.

The maximum entropic stress occurred at ~ 120 ^{o}C and the values increased from 45 to 54 to 67 to 70 MPa as the draw ratio increased from 25 to 35 to 45 to 55. The entropic shrinkage is caused by recoil of extended polymer chains. The lower value indicates the lower extension degree of PAN chains. The entropic peak stresses of fibers with draw ratios of 45 and 55 are comparable, indicating both fibers have similar

orientation of amorphous chains. The interesting thing is that the residual stresses for those fibers almost show similar value regardless of the fiber draw ratio.

2.2.5 Proposed structure of PAN/CNTs composite fibers

The structure of PAN fibers has been proposed to be consisting of two-phases [23, 24], namely ordered regions and disordered regions. In precursor fibers, CNTs are aligned along the fiber axis, and PAN forms ordered and amorphous layered structure. According to above model, CNTs will penetrate many layers of crystalline and amorphous regions, and will affect fiber's thermo-mechanical properties. The stress-temperature evolution was detected in TMA under iso-strain mode (pre-strain = 0.3 %). Temperature was increased from 25 ^{o}C to 175 ^{o}C, and then cooled down to 25 ^{o}C at a rate of 5^{o}C/min. The process was repeated two more times. Stress –temperature curves of PAN and PAN/CNT1 fibers are shown in Figure 2.35.

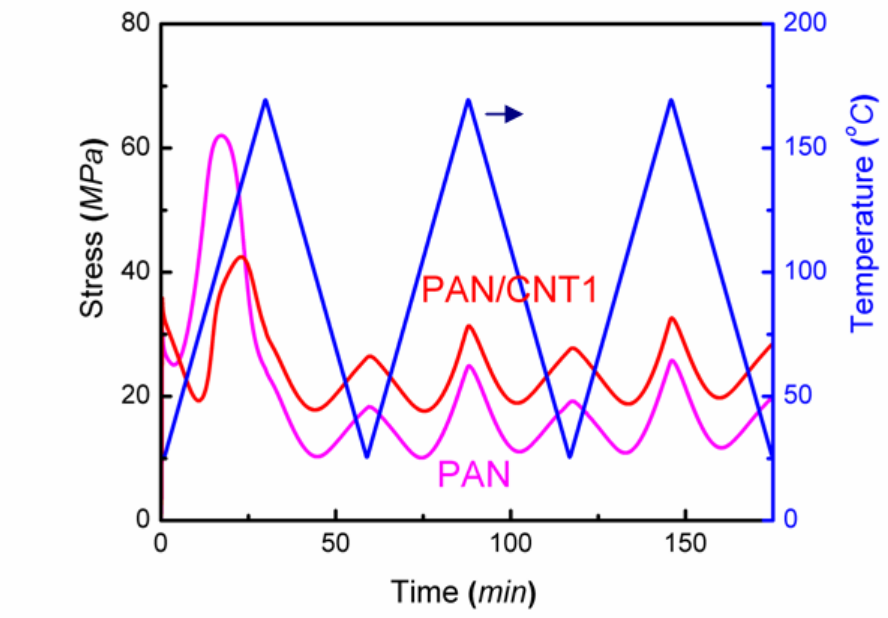

Figure 2.35 Stress curves of PAN and PAN/CNT1 fibers during thermal cycles under iso-strain condition.

In the first cycle, entropic relaxation is observed above 70 ^{o}C. The entropic relaxation from recoil of polymer chains in the amorphous phase cannot reverse during cooling process. The irreversible process means that stretched amorphous chains or segments re-coil and their conformations remain permanently altered. Although both PAN and PAN/CNT fibers were spun under same process and same draw ratio, PAN fibers have much higher entropic stress and lower residual stress than that of PAN/CNT1 fibers, which suggests that more stretched polymer chains recoil in PAN fibers. In the second and third cycles, the stress changes are reversible and indicate fiber structure is very stable. The minimum stresses in the second and third cycles appeared at around 100 ^{o}C, which is around the T_g of PAN fibers. Above 100 ^{o}C, stress changes are caused by entropic force of stretched chains which act as springs; below 100 ^{o}C, fibers are in glassy state, and length changes according to intrinsic thermal shrinkage; cooling reduces length and increases stress. In the second and third cycles, in the temperature range of 100 ^{o}C to 175 ^{o}C, amplitude of entropic stress in PAN/CNT1 fiber is smaller, 13 MPa, than that in PAN fiber, 16 MPa. In the temperature tange of 25 ^{o}C to100 ^{o}C, amplitude of intrinsic thermal shrinkage stress of PAN/CNT1 fiber is larger, 9 MPa, than that of PAN fiber, 8 MPa. Above changes of stresses can be explained by the suggested PAN/CNT model. As temperature increases from 100 to 175 ^{o}C, the shrinkage force caused by entropy is shared by CNTs; therefore, both maximum entropic stress (cycle 1) and entropic stress amplitude (cycle 2&3) are reduced by the addition of CNTs. As temperature decreases from 100 to 25 ^{o}C, assuming PAN and PAN/CNT1 fibers have same coefficient of thermal expansion (CTE), the stress in PAN/CNT1 fibers will increase more than in PAN fibers, since composite fibers have higher modulus than PAN fibers.

The shrinkage behaviors in Figure 2.24 can also be explained by this model. Under low tension, addition of CNTs retains the original structure of fibers, and reduces the entropic shrinkages. Under high tension, the same effect will make fibers harder to be stretched. Similar stress evolution of PAN/MWNT fiber during temperature cycling was measured by TMA and is shown in Figure 2.36.

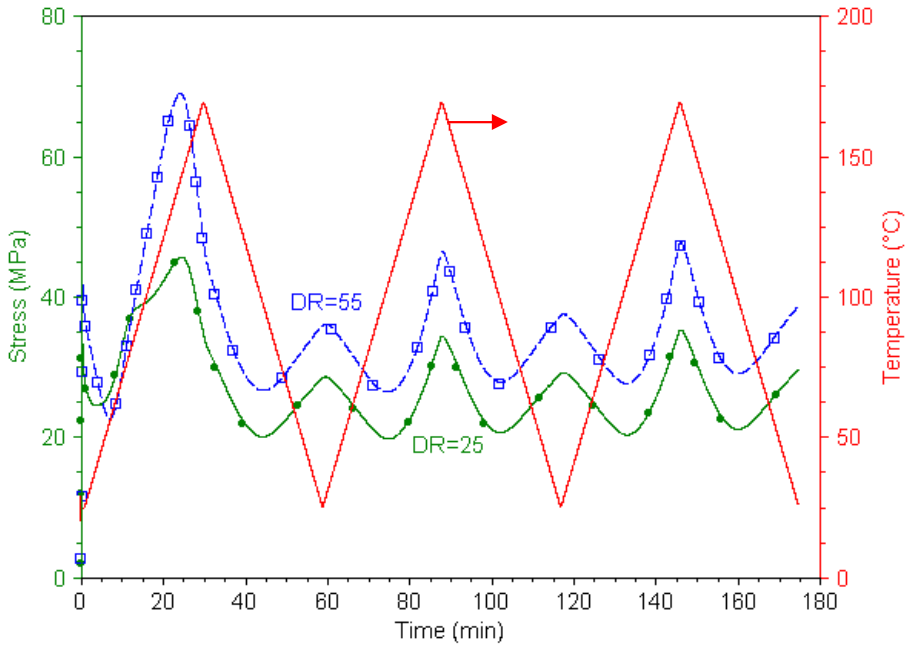

Figure 2.36 Stress curves of PAN/MWNTs (1 wt. %) fibers during thermal cycling under iso-strain condition. DR is draw ratio.

The stress changes in PAN/MWNT fibers are similar to these observed in PAN and PAN/CNT1 composite fibers. For the PAN/MWNT fibers with a higher draw ratio (DR), the PAN molecules will be stretched more, therefore exhibit higher entropic stress and shrinkage than that of fibers with a lower draw ratio. The stress amplitude of PAN/MWNT fiber of draw ratio of 55 is ~ 22 MPa, which was higher than that for the

fiber with draw ratio of 25, which gives stress amplitude of ~ 15 MPa. The higher stress amplitude indicates that the chain segments in amorphous domains are stretched more and possess higher orientation.

2.3 Conclusions

In summary, during the stabilization of gel-spun PAN and PAN/CNT composite fibers, changes in structural, chemical and mechanical properties were studied, and the reinforcement efficiency of different types of CNTs was compared. The stabilization can be divided into two processes; a fast process mainly in the amorphous regions during the early stages of stabilization, and a slow process that occurs in the crystalline regions during the late stages of stabilization. In the fully stabilized fiber, addition of CNTs reduces the formation of β-amino nitrile, and enhances the stress resistance. Ordered PAN structure or PAN crystals lead to the formation of longer conjugated nitrile segments after stabilization. The addition of CNTs enhances the crystallinity of PAN and also affects crystal structure of interphase PAN. This leads to the formation of highly ordered stabilized polymer in the interphase regions, and improves the orientation of stabilized PAN matrix. The surface area of CNTs plays an important role on the reinforcement efficiency in composite fibers; the higher the CNT surface area, the better the reinforcement efficiency. Addition of CNT affects the phase transition behavior of ceramic materials (alumina) as shown in appendix A.

The tension applied during stabilization also plays an important role on the properties of stabilized fibers. Higher stress will lead to better mechanical properties, less β-nitrile and better orientation in stabilized fibers. The final shrinkage of fibers is very sensitive to stabilization conditions, and can be reduced by higher stress or higher

stabilization temperature. Addition of CNTs reduces both chemical and entropic shrinkages of PAN fibers during stabilization, and makes fiber much harder to be stretched. Also, due to the addition of CNTs, the composite fibers can withstand higher tension during stabilization, which is very important to improve the properties of the stabilized fiber. For the structure of PAN fibers, the two phases' structure is suitable, and added CNTs penetrate many layers of crystal and amorphous regions, and improves the stress resistance and reduces the entropic stress and shrinkage.

2.4 References

[1] Cadek M, Coleman JN, Ryan KP, Nicolosi V, Bister G, Fonseca A, Nagy JB, Szostak K, Béguin F, Blau WJ. Reinforcement of polymers with carbon nanotubes: The role of nanotube surface area. Nano Letters 2004; 4(2): 353-6.

[2] Barber AS, Cohen SR, and Wagner HD. Measurement of carbon nanotube-polymer interfacial strength. Applied Physics Letter 2003; 82(23): 4140-2.

[3] Chae HG, Sreekumar TV, Uchida T, A comparison of reinforcement efficiency of various types of carbon nanotubes in polyacrylonitrile fiber. Kumar S. Polymer. 2005; 46(24):10925-35.

[4] Wei C. Adhesion and Reinforcement in Carbon Nanotube Polymer Composite. Appl. Phys. Lett: 2006; 88: 093108.

[5] Liu T. and Kumar S. Quantitative characterization of SWNT orientation by polarized Raman spectroscopy. Chemical Physics Letters 2003; 378(3-4): 257-62.

[6] Dumitrica T, Hua M, Yakobson I. Symmetric-, time-, and temperature-dependent strength of carbon nanotubes. PNAS 2006; 103(16): 6105-9.

[7] Chae HG, Minus ML, Rasheed A, Kumar S. Stabilization and carbonization of gel spun polyacrylonitrile/single wall carbon nanotube composite fibers. Polymer 2007; 48(13): 3781-9.

[8] Devasia R, Nair CPR, Sadhana R, Babu NS, Ninan KN. Fourier transform infrared and wide-angle X-ray diffraction studies of the thermal cyclization reactions of high-molar-mass poly(acrylonitrile-co-itaconic acid). Journal of Applied Polymer Science 2006; 100(4): 3055-62.

[9] Fochler HS, Mooney JR, Ball LE, Boyer RD, Grasselli JG. Infrared and NMR spectroscopic studies of the thermal-degradation of polyacrylonitrile. Spectrochimica Acta Part A Molecular and Biomolecular Spectroscopy 1985; 41(1-2):271-8.

[10] Shimada I, Takahagi T, Fukuhara M, Morita K, Ishitani A. FT-IR study of the stabilization reaction of polyacrylonitrile in the production of carbon-fibers. Journal of Polymer Science Part A: Polymer Chemistry 1986; 24(8):1989-95.

[11] Usami T, Itoh T, Ohtani H, Tsuge S. Structural study of polyacrylonitrile fibers during oxidative thermal degradation by pyrolysis-gas chromatography, solid state C^{13} nuclear magnetic resonance, and fourier transform infrared spectroscopy. Macromolecules 1990; 23(9): 2460-5.

[12] Zhu Y, Wilding MA, Mukhopadhyay SK. Estimation, using infrared spectroscopy, of the cyclization of poly(acrylonitrile) during the stabilization stage of carbon fibre production . Journal of Materials Science 1996; 31(14): 3831-7.

[13] Devasia R, Reghunadhan CP, Sivadasan NP, Katherine BK, Ninan KN. Cyclization reaction in poly(acrylonitrile/itaconic acid) copolymer: An isothermal differential scanning calorimetry kinetic study. Journal of Applied Polymer Science 2003; 88(4): 915-20.

[14] Gallaher KL, Lukco D, Grasselli JG. Investigation of the assignment of the 2190 cm^{-1} infrared band in polyfumaronitrile. Canada Journal of Chemistry. 1985; 63(7):1960-6.

[15] Yu MJ, Bai YJ, Wang CG, Xu Y, Guo PZ. A new method for the evaluation of stabilization index of polyacrylonitrile fibers. Materials Letter 2007; 61(11-12): 2292-4.

[16] Yu MJ, Wang CG, Bai YJ, Wang YX, Xu Y. Influence of precursor properties on the thermal stabilization of polyacrylonitrile fibers. Polymer Bulletin. 2006; 57(5):757-63.

[17] Gupta A, Harrison IR. New aspects in the oxidative stabilization of pan-based carbon fibers. Carbon. 1996; 34(11):1427-45.

[18] Hou YP, Sun TQ, Wang HJ, Wu D. Thermal-shrinkage investigation of the chemical reaction during the stabilization of Polyacrylonitrile fibers. Journal of Applied Polymer Science. 2009; 114: 3668-72.

[19] Fitzer E, Frohs W, Heine M. Optimization of stabilization and carbonization treatment of PAN fibers and structural characterization of the resulting carbon-fibers. Carbon 1986; 24(4): 387-95.

[20] Chae HG, Choi YH, Minus ML, Kumar S. Carbon nanotube reinforced small diameter polyacrylonitrile based carbon fiber. Composites Science and Technology. 2009;69(3-4):406-13.

[21] Kim DY, Kim YC, and Kim CY. Thermal analysis of PAN precursor of carbon fibers. Polymer (Korea) 1985; 9: 518-524.

[22] Bahl OP, Manocha LM. Shrinkage behavior of polyacrylonitrile during thermal treatment. Angewandte Makromolekulare Chemie 1975; 48: 145-59.

[23] Warner SB, Uhlmann DR, Peebles LH. Oxidative stabilization of acrylic fibers 3. Morphology of polyacrylonitrile. Journal of Material Science 1979; 14(8): 1893-8.

[24] Gupta AK, Singhal RP. Effect of co-polymerization and heat-treatment on the structure and x-ray diffraction of polyacrylonitrile. Journal of Polymer Physics Edition 1983; 21(11): 2243-62.

CHAPTER 3

STABILIZATION KINETICS AND EFFECT OF VARIOUS CHEMICAL REACTIONS

During stabilization, PAN fibers undergo complex physical and chemical changes [1-3]. It is known that the chemical reactions include cyclization [4, 5], oxidation [6, 7], dehydration [8], and cross-linking [4]. However, it is difficult to separate these reactions because they occur concurrently. The stabilization reactions of PAN-based fibers have been studied for over 40 years, and there are some points of consensus. However no direct evidence for these reactions and definitive mechanism have been reported. If one can better understand the kinetics [8, 9] and effect of different chemical reactions, then it would help in better optimizing the stabilization process.

Stabilization reactions are exothermic. Based on the heat evolution that can be monitored by DSC, reaction peak temperature can be obtained and reaction activation energy can also be calculated [10, 11]. There are reports on the existence of two DSC exothermic peaks during heat treatment in air, and these peaks were ascribed to different reactions [9, 12]. However, the problems in assigning the peaks to different reactions are that not all reactions show individual peaks, and reactions may be inter-dependent. Watt et al. [6] observed that cyclization reaction strongly affects the oxidation behavior and concluded that the primary reaction caused by heating is cyclization, and cyclized ladder polymer is the prerequisite of oxidation. Cyclization reaction can occur in either inert or

oxidative gas environment [13]; thus, it is possible to separate the reactions by using different gas environments during different stabilization stages.

In this chapter, stabilization kinetics of gel-spun PAN and PAN/carbon nanotube (CNT) composite fibers are discussed. As reported previously [14], gel-spun PAN/CNT composite fibers result in carbon fibers with significantly improved mechanical properties as compared to the comparably processed PAN fibers. The CNT containing gel-spun PAN fibers are considered to be the best candidates for manufacture of the next generation carbon fiber. The detailed stabilization study of the gel-spun fibers was carried out as follows. The stabilization reactions are divided into cyclization, oxidation and additional cross-linking by changing the environmental gas during heat treatment. The same method of changing atmosphere has been used by Fitzer et al. [8] to study the influence of oxygen on stabilization. However in Fitzer et al.'s study no relationship between DSC exothermic peaks and stabilization reactions was investigated. In the current work, the activation energy of individual reaction was calculated from DSC data. The effect of different reactions on the structure, dynamic mechanical properties, and shrinkage of PAN and PAN/CNT composite fibers are investigated.

3.1 Experimental

3.1.1 Materials

PAN (homo-polymer, M_w=250,000 g/mol) and PAN/CNT1 composite fibers are used in this study, which are the same fibers as studied in chapter 2. In this chapter, PAN/CNT composite fiber means PAN/CNT1 composite fiber in chapter 2.

3.1.2 Characterization methods

IR spectra were obtained using spectrometer (Spectrum One, Perkin Elmer Corp.) by collecting 256 scans at a resolution of 2 cm^{-1}. Wide angle X-ray diffraction (WAXD) patterns were obtained by Rigaku micromax-002 using Cu-K_α (λ=0.1542 nm) radiation and Rigaku R-axis IV++ 2D detector. Weight loss during stabilization was recorded by thermo-gravimetric analysis (TGA, Q5000, TA Instruments). The shrinkage and stress variations were monitored by thermal mechanical analyzer (TMA, Q-400, TA Instruments). Heat flow curves were collected by differential scanning calorimeter (DSC, Q-100, TA Instruments). Dynamic mechanical analysis (DMA) experiments were performed on RSA III (TA Instruments). For DMA, a fiber bundle containing 100 filaments was tested under three frequencies, 0.1, 1, and 10 Hz, at a heating rate of 1 ^oC/min.

3.2 Results and discussions

3.2.1 Effect of surrounding gas environments on stabilization reactions

Previous reports [6] have shown that after cyclization in vacuum, no difference was seen for homo-PAN polymer and PAN-co-acid polymer upon further heat-treated in air. For acid containing PAN copolymer, acid will fast initial oxidation reaction and causes the formation of oxidation zone when fibers are stabilized in air; in comparison, no oxidation zone was formed in non-acid containing PAN fibers. However, once both fibers were treated in vacuum at 230 ^oC for 6 hr, and ladder polymer was formed, oxidation zone occurred in the stabilized polymer with or without acid co-monomer, indicating that the formation of ladder polymer is the prerequisite to oxidation. Hence, following this method, it is possible to separate cyclization, oxidation, and further cross-

linking by using nitrogen and air as environments in sequence. Then, by studying the stresses, shrinkage, and reaction activation energy, the effect of CNTs and co-monomers on different kinds of reactions during the complex stabilization process can be better understood and optimized.

PAN fibers were first stabilized in nitrogen, and cooled to room temperature. Subsequently, the treated fibers were further stabilized in air. The heating profile is shown in Figure 3.1. Sample_1, Sample_2, and Sample_3 were collected for further characterizations at different stabilization stages as shown in figure 3.1. The control sample was only stabilized in air from room temperature to 380 ^{o}C at a heating rate of 1 ^{o}C/min.

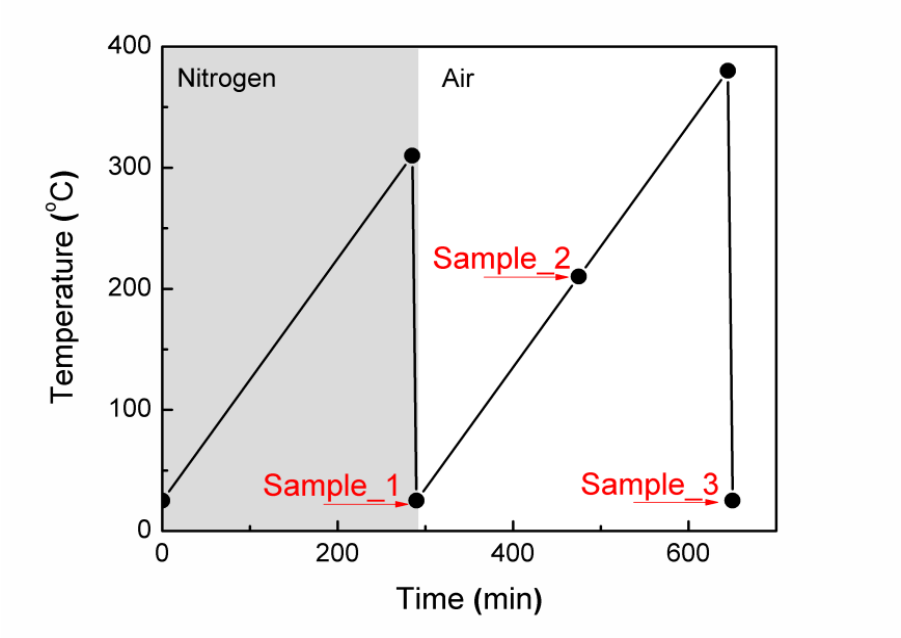

Figure 3.1. Heat treatment profile for stabilization of PAN and PAN/CNT precursor fibers conducted in RSA III in nitrogen followed by air environment. Heating rate is 1^{o}C/min, and then quenched to room temperature using liquid nitrogen.

Figure 3.2 shows DSC curves of PAN fiber heated in different gas environments. The heat flow curve of control PAN fiber (Figure 3.2C) exhibits a broad exothermic peak due to the multiple and complex stabilization reactions. If stabilization is carried out in nitrogen, a sharp and narrow peak caused by cyclization reaction is observed (Sample A in Figure 3.2). Similar result was previously reported by Fitzer et al. [15] Further heat-treatment of this sample (Sample A) in air results in two broad exothermic peaks (Figure 3.2B), indicating that different reactions happen at different temperature, one at around 170 ^{o}C and the other at around 300 ^{o}C.

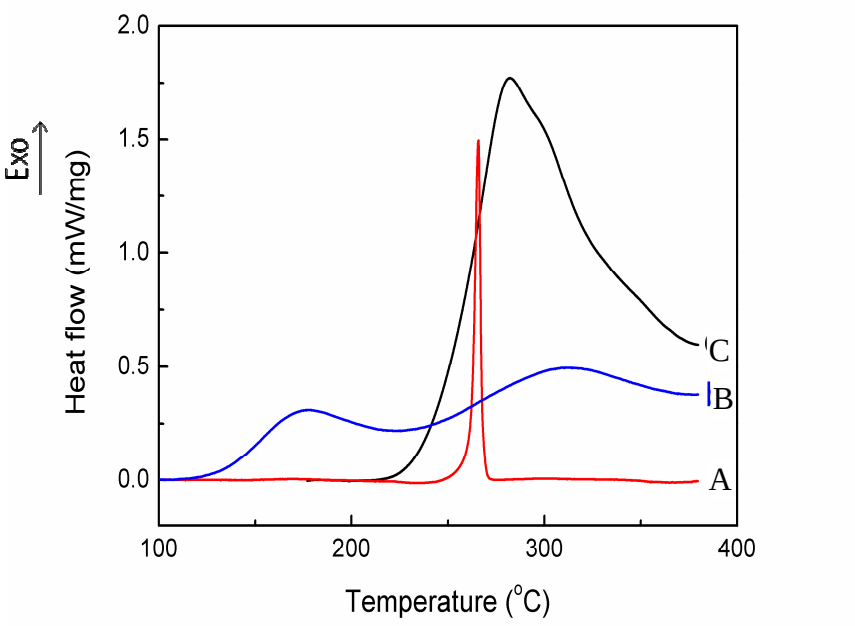

Figure 3.2 DSC heat flow curves of PAN precursor fibers at a heating rate of 1 ^{o}C/min. (A) in nitrogen (B) sample A rerun in air, and (C) in air only.

IR spectra of stabilized fibers were compared, in order to understand the changes in chemical structure, and reactions related to the heat evolution at different temperatures.

Figure 3.3 shows the IR spectra of stabilized PAN fibers using different gas environments.

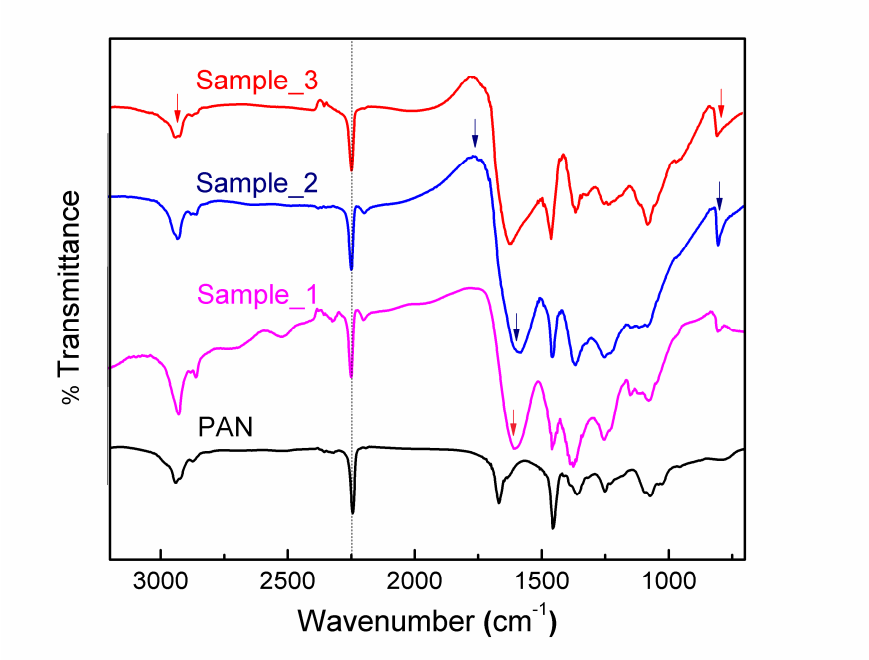

Figure 3.3. IR spectra of Sample_1, Sample_2, Sample_3, and PAN precursor fibers. IR spectra are shifted upward for clarity. Peak at ~804 cm^{-1} (pointed by far right arrow) is due to the formation of C=C-H after dehydration. Peak at ~1617 cm^{-1} (pointed by middle arrow) in Sample_1 and Sample_2 is ascribed to the formation of C=N group due to the cyclization reaction. The deep shoulder appeared at ~1725 cm^{-1} (pointed by far left arrow) is known to be due to the ketonic structure.

In the IR spectra of PAN precursor fibers, the peak at ~2931 cm^{-1} is assigned to C-H vibration in PAN backbone, ~2242 cm^{-1} is assigned to the stretching of C≡N groups, ~1462 cm^{-1} is due to C-C chain vibration. After fibers were heat treated in nitrogen up to 310 ^{o}C (Sample_1), the peak intensity of C≡N group decreases as compared with peaks of C-H and C-C vibration. A new peak appears at ~ 1617 cm^{-1} caused by the formation of C=N groups formed during cyclization reaction. When the same fibers were further treated in air up to 210 ^{o}C (Sample_2), the peak at ~ 804 cm^{-1} due to formation of C=C-

H after dehydration reaction and a deep shoulder at ~ 1725 cm^{-1} due to ketonic structure [12] develop due to oxidation reaction. Both peaks at ~ 804 cm^{-1} and ~ 1725 cm^{-1} are observed simultaneously, suggesting that oxidation and dehydration reactions take place concurrently.

Considering DSC results of samples B and C in Figure 3.2, oxidation temperature is greatly reduced if cyclization occurs prior to oxidation, which also suggests that the oxidation occurs on the cyclized structure. After the temperature was raised to 380 ^oC (Sample_3), intensities of C-H peak at ~ 2931 cm^{-1}, C=C peak at ~ 1617 cm^{-1} and C=C-H peak at ~ 804 cm^{-1} decrease, indicating that hydrogen atoms are eliminated from the cyclized structure, and that additional inter-molecular cross-linking may happen at this stage [12]. Figure 3.4 shows weight loss curves of PAN fibers when heated in TGA in nitrogen, in air, and in nitrogen followed by heating in air. The initial weight loss at around 150 ^oC (~ 3 - 4 wt %) may be due to the absorbed moisture and residual DMF. Significant weight loss occurs above 250 ^oC. It is reported that there is some evolution of HCN groups during stabilization [15, 16], which may lead to major weight loss. Also, it can be observed that heating rate affects the final weight loss (Figure 3.4A and C); at higher heating rates, ultimate weight loss is higher. The higher heating rate will cause faster exothermic rate, since PAN is not a good thermally conductive medium, it causes local overheating and decomposition. Stabilization in air has less weight loss than in nitrogen, since oxygen participates the reactions. For PAN fibers stabilized in air after being cyclized in nitrogen, an increase of weight could be seen at temperature higher than 130 ^oC. The increase can be contributed to oxygen up-take due to oxidation reaction, and confirmed by IR spectra as discussed earlier. Weight reduction in this sample can be

observed at temperatures higher than 330 ^{o}C, which can be attributed to the additional cross-linking or partial decomposition.

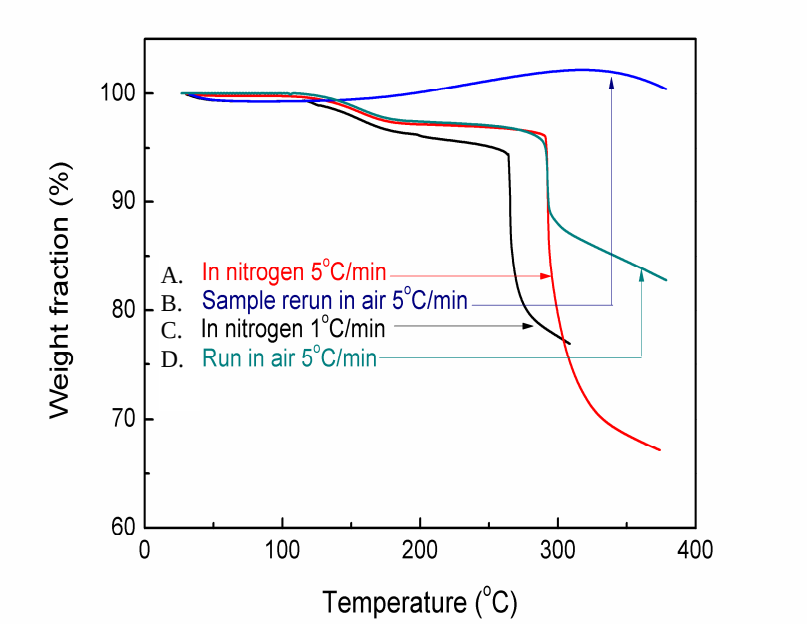

Figure 3.4. Weight loss curves of PAN precursor fibers. A: in nitrogen at a heating rate of 5^{o}C/min; B: sample A rerun in air after running in nitrogen at a heating rate of 5^{o}C/min; C: in nitrogen at a heating rate of 1^{o}C/min; D: in air only at a heating rate of 5^{o}C/min.

The integrated WAXD patterns of stabilized samples at each stage are shown in Figure 3.5. The characteristic PAN crystal peaks (2θ ~17^{o} and 30^{o}) diminish as stabilization progresses. The peak evolved at ~ 26^{o} is due to the formation of cyclic structure. It can be also noted that the intensity of this peak increases with the progress of stabilization reaction, indicating that the content of cyclic structure increases during stabilization. WAXD curves of Sample_3 and control sample show comparable pattern. This suggests that these fibers have similar structure as characterized by WAXD, even though they underwent different stabilization processes.

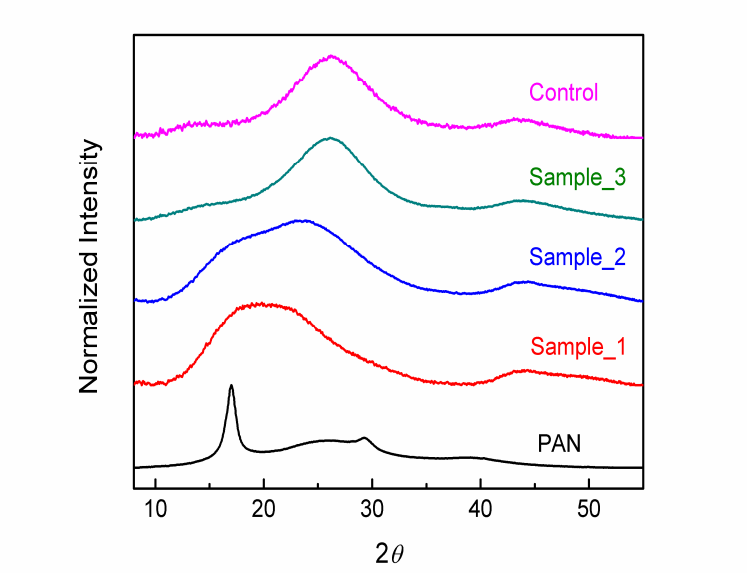

Figure 3.5 Integrated WAXD patterns of PAN precursor fiber and stabilized PAN fibers. Control sample represents PAN fiber stabilized in air from room temperature to 380 ^{o}C at a heating rate of 1 ^{o}C/min. Sample_1, Sample_2, and Sample_3 are the specimen designated in Figure 3.1.

Table 3.1 XRD data of samples 1, 2, 3 and control sample as shown in Figure 3.5.

Sample	**Aromatic structure**		**Peak $_{meridional}$ (^{o})**
	***d* spacing (Å)**	**Peak area (%)**	
Sample 1	3.90	2	43.05
Sample 2	3.66	43	43.27
Sample 3	3.40	48	43.42
Control	3.40	68	43.86

Note: Control sample represents PAN fiber stabilized in air from room temperature to 380 ^{o}C at a heating rate of 1 ^{o}C/min.

The data in Table 3.1 shows that the *d* spacing of formed aromatic structure reduces monotonously, and indicates that the fibers became denser and denser. The final *d* spacing is 3.40 Å, which is very close to the layer-to-layer distance of graphite. The integrated area of aromatic structure increases with the reactions. Also, the peak in meridional scan slightly shifts to higher 2θ value. Suresh et al. [17] reported changes in visco-elastic properties during oxidative stabilization reactions as a function of type and

content of the co-monomer. Using the same method, the effect of different stabilization reactions on the dynamic mechanical properties is compared. The dynamic mechanical property changes during heat treatment monitored using DMA are shown in Figure 3.6. In Figure 3.6A and B, the first tan(δ) peak appears at around 80 ^{o}C, which is T_g of PAN molecules. Different gas environments showed little or no effect on T_g. The second tan(δ) peak in Figure 3.6A at around 280 ^{o}C is due to the chemical reactions during stabilization. tan(δ) peak of PAN fibers stabilized in air (Figure 3.6C) appears at higher temperature (~15 ^{o}C higher) compared with the peak in fibers stabilized in nitrogen (Figure 3.6A). The stabilization in air involves much more complex reactions compared with those in nitrogen, and therefore, shows much broader tan(δ) peak. The tan(δ) peak positions of stabilization reactions show very little frequency dependence, and suggests very high activation energy. For fibers stabilized in air, the storage modulus increases monotonically with increasing temperature, since oxidation, dehydration, and cross-linking can further lead to the improvement in storage modulus. On the other hand, for the fibers heat-treated in nitrogen, the storage modulus decreases after initial increase. As discussed earlier, when the fibers are treated in nitrogen, only cyclization reaction occurs without the occurrence of oxidation and cross-linking reactions. Further heat treatment at higher temperature would result thermal decomposition, which is confirmed by weight loss in TGA experiment conducted in nitrogen as shown in Figure 3.4. When the PAN sample cyclized in nitrogen is further treated in air (Figure 3.6B), the storage modulus increases with increase of temperature. The storage modulus increases rapidly and loss modulus decreases at temperature higher than 300 ^{o}C, which confirms that the additional cross-linking reaction occurs at this stage.

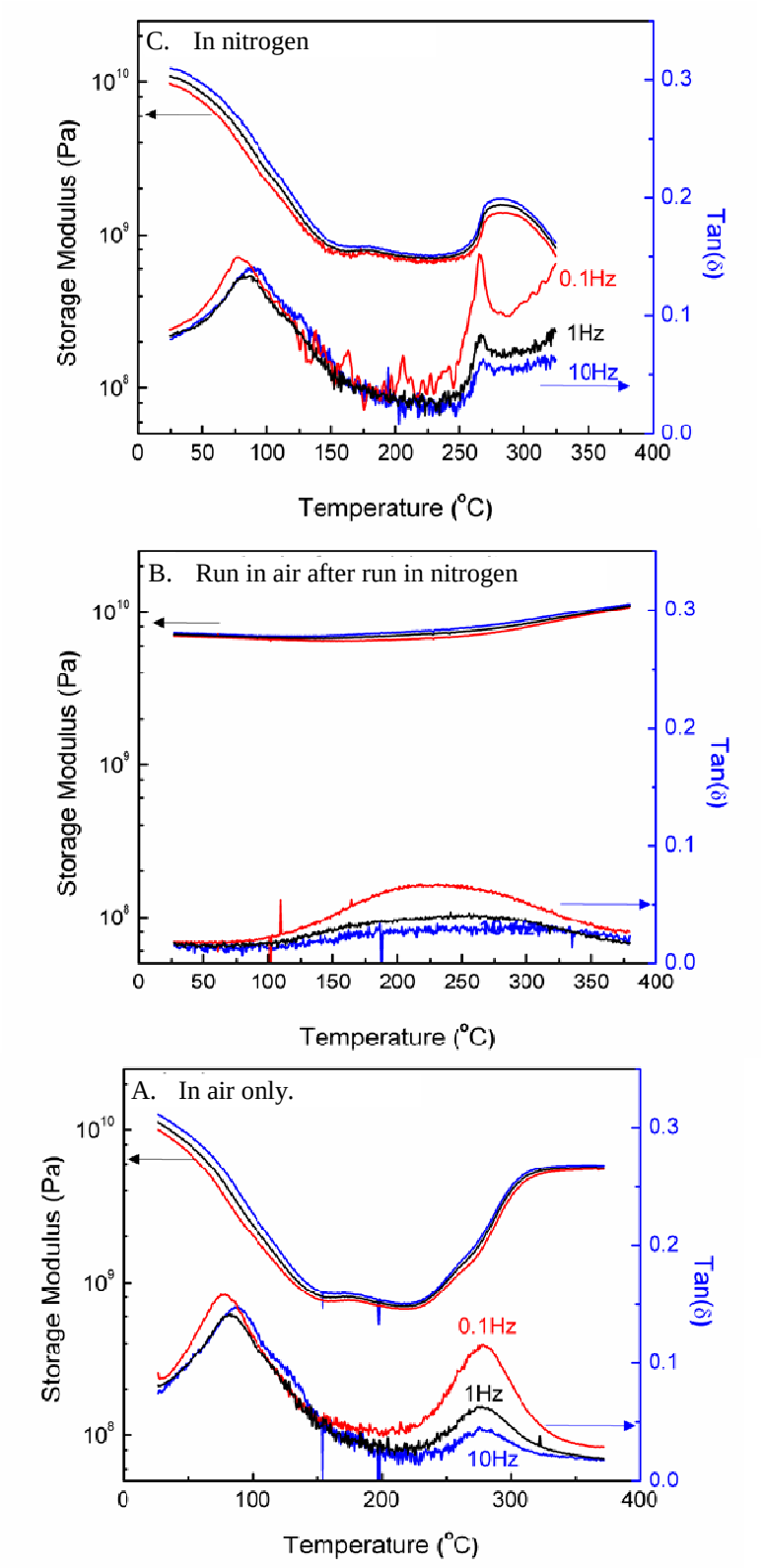

Figure 3.6. Storage modulus and tan(δ) changes of PAN fibers heated in different gas environment at a heating rate of 1°C/min. A: in nitrogen; B: sample A rerun in air after running in nitrogen; C: in air only.

In summary, based on FTIR, XRD, DMA, and DSC results, using nitrogen and air as environments in sequence, stabilization reactions happen in the sequence of cyclization, oxidation and dehydration, followed by the additional cross-linking.

3.2.2 Reaction kinetics and effect of addition of CNTs

Based on the above proposed method of using nitrogen and air in sequence, the effect of additives on individual stabilization reaction can be studied. In this part, the activation energies of PAN and PAN/CNT composite fibers were determined, and the effect of addition of CNTs was studied. Figure 3.7 presents DSC curves of PAN and PAN/CNTs fibers heated in air at different heating rates of 1, 2.5, 5, 10, and 20 ^{o}C/min. Figure 3.8 shows DSC curves of PAN and PAN/CNTs in nitrogen and run again in air at different heating rates from 1 to 15 ^{o}C/min. The exothermic peak shifts to higher temperature and become sharper as the heating rate increases. The peak temperatures and heating rates are listed in Table 3.2.

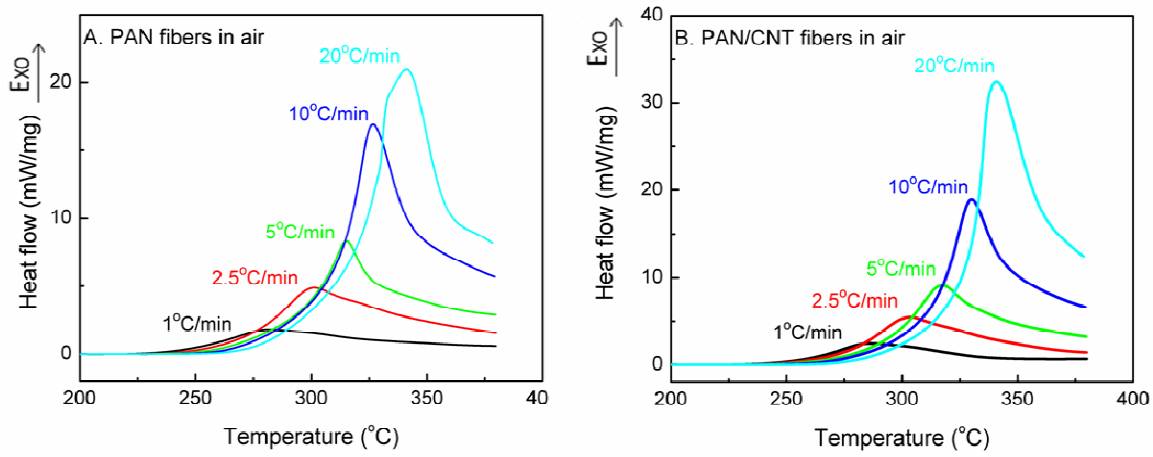

Figure 3.7 DSC heat flow curves of (A) PAN and (B) PAN/CNT composite precursor fibers at different heating rates in air.

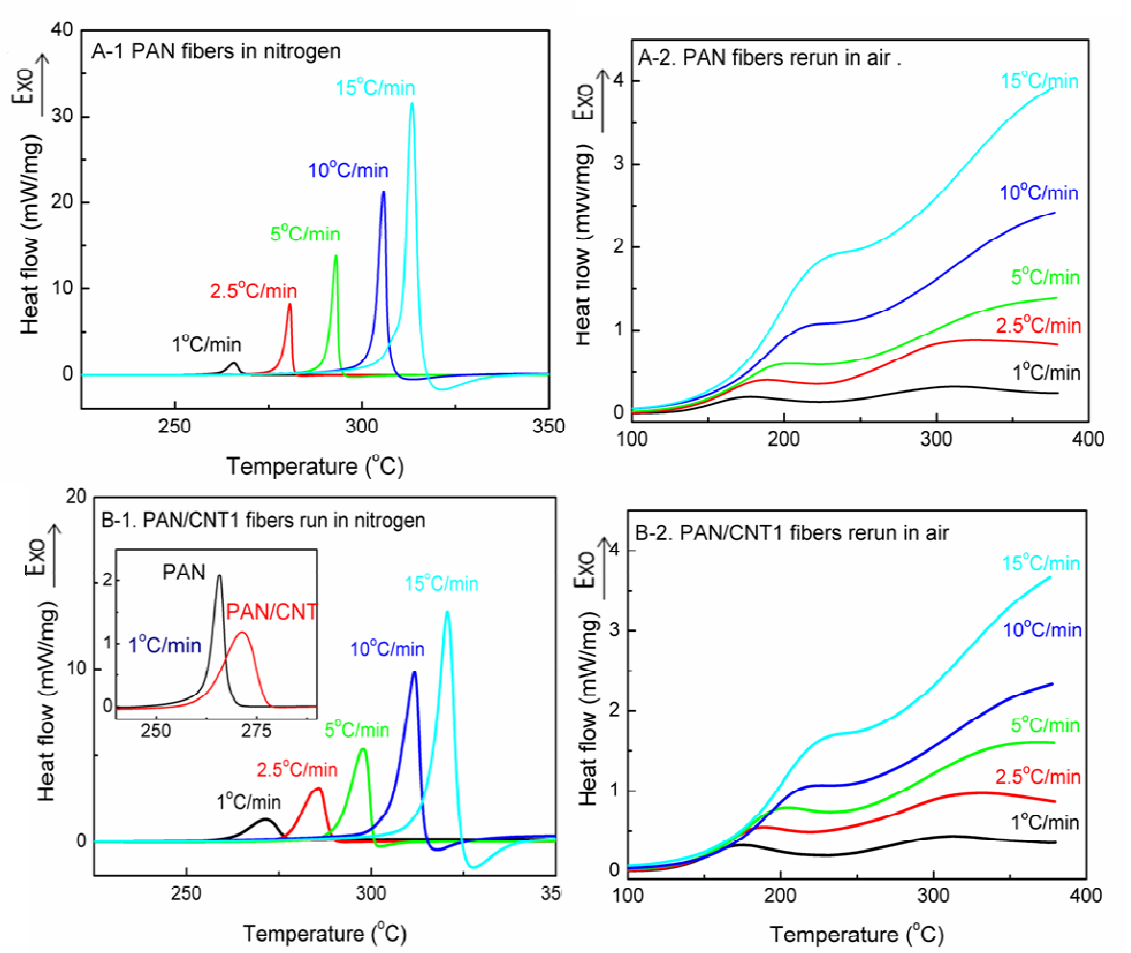

Figure 3.8 DSC curves of PAN and PAN/CNT precursor fibers stabilized at different heating rates. (A-1) PAN precursor fibers in nitrogen, (A-2) PAN fibers rerun in air after running in nitrogen, (B-1) PAN/CNT precursor fibers in nitrogen, and (B-2) PAN/CNT fibers rerun in air after running in nitrogen.

Comparing the exothermic peak of PAN fibers heated in different gas environments, the reactions in air happen in a much broader temperature range and exothermic peak appears at much higher temperature (> 15 ^{o}C higher) than that in nitrogen. It can also be noted that the addition of CNTs elevates peak position to higher temperature (~ 5 ^{o}C) and broaden the exothermic peak of PAN fibers stabilized in nitrogen (inset figure in Figure 3.8B-1).

Table 3.2 DSC data of PAN and PAN/CNT fibers.

Heating rate (°C/min)	In air		In nitrogen		Rerun in air after in nitrogen			
	PAN	PAN/CNT	PAN	PAN/CNT	PAN		PAN/CNT	
	T_s (°C)	T_s (°C)	T_s (°C)	T_s (°C)	T_{s1} (°C)*	T_{s2} (°C)*	T_{s1} (°C)*	T_{s2} (°C)*
1	281.6	286.0	265.9	271.4	173.8	308.5	172.5	309.8
2.5	301.0	303.2	280.7	285.9	182.9	315.3	185.1	316.5
5	315.0	317.1	293.0	298.0	193.3	330.7	197.0	333.3
10	326.4	329.7	305.7	311.7	209.2	--	211.8	--
15	--	--	313.3	320.6	219.0	--	222.6	--
20	340.4	340.4	--	--	--	--	--	--

* T_s: exothermic peak temperature in DSC experiments, 1 and 2 represent the first and second exothermic peaks, respectively.

The FWHMs and heat of stabilization from DSC exothermic peaks in air and in nitrogen are listed in Table 3.3. For stabilization in air, no straight effect on FWHM can be found after the addition of CNTs, since the stabilization in air involves complex chemical reactions, and therefore may be affected by many factors. For stabilization in nitrogen, only cyclization reaction happens. In this case, it is seen that the addition of CNTs significantly broadens the exothermic peak. For heat of stabilization, the addition of CNT reduces the released heat in nitrogen, but increases it in air. It has been reported [18] that the PAN molecules possess more ordered structure in the vicinity of CNT as compared to that in the bulk PAN matrix farther away from CNTs. The studies in chapter 2 show that the addition of CNT promotes the formation of conjugated nitrile and reduce the formation of β-amino nitrile. The different cyclization reactions may lead to different heat of stabilization in nitrogen. Also, since more conjugate nitrile groups are formed in composite fibers, they will react with more oxygen, and release more heat of stabilization in air in comparison with PAN fibers.

Table 3.3. FWHM of DSC exotherms and heat of stabilization.

Heating rate (°C/min)	In air		In nitrogen	
	PAN	PAN/CNT	PAN	PAN/CNT
	FWHM (°C) / $\Delta H_{Stabilization}$ (J/g)			
1	78.0 /5937	57.5 /6583	3.3 /533	9.2 /487
2.5	66.2 /4839	55.9 /5842	2.2 /525	7.0 /465
5	42.9 /2950	50.5 /3541	2.1 /458	5.8 /456
10	33.4 /2502	36.0 /2722	2.3 /419	5.3 /390
15	--	--	2.4 /380	5.0 /248
20	34.4 /1434	31.8 /1798	--	--

Note: FWHM: Full width at half maximum of DSC exothermic peaks.

When heating rate is faster than 10 °C/min, an endothermic peak appears right after the strong exothermic peak in the fibers heated in nitrogen. The endothermic peak is ascribed to the melting of PAN crystals [20]. If the heating rate is fast enough, melting will occur before stabilization reaction. The DSC curves of PAN and PAN/CNTs fibers at a heating rate of 60 °C/min are shown in Figure 3.9. Similar effect of CNTs addition on melting behavior can be found. The CNTs incorporation shifts the melting point to higher temperature and also broadens the endothermic peak.

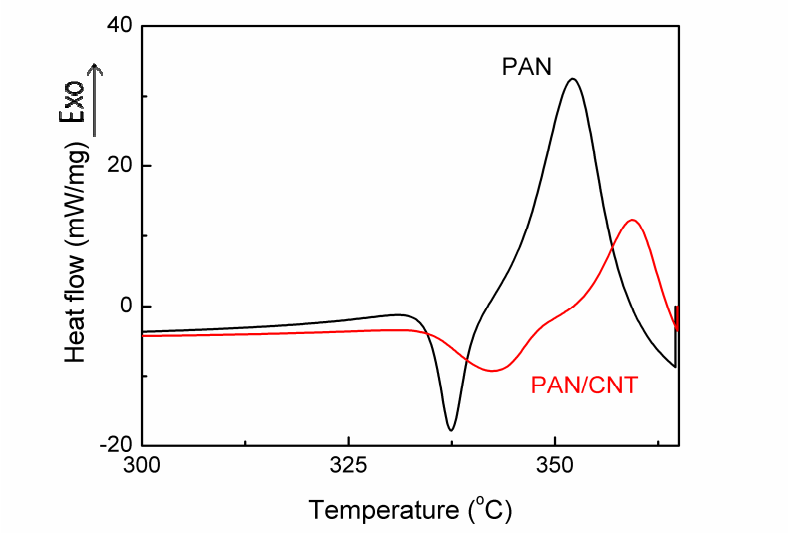

Figure 3.9 DSC curves of PAN and PAN/CNT precursor fibers heat-treated in nitrogen at a heating rate of 60 °C/min.

DSC endothermic peak positions with different heating rates are summarized in Table 3.2. The activation energy can be obtained by fitting data by Ozawa's Equation [10], $-\frac{E_a}{R} = 2.15\frac{d(\log(\phi))}{d\left(1/T_S\right)}$, and Kissinger's equations [11], $-\frac{E_a}{R} = \frac{d\left[\ln\left(\phi/T_S^2\right)\right]}{d\left(1/T_S\right)}$, where E_a is the activation energy, φ is the heating rate (^{o}C/min), and T_S is exothermic peak temperature (K). Above two equations are used to estimate the activation energy irrespective of the detailed reaction mechanism. By plotting $\ln(\varphi/T_S^2)$ versus $1/T_S$ according to Kissinger's equation, and $\log(\varphi)$ versus $1/T_S$ according to Ozawa's equation, the slope of linear fitting line can be used to calculate E_a. Since only cyclization happens in nitrogen, the reaction order can be obtained by the shape of the peak. The order of reaction can be calculated by equation $n = 1.26\sqrt{\frac{a}{b}}$ [15]. The value of 'a' and 'b' can be obtained from the tangential lines in DSC curve as shown in Figure 3.10.

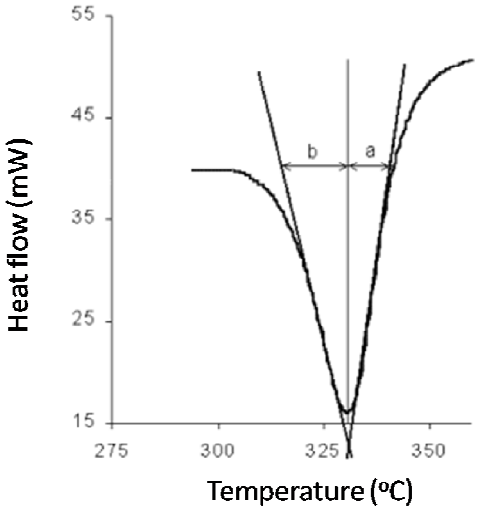

Figure 3.10 Method of calculating reaction order by curve shape. [15]

The addition of CNTs has no effect on reaction order of the cyclization, which is close to 1 with or without CNTs. The plots of Ozawa and Kissinger's curves are shown in Figure 3.11.

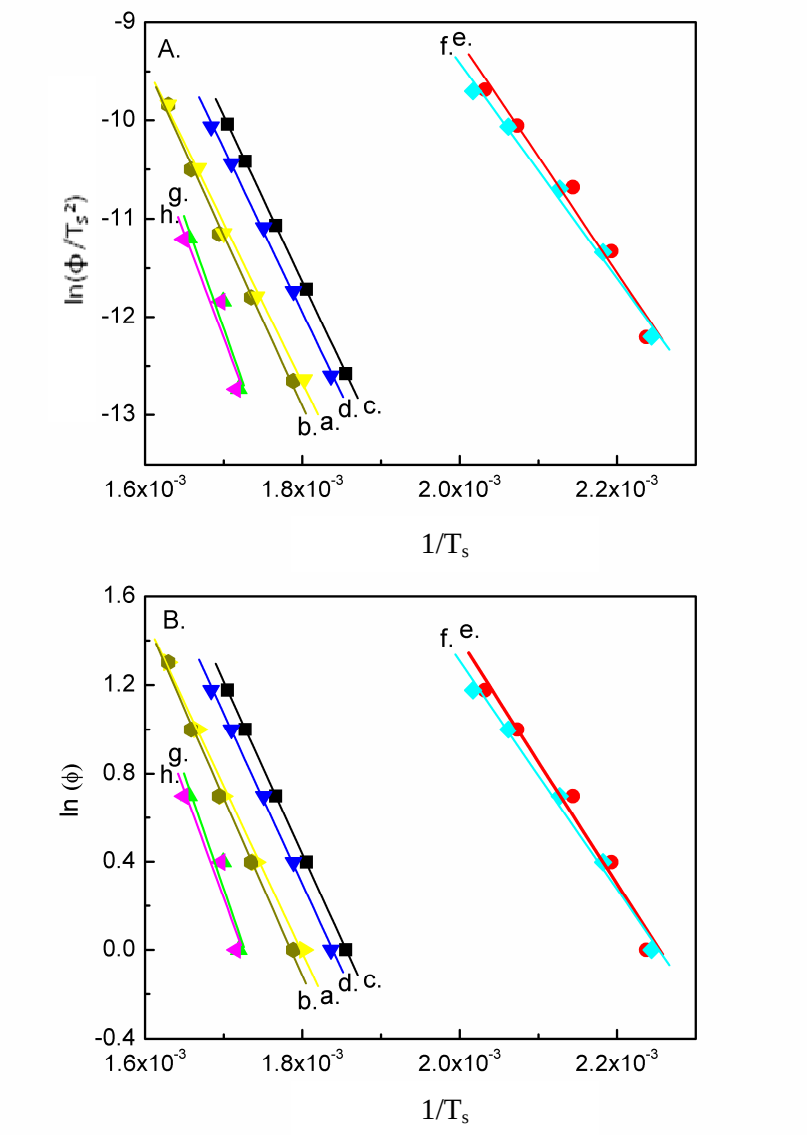

Figure 3.11 Plots according to (A) Kissinger's equation and (B) Ozawa's equation for a. PAN fibers in air, b. PAN/CNT fibers in air, c. cyclization peak of PAN fibers in nitrogen, d. cyclization peak of PAN/CNT fibers in nitrogen, e. oxidation peak of PAN fibers rerun in air after running in nitrogen, f. oxidation peak of PAN/CNT fibers rerun in air after running in nitrogen, g. additional cross-linking peak of PAN fibers rerun in air after running in nitrogen, and h. additional cross-linking peak of PAN/CNT fibers rerun in air after running in nitrogen.

The activation energies related to different reactions are named as cyclization reaction activation energy ($E_{a\text{-Cyclization}}$), oxidation reaction activation energy ($E_{a\text{-Oxidation}}$), and cross-linking reaction activation energy ($E_{a\text{-Cross-linking}}$). Based on calculated activation energy, the pre-exponential factor A in the Arrhenius equation, $\kappa = Ae^{-E_a/RT}$, could be calculated using the equation $A = \frac{\phi E_a}{RT_s^2} e^{E_a/RT_s}$ [21] Where, T_s is the temperature of DSC exothermic Peak, E_a is reaction activation energy. The exponential factor 'A' was calculated from the DSC data at the heating rate of 1 ^oC/min, and the calculated results are listed in Table 3.4.

Table 3.4. Calculated kinetic parameters of PAN and PAN/CNTs fibers.

		From Kissinger's Equation		From Ozawa's Equation	
		E_a (kJ/mol)*	A (s^{-1})*	E_a (kJ/mol)*	A (s^{-1})*
PAN	In air	135.4	3.0×10^{11}	135.9	3.3×10^{11}
	$E_{a\text{-Cyclization}}$	140.2	2.2×10^{12}	140.1	2.2×10^{12}
	$E_{a\text{-Oxidation}}$	98.1	1.7×10^{10}	99.2	2.3×10^{10}
	$E_{a\text{-Cross-linking}}$	188.6	5.8×10^{15}	186.0	3.3×10^{15}
PAN/CNT	In air	145.0	2.0×10^{12}	145.0	2.0×10^{12}
	$E_{a\text{-Cyclization}}$	138.5	1.1×10^{12}	138.7	1.1×10^{12}
	$E_{a\text{-Oxidation}}$	91.1	2.6×10^{9}	92.7	4.1×10^{9}
	$E_{a\text{-Cross-linking}}$	176.8	4.4×10^{14}	175.0	3.0×10^{14}

* E_a is activation energy and A is the exponential factor in the Arrhenius equation.

Among all types of reactions, oxidation reaction exhibits the minimum activation energy. Other researchers [9, 13, 22] reported multiple peaks in DSC curves; by deconvolution, cyclization and oxidation peaks were separated. The reported value of oxidation activation energy, 118 kJ/mol [9], is higher than the value calculated in the current study. The reason is that oxidation reaction is limited by cyclization reaction. Since oxidation reaction happens at much lower temperature (< 200 ^oC) in cyclized PAN

fibers than that in control PAN fibers (> 250 ^{o}C), it suggests that the oxidation reaction prefers to react with cyclized ladder polymer, and not directly with PAN molecules. For stabilization of PAN only in air, the oxidative exotherm will be delayed till the temperature is high enough to form the cyclized structure. In this study, cyclized polymer was formed before oxidation reaction. This would be the main reason behind different activation energy of oxidation in present work as compared to that study reported in literature [9]. Based on the data in Table 3.4 and Arrhenius equation, the rate coefficients of cyclization and oxidation reaction of PAN stabilized in air at 281.6 ^{o}C are calculated to be 0.13 and 9.2 sec^{-1}, respectively. It suggests that oxidation is much faster than cyclization at this temperature. Since oxygen preferably reacts with cyclized PAN, by comparing the rates of cyclization and oxygen diffusion, one can determine whether the stabilization is limited by reaction or by oxygen diffusion.

The activation energy as a function of exothermic peak position is plotted in Figure 3.12, and shows a linear relationship with peak temperature. Reaction with higher activation energy requires higher temperature to initiate. Comparing PAN and PAN/CNT composite fiber, addition of CNTs decreases the activation energies of oxidation and additional cross-linking reactions, while it lowers the activation energy of cyclization reaction marginally. For the composite fibers, it has been reported that the addition of CNTs increases the content of planar zigzag structure in PAN fibers, crystallinity, and crystal size, and also induces highly ordered ladder polymer around the CNTs after stabilization. Since there is almost no difference for the cyclization activation energies of PAN and PAN/CNT composite fibers, it suggests that the above structural changes do not affect the mechanism of cyclization reaction. From FTIR studies (chapter 2) of nitrile

band in stabilized fibers, addition of CNTs improves the segment length of conjugated nitrile in stabilized fibers, and makes the cyclized polymer easier to react with oxygen and further cross-link together. This explains lower activation energy of oxidation and cross-linking during stabilization of composite fibers.

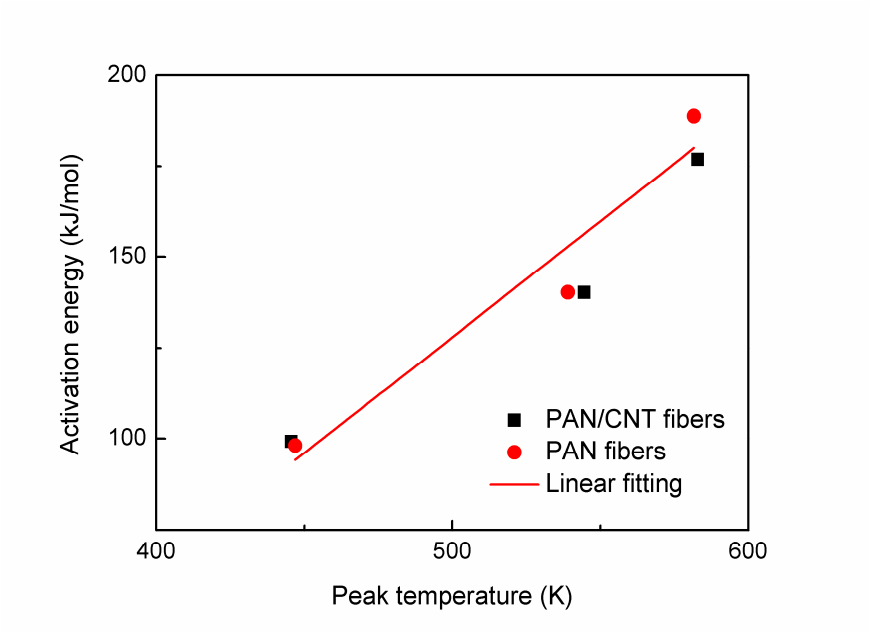

Figure 3.12 Plot of reaction activation energies versus DSC exothermic peak positions. A linear relationship between reaction activation energy and reaction temperature can be observed.

3.2.3 Effect of reactions on shrinkage behavior

The PAN/CNT composite fibers were stabilized in TMA following the procedure in Figure 3.1. The length changes of PAN/CNT fiber stabilized in air after stabilization in nitrogen is shown in Figure 3.13.

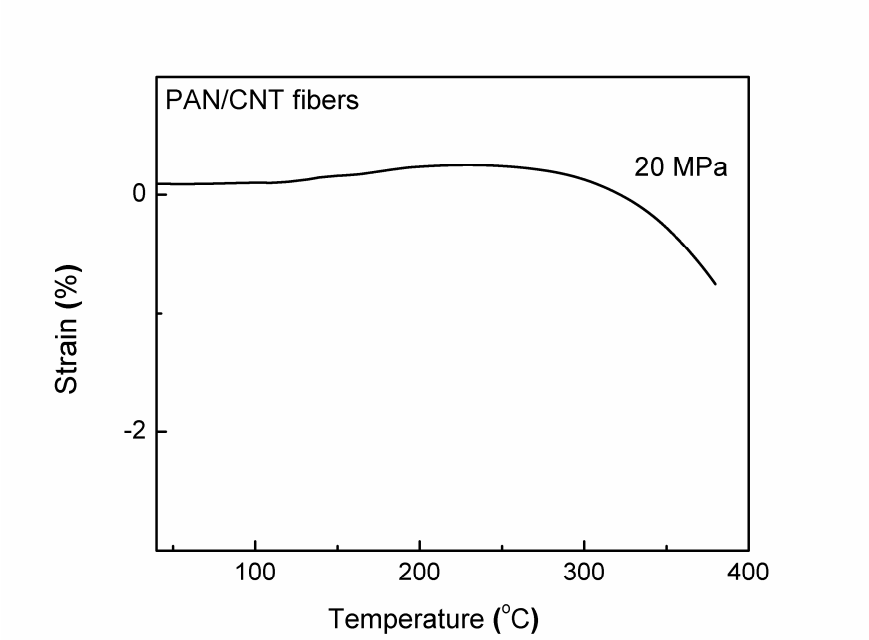

Figure 3.13 Strain curve of PAN/CNT composite fibers in air under the tension of 20 MPa at a heating rate of 1 ^{o}C/min. Before the experiment, fiber was pre-stabilized in nitrogen to 320 ^{o}C at a heating rate of 1 ^{o}C/min. Negative value represents shrinkage.

Cyclization is an important reaction during stabilization because it constructs the main structural frame of the resulting carbon fiber. Shrinkage behavior is mainly caused by cyclization reactions. Once cyclization reaction is completed in nitrogen, length remains constant during further oxidation and cross-linking reactions (less than 0.25% shrinkage at about 380 ^{o}C in Figure 3.13). Figure 3.14 shows shrinkage curves of PAN/CNT fiber stabilized under a tension of 4 MPa in air and in nitrogen.

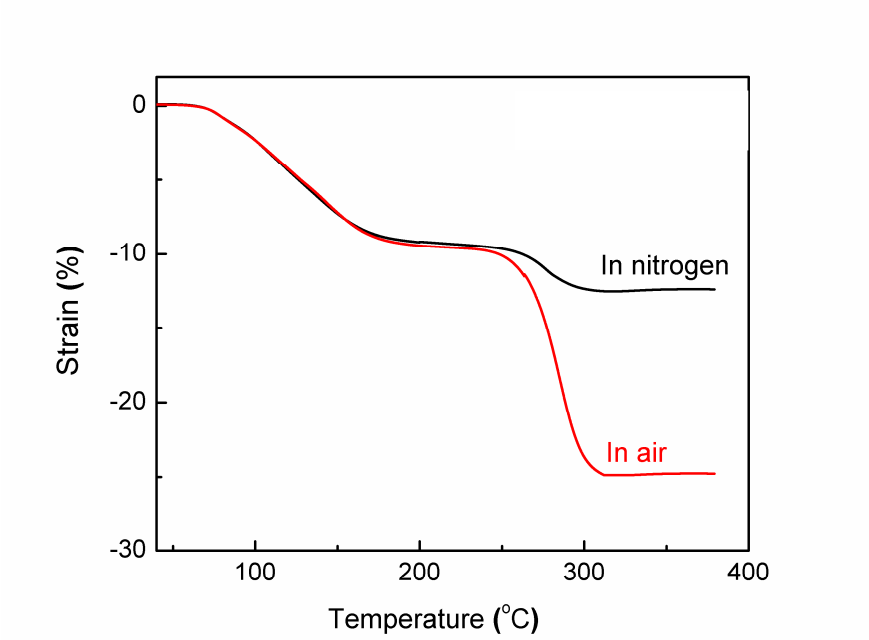

Figure 3.14 Strain curves of PAN/CNT precursor fibers under the tension of 4 MPa in air and in nitrogen at a heating rate of 1 °C/min.

Entropic shrinkage happens at temperature below 200 °C, and is not affected by the gas environment. However, reaction shrinkage shows significant difference depending on if fibers are stabilized in air or in nitrogen. It can be observed that the reaction shrinkage in air is much larger than that in nitrogen. Wang et al. [23] reported that no difference was found for the shrinkage of PAN fibers stabilized in air or argon, however other results [13,24,25] showed that shrinkage of PAN fibers stabilized in air is much larger than that in the inert gas. As for intra-molecular cyclization, the length of polymer chains remains unchanged for planar zigzag conformation and slightly increases for helical conformation. Inter-molecular cyclization contributes substantially to the reaction shrinkage [16]. Reaction shrinkage in air (Figure 3.14) is much larger than in nitrogen, which indicates that cyclization in air involved more inter-molecular cyclization reaction as compared to those in nitrogen. For copolymer, PAN fibers containing acid co-

monomer which initiates cyclization by ionization, it was reported that higher content of copolymer leads to larger reaction shrinkage [16]. When fibers are stabilized in air, the formed oxidative structure can initiate cyclization [8], which may lead to larger shrinkage.

To better understand the effect of oxygen on shrinkage, stress and strain changes of PAN and PAN/CNT composite fibers under various conditions were investigated (Figure 3.15). Higher stress reduces both entropic and reaction shrinkages during stabilization both in nitrogen and in air as discussed in chapter 2. For PAN fibers stabilized in nitrogen, when applied tension increases from 0.4 to 4 MPa, chemical shrinkage reduces from 20% to 5%, while entropic shrinkage reduces from 16% to 12%. If stress is increased to 20 MPa, a stretching process occurs, and fiber length increases. In comparison, if fibers are stabilized in air under the same stress of 20 MPa, large total shrinkage of above 10 % occurs.

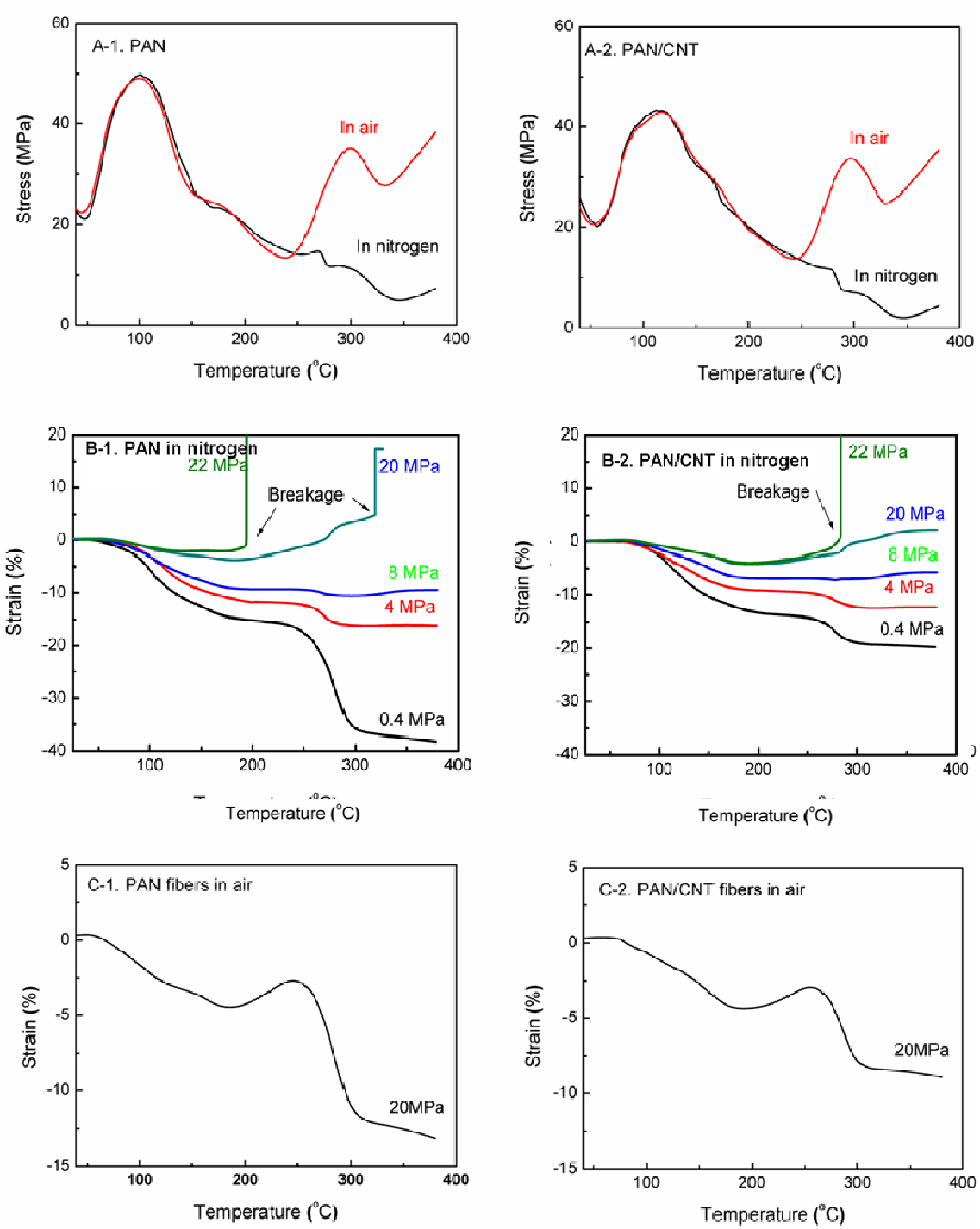

Figure 3.15 (A-1) and (A-2) are stress variation curves of PAN and PAN/CNT precursor fibers stabilized in air and in nitrogen in a constant length mode, respectively. (B-1) and (B-2) are strain variation curves of PAN and PAN/CNT precursor fibers stabilized in nitrogen under various constant pretensions, respectively. (C-1) and (C-2) are strain variation curves of PAN and PAN/CNT precursor fibers stabilized in air under a constant tension of 20 MPa, respectively. Heating rate is 5 ^{o}C/min.

For stabilized fibers, if more inter-molecular cyclization happens, fibers will be much stiffer and show better resistance to external force [26]. Otherwise, if more intra-molecular cyclization occurs, the polymer chains will lose their cohesive energy and can easily slides pass each other. When stabilized in nitrogen, a tension as low as 8 MPa reduces the reaction shrinkage to almost zero. The stress evolution during stabilization under constant length mode is shown in Figure 3.15A. For fibers stabilized in air, reaction stress significantly increases during stabilization, whereas in nitrogen, the stress decreases. Shrinkage curves under different tensions in nitrogen are shown in Figure 3.15B. With increase in tension, the reaction shrinkage reduces, and stretching occurs at tensions higher than 8 MPa. In comparison, PAN fibers stabilized under a constant stress of 20 MPa in air (Figure 3.15C), reaction shrinkage is more than 10 %. The formed ladder polymer stabilized in nitrogen is much easier to slip than that stabilized in air, which also indicates that cyclization reaction in nitrogen prefers intra-molecular propagation that leads to poor inter-chain adhesion. The stress changes of fibers in nitrogen in constant length mode are shown in Figure 3.15A. Before cyclization starts at ~ 270 ^{o}C, the residual stress of ~ 17 and 15 MPa is seen in PAN and PAN/CNT composite fibers respectively (Figure 3.15A), which are higher than 8 MPa. Under this high tension, polymer chains begin to slip past each other and fibers are stretched. Therefore, stress decreases during stabilization in nitrogen.

In order to obtain high modulus carbon fiber, orientation of stabilized PAN and final carbon fibers must be maintained during processing. Therefore, shrinkage should be minimized and the maximum stress should be applied (chapter 2). The addition of CNT reduces shrinkage in two ways: 1. Shrinkage curves of PAN/CNT composite fibers with

PAN fibers (Figure 3.15B and C) shows that the addition of CNTs slightly reduces the entropic shrinkage, but greatly reduces the chemical shrinkage both in nitrogen or in air, especially when fibers are stabilized under low tension. 2. During heating in nitrogen (Figure 3.15B) at a rate of 5 ^{o}C/min under a tension of 20 MPa, the fibers with the addition of CNTs did not break even up to 380 ^{o}C; while control PAN fibers broke at a temperature ~ 320 ^{o}C. The addition of CNTs increases the tension that fibers can bear during stabilization, which can lead to better properties of stabilized fibers as discussed in chapter 2.

3.3 Conclusions

In summary, this study shows the effect of different chemical reactions and CNT addition on the stabilization behavior of PAN fiber. To clearly investigate this effect, precursor fibers were stabilized using nitrogen and air in sequence. It has been shown that, following this method, the complex chemical reactions can be separated into cyclization, oxidation and dehydration, and additional cross-linking. Separating reactions is helpful to better understand the effect of different reactions on the structure changes during stabilization. It is also found that the additional cross-linking reaction has the highest activation energy followed by cyclization and oxidation reaction. Addition of CNTs in PAN fibers marginally reduces the activation energy of cyclization reaction, and lowers the activation energy of oxidation and cross-linking reactions, considerably. It would be better to understand the limitation of reactions if one can compare the rate of different reactions with gas (oxygen) diffusion coefficient, and optimize the stabilization reaction. The cyclization occurred in air involves more inter-molecular cyclization, and leads to larger shrinkage as compared to that of fibers stabilized in nitrogen. For

PAN/CNTs composite fibers, the addition of CNTs reduces both entropic and reaction shrinkages. Also, it improves the level of tension that can be applied during stabilization.

3.4 References

[1] Bashir Z. A critical review of the stabilisation of polyacrylonitrile. Carbon. 1991;29(8):1081-90.

[2] Gupta A, Harrison IR. New aspects in the oxidative stabilization of PAN-based carbon fibers: II. Carbon. 1997;35(6):809-18.

[3] He DX, Wang CG, Bai YJ, Lun N, Zhu B, Wang YX. Microstructural evolution during thermal stabilization of PAN fibers. Journal of Materials Science. 2007;42(17):7402-7.

[4] Josef S. Discoloration effect in acrylonitrile polymers. Journal of Polymer Science. 1958;28(117):438-9.

[5] Coleman MM, Sivy GT. Fourier transform ir studies of the degradation of polyacrylonitrile copolymers--I: Introduction and comparative rates of the degradation of three copolymers below 200°c and under reduced pressure. Carbon. 1981;19(2):123-6.

[6] Watt W, Johnson W. Mechanism of oxidization of polyacrylonitrile fibers. Nature. 1975;257(5523):210-2.

[7] Rangarajan P, Bhanu VA, Godshall D, Wilkes GL, McGrath JE, Baird DG. Dynamic oscillatory shear properties of potentially melt processable high acrylonitrile terpolymers. Polymer. 2002;43(9):2699-709.

[8] Fitzer E, Müller DJ. The influence of oxygen on the chemical reactions during stabilization of pan as carbon fiber precursor. Carbon. 1975;13(1):63-9.

[9] Ouyang Q, Cheng L, Wang H, Li K. Mechanism and kinetics of the stabilization reactions of itaconic acid-modified polyacrylonitrile. Polymer Degradation and Stability. 2008;93(8):1415-21.

[10] Ozawa T. A new method of analyzing thermogravimeteric data. Bull Chem Soc Jpn. 1965;38(11):1881-&.

[11] Kissinger HE. Reaction Kinetics in Differential Thermal Analysis. Analytical Chemistry. 1957;29(11):1702-6.

[12] Mittal J, Bahl OP, Mathur RB, Sandle NK. IR studies of PAN fibres thermally stabilized at elevated temperatures. Carbon. 1994;32(6):1133-6.

[13] Gupta A, Harrison IR. New aspects in the oxidative stabilization of pan-based carbon fibers. Carbon. 1996;34(11):1427-45.

[14] Chae HG, Minus ML, Rasheed A, Kumar S. Stabilization and carbonization of gel spun polyacrylonitrile/single wall carbon nanotube composite fibers. Polymer. 2007 Jun;48(13):3781-9.

[15] Fitzer E, Frohs W, Heine M. Optimization of stabilization and carbonization treatment of PAN fibres and structural characterization of the resulting carbon fibres. Carbon. 1986;24(4):387-95.

[16] Sivy GT, Gordon Iii B, Coleman MM. Studies of the degradation of copolymers of acrylonitrile and acrylamide in air at 200°C. Speculations on the role of the preoxidation step in carbon fiber formation. Carbon. 1983;21(6):573-8.

[17] Suresh KI. Viscoelastic properties of polyacrylonitrile terpolymers during thermo-oxidative stabilization (cyclization). Polymers for Advanced Technologies. 2008;19(7):831-7.

[18] Chae HG, Minus ML, Kumar S. Oriented and exfoliated single wall carbon nanotubes in polyacrylonitrile. Polymer. 2006;47(10):3494-504.

[19] Chae HG, Choi YH, Minus ML, Kumar S. Carbon nanotube reinforced small diameter polyacrylonitrile based carbon fiber. Composites Science and Technology. 2009;69(3-4):406-13.

[20] Dunn P, Ennis BC. Thermal analysis of polyacrylonitrle. 1. Melting of polyacrylonitrle. Journal of Applied Polymer Science. 1970;14(7):1795-9.

[21] Reghunadhan NCP, Krishnan K, Ninan KN. Differential scanning calorimetric study on the Claisen rearrangement and thermal polymerisation of diallyl ether of bisphenols. Thermochimica Acta. 2000;359(1):61-7.

[22] Ouyang Q, Cheng L, Wang HJ, Li KX. DSC study of stabilization reactions in poly(acrylonitrile-co-itaconic acid) with peak resolving method. J Therm Anal Calorim. 2008 Oct;94(1):85-8.

[23] Wang PH. Aspects on prestretching of PAN precursor: Shrinkage and thermal behavior. Journal of Applied Polymer Science. 1998 Feb;67(7):1185-90.

[24] Parkash OM, Bahl LMM. Shrinkage behaviour of polyacrylonitrile during thermal treatment. Angewandte Makromolekulare Chemie. 1975;48(1):145-59.

[25] Kim DY, Kim YC, Kim CY. Thermal Analysis of PAN Precursors of Carbon Fibers. Polymer (Korea). 1985;9(6):7.

[26] Hou YP, Sun TQ, Wang HJ, Wu D. Effect of heating rate on the chemical reaction during stabilization of polyacrylonitrile fibers. Text Res J. 2008 Sep;78(9):806-11.

CHAPTER 4

EFFECT OF STABILIZATION CONDITIONS ON THE RESULTING CARBON FIBERS

In the process of converting PAN precursor fibers into carbon fibers, oxidative stabilization which involves complex physical and chemical changes, is very important for obtaining high-performance carbon fibers [1-3] and needs to be carefully optimized, as the degradation of PAN may occur during this high temperature stabilization. The stabilization is strongly dependent on the precursor fiber properties, fiber diameter, co-monomer type, co-monomer content, etc.

For stabilization of PAN fibers in batch process, there are three controllable processing parameters including applied tension, temperature, and residence time. Based on the relationship of temperature and time, there are three possible heat-treatment profiles [4] including slow ramping, isothermal, and stepwise heating. In the present work, isothermal and stepwise temperature profiles were adopted. Based on the properties of the resulting carbon fibers, the effects of different stabilization processing parameters are compared and the best conditions are proposed for the composite fiber used in this study. In addition, the relationship between processing parameters and the resulting carbon fiber properties are discussed. Furthermore, for a methodological study of stabilization, different characterization methods, including shrinkage behavior, DMA, FTIR, and WAXD, are compared to obtain the best processing parameters. Characterization of stabilized fibers can be done in two ways: 1. real-time monitoring of property variations during stabilization, and 2. post processing characterization – i.e. the

characterization performed after stabilization. Here, the relationships between various characterization methods and optimum stabilization time are studied. A new method of monitoring dynamic mechanical properties was used in this study, which can narrow down the optimum stabilization time range.

4.1 Experimental

4.1.1 Materials

PAN polymer used in this study is same as that used for the studies discussed in chapters 2 and 3. CNT is same as that named as CNT1 in chapter 2. Composite fiber contains 1 wt% CNTs with respect to the polymer. The preparation of spinning solutions (15 wt. % PAN/CNT in DMAc) [5] and fiber spinning process are the same as described in chapter 2. A spinneret with 7 holes was used, and total draw ratio was 13.2. The properties of PAN/CNT fibers are summarized in Table 4.1.

Table 4.1 Mechanical and structural properties of PAN/CNT precursor fiber.

	PAN/CNT fiber
Tensile strength (GPa)	0.83 ± 0.09
Tensile modulus (GPa)	23.8 ± 2.4
Strain to failure (%)	6.6 ± 0.6
Diameter (μm)	8.3
f_{PAN}*	0.86
PAN crystal size (nm)**	9.5

*Note: * f*: Herman's orientation factor was calculated from azimuthal scan of PAN (110), (200) diffraction peak. **PAN crystal size was determined from (110) ,(200) reflection, using Scherrer's equation.

The precursor fibers have much better modulus and smaller diameter as compared with that used in chapter 2. The stabilization was carried out in a tube furnace

manufactured by Micropyretics Heaters International (Cincinnati, OH). The temperature inside the furnace was measured by a temperature probe and was used for the experiment.

4.1.2 Characterization methods

FTIR data was collected using infrared spectrometer (FTIR, Spectrum One, Perkin Elmer Corp.). 128 scans were collected with a resolution of 4 cm^{-1}. WAXD patterns were obtained by Rigaku micromax-002 using CuK_α (λ=0.1542 nm) radiation and a Rigaku R-axis IV++ detector. Shrinkage behavior and dynamic mechanical properties were measured by TMA (TA Q-400) manufactured by TA Instruments-Waters LLC. For DMA, a constant tension of 25 MPa (Stress calculation is based on the diameter of the precursor fiber) was applied, and force amplitude was set to be 4 MPa and the frequency was 1 Hz. The mechanical properties of single carbon fibers were tested on an RSA III solid analyzer (Rheometric Scientific Co.) at a crosshead speed of 0.1 %/s with a gauge length of 6 mm. Microstructure of carbon fibers was observed on S-800 and leo 1530 SEMs at an operating voltage of 10 kV, and the cross-sectional area was calculated using ImageJ image analysis software (NIH).

4.2 Results and discussions

4.2.1 Determining optimum stabilization time by real-time characterization method

Shrinkage behavior during stabilization was measured by TMA. As discussed in chapter 3, the shrinkage of PAN fiber can be divided into entropic shrinkage and reaction shrinkage. In this study, entropic relaxation was pre-released by heating the fiber from room temperature to 200 ^oC under 4 MPa at a heating rate of 5 ^oC/min; subsequently, temperature was quickly raised to desired temperature (typically in less than 40 sec), and

the reaction shrinkage was monitored. Figure 4.1 shows the isothermal reaction shrinkage curves obtained both in atmosphere of nitrogen and in air at various temperatures.

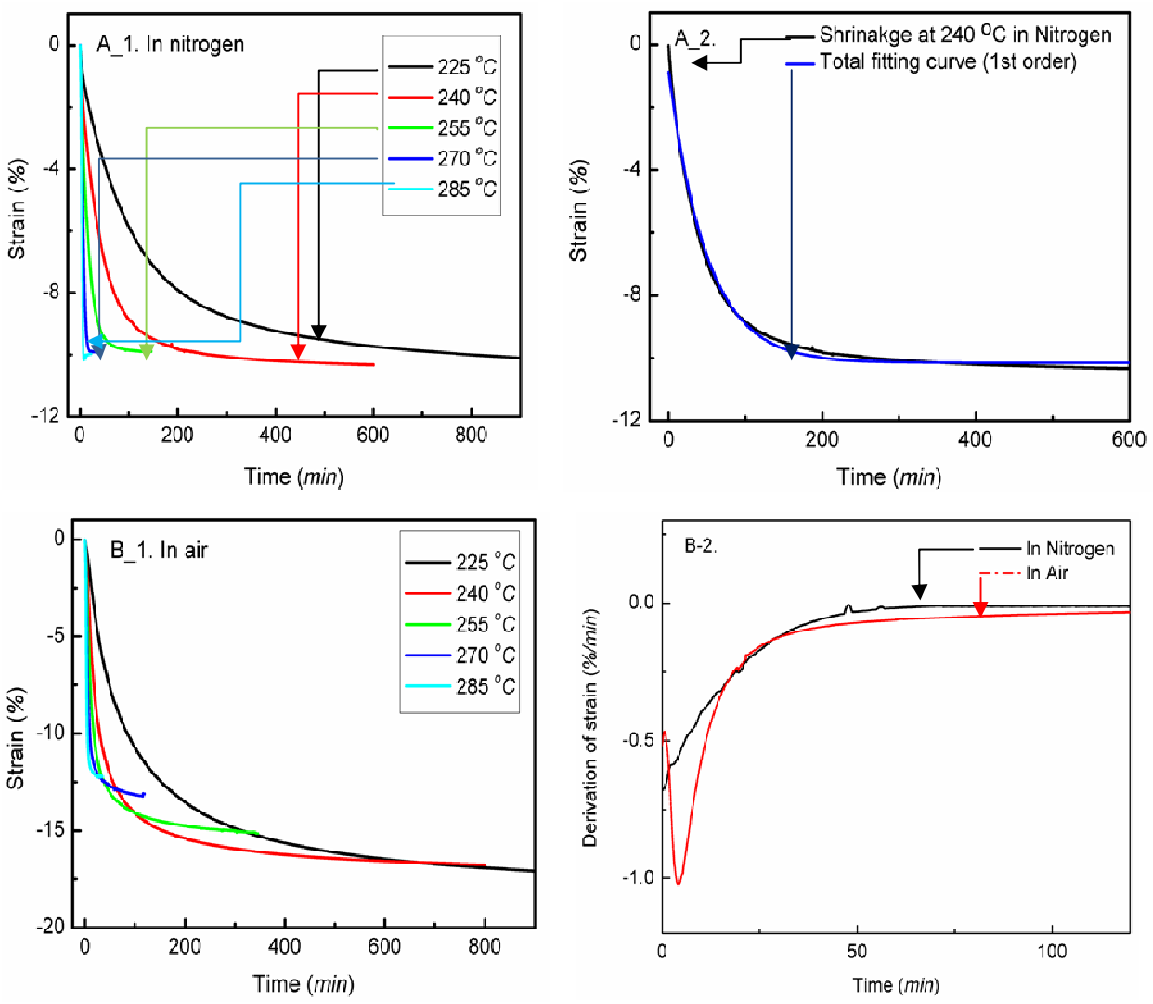

Figure 4.1 Chemical reaction shrinkage behavior of PAN/CNT composite fiber isothermally stabilized at various temperatures under a constant stress of 4 MPa. (A_1) in nitrogen, (A_2) comparison of experimental and fitting results. Curve fitting conducted using exponentially decaying function as described in the text, (B_1) in air, and (B_2) derivatives of strain with time for stabilizations at 255 ^{o}C in air and in nitrogen.

As can be seen from Figures 4.1(A_1) and (B_1), the stabilization temperature has little effect on the final reaction shrinkage of the fibers stabilized in nitrogen,

whereas, in air, a lower stabilization temperature results in a larger reaction shrinkage. Regardless of stabilization temperature, reaction shrinkage occurring during stabilization in air is larger than that in nitrogen. This is consistent with previous literature reports [6, 7] and the shrinkage results in chapter 3. The different shrinkage behaviors in different gas environments are due to different cyclization mechanisms. The cyclization reaction in air involves more inter-molecular reactions, such as oxidation and cross-linking, than that in nitrogen. Figure 4.1(B_2) shows the derivative of the reaction shrinkage-time curves obtained in air and in nitrogen at 255 ^{o}C. While the shrinkage in nitrogen slows down with time, there is an acceleration period (~ 5 min) for reaction shrinkage in air. Shrinkage rate is much faster in air as comparison with that in nitrogen. After ~ 60 min, shrinkage in nitrogen reaches a plateau; however, shrinkage in air requires more time to come to completion. The reaction shrinkage was reported to be correlated with the cyclization reaction [8, 9], and could be used to calculate the reaction activation energy. Reaction shrinkage was fitted by the equation, $L(t) = L(1-e^{-bt})$, where, L is chemical shrinkage, b is exponential parameter, and t is time. One example of fitted curve is shown in Figure 4.1(A_2). The exponential parameter *b* has Arrhenius-type dependence on the absolute reaction temperature and can be used to calculate the reaction activation. Using above equation to fit the shrinkage curves in air, it was found that correlation coefficient R^2 of fitting curve was only 0.96, which is much lower than that for the samples stabilized in nitrogen, $R^2 > 0.99$. The probable reason is that stabilization in air involves more complex reactions than that in nitrogen. To improve curve fitting, for the shrinkage in air, second order fitting was used, and the R^2 was improved to over 0.995. The second

order decay is fitted by the equations, $L(t) = L - L_1 \times \exp(-x/t_1) - L_2 \times \exp(-x/t_2)$,

$b_1 = 1/t_1$, $b_2 = 1/t_2$, $b = b_0 \exp(-\frac{E_a}{RT})$. The fitting results are listed in Table 4.2.

Table 4.2 Curve fitting results of PAN/CNT fibers stabilized in air at various temperatures under a constant tension of 4 MPa.

Curve fitting results		Temperature (^{o}C)				
		225	240	255	270	285
1st order	*Ln(b)*	-4.82	-3.87	-2.94	-1.81	-0.94
2nd order	L_1	8.35	4.66	3.44	2.03	--
	$ln(b_1)$	-5.46	-5.08	-4.44	-3.87	--
	L_2	8.35	12.47	12.77	14.14	16.88
	$ln(b_2)$	-3.76	-2.99	-2.32	-1.50	-0.92

In the plot of *ln(b)* versus *1/T*, the slope of fitted line is linear to activation energy. The fitting lines are shown in Figure 4.2. The calculated value of activation energy from first order fitting is close to the cyclization reaction activation energy calculated from DSC data in chapter 3, 138.5 kJ/mol. The difference may be caused by different fiber spinning conditions adopted in these studies. From second order fitting, two activation energies can be obtained, one is 110.6 kJ/mol and the other is 80.9 kJ/mol. The activation energy of 80.9 kJ/mol is close to the oxidation reaction's activation energy, which is 91.1 kJ/mol. Also the reaction with the activation energy of 80.9 kJ/mol needs longer time to complete. Therefore, it can be considered that the lower activation energy reaction is the oxidation reaction. The reaction with higher activation energy can be related to cyclization. Lower cyclization reaction activation energy in air (110.6 kJ/mol) than in nitrogen (138.5 kJ/mol) suggests that oxygen present in air facilitates the cyclization reaction. In the derivation curves of PAN/CNT1 fibers in nitrogen and in air (Figure

4.1B-2), an initial accelerating period can be observed for shrinkage in air, which also indicates that oxygen stimulates cyclization reaction.

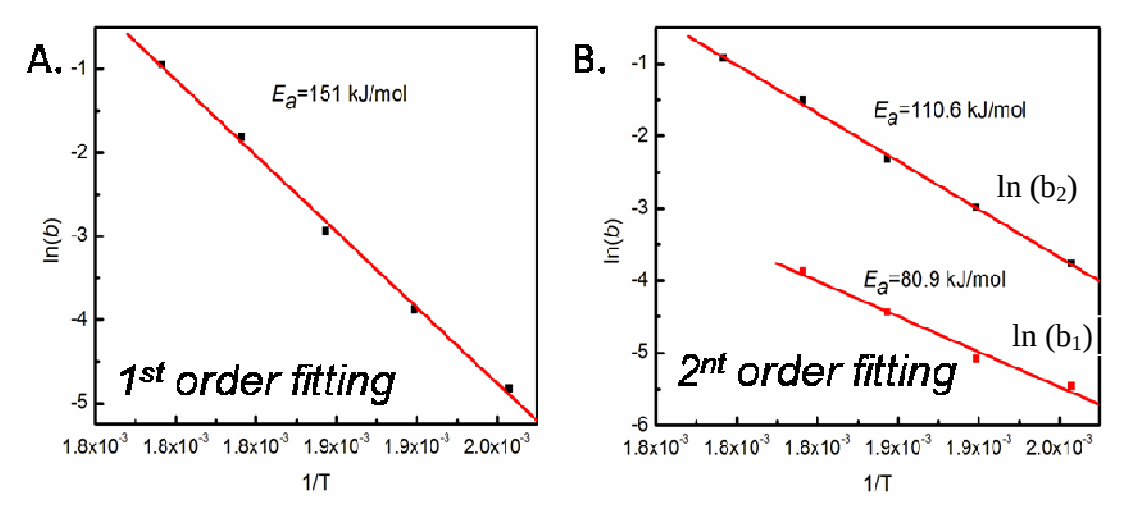

Figure 4.2 Arrhenius-type of dependence of *b* and *T* of shrinkage of PAN/CNT fibers in air. A: first order fitting; B: second order fitting.

The calculated activation energy by first order decay, and transition time that is required for shrinkage to reach its maximum value are listed in Table 4.3. Since reaction shrinkage has direct relationship with stabilization reaction, it is possible to use it as criteria to find the optimum residence time.

Table 4.3. Residence time and reaction activation energy from reaction shrinkage data.

Environment	Transition time (min)*					Activation energy** (kJ/mol)
	225 °C	240 °C	255 °C	270 °C	285 °C	
Nitrogen	600	240	130	30	10	151
Air	800	420	240	120	30	142

Note: * Transition time is defined as the time when shrinkage reaches the maximum value. ** Activation energy was calculated from first order fitting of the shrinkage data.

From Table 4.3, it can be seen that fibers stabilized in air need more time for reaction completion than fibers stabilized in nitrogen. Also, for stabilization reactions in air, the oxidative reaction happens after the cyclization reaction. This reaction can be limited either by the cyclization reaction or by oxygen diffusion. Since the stabilization reactions in air occur over longer time than that in nitrogen, it suggests that the stabilization in air is limited by the oxygen diffusion. In the later stages of stabilization, reaction shrinkage in air changes slowly with the stabilization time, making it difficult to determine the accurate time of the end of the reactions. The curing process of thermosetting materials has been widely studied by investigating dynamic mechanical properties [10, 11]. By comparing the transition of storage modulus and loss tangent, gelation time can be obtained and the extent of chemical conversion can be calculated. During the oxidative stabilization of PAN, cyclization and other reactions lead to cyclization and cross-linking etc. Changes in visco-elastic properties during oxidative stabilization have been reported and were used to compare the influence of the precursor polymer [12]. Here, storage modulus and loss modulus were recorded by TMA as a function of stabilization time (Figure 4.3). Same temperature profile as in the shrinkage experiments was used to monitor the variation of dynamic mechanical properties. During the isothermal stabilization, the storage modulus continuously increases and reaches a plateau; whereas, loss modulus reaches its maximum value and then slowly decreases.

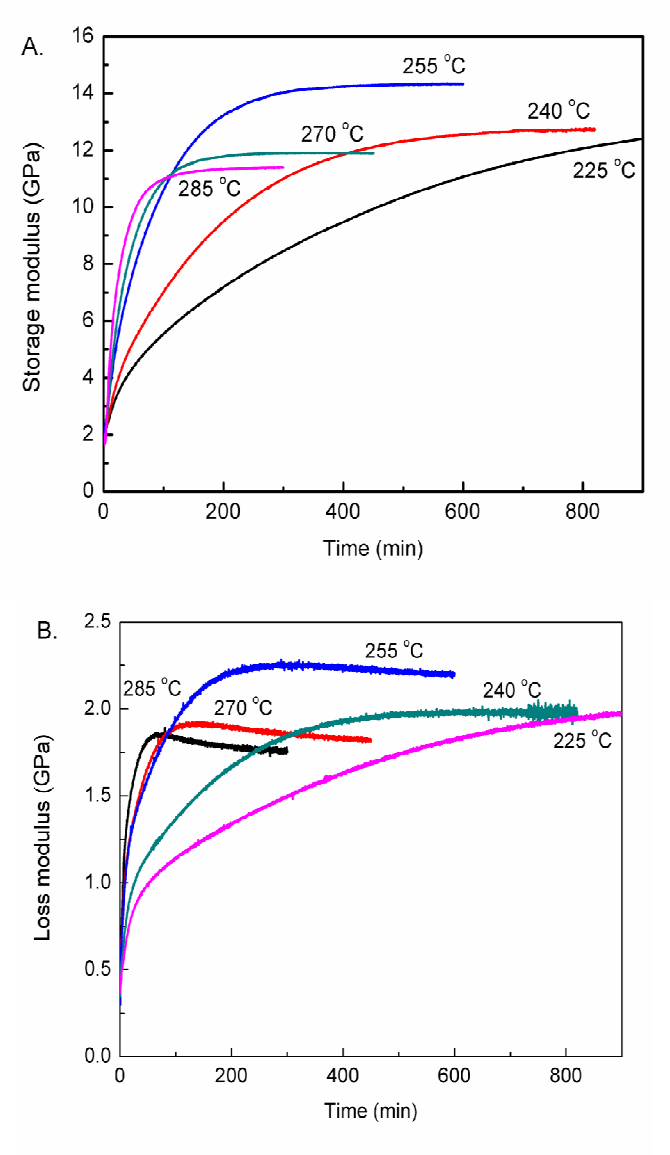

Figure 4.3 Dynamic mechanical behavior of fiber isothermally stabilized at different temperatures under air. (A) Storage modulus and (B) loss modulus.

From the studies reported in chapters 2 and 3, the sequence of stabilization reactions in homo-polymer PAN is known to be cyclization, then oxidation, followed by additional cross-linking. Different reactions show different effect on the dynamic mechanical properties. The cyclization reaction increases the storage modulus, whereas destruction of PAN crystals leads to increase of loss modulus. The additional cross-

linking reactions lead to further increase in storage modulus and decrease in loss modulus. The transition times, defined as the time that either storage or loss modulus reaches its maximum value, are listed in Table 4.4.

Table 4.4 Transition times obtained from dynamic mechanical test for stabilization in air.

	Transition time (min)*				
	225 °C	240 °C	255 °C	270 °C	285 °C
Loss modulus	820	510	260	120	70
Storage modulus	>900	700	420	270	190

Note: * Transition time is defined as the time when modulus reaches the maximum value.

The transition time of storage modulus indicates all stabilization reactions are completed; however, it may lead to over-stabilization since reactions will continue to occur during the heating stage of carbonization process, including thermal degradation. The transition time of loss modulus indicates that oxidative reaction is almost complete and additional cross-linking reactions become dominant. Therefore, the optimum stabilization time may be between these two transition times.

4.2.2 Determining optimum stabilization time by post-process characterization methods

PAN/CNT composite fibers were first stabilized in air, and then carbonized in argon to produce carbon fibers to determine the optimum stabilization time. In this study, 255 °C was used as the stabilization temperature, since the storage modulus of fibers stabilized at 255 °C was the highest among all the other fibers stabilized at different temperatures. The optimum stabilization time determined by shrinkage and dynamic mechanical property experiments lies in the range of 240 ~ 420 minutes. During

carbonization, temperature was increased from room temperature to 1100 ^{o}C at a heating rate of 5 ^{o}C/min, and then the sample was isothermally carbonized for 10 min. During stabilization and carbonization, constant tension of 35 MPa and 4 MPa were applied, respectively, using a pair of graphite clamps.

The chemical and physical structural changes of the stabilized fiber were characterized by FTIR and WAXD. Figure 4.4A shows the infrared spectra of the stabilized fibers. With increasing stabilization time, the peak intensity of nitrile band (at 2243 cm^{-1}) continuously decreases and broadens, as well a broad peak appeares and increases at around 1595 cm^{-1}, which is due to the formation of ladder polymer. The stabilization index (I_s) [13] is defined as the ratio of peak height of 1595 cm^{-1} to the peak height of 2243 cm^{-1}, which is proportional to the ratio of ladder polymer over the residual nitrile group (Figure 4.4B). It can be observed that I_s continuously increases with increase in stabilization time. As mentioned earlier, nitrile band becomes broader during stabilization, which is caused by the formation of β-amino nitrile at 2194 cm^{-1} and conjugated nitrile at 2218 cm^{-1}. As the stabilization progresses, amount of unreacted nitrile reduces, and that of β-amino nitrile and conjugated nitrile increase, leading to changes of the nitrile band shape and position. The dependence of the peak position of nitrile band on stabilization time is shown in Figure 4.4B. After the fiber was stabilized for over 200 minutes, a transition of the peak position of nitrile band was observed. A very low fraction of unreacted nitrile still remains even after fiber was stabilized for 300 minutes, due to the isolation of these nitrile groups and the difficulty of forming them into ladder structure.

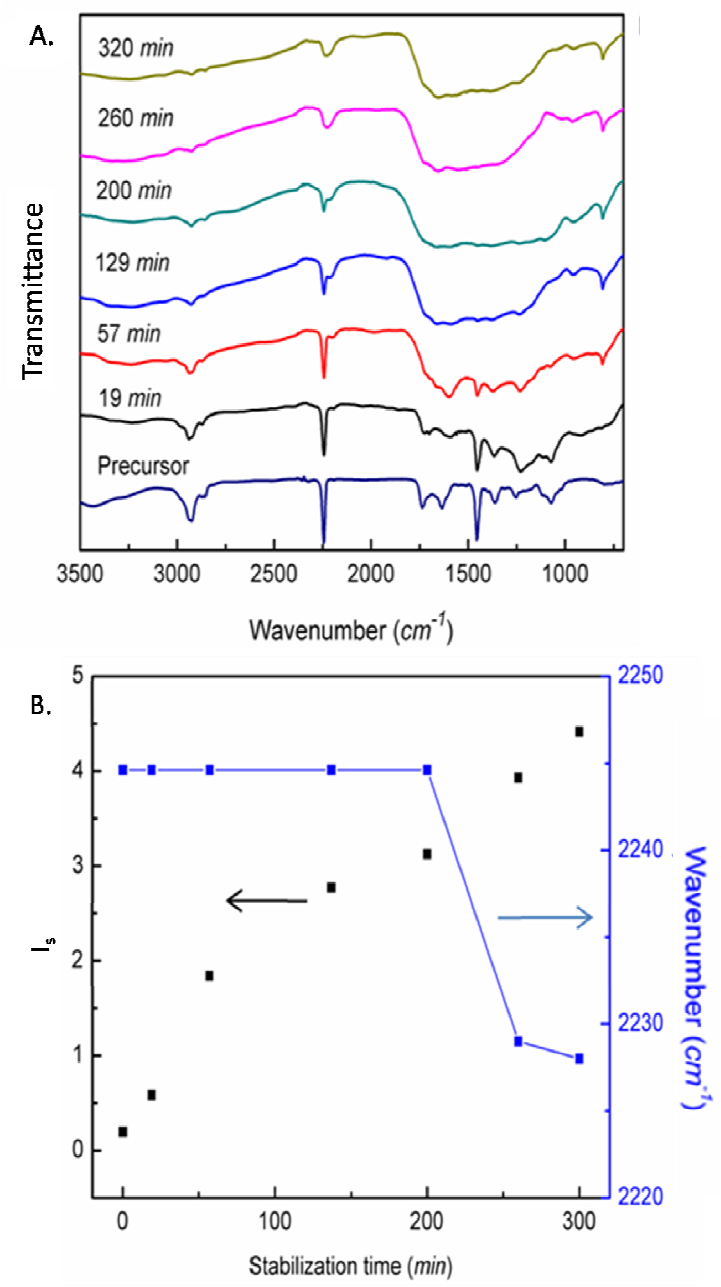

Figure 4.4 FTIR results of fibers stabilized at 255 ^{o}C for various times under air. (A) FTIR spectra and (B) Stabilization index I_s and peak position of nitrile band. FTIR spectra in (A) are shifted upward for clear comparison.

The ladder polymer formation in stabilized fibers was characterized by WAXD. The integrated XRD curves, Herman's orientation factor of formed aromatic structure,

and stabilization index are shown in Figure 4.5. Based on the change of intensity of the PAN (200),(110) peak, the stabilization index (I'_s) [14] is calculated by equation $I'_s = \frac{I_0 - I}{I_0}$ and shown in Figure 4.5B, where, I_0 is Intensity of PAN (200),(110) peak in precursor fibers, and I is Intensity in stabilized fibers. In the integrated WAXD patterns shown in Figure 4.5A, the diffraction peak at $2\theta=16.7^o$ corresponding to the (200), (110) planes of PAN crystal decreases during stabilization and almost disappears after thermal treatment for 260 minutes at 255 ^{o}C. The stabilization index, I'_s, increases rapidly at first, then increases slowly. After the fibers were stabilized at 255 ^{o}C for 260 min, I'_s is more than 0.9. The increase of peak intensity at $2\theta \sim 25.5^o$ is due to the formation of cyclized ladder structure. The orientation of the ladder polymer is also calculated from the azimuthal scan and is shown in Figure 4.5B. The Herman's orientation factor of the ladder polymer increases during stabilization, reaches the maximum value at 260 min, and subsequently at further prolonged stabilization decreases, possibly because of degradation by over-stabilization.

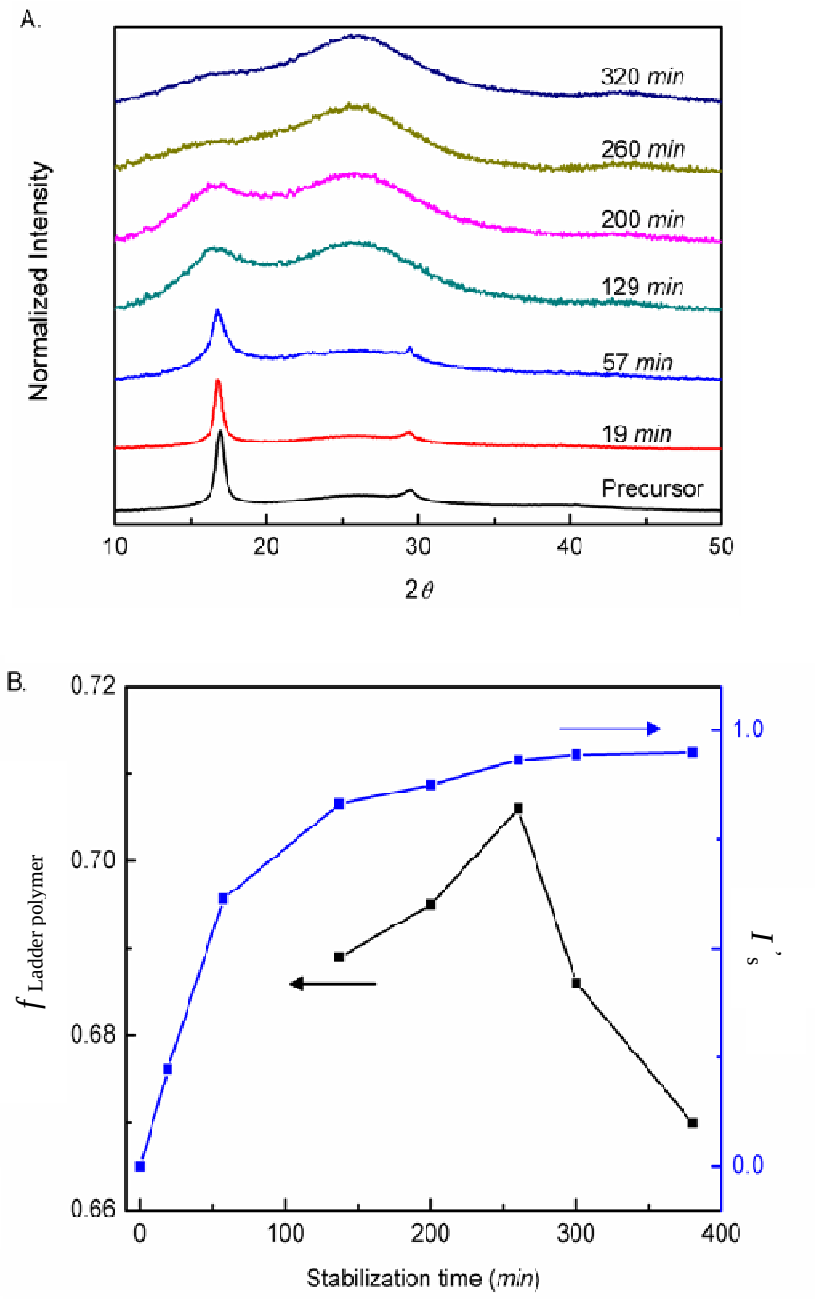

Figure 4.5 WAXD results of fibers stabilized at 255 ^{o}C for various times. (A) Integrated scans and (B) variation of $f_{\text{Ladder polymer}}$ (Herman's orientation factor of stabilized ladder polymer) and I'_{s} (stabilization index) as a function of stabilization time. Intensity profiles of integrated scans in (A) are shifted upward for clear comparison.

The mechanical properties of the resulting carbon fibers are listed in Table 4.5. The stabilization time shows significant effect on the final tensile properties of the resulting carbon fiber. Based on the tensile properties of carbon fibers, the best stabilization time was around 260 minutes at 255 ^{o}C. Either longer or shorter stabilization time reduces the strength of the resulting carbon fibers. The variations of mechanical properties of the ultimate carbon fiber are in agreement with the structural analysis results of the stabilized fibers.

Table 4.5 Mechanical properties of resulting carbon fibers after stabilized at 255 ^{o}C under 35 MPa with various stabilization times. Carbonization was carried out at 1100 ^{o}C using 4 MPa of pre-tension. Fiber diameter is about 4.7 μm.

Stabilization time (min)	Tensile strength (GPa)	Tensile modulus (GPa)	Strain to failure (%)
19	0.79 ± 0.10	134 ± 11	0.60 ± 0.09
57	0.85 ± 0.08	173 ± 16	0.49 ± 0.13
130	1.05 ± 0.11	188 ± 12	0.57 ± 0.08
200	1.34 ± 0.12	197 ± 23	0.67 ± 0.11
260	1.58 ± 0.14	204 ± 16	0.80 ± 0.09
320	1.48 ± 0.09	207 ± 12	0.75 ± 0.12

4.2.3 Effect of tension on the resulting carbon fibers

It has been reported that the tension applied during thermal treatment to manufacture the carbon fibers is very important to enhance the mechanical properties of the resulting carbon fibers [1, 15-17]. In the current experiment, the applied tension during stabilization and carbonization was kept constant at 35 MPa. The mechanical properties of the resulting carbon fiber are listed in Table 4.6. The average fiber diameter was calculated from the fiber cross-section images observed under SEM. The applied tension during carbonization shows significant influence on the final properties of

resulting carbon fibers. With an increase in the tension from 4 MPa to 35 MPa, the strength of the resulting carbon fiber increased from 1.6 GPa to 3.6 GPa when stabilization time was 260 min. In addition, it should also be noted that the residence time during stabilization is very important to the resulting carbon fiber properties. As listed in Table 4.6, stabilization time was incremented in 15 min steps from 230 min to 290 min. A 15 min difference in stabilization time reduces the tensile strength by up to 10% in comparison with that of the best sample stabilized for 260 min.

Table 4.6 Mechanical properties of resulting carbon fibers after stabilized at 255 ^{o}C with various stabilization times. Carbonization was carried out at 1100 ^{o}C using 35 MPa of pre-tension. Carbon fiber diameter is about 4.5 μm.

Stabilization time (min)	Tensile strength (GPa)	Tensile modulus (GPa)	Strain to failure (%)
230	2.55 ± 0.53	214 ± 34	1.16 ± 0.13
245	3.24 ± 0.43	246 ± 22	1.20 ± 0.13
260	3.60 ± 0.40	245 ± 19	1.47 ± 0.25
275	3.17 ± 0.50	246 ± 24	1.24 ± 0.16
290	2.74 ± 0.42	225 ± 34	1.17 ± 0.24

Figure 4.6 shows the cross-sections of the stabilized fibers and the resulting carbon fibers cut by a sharp blade. Fibrous structure can be seen and it shows very uniform distribution of CNTs through the whole cross-section of fibers, which indicates that carbon nanotubes are well dispersed in PAN matrix.

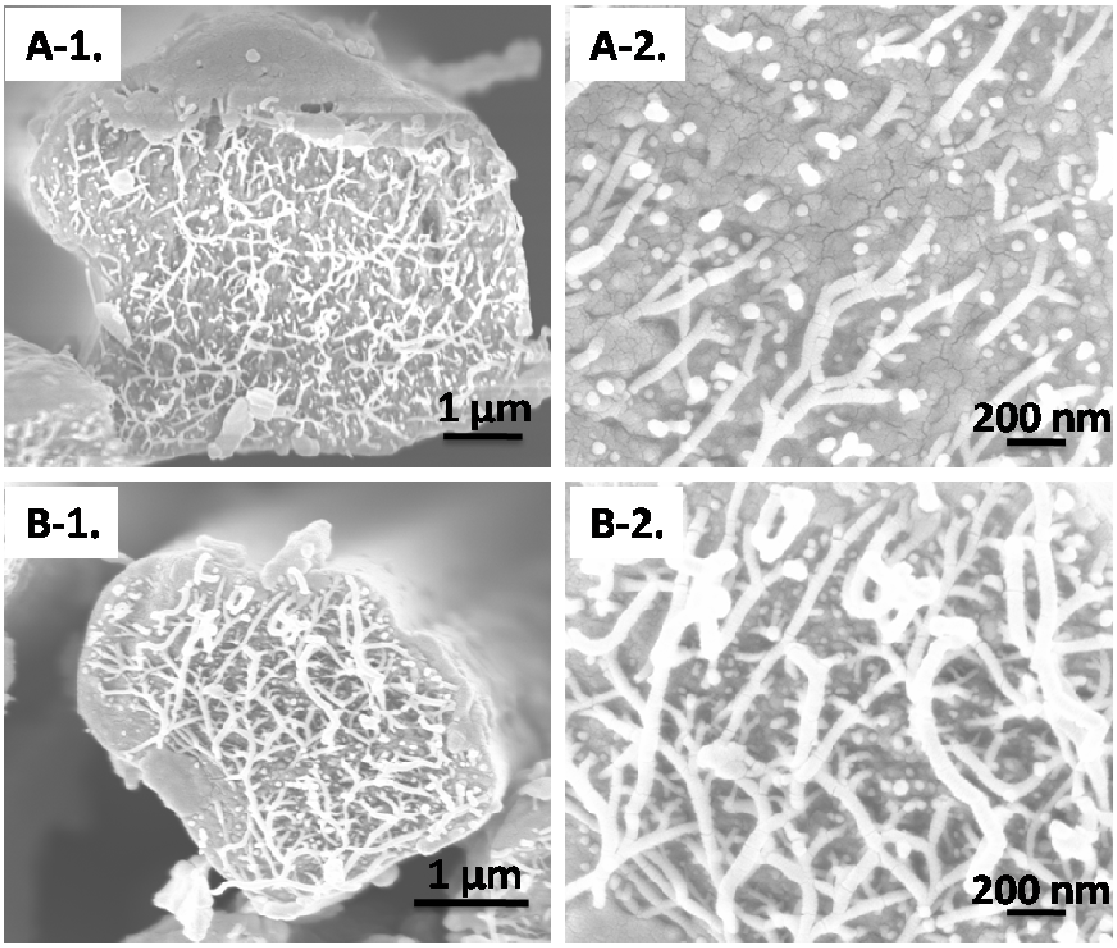

Figure 4.6 Cross-sectional images by SEM. A-1, A-2: The precursor fiber was stabilized at 255 ^{o}C for 260 minutes under a constant stress of 35 MPa. B-1, B-2: Stabilized fibers were further carbonized at 1100 ^{o}C under a constant stress of 35 MPa. Fibrillar structure exhibits that CNTs are uniformly distributed throughout the fiber cross-section.

To further explore the effect of applied tension, the constant stress during stabilization and carbonization was increased from 35 MPa to 46 MPa. The mechanical properties of the resulting carbon fibers are listed in Table 4.7. Comparing the best stabilization time under different tensions in Table 4.6 and Table 4.7, it can be seen that higher tension reduces the optimum stabilization time.

Table 4.7 Mechanical properties of resulting carbon fibers after stabilized at 255 °C with various stabilization times. Carbonization was carried out at 1100 °C. A tension of 46 MPa was applied during treatment. Carbon fiber diameter is about 4.4 µm.

Stabilization time (min)	Tensile strength (GPa)	Tensile modulus (GPa)	Strain to failure (%)
200	3.10 ± 0.42	266 ± 16	1.17 ± 0.12
215	3.78 ± 0.51	271 ± 35	1.33 ± 0.14
230	4.03 ± 0.46	289 ± 32	1.40 ± 0.13
245	3.83 ± 0.47	291 ± 32	1.34 ± 0.16
260	3.02 ± 0.57	256 ± 42	1.20 ± 0.13

The shrinkage curves of the fibers under different tensions during stabilization detected by TMA are shown in Figure 4.7. Higher stress leads to less shrinkage or even stretching of the fiber.

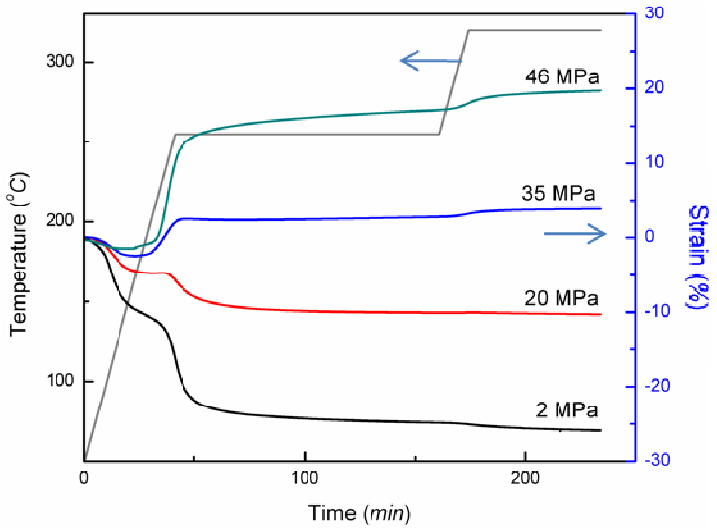

Figure 4.7 Shrinkage behavior of fibers stabilized under various stresses, showing the significant effect of stress on the shrinkage by chemical reaction. This suggests that the higher stress can minimize fiber shrinkage or even stretch the fiber (46 MPa). Heating profile for these experiments is also shown in the figure.

In the case of stabilized fiber using 35 MPa and 46 MPa, the fiber is stretched to ~ 4 %, and to over 20 %, respectively. Assuming poisson's ratio is 0.5, the diameter of

stabilized fiber under 46 MPa will be ~ 8 % smaller than that under 35 MPa. The smaller diameter fiber shortens the oxygen diffusion distance to the center of fiber, and ultimately reduces the diffusion time. Since the stabilization reaction is limited by oxygen diffusion, the higher applied stress may expedite the stabilization reaction.

Herman's orientation factors of the stabilized fibers and the carbonized fibers were calculated from azimuthal scans, and they were found to slightly increase from 0.69 to 0.70 and from 0.88 to 0.90, respectively, when the applied stress was increased from 35 MPa to 46 MPa. The modulus of resulting carbon fiber with optimum stabilization time improved from 245 GPa to 289 GPa. The higher orientation of the carbon structure leads to higher modulus of the resulting carbon fibers. It is noted that no compliance correction was applied to the modulus data. The tensile strength of resulting carbon fibers also improved from 3.60 GPa to 4.03 GPa.

The 46 MPa tension is the highest tension that can be applied during thermal treatment without breaking the fiber. To obtain the best properties of resulting carbon fibers, the maximum tension should be applied during heating treatment. It was [18] reported that not the highest tension, but a suitable tension shows the best effect on the mechanical properties of resulting carbon fibers. In the present study, the highest tension is found to be the best one to enhance carbon fiber properties. This discrepancy may lie in the fact that the stabilization time which is affected by the applied tension was not considered in the previous literature, and a fixed stabilization time was used. Here, if the stabilization time is fixed at 260 min, the tensile properties of the resulting carbon fiber will decrease when applied stress is increased from 35 to 46 MPa; however, the optimum stabilization time depends on both tension and temperature, and must be considered.

4.2.4 Effect of stabilization temperature on the resulting carbon fibers

It is discussed in previous chapter that the different stabilization reactions were separated by using nitrogen and air as gas environments sequentially. Same method is used here and the DSC curves are shown in Figure 4.8.

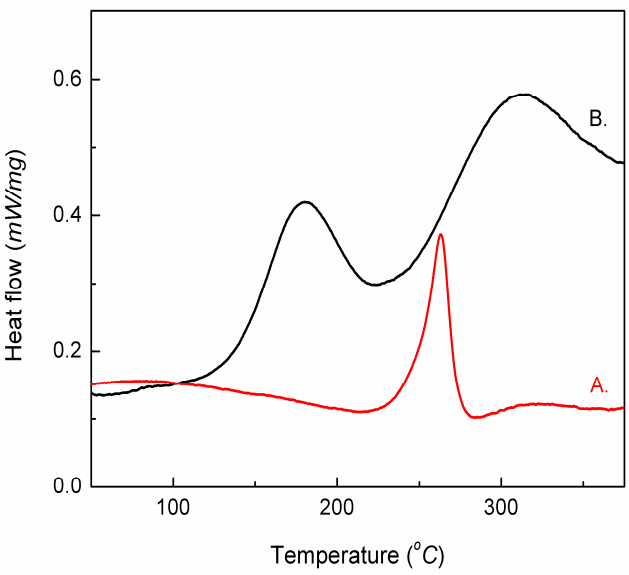

Figure 4.8 DSC curves of PAN/CNT composite precursor fiber at a heating rate of 1 ^{o}C/min. (A) in nitrogen and (B) Sample A re-run in air.

When the fiber is re-heated in air after in nitrogen, two exothermic peaks related to oxidation reaction and additional cross-linking reaction, respectively, appear. It has been found that the additional cross-linking reaction happens at a temperature over 300 ^{o}C [20, 21]. If the additional cross-linking reaction is enhanced, will it improve the final mechanical properties of the resulting carbon fiber? To answer this question, after the fiber was isothermally stabilized at 255 ^{o}C for 120 minutes, temperature was raised to 320 ^{o}C at a rate of 5 ^{o}C/min, and fiber was isothermally stabilized for various times. 320 ^{o}C is the exothermic peak temperature of the additional cross-linking reaction in DSC

curve (Figure 4.8, curve B). Stabilized fibers were then carbonized at 1100 ^{o}C. The dynamic mechanical properties measured during stabilization are shown in Figure 4.9. For stabilization at 320 ^{o}C, the transition times for loss and storage moduli are 10 min and 45 min, respectively. According to these moduli transition times, the stabilization time at 320 ^{o}C was step-wisely changed from 15 min to 35 min.

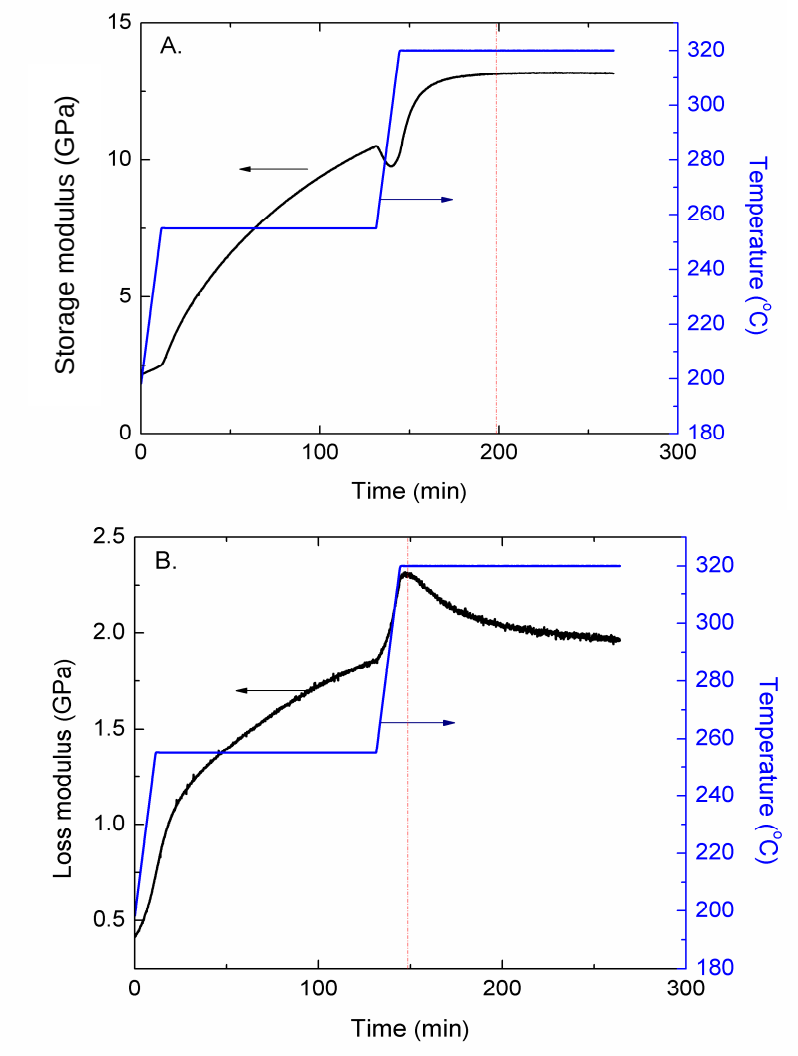

Figure 4.9 Dynamic mechanical behavior of PAN/CNT precursor fiber during stepwise stabilization in air. Heating profile is also given in the plot. Stabilization temperatures are 255 and 320 ^{o}C, and heating rate was 5 ^{o}C/min. (A) Storage modulus and (B) loss modulus.

The mechanical properties of the resulting carbon fibers are listed in Table 4.8. Comparing the data in Table 4.6 and in Table 4.8, the total stabilization time is reduced while stabilization temperature is increased. Final properties of the resulting carbon fibers become much more sensitive to stabilization time when stabilization temperature is higher. Comparing the fibers further stabilized for 22.5 min at 320 ^{o}C to that stabilized only at 255 ^{o}C for 260 min at a same tension of 35 MPa, the tensile strength of the resulting carbon fibers improved from 3.60 GPa to 3.97 GPa, and tensile modulus improved from 245 GPa to 286 GPa. When the fibers are further stabilized at a high temperature, the additional cross-linking reaction is enhanced, significantly improving the tensile modulus of the resulting carbon fibers while the elongation at break remains at the same level.

Table 4.8 Mechanical properties of resulting carbon fibers after stabilization at 255 ^{o}C for 120 minutes, then at 320 ^{o}C for various stabilization times. Carbonization was carried out at 1100 ^{o}C using 35 MPa of pre-tension. Carbon fiber diameter is about 4.4 μm.

Stabilization time (min)	Tensile strength (GPa)	Tensile modulus (GPa)	Strain to failure (%)
15	3.17 ± 0.63	282 ± 29	1.14 ± 0.20
20	3.24 ± 0.43	294 ± 23	1.24 ± 0.14
22.5	3.97 ± 0.42	286 ± 31	1.42 ± 0.15
25	3.74 ± 0.50	267 ± 32	1.34 ± 0.14
35	2.86 ± 0.62	262 ± 30	1.08 ± 0.10

The Integrated XRD curves of the stabilized fibers are shown in Figure 4.10. The PAN (200), (110) diffraction peak completely disappears. It can be observed that the peak from aromatic structure slightly shifted its peak position from 25.05 to 25.12 when the stabilization temperature was raised from 255 ^{o}C to 320 ^{o}C, indicating that the additional cross-linking reaction makes the stabilized fiber more compact.

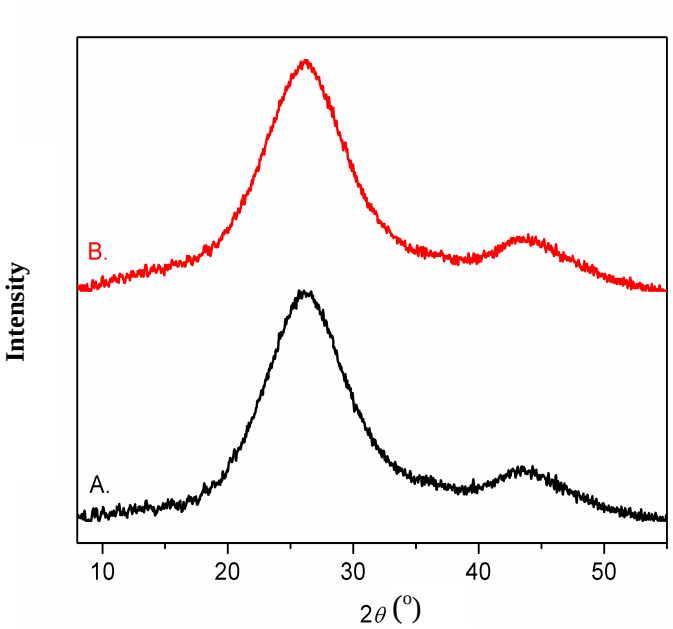

Figure 4.10 Integrated WAXD scans of stabilized PAN/CNT composite fibers. (A) Stabilized at 255 °C for 120 min then 320 °C for 22.5 min and (B) stabilized at 255 °C for 260 min. Both fibers exhibit comparable structure. Intensity profile of sample B is shifted upward for clear comparison.

Azimuthal scans of the stabilized fibers are also shown in Figure 4.11. Sharp peaks can be found in both of the azimuthal curves, due to the highly ordered ladder polymer formed due to the addition of CNTs [21]. Using the same curve fitting method described elsewhere [21], the contributions from the highly ordered regions and the matrix can be deconvoluted. This curve fitting data is listed in Table 4.9. The Herman's orientation factor of the fiber further stabilized at 320 °C is slightly lower than the fibers stabilized at 255 °C; however, the fraction of highly ordered region increases from 2.5 % to 3.3 % upon further stabilization. The Herman's orientation factors for the carbonized fiber are 0.88 and 0.87 for the fiber stabilized at 255 °C and the fiber further stabilized at 320 °C, respectively.

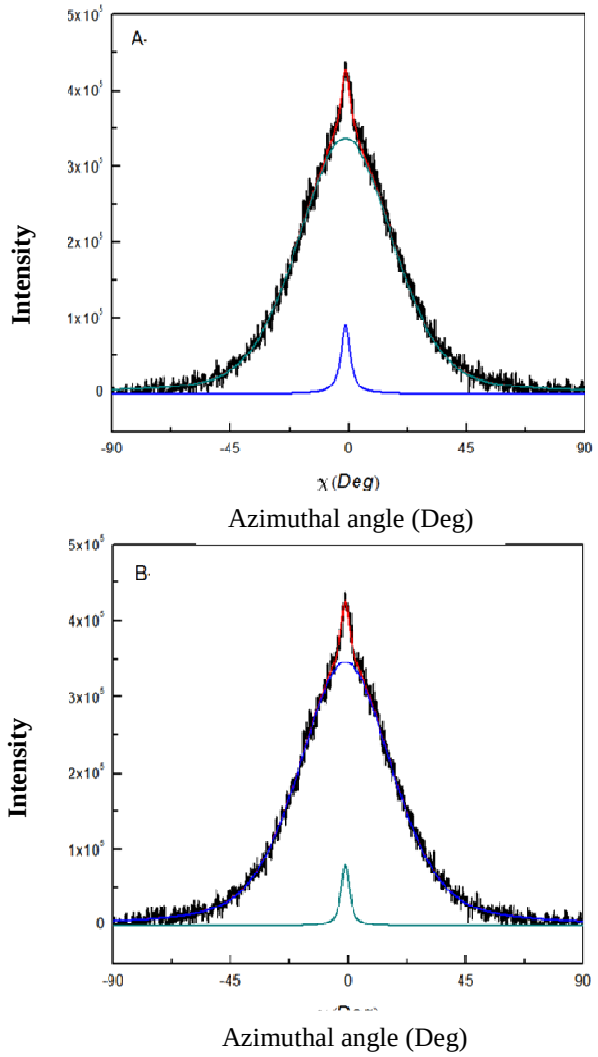

Figure 4.11 Azimuthal WAXD scans of 2θ ~25^{o} in stabilized PAN/CNT composite fibers. (A) Stabilized at 255 ^{o}C for 120 min then 320 ^{o}C for 22.5 min and (B) stabilized at 255 ^{o}C for 260 min.

Table 4.9 WAXD analysis results of azimuthal scans of 2θ ~25^{o} for the stabilized fibers.

Stabilization conditions	f Overall	Highly ordered region		Matrix	
		f	Area (%)	f	Area (%)
At 255 ^{o}C for 260 min	0.69	0.95	2.5	0.68	97.5
At 255 ^{o}C for 120 min, then 320 ^{o}C for 22.5 min	0.68	0.94	3.3	0.67	96.7

The improvement of the modulus in the resulting carbon fibers with elevated stabilization temperature at 320 ^{o}C is due to the higher volume fraction of the highly

ordered phase caused by the additional cross-linking reactions. Raman spectra of the stabilized fibers and the carbonized fibers are shown in Figure 4.12. The intensity of the peak at 1585 cm^{-1} increases when the fibers are further stabilized at 320 ^{o}C. This peak comes from the tangential vibration of graphitic structure (G-band) and indicates that additional cross-linking reaction at 320 ^{o}C leads to the formation of a 2-D graphitic structure. Such kind of structure is not observed in the fibers stabilized at a relatively low temperature of 255 ^{o}C. The Raman spectra of the carbonized fibers show similar results.

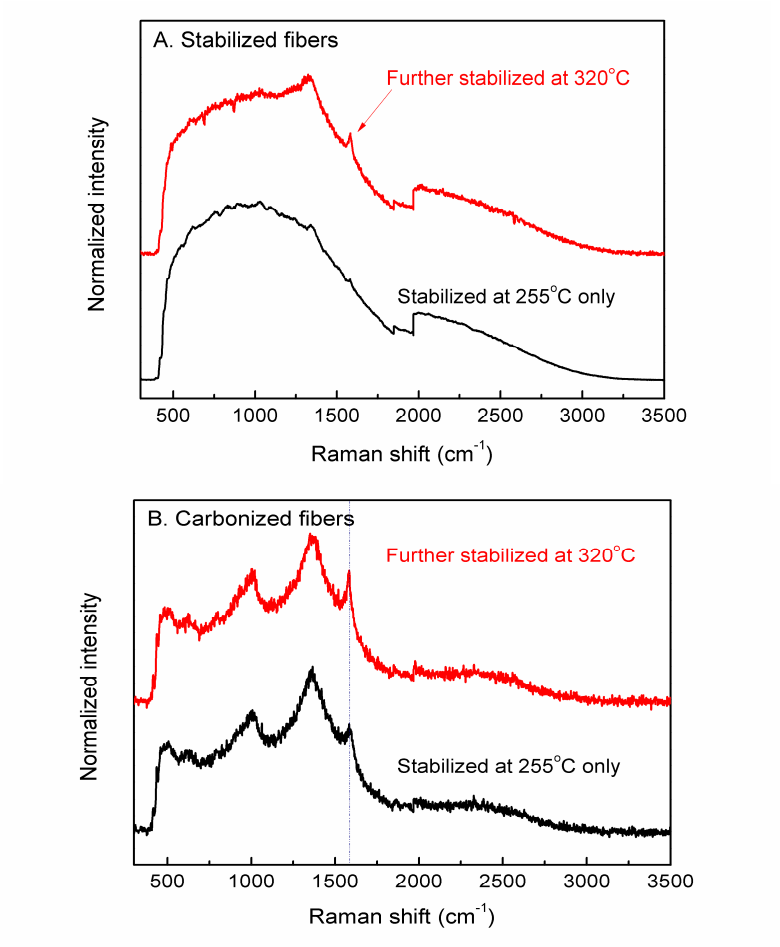

Figure 4.12 Raman spectra of (A) stabilized fiber and (B) carbon fiber undergo different stabilization conditions. Top spectrum is from the fiber stabilized at 255 ^{o}C for 2 hr, then at 320 ^{o}C for 22.5 min. Bottom spectrum is from the fiber stabilized at 255 ^{o}C only.

4.2.5 Effect of carbonization temperature on the resulting carbon fibers

For fibers further stabilized at 320 ^{o}C for 22.5 minutes under a stress of 35 MPa, carbonization was carried out at various temperatures, 1100, 1300, and 1500 ^{o}C. The mechanical properties of the resulting carbon fibers are listed in Table 4.10. With increase in carbonization temperature, the fiber diameter and the elongation at break decreased and the modulus increased. The higher carbonization temperature at 1300 ^{o}C marginally improves the strength of the resulting carbon fiber. Subsequent carbonization at 1500 ^{o}C results in significant decrease in tensile strength as well as decrease in strain to failure. The images of carbon fiber surfaces observed by SEM are shown in Figure 4.13. The surface of fibers carbonized at 1100 ^{o}C is very smooth. When carbonization temperature was increased to 1300 ^{o}C, the surface of the carbon fiber becomes rough with particle-like structure, with a diameter of tens of nm, appearing on the surface. When the carbonization temperature was increased to 1500 ^{o}C, a porous structure can be seen on the fiber surface with dimensions on the order of about 50 nm. These surface defects decrease the tensile strength of the resulting carbon fibers. Since carbonization was done in batch process, the exposure time of fibers to carbonization temperature of over 1000 ^{o}C is typically more than 4 hr. As compared to the industrial carbon fibers production set-up. This exposure time is very long and it is conceivable that thermal degradation may occur during carbonization leading to poor mechanical properties of the resulting carbon fibers. Additionally, as pointed out by Watt [22], the decrease in strength at 1500 ^{o}C may have been due to impurities such as foreign particles present in the environment during fiber spinning and heat treatment. These impurities will lead to defects in the carbon fiber structure, and will lower the fiber properties.

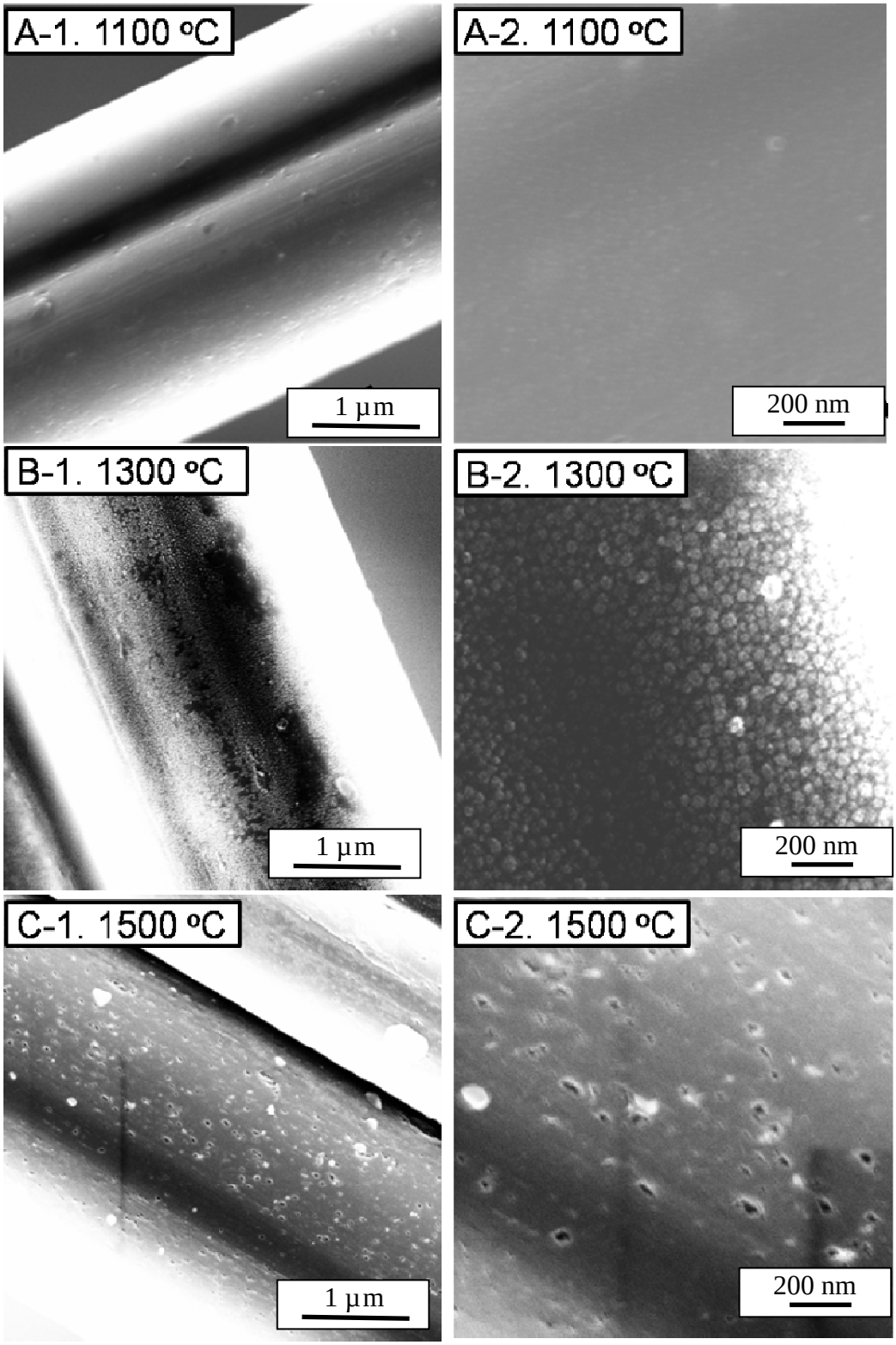

Figure 4.13. Surface morphologies of carbonized fibers after stabilized at 255 ^{o}C for 120 minutes and then stabilized at 320 ^{o}C for 22.5 minutes under a tension of 35 MPa. A: Carbonized at 1100 ^{o}C; B: Carbonized at 1300 ^{o}C; C: Carbonized at 1500 ^{o}C.

Table 4.10 Mechanical properties of resulting carbon fibers after stabilized at 255 ^{o}C for 120 minutes, then at 320 ^{o} for 2.25 minutes and carbonized at various temperatures using 35 MPa of pre-tension.

Temp $_{Carbonization}$ (^{o}C)	Diameter (μm)	Tensile strength (GPa)	Tensile modulus (GPa)	Strain to failure (%)
1100	4.4	3.97 ± 0.42	286 ± 31	1.42 ± 0.15
1300	4.1	4.09 ± 0.53	324 ± 32	1.25 ± 0.15
1500	3.7	2.78 ± 0.41	352 ± 38	0.86 ± 0.14

4.3 Conclusions

To produce carbon fibers with the best mechanical properties, the three controllable batch process parameters including temperature, applied tension and stabilization time were optimized and carefully controlled. It is demonstrated that the highest tension without breaking the fiber should be applied during stabilization and carbonization. To obtain the optimum stabilization time, a new method is suggested which monitors changes in the dynamic mechanical properties. Additional stabilization above 300 ^{o}C improves the carbon fiber properties significantly by enhancing the additional cross-linking reaction. The optimum stabilization time depends on both the applied tension and temperature during stabilization. Higher applied tension reduces the stabilization time. By optimizing thermal treatment, carbon fibers with an average tensile strength as high as 4 GPa were obtained by carbonizing at a temperature of 1100 ^{o}C.

4.4 References

[1] Dalton S, Heatley F, Budd PM. Thermal stabilization of polyacrylonitrile fibres. Polymer. 1999; 40(20): 5531-43.

[2] Ko TH, Ting HY, Lin CH. Thermal stabilization of polyacrylonitrile fibers. Journal of Applied Polymer Science. 1988; 35(3):631-40.

[3] Rahaman MSA, Ismail AF, Mustafa A. A review of heat treatment on polyacrylonitrile fiber. Polymer Degradation and Stability. 2007 Aug; 92(8):1421-32.

[4] Fitzer E, Frohs W, Heine M. Optimization of stabilization and carbonization treatment of PAN fibres and structural characterization of the resulting carbon fibres. Carbon. 1986;24(4):387-95.

[5] Chae HG, Minus ML, Kumar S. Oriented and exfoliated single wall carbon nanotubes in polyacrylonitrile. Polymer. 2006;47(10):3494-504.

[6] Gupta A, Harrison IR. New aspects in the oxidative stabilization of pan-based carbon fibers. Carbon. 1996; 34(11):1427-45.

[7] Bahl OP, Manocha LM. Shrinkage behaviour of polyacrylonitrile during thermal treatment. Angewandte Makromolekulare Chemie. 1975; 48(1):145-59.

[8] Johannis Simitzis SS. Correlation of chemical shrinkage of polyacrylonitrile fibres with kinetics of cyclization. Polymer International. 2008;57(1):99-105.

[9] Hou Y, Sun T, Wang H, Wu D. A new method for the kinetic study of cyclization reaction during stabilization of polyacrylonitrile fibers. Journal of Materials Science. 2008;43(14):4910-4.

[10] Ramis X, Cadenato A, Morancho JM, Salla JM. Curing of a thermosetting powder coating by means of DMTA, TMA and DSC. Polymer. 2003;44(7):2067-79.

[11] Cadenato A, Salla JM, Ramis X, Morancho JM, Marroyo LM, Martin JL. Determination of gel and vitrification times of thermoset curing process by means of TMA, DMTA and DSC techniques - TTT diagram. 1997: John Wiley & Sons Ltd; 1997. 269-79.

[12] Suresh KI, Thomas KS, Rao BS, Nair CPR. Viscoelastic properties of polyacrylonitrile terpolymers during thermo-oxidative stabilization (cyclization). Polymers for Advanced Technologies. 2008;19(7):831-7.

[13] Ouyang Q, Cheng L, Wang H, Li K. Mechanism and kinetics of the stabilization reactions of itaconic acid-modified polyacrylonitrile. Polymer Degradation and Stability. 2008;93(8):1415-21.

[14] Yu MJ, Bai YJ, Wang CG, Xu Y, Guo P-Z. A new method for the evaluation of stabilization index of polyacrylonitrile fibers. Materials Letters. 2007; 61(11-12): 2292-4.

[15] Yu MJ, Wang CG, Bai YJ, Wang YX, Zhu B. Evolution of tension during the thermal stabilization of polyacrylonitrile fibers under different parameters. Journal of Applied Polymer Science. 2006;102(6):5500-6.

[16] Wu GP, Lu CX, Ling LC, Hao AM, He F. Influence of tension on the oxidative stabilization process of polyacrylonitrile fibers. Journal of Applied Polymer Science. 2005;96(4):1029-34.

[17] Deurbergue A, Oberlin A. Stabilization and carbonization of pan-based carbon fibers as related to mechanical properties. Carbon. 1991;29(4-5):621-8.

[18] Bahl OP, Mathur RB. Effect of load on the mechanical-properties of carbon-fibers from PAN precursor. Fibre Science & Technology. 1979;12(1):31-9.

[19] Gupta A, Harrison IR. New aspects in the oxidative stabilization of PAN-based carbon fibers: II. Carbon. 1997;35(6):809-18.

[20] Mittal J, Bahl OP, Mathur RB, Sandle NK. IR studies of PAN fibres thermally stabilized at elevated temperatures. Carbon. 1994; 32(6):1133-6.

[21] Chae HG, Choi YH, Minus ML, Kumar S. Carbon nanotube reinforced small diameter polyacrylonitrile based carbon fiber. Composites Science and Technology. 2009; 69(3-4): 406-13.

[22] Moreton R, Watt W. Tensile strengths of carbon-fibers. Nature. 1974; 247 (5440): 360-1.

CHAPTER 5

EFFECT OF PRECURSOR FIBER COMPOSITION ON THE PROPERTIES OF THE RESULTING CARBON FIBERS

Although thermal treatment protocol of PAN fibers is vital for the ultimate properties of the resulting carbon fibers, properties of PAN precursor fibers are also equally important. How physical and chemical structures of precursor fibers affect the properties of the resulting carbon fibers? To produce ultra-strong carbon fibers, what is the best structure of precursor fibers? Since the physical and chemical changes during thermal treatment are so complex, answers to these questions are not easily obtained. It is commonly agreed that higher orientation, smaller fiber diameter and round shape of the precursor fiber are key requirements for achieving high mechanical properties carbon fibers. However, the direct relationship between properties of precursor fibers and the resulting carbon fibers are seldom reported. In order to improve the mechanical properties of carbon fibers, each manufacturing process must be carefully optimized. Finding the relationship between the physical and chemical structures of precursor fibers and the mechanical properties of the resulting carbon fibers will provide criteria for choosing the suitable PAN polymer and for optimizing fiber spinning process.

In this chapter, preliminary studies are conducted to optimize PAN precursor fibers. In chapter 2 to 4, stabilization process of PAN fibers was optimized, and the resulting carbon fiber with the best possible tensile property was achieved. Based on proposed optimum stabilization conditions, properties of the best carbon fibers are compared with their precursor fibers, and their relationship is studied.

5.1 Experimental

Three types of PAN/CNT composite fibers were used in this study. The properties of the precursor fibers used in this chapter are listed in Table 5.1.

Table 5.1 Properties of PAN/CNTs composite fibers.

PAN	Homo-polymer	4 % MAA	2 % IA
M_w (g/mol)	250K	240K	520K
CNTs	1 wt. %, XO122UA		
Spinning method	Sheath-core method, sheath was dissolved	Sheath-core method, sheath was dissolved	Single component
Abbreviation	$P_{250K\text{-}Homo}$	$P_{240K\text{-}MA}$	$P_{520K\text{-}IA}$
Diameter (μm)	7.4	6.3	11.2
Strength (GPa)	1.1 ± 0.1	1.0 ± 0.2	0.85 ± 0.06
Modulus (GPa)	25.7 ± 2.1	24.6 ± 3.3	20.7 ± 1.4
Elongation at break (%)	8.0 ± 0.6	7.0 ± 1.1	6.9 ± 0.3
Crystallinity (%)	58	62	51
Crystal size (nm)	9.3	9.5	8.7
f_{PAN}	0.893	0.891	0.883

Note: MAA: Methylacrylic acid; IA: Itaconic acid. f_{PAN}: Herman's orientation factor of PAN crystals using (200), (110) planes.

$P_{250K\text{-}Homo}$ and $P_{240K\text{-}MA}$ precursor fibers were spun using sheath-core bicomponents spinning method. PMMA/DMAc (30 wt.%) solution was used as sheath solution, and PAN/CNT /DMAc solution was used as core solution. Fibers were spun by bi-components solution extruder through a designed spinneret. After drawing, the PMMA sheath was dissolved by nitrile methane, and core part was left. $P_{520K\text{-}IA}$ precursor fiber was spun by single-hole spinneret. Mechanical properties of $P_{250K\text{-}Homo}$ and $P_{240K\text{-}MA}$ precursor fibers were quite good, whereas $P_{520K\text{-}IA}$ precursor fiber had relatively poor mechanical properties. Stabilization and carbonization processes were carried out in the same tube furnace used in chapter 4, and same characterization methods were used.

5.2 Optimization of stabilization processes

5.2.1 Stabilization temperature

The conclusions drawn in previous chapters are used to optimize the stabilization conditions for the three precursor fibers. DSC experiments were conducted to find the suitable stabilization temperatures. The DSC thermo-grams in nitrogen and in air for three precursor fibers are shown in Figure 5.1. Figure 5.1A shows that the addition of co-monomer lowers the reaction peak temperature by ~ 15 ^{o}C. The exothermic peak temperature of $P_{520K\text{-}IA}$ is ~2 ^{o}C lower than that of $P_{240K\text{-}MA}$. A shoulder peak can be seen on the lower temperature side (indicated by arrow) of main exothermic peak of $P_{520K\text{-}IA}$ fibers. The $P_{520K\text{-}IA}$ exotherm shows the lowest on-set temperature at 207.7 ^{o}C, while that for $P_{250K\text{-}Homo}$ is at 261 ^{o}C. For reactions in air (Figure 5.1B), the addition of co-monomers initiates the cyclization reactions at much lower temperatures than that in the homo-polymer, decreases exotherm intensity and broadens it to a wider temperature range. These factors benefit the control of temperature for lower heat generation rate. The stabilization reaction in PAN fibers with co-monomers is faster than that in homo-PAN fibers.

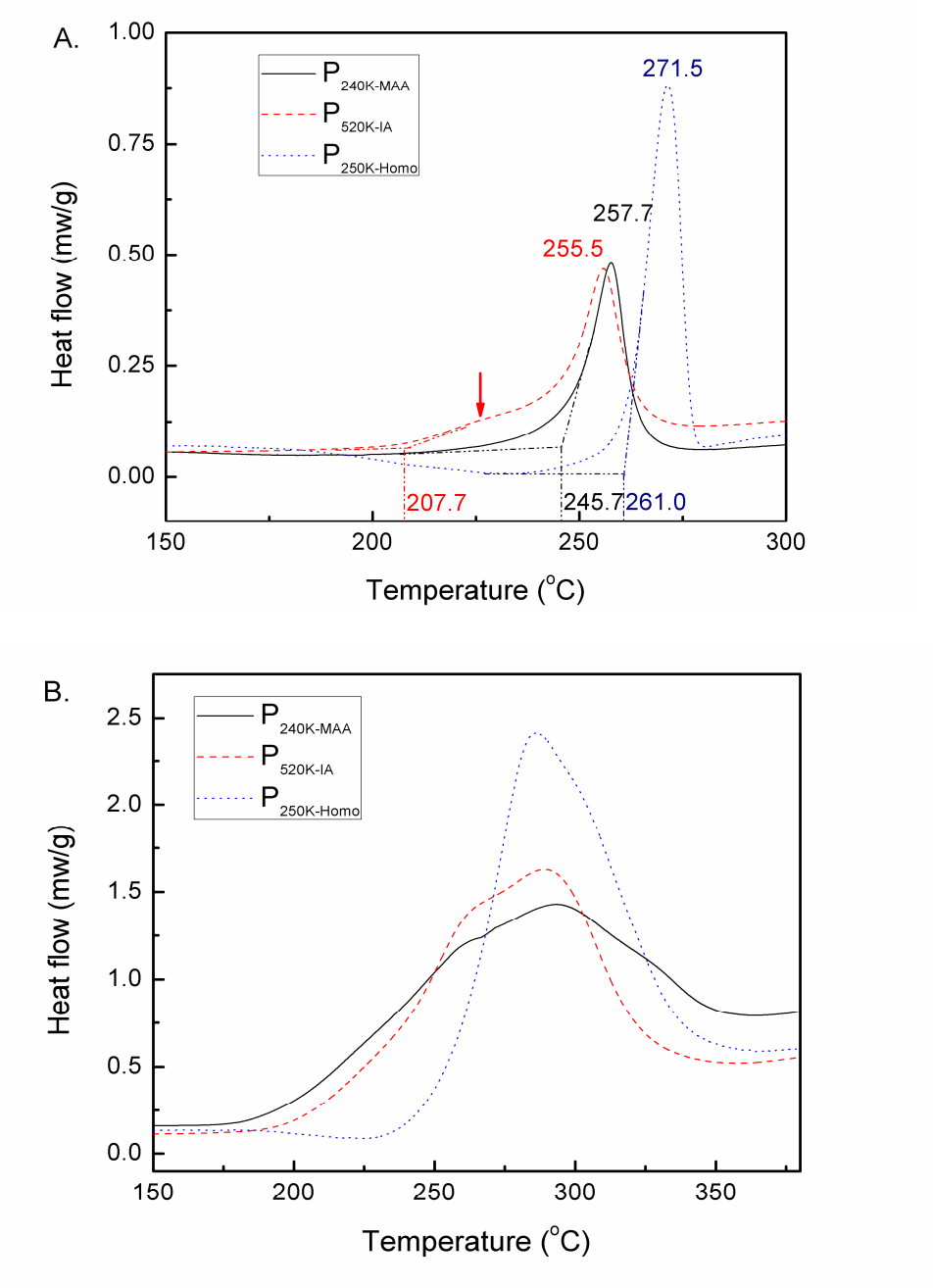

Figure 5.1 DSC curves of precursor fibers $P_{250K\text{-}Homo}$, $P_{240K\text{-}MA}$, and $P_{520K\text{-}IA}$ at a heating rate of 1 °C/min. A. In nitrogen; B. In air.

The DSC samples of Figure 5.1A were re-run in air, and the resulting DSC curves are shown in Figure 5.2. As mentioned in chapter 3, the second DSC peak at higher temperature belongs to additional cross-linking reactions. Copolymer fibers show

stronger exotherm than homo-polymer fibers, suggesting that more additional cross-linking reactions happen in copolymer fibers. The stabilized fibers with further cross-linking have been found to produce higher modulus carbon fibers (Chapter 4). In chapter 4, the best stabilization temperature profile for homo-polymer PAN fibers is reported to be 255 ^{o}C for 2 hr, then 320 ^{o}C for a suitable time. Here, for co-polymer PAN-fibers, same temperatures were used, however the stabilization time at 255 ^{o}C was shortened from 2 hr to 1 hr. The temperature profiles are shown in Figure 5.3.

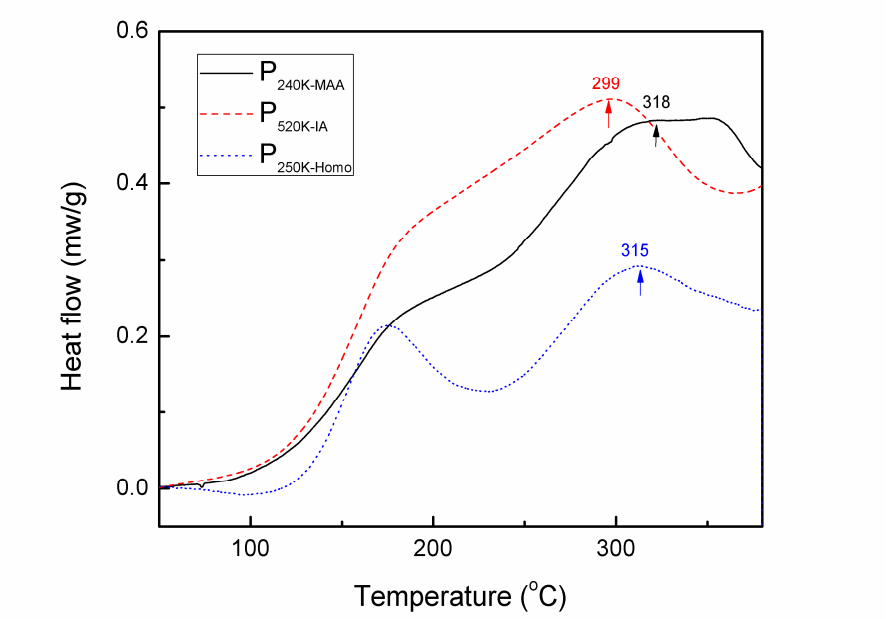

Figure 5.2 DSC curves of samples $P_{250K\text{-}Homo}$, $P_{240K\text{-}MA}$, and $P_{520K\text{-}IA}$ in Figure 5.2-A were re-run in air at a heating rate of 1 ^{o}C/min.

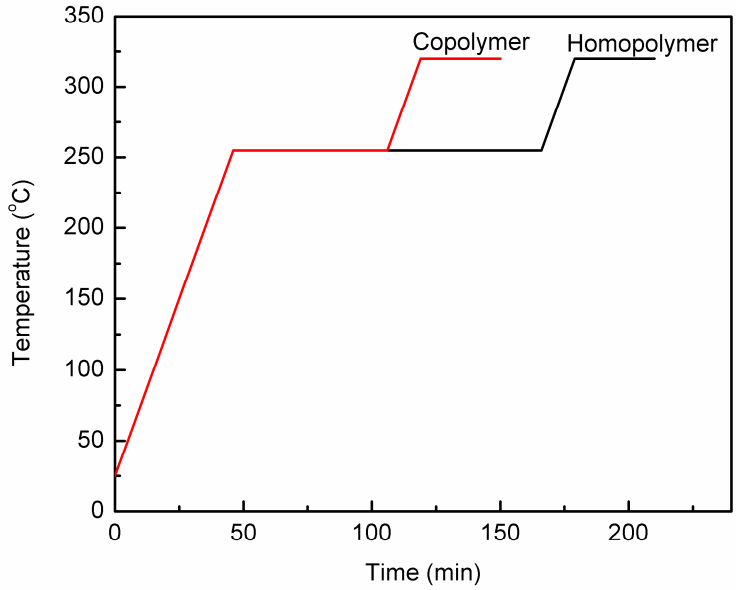

Figure 5.3 Temperature profiles for fiber stabilization.

5.2.2 Applied tension

The applied tension during thermal treatment was analyzed by TMA. The shrinkage curves of three precursor fibers under various stresses are shown in Figure 5.4. Based on the TMA results, the maximum stresses which can be applied on $P_{250K\text{-}Homo}$, $P_{240K\text{-}MA}$, and $P_{520K\text{-}IA}$ precursor fibers during thermal treatment are 49 MPa, 45 MPa and 55 MPa, respectively.

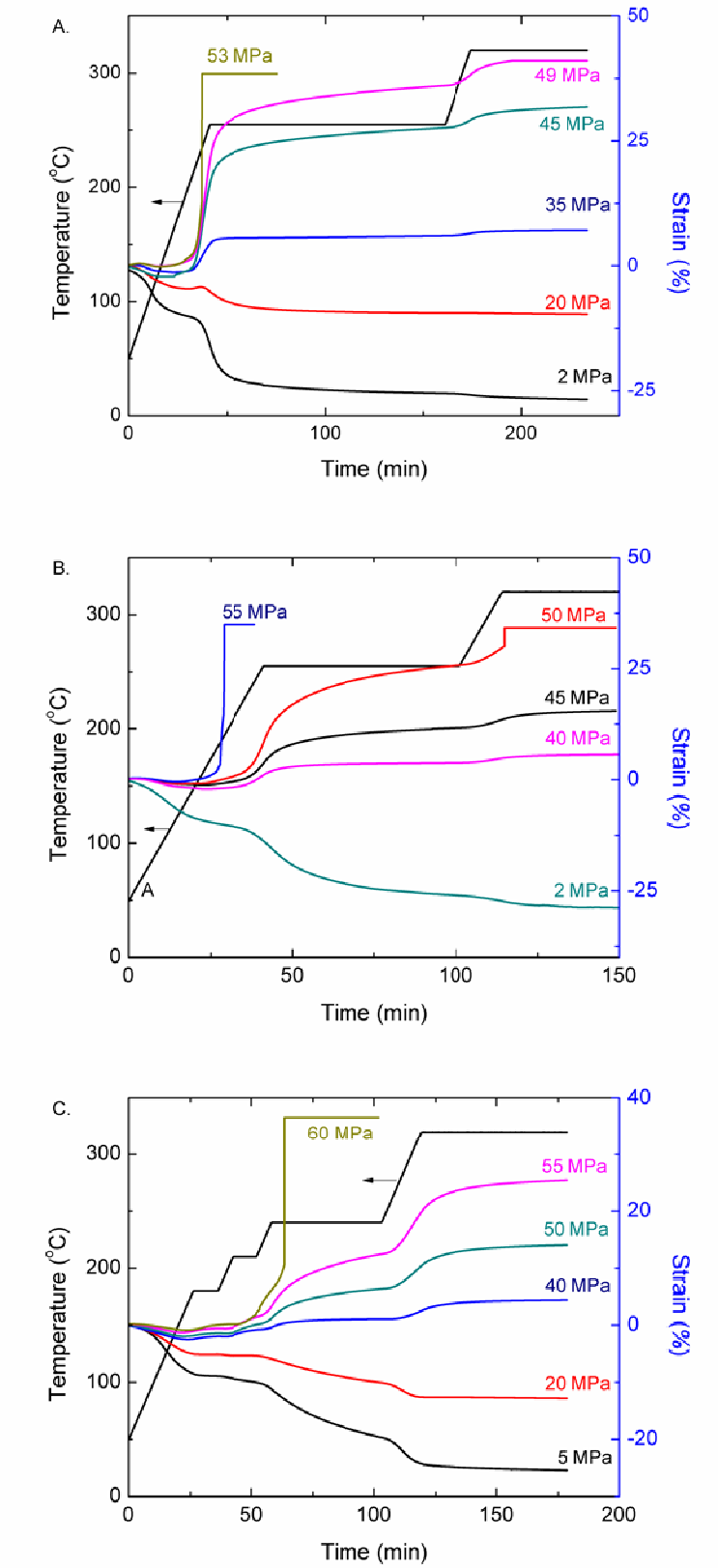

Figure 5.4 Shrinkage curves of precursor fibers under various tensions in air. A: $P_{250K\text{-}Homo}$, B: $P_{240K\text{-}MA}$, C: $P_{520K\text{-}IA}$.

5.2.3 Optimum stabilization conditions

Stabilized fibers were carbonized at 1100 ^{o}C, and the optimum stabilization conditions were determined from the tensile properties of the resulting carbon fibers. The mechanical properties of the resulting carbon fiber with varying stabilization times are listed in Table 5.2.

Table 5.2 Mechanical properties of carbonized fibers at 1100 ^{o}C with varying stabilization times.

Stabilization time at 320 ^{o}C (min)	Tensile strength (GPa)	Tensile modulus (GPa)	Elongation at break (%)
P_{250K}, Diameter ~ 4.0 µm, applied tension = 49 MPa.			
17.5	3.32±0.50	266±26	1.26±0.24
22.5	4.09±0.59	262±18	1.60±0.20
25	4.36±0.44	265±21	1.68±0.21
27.5	3.94±0.31	246±12	1.62±0.12
32.5	3.24±0.26	242±18	1.37±0.08
$P_{240K-MA}$, Diameter ~ 2.9 µm, applied tension = 45 MPa.			
10	3.14±0.52	284±41	1.13±0.26
20	3.57±0.50	283±22	1.28±0.12
25	4.27±0.61	297±29	1.45±0.20
30	3.72±0.54	294±26	1.30±0.22
40	3.38±0.48	295±17	1.18±0.14
$P_{520K-IA}$, Diameter ~ 6.6 µm, applied tension = 53 MPa.			
0.1	1.79±0.29	218±16	0.84±0.14
10	1.58±0.26	209±12	0.75±0.12

When P_{250K} and $P_{240K-MA}$ precursor fibers are stabilized at 320 ^{o}C for 25 min, the resulting carbon fibers possess the best mechanical properties. For $P_{520K-IA}$ precursor fibers, by decreasing stabilization time at 320 ^{o}C from 10 min to 0.1 min, mechanical properties of carbon fibers are improved, which indicates that even for fibers stabilized for as little as 0.1 min at 320 ^{o}C, over stabilization occurs. Thus following stabilization process was used for $P_{520K-IA}$ precursor fibers. Fibers were stabilized at 180 ^{o}C for 10

min, 210 ^{o}C for 10 min, 240 ^{o}C for 45 min, then 320 ^{o}C for various times. Lower stabilization temperature may slow down the reaction rate. The mechanical properties of the resulting carbon fibers at 1100 ^{o}C are listed in Table 5.3.

Table 5.3 Mechanical properties of carbonized $P_{520K\text{-}IA}$ fibers at 1100 ^{o}C with varied stabilization times.

Stabilization time at 320 ^{o}C (min)	Tensile strength (GPa)	Tensile modulus (GPa)	Elongation at break (%)
0.1	2.96±0.50	251±27	1.19±0.15
10	2.51±0.29	223±18	1.14±0.13
20	1.94±0.32	196±16	1.00±0.17
30	1.62±0.41	198±16	0.82±0.22

Based on mechanical properties in Table 5.3, $P_{520K\text{-}IA}$ precursor fibers seem to be still over-stabilized even both stabilization temperature and times were decreased. For the third stabilization trial of $P_{520K\text{-}IA}$ precursor fibers, stabilization time at 320 ^{o}C was fixed at 0.1 min, and stabilization time at 240 ^{o}C was varied. The tensile properties of carbonized fibers are listed in Table 5.4.

Table 5.4 Tensile properties of carbonized $P_{520K\text{-}IA}$ fibers at 1100 ^{o}C with varied stabilization times at 240 ^{o}C.

Stabilization time at 240 ^{o}C (min)	Tensile strength (GPa)	Tensile modulus (GPa)	Elongation at break (%)
15	3.10±0.61	217±21	1.42±0.22
25	3.74±0.62	251±23	1.51±0.24
35	3.08±0.43	238±16	1.31±0.20

Comparing the optimum stabilization time in $P_{520K\text{-}IA}$ and $P_{240K\text{-}MA}$, co-monomer IA makes the stabilization reactions much faster as compared to that by co-monomer MAA. The detailed reaction mechanisms of different co-monomers are still unclear, and

need more investigation. From the mechanical properties in Tables 5.3 and 5.4, it becomes clear that the tensile modulus of carbon fibers shows a platform when stabilization conditions are closed to the optimum conditions. Under or over stabilization decreases the modulus significantly. To verify if above stabilization conditions are the best conditions, stabilization temperature and times were further varied, and mechanical properties of the resulting carbon fibers are listed in Table 5.5. For $P_{520K\text{-}IA}$ fibers stabilized at 210 ^{o}C in the first stabilization stage (Table 5.5), when the stabilization time is increased from 60 min to 90 min, modulus of carbon fibers improves significantly. However, comparing Sample_3 with Sample_4, stabilization at 320 ^{o}C for 10 min seems to result in over-stabilization and decreased the tensile modulus of the carbon fibers. By varying the stabilization temperature in the first step from 210 ^{o}C to 230 ^{o}C, modulus of the carbon fibers (251 GPa) is same as that for the carbon fiber obtained under optimized stabilization condition in Table 5.4.

Table 5.5 Mechanical properties of carbonized $P_{520K\text{-}IA}$ fibers at 1100 ^{o}C with varying stabilization conditions.

	Stabilization conditions	Tensile strength (GPa)	Tensile modulus (GPa)	Elongation at break (%)
Sample_1	210 ^{o}C–60 min, then 320 ^{o}C–10 min.	1.62±0.36	141±14	1.16±0.10
Sample_2	210 ^{o}C–90 min, then 320 ^{o}C–10 min.	2.78±0.32	208±11	1.35±0.12
Sample_3	210 ^{o}C–120 min, then 320 ^{o}C–10 min.	2.07±0.38	203±11	1.04±0.18
Sample_4	210 ^{o}C–120 min, then 300 ^{o}C–10 min.	2.87±0.59	248±20	1.17±0.22
Sample_5	220 ^{o}C–60 min, then 300 ^{o}C–10 min.	2.76±0.41	251±14	1.11±0.16
Sample_6	230 ^{o}C–60 min, then 300 ^{o}C–10 min.	2.82±0.45	212±12	1.35±0.18

5.3 Important factors in the manufacture of carbon fibers

5.3.1 Effect of precursor fibers on carbonized fibers

To understand how properties of precursor fibers affect the properties of the resulting carbon fibers, the optimum stabilization conditions, mechanical properties and herman's orientation factor of carbonized fibers are summarized in Table 5.6.

Table 5.6 Optimum stabilization conditions, mechanical properties and Herman's orientation factor* of carbonized fibers at 1100 ^{o}C.

Sample	Stabilization conditions	f Herman's orientation factor		Tensile strength (GPa)	Tensile modulus (GPa)	Strain at failure (%)
		Stabilized fiber	Carbonized fiber			
P_{250K}	255 ^{o}C-120 min 320 ^{o}C–25 min	0.644	0.83	4.36±0.44	265±21	1.68±0.21
$P_{240K\text{-}MAA}$	255 ^{o}C–60 min 320 ^{o}C–25 min	0.640	0.80	4.27±0.61	297±29	1.45±0.20
$P_{520K\text{-}IA}$	240 ^{o}C–25 min 320 ^{o}C–0.1 min	0.637	0.79	3.74±0.62	251±23	1.51±0.24

* Herman's orientation factor was calculated from azimuthal scans at 2θ ~25^{o} for stabilized fibers and 2θ =24.7^{o} for carbonized fibers.

By comparing Table 5.1 and 5.6, it becomes clear that the addition of co-monomer shortens the optimum stabilization times. Precursor P_{250K} and $P_{240K\text{-}MAA}$ fibers possess similar tensile strength and modulus value. Applied tension on copolymer $P_{240K\text{-}MAA}$ fibers is 45 MPa, which is lower than that (49 MPa) applied on homo-polymer P_{250K}. It can also be observed that addition of co-monomer MAA improved modulus of the resulting carbon fibers, although Herman's orientation factor of carbon fibers manufactured from $P_{240K\text{-}MAA}$ is even lower than that of carbonized P_{250K}. From Figure 5.2, the cross-linking exotherm of co-monomer fibers has higher intensity than that of the homo-polymer fibers, which suggests that more cross-linking reactions happened. In

Figure 5.4, under a tension of 2 MPa, $P_{240K\text{-}MAA}$ fiber has a chemical shrinkage of 18 % which is larger than that of P_{250K} fibers (16 %). Based on the conclusions in chapter 3, higher shrinkage is caused by more inter-molecular cyclization reactions. When fibers were further stabilized at higher temperature to improve cross-linking, modulus of the resulting carbon fibers improved (discussed in chapter 4). Here, the addition of co-monomer enhances degree of cross-linking in stabilized fibers, and further improves the modulus in the carbonized fibers.

Precursor $P_{520K\text{-}IA}$ fibers possess relatively poor mechanical properties as compared to those of P_{250K} and $P_{240K\text{-}MAA}$ precursor fibers. The carbonized $P_{520K\text{-}IA}$ fibers show the lowest molecular orientation and tensile modulus among all carbonized fibers. For precursor fibers, the better molecular orientation leads to the higher tensile modulus. Strength is influenced by defects, besides the morphological properties, whereas modulus depends upon the intrinsic properties of the fibers. Therefore, under optimum stabilization conditions, the better molecular orientation and thereby higher modulus in precursor fibers will increase the modulus of the resulting carbon fibers.

5.3.2 Effect of carbonization temperatures

In chapter 4, it is found that when carbonization temperature increases from 1100 ^{o}C to 1300 ^{o}C, the modulus and strength of carbon fibers improve. When carbonization temperature further increases to 1500 ^{o}C, although modulus of carbon fibers increases, elongation at break and tensile strength are greatly reduced due to the defects formed on the surface. Here, the detailed effect of carbonization temperature on mechanical properties of carbon fibers is studied. The mechanical properties of carbonized fibers at elevated carbonization temperatures are listed in Table 5.7.

Table 5.7 Mechanical properties of carbonized fibers at elevated temperatures.*

Carbonization Temperature (°C)	Diameter (μm)	Tensile strength (GPa)	Tensile modulus (GPa)	Elongation at break (%)
P_{250K}, applied tension = 49 MPa.				
1100	3.97	4.36±0.44	265±21	1.68±0.21
1300	3.77	4.56±0.41	280±12	1.67±0.14
1350	3.70	4.50±0.36	289±18	1.59±0.09
1400	3.66	4.73±0.52	299±14	1.62±0.19
1500	3.47	2.74±0.28	338±26	0.85±0.13
$P_{240K\text{-}MA}$, applied tension = 45 MPa.				
1100	2.94	4.27±0.61	297±29	1.45±0.20
1300	2.81	4.84±0.62	332±28	1.47±0.16
1500	2.76	2.60±0.34	355±27	0.70±0.12
$P_{520K\text{-}IA}$, applied tension = 53 MPa.				
1100	6.60	3.74±0.62	251±23	1.51±0.24
1300	6.10	4.07±0.44	272±22	1.49±0.12

*Stabilization conditions listed in Table 5.6 were used for the respective fibers.

The higher carbonization temperature reduces the diameter of carbonized fibers and improves their modulus. Based on the highest tensile properties, the best carbonization temperature for strength appears to be about 1400 °C for $P_{250K\text{-}Homo}$. If carbonization temperature is higher than 1400 °C, elongation at break decreases dramatically. Figure 5.5 shows the surface images of fibers carbonized at elevated temperatures. Phenomena reported in Figure 4.13 in chapter 4 is observed here. Higher carbonization temperature causes more surface defects. For homo-polymer and co-monomer fibers, carbonization at 1300 °C leads particle-like structure on the fiber surface, and carbonization at 1500 °C leads to grooves. These defects result in stress concentration in carbon fiber and reduce elongation at break.

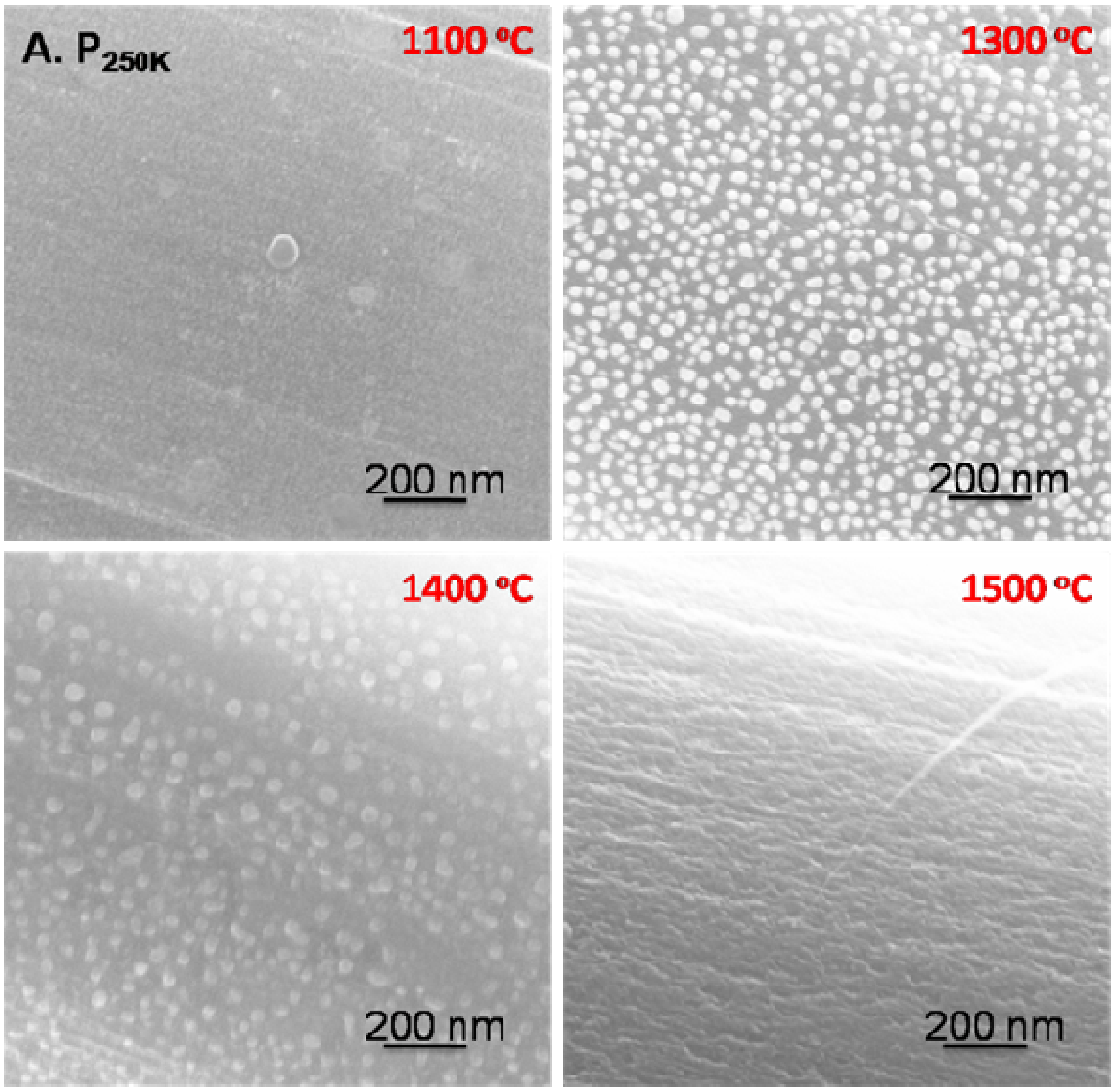

(Continued on next page)

(Continued)

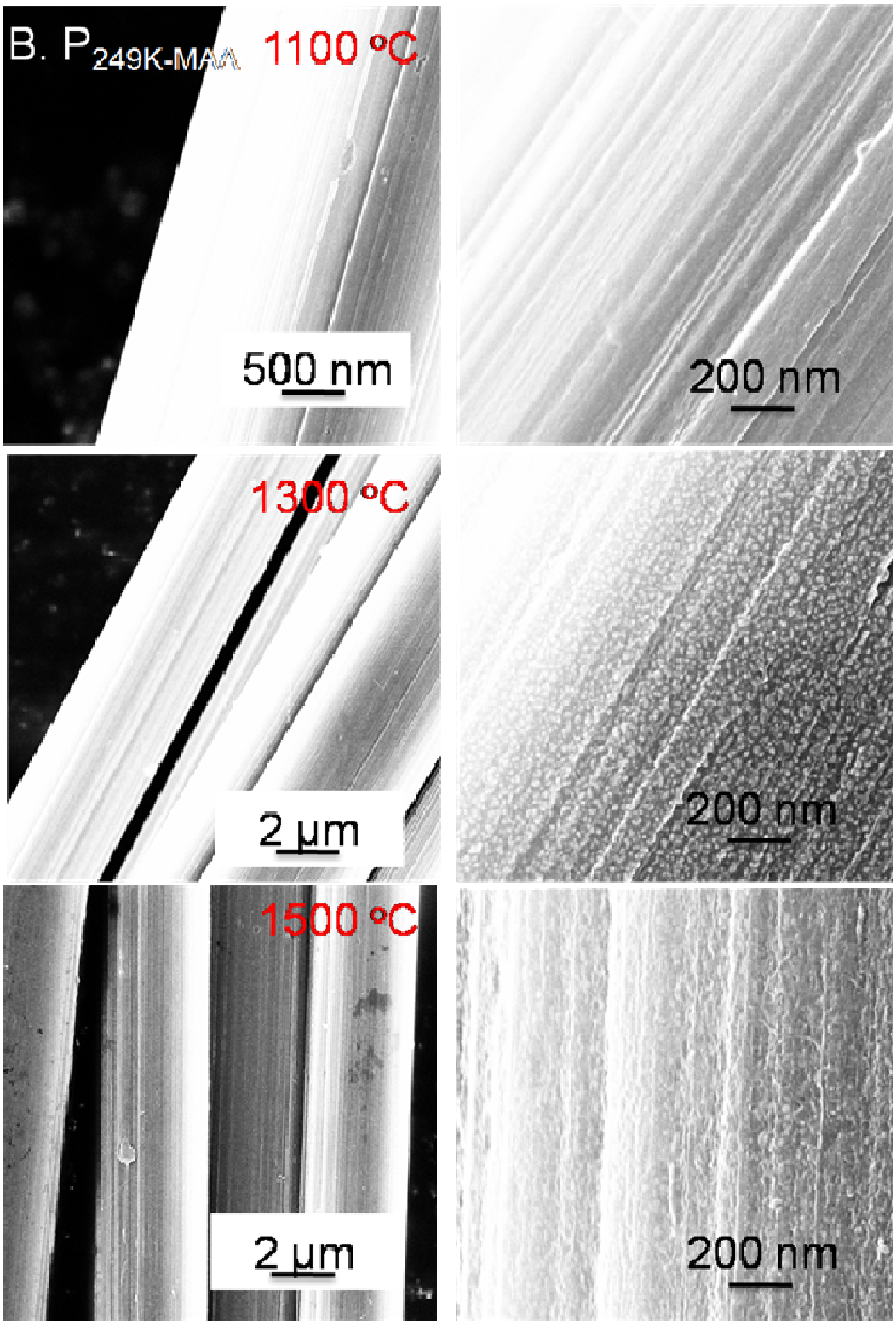

Figure 5.5 SEM surface images of fibers carbonized at elevated temperatures. A: P_{250K} fibers; B: $P_{240K\text{-}MAA}$ fibers.

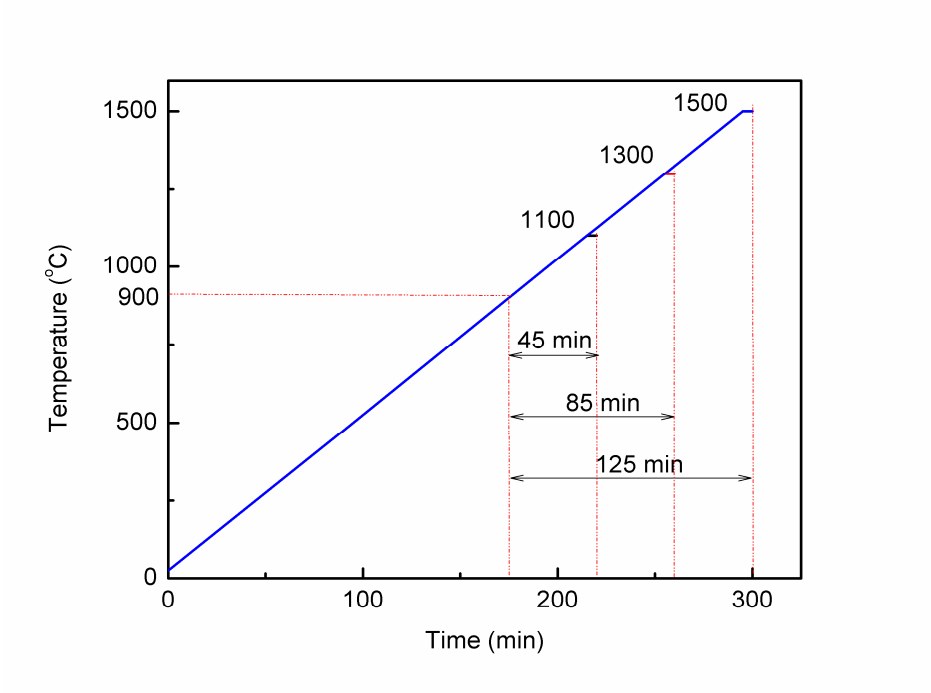

Figure 5.6 Carbonization temperature profiles.

Figure 5.6 shows temperature profiles of carbonization. Comparing residence time above 900 ^{o}C during carbonization, for carbonization at 1500 ^{o}C, residence time above 900 ^{o}C was 80 min longer than that for the sample carbonized at 1100 ^{o}C. Also, the temperature is much higher. The longer exposure time at higher temperature may lead to surface defects. Also, any trace of humidity, oxygen, and impurities, in purging gas of argon will lead to decomposition of carbon fiber surfaceunder these prolonged carbonization conditions.

5.3.3 Effect of precursor fiber aging time

Bahl et al. [1] reported that after long time on the shelf, properties of the solution-spun PAN precursor fiber changed, and the resulting carbon fiber properties decreased. In the present experiments, when the fibers stored for 4-6 months in the cabinet at room

temperature were stabilized at the same tension which was found safe in previous experiments, fiber bundles always broke. The properties of the precursor fibers are important for processing parameters and for determining the properties of the resulting carbon fibers. Therefore, it is important to know if the precursor fiber properties changed with the storage time for gel-spun PAN and PAN/CNT fibers. And if yes, how fast do they change? In this section, the effect of shelf time on the mechanical properties and physical structure of P_{250K} and $P_{240K\text{-}MAA}$ fibers are studied. Table 5.8 shows the mechanical properties after 1 - 2 years shelf.

Table 5.8 Mechanical properties of P_{250K} and $P_{240K\text{-}MAA}$ fibers before and after 1 - 2 years shelf.

Fibers	P_{250K}	$P_{240K\text{-}MAA}$
Spun Date	February 2009	June 2009
Diameter (μm)	7.4	6.3
Tensile strength (GPa)	1.1 ± 0.1	1.0 ± 0.2
Tensile modulus (GPa)	25.7 ± 2.1	24.6 ± 3.3
Elongation at break (%)	8.0 ± 0.6	7.0 ± 1.1
	Re-test Date: April 2010*	
Tensile strength (GPa)	0.82± 0.11	0.91 ± 0.15
Tensile modulus (GPa)	20.2 ± 1.6	23.6 ± 2.0
Elongation at break (%)	8.4 ± 1.4	7.5 ± 1.2

* Before testing, fibers were dried in vacuum oven at 60 ^{o}C for 2 days.

It can be seen that both strength and modulus significantly decreased after long shelf-time, while elongation at breakage increased moderately. These changes in properties are caused by molecular relaxation. The physical structures of the precursor fibers are examined by XRD (Table 5.9). It can be seen that after long shelf-time, PAN orientation and crystal size decreases, and meridional peak shifts to higher 2θ value. These observations suggest molecular relaxation in fibers and are consistent with the

observed changes in mechanical properties. These changes are detrimental for producing good quality carbon fibers.

Table 5.9 Structural parameters of $P_{250K\text{-}homo}$ and $P_{240K\text{-}MAA}$ fibers before and after aging as determined by WAXD.

Fibers	P_{250K}		$P_{240K\text{-}MAA}$	
Testing Date	February 2009	April 2010	June 2009	April 2010
FWHM*	0.7	1	0.9	1.1
Herman's Orientation Factor**	0.893	0.867	0.891	0.882
Meridional Peak Position	39.5 ^{o}	39.8^{o}	39.4 ^{o}	39.5 ^{o}

* FWHM was calculated from PAN (200), (110) peak in equatorial scan, ** Herman's orientation factor was calculated from PAN (200), (110) planes.

5.4 Conclusions

Addition of acid co-monomer reduces over all stabilization time. Comparing co-monomers IA and MAA, addition of IA makes stabilization reactions much faster. Higher modulus and orientation of precursor fibers results in improved modulus of the carbon fibers. Carbonization for longer time at higher temperature causes defects on carbonized fiber surface. For batch process, the highest tensile strength fibers were obtained in the temperature range of from 1300 to 1400 ^{o}C. When carbonization temperature is higher than 1400 ^{o}C, surface defects greatly reduce the elongation at break and strength. PAN/CNT precursor fiber properties deteriorate with aging at room temperature, resulting in lower carbon fiber properties.

5.5 References

[1] Bahl OP, Mathur RB, Matta VK, On the shelf-life of PAN precursor. Carbon, 1989, 27(27): 494-5.

CHAPTER 6

CONCLUSIONS AND RECOMMENDATIONS

6.1 Conclusions

1. PAN/CNT (1 wt. %) composite fibers were spun by dry-jet gel-spinning. Three types of CNTs were used. Addition of CNTs improves fiber tensile strength, tensile modulus, and greatly increases the activation energy of T_g. Fiber modulus reinforcement efficiency shows linear relationship with the CNT BET surface area. Added CNTs appear to penetrate many layers of PAN crystalline and amorphous regions, improving the stress resistance, and reducing the fiber entropic stress and shrinkage.
2. Effect of different types of CNTs on stabilization process was compared. For optimally stabilized fiber, addition of CNTs reduces the fraction of β-amino nitrile. For determining the optimum stabilization time, nitrile band absorbance in FTIR and the Herman's orientation of formed ladder polymer determined from X-ray difraction show consistent results and can be used as the criteria for this purpose. The content of residual catalyst in the range of 1 – 4 wt. % shows little effect on the mechanical properties of the stabilized fibers.
3. The tension applied during stabilization also plays an important role on the properties of the stabilized fibers. Higher tension leads to better mechanical properties, longer segment length of conjugated nitrile, and better molecular orientation. The final shrinkage of fibers is very sensitive to applied tension, and can be significantly reduced by higher stress or higher stabilization temperature. Also, addition of CNTs

improves the maximum applied stress during stabilization, which is very important to enhance the properties of carbon fibers.

4. Complex stabilization reactions can be separated by using nitrogen and air environments in sequence. Additional cross-linking reaction occurs at a temperature higher than 300 ^{o}C. It was also found that the additional cross-linking reaction has the highest activation energy followed by activation energy of cyclization and oxidation reactions. Addition of CNTs in PAN fibers reduces the activation energy of cyclization reaction marginally, whereas it lowers the activation energy of oxidation and cross-linking reactions significantly.
5. To produce carbon fibers with highest mechanical properties, the highest tension that fiber can bear should be applied during stabilization and carbonization. To obtain the optimum stabilization time, a new method is proposed to monitor the changes in dynamic mechanical properties in order to narrow down the stabilization time range. Additionally, further stabilization above 300 ^{o}C improves the carbon fiber properties. The optimum stabilization time depends on both applied tension and temperature. Higher applied tension reduces the stabilization time.
6. Addition of methacrylic as well as itaconic acid co-monomers in PAN reduces the overall stabilization time, and improves tensile modulus of the resulting carbon fibers. Higher modulus and orientation of precursor fibers resulted in improved modulus of the carbonized fibers.

6.2 Recommendations for future works

1. Cross-section of carbonized fibers showed irregular shape. Attempts should be made to process precursor fibers with circular cross-section. This will result in more

uniform oxygen diffusion during stabilization and will also result minimization of the total surface area and hence minimization of surface defects.

2. The effect of heating rate during stabilization on the properties of gel spun PAN/CNT based carbon fibers has not been studied. Similarly, what is the maximum number of temperature steps and at what temperatures and for what duration, has yet to be studied.
3. The effect of broader range of co-monomer composition on stabilization temperature profile needs to be studied for the gel spun PAN/CNT fibers.
4. The effect of shelf-time of the gel-spun fibers on carbonized fiber properties needs further investigation.
5. It is recommended that fiber tensile properties should be measured at different gauge lengths, and data should be analyzed by Weibull distribution.

APPENDIX A

EFFECT OF CARBON NANOTUBES ON PHASE TRANSFORMATION AND MORPHOLOGY OF ALUMINA

A.1 Introduction

Aluminum oxide (Al_2O_3, alumina) is an important [1, 2] oxide ceramic material. Alumina has strong ionic bonding, which leads to high hardness, wear resistance, chemical resistance and good thermo-chemical properties. Alumina is widely used in many fields, such as aluminum production, abrasives, refractories, ceramics, and electrical insulation. However, in structural applications, alumina is limited by its brittleness. CNTs are used as reinforcement materials mostly in polymer materials, but seldom used in metal and ceramic materials. Incorporating CNTs to reinforce ceramic materials and to overcome their intrinsic brittleness is quite attracting [3]. Also, CNTs have been found to show strong nucleation effect, and can induced crystallization of many kinds of polymers [4, 5]. It is interesting to study the effect of CNT on the crystal structure of ceramic materials. The addition of CNTs in alumina matrix has been found to improve both hardness and fracture toughness [6-10]. Good dispersion of CNTs is a general prerequisite for a good reinforcement. In the literatures, three processing methods have been reported to prepare alumina/CNT composite materials: 1. In-situ grown CNTs by CVD method inside alumina powders [9, 11-13], 2. Colloidal processing [6, 14] and powder mixing [15, 16], 3. precursor [8, 17] and sol-gel methods [7, 18] In the current study, alumina/FWNT composite precursor was prepared by sol-gel method, and then converted to alumina by thermal sintering. The advantages of sol-gel method are gel

network structure can prevent aggregation of dispersed CNTs and alumina gel can be spun to produce alumina fibers. Alumina has many crystallographic forms, including α-alumina, γ-alumina, θ-alumina, η-alumina, and δ-alumina etc. To-date, there are no report showing the effect of CNTs on the crystallographic transition of sintered alumina. In this study, it is found that addition of 1 wt % FWNTs stabilizes the transition phase alumina, and significantly elevates the phase transition temperature of alumina and affects morphology of the composite materials.

A.2 Experimental

A.2.1 Sol-Gel method

FWNTs (lot no. XO122UA) containing ~ 1 wt% catalyst residual (average wall number ~ 4) was obtained from Unidym, Inc (Houston, TX). Alumina precursor solution was synthesized using sol-gel method reported by Maki and Sakka [19]. First, aluminum cation hydrolyses in water, and then hydrolyzed product condenses together after refluxing at 100 ^{o}C. The reaction mechanism is shown below.

Hydrolysis

$$Al_3^{+}(aq) + 6H_2O(l) <-> [Al(H_2O)_6]_3^{+}\ (aq)$$

$$[Al(H_2O)_6]_3^{+}(aq)\ + H_2O(l) \rightarrow\ [Al(H_2O)_5OH]_2^{+}(aq) + H_3O{+}(aq)$$

Condensation

$$2[Al(H_2O)_5OH]_2^{+}(aq) \rightarrow [Al_2(H_2O)_{10}O]_4^{+} + H_2O$$

In order to well disperse FWNT in alumina precursor solution, alumina/FWNTs composite precursor solution was prepared by following steps: Step 1: CNTs were dispersed in DMF at a concentration of 50 mg/L after bath ultra-sonication for 24 hr; Step 2: 2 wt% poly(vinyl alcohol) (PVA, M_W ~ 150,000 g/mol, Sigma-Aldrich Corp.)/DMSO solution was prepared; Step 3: Equal volume of CNTs solution was poured into PVA/DMSO solution, mixed solution was evaporated at 100 ^oC under vacuum; Step 4: Step-3 was repeated until desired amount of CNTs was dispersed in solution; Step 5: CNTs solution was mixed with precursor solution before aging process by mechanical stirring. Both composite and control alumina solutions were aged at 60 ^oC until solution became very viscous (~ 2-3 days, suitable for spinning), and gel were dried at 80 ^oC (dried gel). Composite dried gel was black non-transparent solid; while control dried gel was yellow semi-transparent solid. Composite dried gels was pre-treated at 450 ^oC in air for 30 min in box furnace to remove PVA, same pre-treatment was also done on control dried gel to ensure exactly same thermal treatment history. Pre-treated samples were further sintered at various temperatures from 900, 1000, 1100 to 1150 ^oC in Argon (heating rate was 5 ^oC/min, and then held for 2 hr).

A.2.2 Characterizations

Thermal Gravimetric Analysis (TGA) was done on TA Q-500 (TA Instruments Corp.). Wide angle X-ray diffraction (WAXD) patterns were recorded by Rigaku micromax-002 (Cu K_α radiation, λ=0.1542 nm) with Rigaku R-axis IV++ detector. Glass capillary was used as a sample container. Surfaces of sintered samples were observed by Leo 1530 Scanning Electron Microscopy (SEM) at an operate voltage of 10 kV after gold sputtering. Porosity was tested on Porosimeter ASAP 2020 (Micromeritics Corp.).

A.3 Results and discussions

Figure A.1 shows TGA curves of FWNT and PVA treated in air at 450 ^{o}C for 30 minutes. Over 97 wt % PVA decomposed, while 90 wt % FWNT still remained. Same treatment was done on composite dried gels to remove residual PVA.

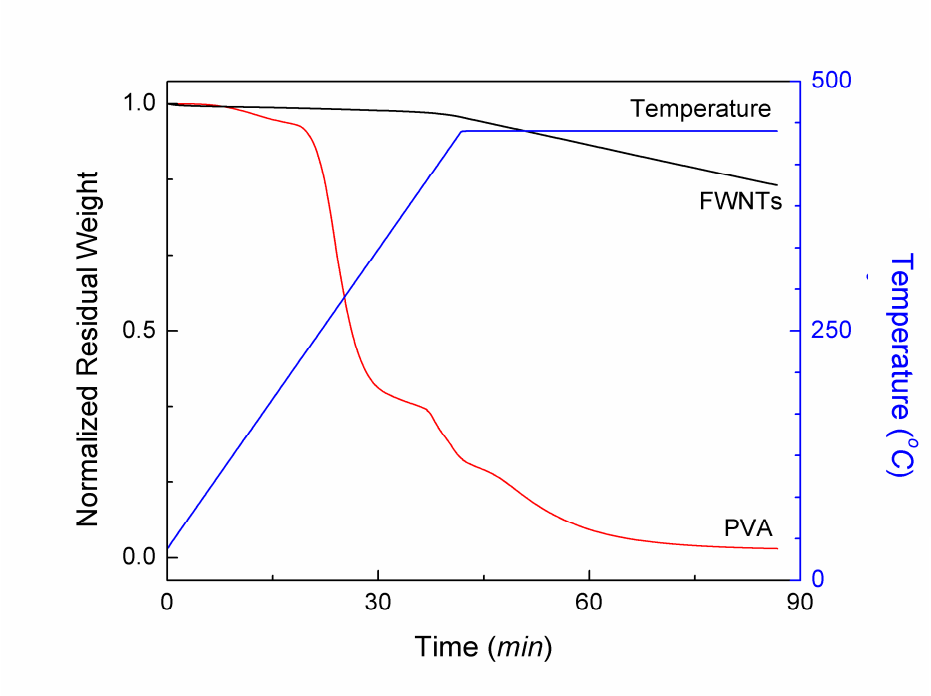

Figure A.1. TGA curves of PVA and FWNT in air. After treated at 450 ^{o}C for 30 min in air, over 97 wt% PVA is burned out, while most FWNTs survived.

Control dried gels were also pre-treated with the same procedure to ensure exactly same thermal treatment process. TGA curve of composite dried gel is shown in Figure A.2. There is weight loss of ~ 32 % in the temperature range between 100 ^{o}C and 400 ^{o}C due to pyrolysis.

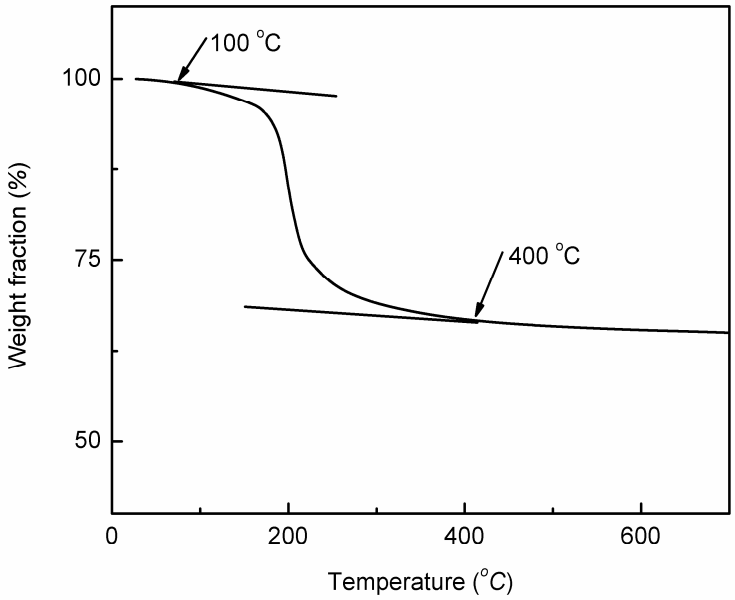

Figure A.2. TGA curve of composite dried gel in nitrogen at a heating rate of 5 ^{o}C/min.

Figure A.3 shows surface morphologies of the pre-treated gels. For composite dried gel, CNTs were uniformly dispersed without obvious agglomeration. Some CNT bundles pulled out, and some lied on the surface. Control samples showed relatively smooth surface. XRD patterns are shown in Figure A.4. Both control and composite samples shows similar broad peaks at ~ 24 ^{o}, which indicates an amorphous alumina phase.

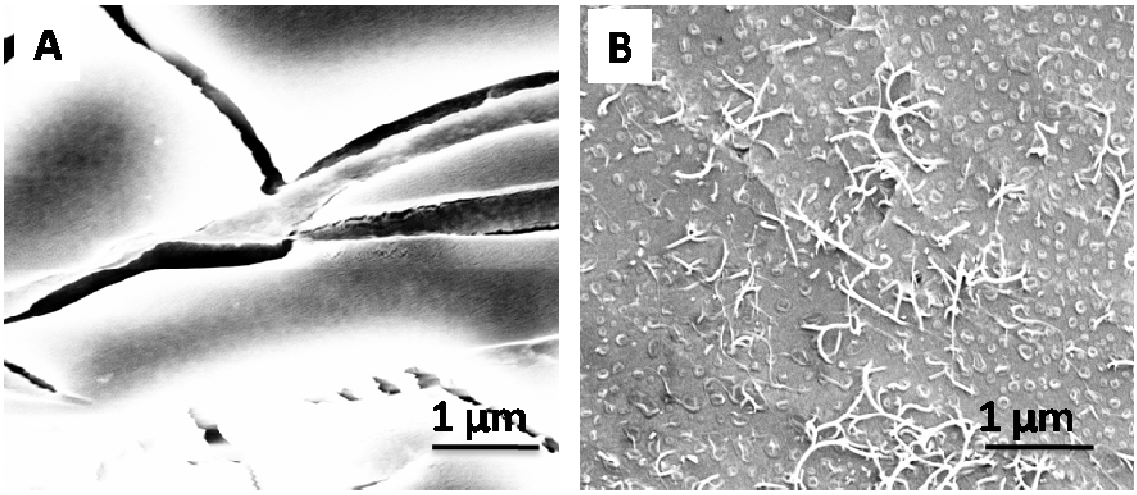

Figure A.3. SEM images of pre-treated dried gels. A. Control sample; B. Composite sample. Pre-treatment process: Dried gels were heated in box furnace to 450 ^{o}C at a heating rate of 5 ^{o}C/min in air, and then held at 450 ^{o}C for 30 min.

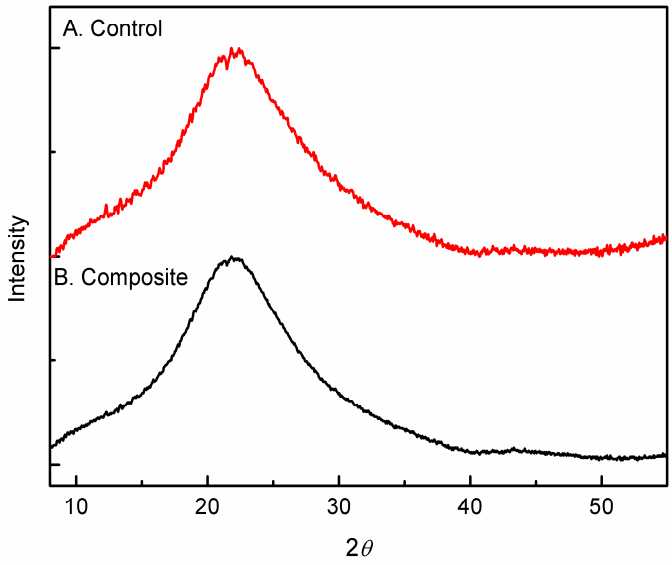

Figure A.4. Integrated XRD patterns of samples shown in Figure A.3. A. control sample; B. composite sample.

Pre-treated dried gels were further sintered at higher temperature from 900 ^{o}C to 1150 ^{o}C. After sintering, gray color control alumina was very brittle and easily broke into small pieces, while composite alumina had relatively better structural integrity. SEM images of alumina/FWNTs composite and control alumina after sintering at 900 ^{o}C and 1150 ^{o}C are shown in Figure A.5.

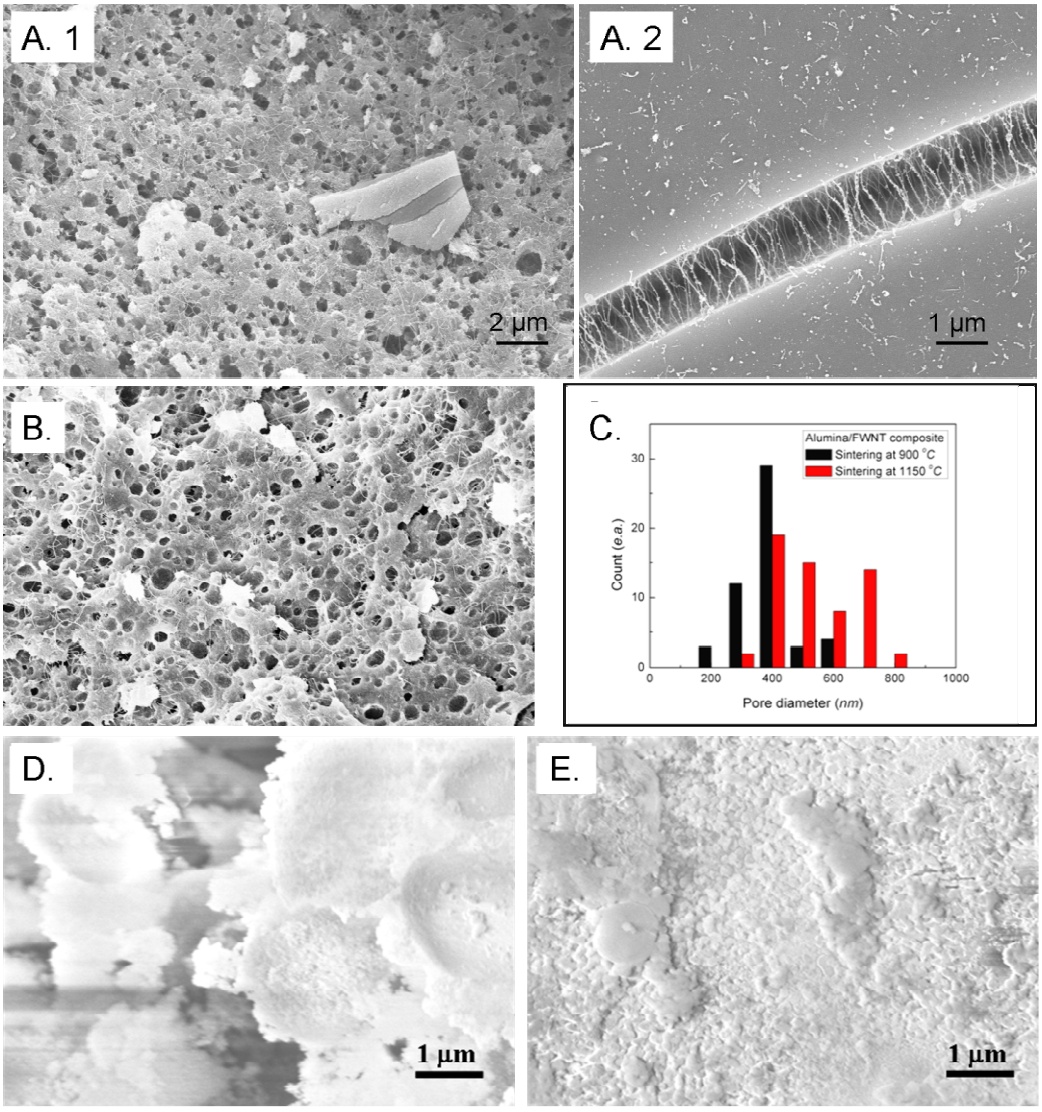

Figure A.5. SEM images of alumina after sintering. A. Composite alumina treated at 900 ^{o}C for 2 hr; B. Composite alumina treated at 1150 ^{o}C for 2 hr; C. Pore size distribution of composites; D. Control alumina treated at 900 ^{o}C for 2 hr; E. Control alumina treated at 1150 ^{o}C for 2 hr.

It can be seen that FWNTs were uniformly dispersed through whole alumina matrix. Figure A.5(A2) shows a formed crack in composite, FWNTs were pulled out from matrix and formed bridges between two fracture surfaces. The bridging effect by the addition of CNT would retard crack propagation and improve the fracture toughness [7]. Additionally, FWNTs also affected morphologies of alumina matrix, and led to the formation of macro-porous structure inside matrix after sintering (Figure A.5-A1); however, the surface of composite alumina is pore-free and relatively smooths (Figure A.5-A2). For all alumina/FWNTs composite sintered samples, macro-size pores ranging from 100 nm to around 2 μm formed inside matrix. Figure A.5.B shows alumina/FWNTs composite sintered at 1150 ^{o}C. The size distributions of these macro-pores are shown in Figure A.5.C. It can be found that higher sintering temperature leads to larger macro-pore size. For example, for composite sintered at 900 ^{o}C, most pores has a diameter around 400 nm or less; while for composite sintered at a higher temperature at 1150 ^{o}C, a dramatic increase in the number of pores with a diameter of 800 nm or larger can be observed. Figure A.4.D and E show control samples sintered at 900 ^{o}C and 1150 ^{o}C respectively. Compared with composite samples, control alumina showed a dense structure through the whole body.

Figure A.6 shows a fracture surface of alumina/FWNT composite sintered at 1000 ^{o}C. A gradient structure of pore size distribution can be observed for the region close to the free surface. For the region near free surface (depth < 4 μm), significant pores were not formed. Figure A.5.A2 shows that composite alumina sintered at 900 ^{o}C showed a non-porous surface. At the depth of 4 to 6 μm, small pores were formed, while > 6 μm below the surface, larger pores were observed. During sintering, alumina precursor was

converted to denser alumina. Densification process led to volume shrinkage. While pyrolyzing control alumina precursor, it can freely shrink and formed dense structure without significant pores; however, for alumina/FWNTs composite, the addition of CNTs restricted the volume shrinkage during pyrolysis, resulting in macro pores. The pore-size uniformity of created macro-pores was due to good CNT dispersion.

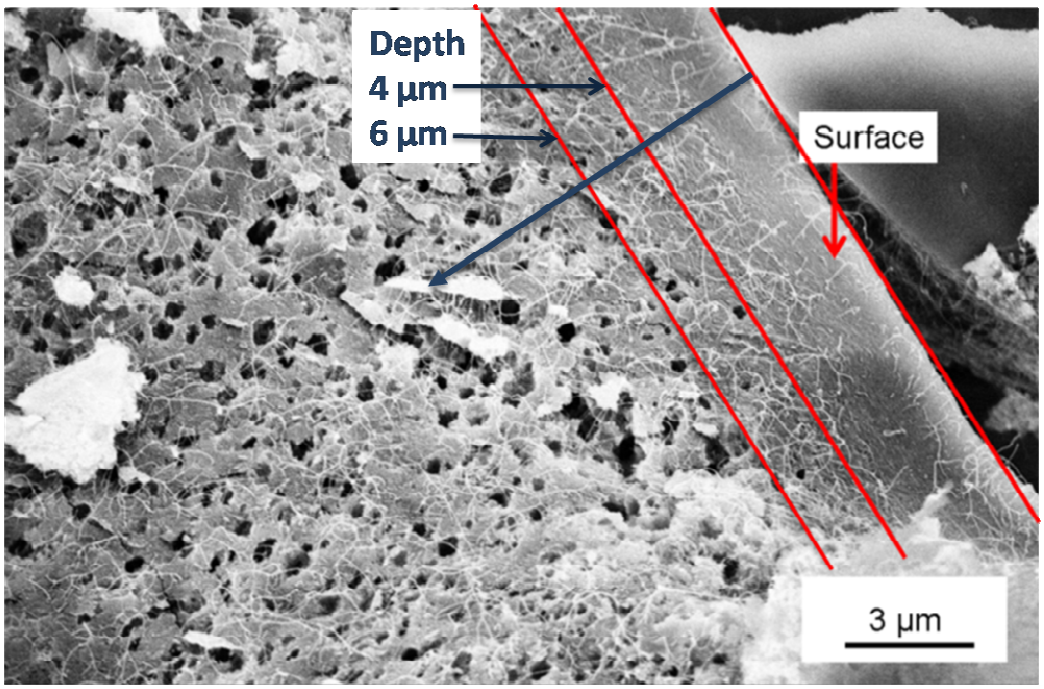

Figure A.6. SEM of cross-section of alumina/FWNTs composite sintered at 1000 ^{o}C for 2 hr.

Alumina can form polymorphous crystals including α-alumina (the most stable form), γ-alumina, θ-alumina, and η-alumina etc (meta-stable forms). The crystal structure was characterized by WAXD, and the results are shown in Figure A.7. The diffraction peaks in XRD curves are deconvoluted by XRD analysis software.

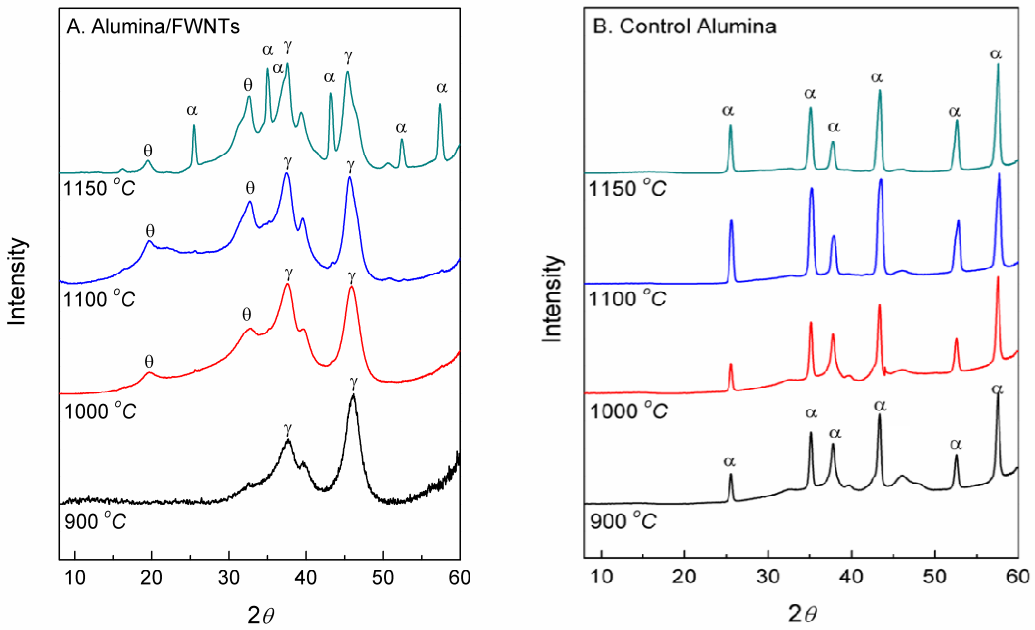

Figure A.7. XRD curves of alumina/FWNTs composite and control alumina sintered at 900 °C, 1000 °C, 1100 °C and 1150 °C for 2 hr.

From width of individual crystal peak, average grain size (Table A.1) can be calculated by Scherrer's equation, $D_p = \frac{0.94\lambda}{\beta_{1/2}\cos(\theta)}$, where, λ: wavelength of X-ray (0.1542 nm); β: peak width; θ: peak position.

Table A.1. Grain sizes of alumina calculated from XRD patterns.

Samples		Grain size (*nm*) at different sintering temperatures			
		900 ^{o}C	1000 ^{o}C	1100 ^{o}C	1150 ^{o}C
Control	α-form (012)	24	18	19	20
	α-form (104)	22	15	16	17
	α-form (110)	23	14	15	16
	α-form (113)	22	14	15	18
	α-form (024)	22	15	15	16
	α-form (116)	15	12	15	17
Composite	γ-form (2θ=38)	4	4	--	--
	γ-form (2θ =47)	3	4	4	4
	θ-form (2θ =20)	NA	2	4	7
	α-form (012)	NA	NA	NA	20
	α-form (113)	NA	NA	NA	18
	α-form (024)	NA	NA	NA	17
	α-form (116)	NA	NA	NA	17

Note: Crystal size is calculated from Scherrer's equation, $D_p = \frac{0.94\lambda}{\beta_{1/2}\cos(\theta)}$. (--) means that peak is overlapped with others and ca not be deconvoluted. (NA) means no such crystal form exists.

For control sample, when it was sintered at 900 ^{o}C, α-alumina with neglectable amount of γ-alumina was formed, while at higher sintering temperature, only α-alumina existed. Whereas, for alumina/FWNTs composite sintered at 900 ^{o}C, only γ-alumina existed. As sintering temperature increased, θ-alumina appeared and its fraction increased, and α-alumina only appeared at 1150 ^{o}C. Comparing grain sizes of two kinds of alumina forms, γ-alumina and θ-alumina had very fine crystals (around 4 nm), while α-alumina had relatively large crystals (around 20 nm).

α-alumina has the density of ~ 3.99 g/cm^3, while precursor density is ~3 g/cm^3, γ-alumina density is 3.65-3.67 g/cm^3 and θ-alumina density is 3.60-3.65 g/cm^3[20]. For alumina/FWNTs composite, mixture of denser α-alumina and lighter γ-alumina was

formed after sintering at 1150 °C while only γ-alumina existed after sintering at 900 °C. The densification after sintering at higher temperatures causes more volume shrinkage, which leads to increase of pore volume (Figure A.5.C). The micro-porosity of alumina/FWNTs composites was characterized by nitrogen gas absorption analysis. Surface area and pore volume distribution are shown in Figure A.8, and calculated BET surface areas are listed in Table A.2.

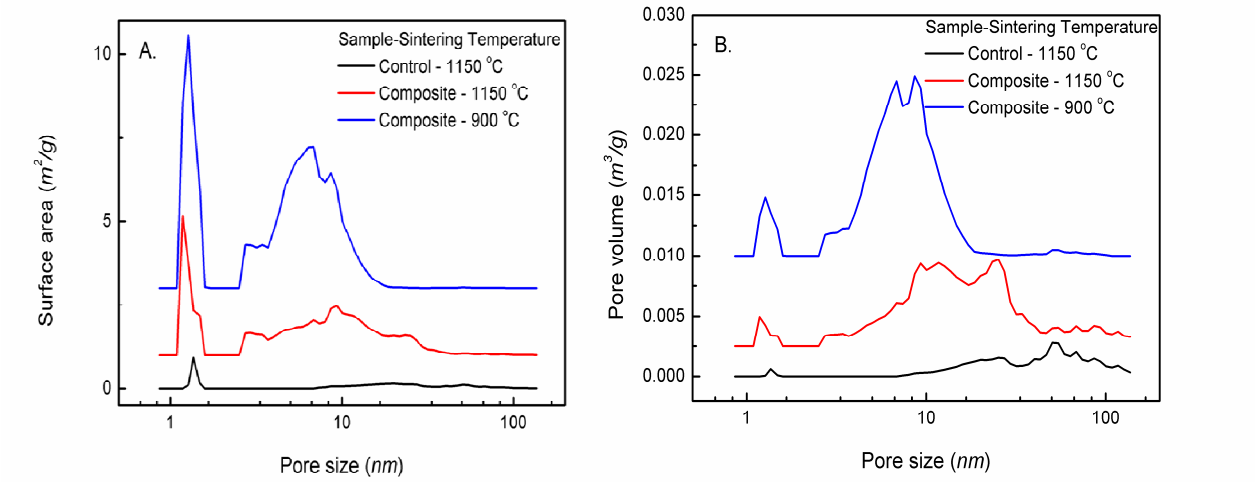

Figure A.8. Porosity test of alumina/FWNTs composite and control alumina.
A. Surface area; B. Pore volume.

Table A.2. BET surface area of alumina calculated from Figure 8.

Sample	Sintering Temperature (°C)	BET surface area (m^2/g)
Composite alumina	900	137.9±1.1
	1150	57.4±0.2
Control alumina	1150	15.3±0.1

For samples sintered at 1150 °C, the BET surface area of alumina/FWNTs composite is ~ 57.4 m^2/g, which is much higher than that for control alumina, ~ 15.3 m^2/g. The BET surface area of FWNT itself is ~ 659 m^2/g. Since the weight fraction of

CNTs in alumina composite is only 1 wt %, the increase of BET surface area caused by the addition of CNTs will be less than 7 m^2/g. Figure 8.B shows that micro-pores within the range from 4 nm to 40 nm are greatly improved by the addition of CNTs. For composite alumina sintered at 900 ^oC, pure γ-alumina was formed. Transition alumina, especially γ-alumina, is reported to have fine particle size and high surface area. The BET surface area of composite alumina sintered at 900 ^oC reaches ~ 138 m^2/g, and most pores are in the range of 3 nm to 20 nm. The increase of surface area and micro-pores was caused by the formation of transition alumina and macro-porous structure induced by CNTs.

γ-alumina has a spinel structure with *fcc* packing oxygen anions layers, while α-alumina has a corundum structure with trigonal symmetry [20, 21]. Significant research [22-24] has focused on the phase transition in alumina and from meta-stable alumina to stable α-alumina, however, detailed mechanism for the phase transition is still uncertain. Among these studies, the common method adopted to alter the phase transition of alumina is doping. It was found that dopants significantly influent phase transformation of alumina. Mn^{2+} and Cu^{2+} [22], and ZnF_2 [23] can accelerate the phase transformation to α-alumina, while Ca^{2+}, Sr^{2+}, Ba^{2+}, K^+, and Cs^+ [24] will retard the transition. The reason was ascribed to the radius of additive cations that > 33 % difference compared with Al^{3+} may stabilize less dense alumina form, but still there are some exceptions. Here, the addition of FWNTs was found to stabilize transition alumina and strongly affected phase transition temperature from alumina precursor to transition alumina to stable α-alumina. Without FWNTs, phase transition sequence is amorphous- $\rightarrow$ α-alumina; with FWNTs, the sequence is amorphous- $\rightarrow$ γ-alumina $\rightarrow$ θ-alumina $\rightarrow$ α-

alumina. Also, the phase transition temperature to α-alumina was greatly increased from equal or lower than 900 ^{o}C to higher than 1150 ^{o}C. At a sintering temperature of 900 ^{o}C, highly pure γ-alumina was formed for the composite precursor. As for γ-alumina, it has high porosity and catalytic surface activity. Therefore γ-alumina/FWNTs composite has potential to be used in high temperature catalyzing carrier. CNTs can be regarded as rolled up graphene sheets. Unlike the ion dopants, CNTs are neutral and do not integrate in the crystal structure of alumina. Previous results [4, 5] show that CNTs have strong nucleation effect in polymer system, and can affect crystal morphology; similar effect can be expected in inorganic materials. The possible route is that CNT surfaces trigger alumina precursors, and induce and stable nucleation and growth of transition alumina. The detailed mechanism needs further experiments.

A.3 Conclusions

In conclusion, the effect of addition of FWNTs on the morphology and crystal structure of alumina precursor prepared by sol-gel method was investigated. The phase transition sequence and temperature of γ-alumina to α-alumina were strongly affected by the addition of CNTs.

1) Addition of CNTs induced phase transition sequence of alumina from amorphous- $\rightarrow$ γ-alumina $\rightarrow$ θ-alumina $\rightarrow$ α-alumina; while control alumina only showed amorphous- $\rightarrow$ α-alumina.
2) Addition of CNTs stabilized transition alumina, and no α-alumina was formed in composite alumina when the sintering temperature was below 1150 ^{o}C; whereas α-alumina was formed in the control alumina after sintering at a temperature as low as 900 ^{o}C.

3) Composite alumina sintered at 900 ^{o}C contained only γ-alumina, and had a BET surface area of 138 m^2/g. Additionally, the addition of FWNTs also induced both macro- and micro- porosity inside alumina matrix with a pore-size range from 4 nm to 800 nm.

A.4 References

[1] Gao L, Jiang L, Sun J. Carbon nanotube-ceramic composites. Journal of Electroceramics. 2006;17(1):51-5.

[2] Hu Y, Shenderova OA, Hu Z, Padgett CW, Brenner DW. Carbon nanostructures for advanced composites. Reports on Progress in Physics. 2006;69(6):1847-95.

[3] Cho J, Boccaccini A, Shaffer M. Ceramic matrix composites containing carbon nanotubes. Journal of Materials Science. 2009;44(8):1934-51.

[4] Li L, Li B, Hood MA, Li CY. Carbon nanotube induced polymer crystallization: The formation of nanohybrid shish-kebabs. Polymer. 2009;50(4):953-65.

[5] Assouline E, Lustiger A, Barber AH, Cooper CA, Klein E, Wachtel E, et al. Nucleation ability of multiwall carbon nanotubes in polypropylene composites. Journal of Polymer Science Part B: Polymer Physics. 2003;41(5):520-7.

[6] Sun J, Gao L, Li W. Colloidal Processing of Carbon Nanotube/Alumina Composites. Chemistry of Materials. 2002;14(12):5169-72.

[7] Mo CB, Cha SI, Kim KT, Lee KH, Hong SH. Fabrication of carbon nanotube reinforced alumina matrix nanocomposite by sol-gel process. Materials Science and Engineering A. 2005;395(1-2):124-8.

[8] Cha SI, Kim KT, Lee KH, Mo CB, Hong SH. Strengthening and toughening of carbon nanotube reinforced alumina nanocomposite fabricated by molecular level mixing process. Scripta Materialia. 2005;53(7):793-7.

[9] Xia Z, Curtin WA, Sheldon BW. Fracture Toughness of Highly Ordered Carbon Nanotube/Alumina Nanocomposites. Journal of Engineering Materials and Technology. 2004;126(3):238-44.

[10] Zhan GD, Kuntz JD, Wan J, Mukherjee AK. Single-wall carbon nanotubes as attractive toughening agents in alumina-based nanocomposites. Nat Mater. 2003;2(1):38-42.

[11] An JW, Lim DS. Synthesis and characterization of alumina/carbon nanotube composite powders. J Ceram Process Res. 2002;3(3):174-7.

[12] Kumari L, Zhang T, Du GH, Li WZ, Wang QW, Datye A, et al. Thermal properties of CNT-Alumina nanocomposites. Composites Science and Technology. 2008;68(9):2178-83.

[13] Zhang T, Kumari L, Du GH, Li WZ, Wang QW, Balani K, et al. Mechanical properties of carbon nanotube-alumina nanocomposites synthesized by chemical vapor deposition and spark plasma sintering. Composites Part A: Applied Science and Manufacturing. 2009;40(1):86-93.

[14] Poorteman M, Traianidis M, Bister G, Cambier F. Colloidal processing, hot pressing and characterisation of electroconductive MWCNT-alumina composites with compositions near the percolation threshold. Journal of the European Ceramic Society. 2009;29(4):669-75.

[15] Lim DS, You DH, Choi HJ, Lim SH, Jang H. Effect of CNT distribution on tribological behavior of alumina-CNT composites. Wear. 2005;259(1-6):539-44.

[16] Jiang D, Thomson K, Kuntz JD, Ager JW, Mukherjee AK. Effect of sintering temperature on a single-wall carbon nanotube-toughened alumina-based nanocomposite. Scripta Materialia. 2007;56(11):959-62.

[17] Yamamoto G, Omori M, Yokomizo K, Hashida T, Adachi K. Structural characterization and frictional properties of carbon nanotube/alumina composites prepared by precursor method. Materials Science and Engineering: B. 2008;148(1-3):265-9.

[18] Chu BTT, Tobias G, Salzmann CG, Ballesteros B, Grobert N, Todd RI, et al. Fabrication of carbon-nanotube-reinforced glass-ceramic nanocomposites by ultrasonic in situ sol-gel processing. J Mater Chem. 2008;18(44):5344-9.

[19] Maki T, Sakka S. Preparation of alumina fibers by sol-gel method. Journal of Non-Crystalline Solids. 1988;100(1-3):303-8.

[20] Igor Levin DB. Metastable Alumina Polymorphs: Crystal Structures and Transition Sequences. Journal of the American Ceramic Society. 1998;81(8):1995-2012.

[21] Macêdo M, Bertran C, Osawa C. Kinetics of the γ → α-alumina phase transformation by quantitative X-ray diffraction. Journal of Materials Science. 2007;42(8):2830-6.

[22] Okada, K. and A. Hattori. Effect of Divalent Cation Additives on the gamma-Al_2O_3-to-alpha-Al_2O_3 Phase Transition. Journal of the American Ceramic Society. 2000;83(4):928-32.

[23] Wu Y, Zhang Y, Pezzotti G, Guo J. Influence of AlF_3 and ZnF_2 on the phase transformation of gamma to alpha alumina. Materials Letters. 2002;52(4-5):366-9.

[24] Okada K, Hattori A, Kameshima Y, Yasumori A, Das RN. Effect of monovalent cation additives on the gamma-Al_2O_3-to-alpha-Al_2O_3 phase transition. Journal of the American Ceramic Society. 2000; 83(5):1233-6.

APPENDIX B

COMPARING OVERLAPPED DATA SETS BY STATISTICAL METHOD

B.1 Gaussian Distribution

For the mechanical properties of fibers, average value and standard deviation are normally used to represent the value of the tensile strength, tensile modulus and elongation at breakage. $\bar{v} = \frac{1}{N}\sum_{i=1}^{N} v_i$, $s = \sqrt{\frac{1}{N-1}\sum_{i=1}^{N}\left(\bar{v} - v_i\right)^2}$, where v is data value, N is number of data points, and s is the standard deviation. Most phenomena can be fitted by Gaussian distribution, $f(x) = \frac{1}{\sqrt{2\pi s^2}} e^{\frac{-(x-\bar{v})^2}{2s^2}}$, where $f(x)$ is function of probability, $\bar{v}$ is the average value. The typical cumulative probability of Gaussian distribution is shown in Figure B.1.

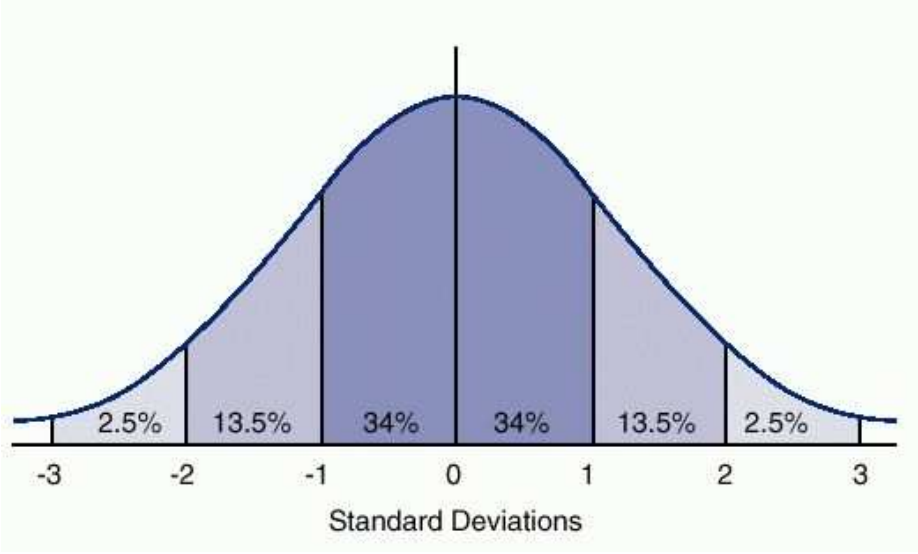

Figure B.1. Cumulative probability curve of Gaussian distribution.

B.2 Criterion for Gaussian Distribution

To determine if a given data serial can be described by Gaussian distribution, χ^2 method is used as criteria. To calculate χ^2, the data serial is divided into several regions (the number of divided regions is defined as *j*), and the cumulative probability (p_i) of each region based on Gaussian distribution is calculated (Figure B.1). $N = \sum_{i=1}^{k} n_i$, where *k* is the number of a certain divided region. The value of χ^2 is calculated by $\chi^2 = \sum_{i=1}^{j} \frac{(n_i - Np_i)^2}{Np_i}$ (Equation B.1). The degree of freedom (df) is defined as $df = j - 1$. The value of χ^2 is used to describe how far real data deviates from the ideal Gaussian distribution. The χ^2 value and its probability based on a Gaussian distribution are listed in Table B.1.

Table B.1. χ^2 value and its probability based on a Gaussian distribution.

	Probability based on Gaussian distribution											
df	0.995	0.990	0.975	0.950	0.900	0.750	0.500	0.250	0.100	0.050	0.025	0.010
1	0.0000393	0.000157	0.000982	0.00393	0.0158	0.102	0.455	1.32	2.71	3.84	5.02	6.63
2	0.0100	0.0201	0.0506	0.103	0.211	0.575	1.390	2.77	4.61	5.99	7.38	9.21
3	0.0717	0.115	0.216	0.352	0.584	1.21	2.37	4.11	6.25	7.81	9.35	11.3
4	0.207	0.297	0.484	0.711	1.06	1.92	3.36	5.39	7.78	9.49	11.1	13.3
5	0.412	0.554	0.831	1.15	1.61	2.67	4.35	6.63	9.24	11.1	12.8	15.1
6	0.676	0.872	1.24	1.64	2.20	3.45	5.35	7.84	10.6	12.6	14.4	16.8
7	0.989	1.24	1.69	2.17	2.83	4.25	6.35	9.04	12.0	14.1	16.0	18.5
8	1.34	1.65	2.18	2.73	3.49	5.07	7.34	10.2	13.4	15.5	17.5	20.1
9	1.73	2.09	2.70	3.33	4.17	5.90	8.34	11.4	14.7	16.9	19.0	21.7
10	2.16	2.56	3.25	3.94	4.87	6.74	9.34	12.5	16.0	18.3	20.5	23.2
11	2.60	3.05	3.82	4.57	5.58	7.58	10.3	13.7	17.3	19.7	21.9	24.7
12	3.07	3.57	4.40	5.23	6.30	8.44	11.3	14.8	18.5	21.0	23.3	26.2
13	3.57	4.11	5.01	5.89	7.04	9.30	12.3	16.0	19.8	22.4	24.7	27.7
14	4.07	4.66	5.63	6.57	7.79	10.2	13.3	17.1	21.1	23.7	26.1	29.1
15	4.60	5.23	6.26	7.26	8.55	11.0	14.3	18.2	22.3	25.0	27.5	30.6
16	5.14	5.81	6.91	7.96	9.31	11.9	15.3	19.4	23.5	26.3	28.8	32.0
17	5.70	6.41	7.56	8.67	10.1	12.8	16.3	20.5	24.8	27.6	30.2	33.4
18	6.26	7.01	8.23	9.39	10.9	13.7	17.3	21.6	26.0	28.9	31.5	34.8
19	6.84	7.63	8.91	10.1	11.7	14.6	18.3	22.7	27.2	30.1	32.9	36.2
20	7.43	8.26	9.59	10.9	12.4	15.5	19.3	23.8	28.4	31.4	34.2	37.6
21	8.03	8.90	10.3	11.6	13.2	16.3	20.3	24.9	29.6	32.7	35.5	38.9
22	8.64	9.54	11.0	12.3	14.0	17.2	21.3	26.0	30.8	33.9	36.8	40.3
23	9.26	10.20	11.7	13.1	14.8	18.1	22.3	27.1	32.0	35.2	38.1	41.6
24	9.89	10.90	12.4	13.8	15.7	19.0	23.3	28.2	33.2	36.4	39.4	43.0
25	10.50	11.50	13.1	14.6	16.5	19.9	24.3	29.3	34.4	37.7	40.6	44.3
26	11.20	12.20	13.8	15.4	17.3	20.8	25.3	30.4	35.6	38.9	41.9	45.6
27	11.80	12.90	14.6	16.2	18.1	21.7	26.3	31.5	36.7	40.1	43.2	47.0
28	12.50	13.60	15.3	16.9	18.9	22.7	27.3	32.6	37.9	41.3	44.5	48.3
29	13.10	14.30	16.0	17.7	19.8	23.6	28.3	33.7	39.1	42.6	45.7	49.6
30	13.80	15.00	16.8	18.5	20.6	24.5	29.3	34.8	40.3	43.8	47.0	50.9

If a data set can be described by Gaussian distribution, the probability of χ^2 should be higher than 0.05. For example, when df=5 and the probability is 0.05, the value of χ^2 is 11.1. If the calculated χ^2 is less than 11.1, then the given data set can be described by Gaussian distribution. Otherwise, the given data set can not be described by the Gaussian distribution.

Here, two data sets for the tensile strength of stabilized PAN fibers are compared. Both fiber samples were stabilized in DMA chamber under the same conditions, except that a constant dynamic vibration (0.3 %) was applied on Sample 2. Tensile strength values for various tests for these two samples are as follows:

Sample 1: 0.265 0.413 0.423 0.303 0.332 0.413 0.410 0.538 0.584 0.468 0.341 0.427 0.444 0.441 0.389 0.451 (GPa)

Sample 2: 0.511 0.369 0.556 0.438 0.397 0.352 0.509 0.490 0.457 0.547 0.368 0.637 0.523 0.565 0.590 0.336 (GPa)

The average value and standard deviation of the above two data sets are listed in Table B.2.

Table B.2. Summary of tensile strength values of Sample 1 and Sample 2.

	Sample 1	Sample 2
Number of data points	16	16
Average value (GPa)	0.413	0.478
Standard deviation (GPa)	0.080	0.093
Max value (GPa)	0.584	0.637
Min value (GPa)	0.265	0.336

To determine if the above data sets can be described by Gaussian distribution, χ^2 criterion is used and the value of χ^2 is calculated and is shown in Table B.3.

Table B.3. Calculation of χ^2 according to Equation 1.

Number of Data Points	Anticipated#	Sample 1	Sample 2
$-\infty \leftrightarrow \bar{v}-2s$	0.4	0	0
$\bar{v}-2s \leftrightarrow \bar{v}-s$	2.16	2	4
$\bar{v}-s \leftrightarrow \bar{v}$	5.44	5	3
$\bar{v} \leftrightarrow \bar{v}+s$	5.44	7	7
$\bar{v}+s \leftrightarrow \bar{v}+2s$	2.16	1	2
$\bar{v}+2s \leftrightarrow +\infty$	0.4	1	0
χ^2		2.418	3.921

* $\bar{v}$: average value; s: standard deviation; χ^2 is calculated by Equation 1.

The calculated χ^2 value is far less than 11.1, which indicates that above two data sets can be described by the Gaussian distribution function.

B.3 t-test method [1]

Data in Table B.2 shows that the tensile strength values of Sample 1 and Sample 2 overlap with each other. How this data set can be used to assess, if there is significant difference between the two samples? The problem can be solved by statistical method. To determine how significant the difference is between two samples with Gaussian distribution, *t*-distribution can be used. *t* value can be calculated by equation, $t = \frac{\left|\overline{v_1} - \overline{v_2}\right|}{\sqrt{\frac{s_1^2}{N_1 - 1} + \frac{s_2^2}{N_2 - 1}}}$, when s_1 (standard deviation of Sample 1) and s_2 (standard deviation of Sample 2). For the above two data sets the ratio of s_1 to s_2, is 0.86. If the ration of s_1/s_2 is between 0.2 to 5, then t test can be used. Therefore, for the above data set, t test can be applied. The critical *t* value and the probability of TYPE I error are listed in Table B.4.

Table B.4. Critical t values for 1 to 100 degrees of freedom (df) and for two types of α values (1 side and 2 sides). α is the probability of Type I error. [1]

α(1 tail)	0.05	0.025		0.05	0.025		0.05	0.025		0.05	0.025		0.05	0.025
α(2 tail)	0.10	0.050		0.10	0.050		0.10	0.050		0.10	0.050		0.10	0.050
df			df			df			df			df		
1	6.3138	12.707	21	1.7207	2.0796	41	1.6829	2.0196	61	1.6702	1.9996	81	1.6639	1.9897
2	2.9200	4.3026	22	1.7172	2.0739	42	1.6820	2.0181	62	1.6698	1.9990	82	1.6636	1.9893
3	2.3534	3.1824	23	1.7139	2.0686	43	1.6811	2.0167	63	1.6694	1.9983	83	1.6634	1.9889
4	2.1319	2.7764	24	1.7109	2.0639	44	1.6802	2.0154	64	1.6690	1.9977	84	1.6632	1.9886
5	2.0150	2.5706	25	1.7081	2.0596	45	1.6794	2.0141	65	1.6686	1.9971	85	1.6630	1.9883
6	1.9432	2.4469	26	1.7056	2.0555	46	1.6787	2.0129	66	1.6683	1.9966	86	1.6628	1.9879
7	1.8946	2.3646	27	1.7033	2.0518	47	1.6779	2.0117	67	1.6679	1.9960	87	1.6626	1.9876
8	1.8595	2.3060	28	1.7011	2.0484	48	1.6772	2.0106	68	1.6676	1.9955	88	1.6623	1.9873
9	1.8331	2.2621	29	1.6991	2.0452	49	1.6766	2.0096	69	1.6673	1.9950	89	1.6622	1.9870
10	1.8124	2.2282	30	1.6973	2.0423	50	1.6759	2.0086	70	1.6669	1.9944	90	1.6620	1.9867
11	1.7959	2.2010	31	1.6955	2.0395	51	1.6753	2.0076	71	1.6666	1.9939	91	1.6618	1.9864
12	1.7823	2.1788	32	1.6939	2.0369	52	1.6747	2.0066	72	1.6663	1.9935	92	1.6616	1.9861
13	1.7709	2.1604	33	1.6924	2.0345	53	1.6741	2.0057	73	1.6660	1.9930	93	1.6614	1.9858
14	1.7613	2.1448	34	1.6909	2.0322	54	1.6736	2.0049	74	1.6657	1.9925	94	1.6612	1.9855
15	1.7530	2.1314	35	1.6896	2.0301	55	1.6730	2.0041	75	1.6654	1.9921	95	1.6610	1.9852
16	1.7459	2.1199	36	1.6883	2.0281	56	1.6725	2.0032	76	1.6652	1.9917	96	1.6609	1.9850
17	1.7396	2.1098	37	1.6871	2.0262	57	1.6720	2.0025	77	1.6649	1.9913	97	1.6607	1.9847
18	1.7341	2.1009	38	1.6859	2.0244	58	1.6715	2.0017	78	1.6646	1.9909	98	1.6606	1.9845
19	1.7291	2.0930	39	1.6849	2.0227	59	1.6711	2.0010	79	1.6644	1.9904	99	1.6604	1.9842
20	1.7247	2.0860	40	1.6839	2.0211	60	1.6706	2.0003	80	1.6641	1.9901	100	1.6602	1.9840

For Sample 1 and Sample 2, the calculated *t* value is 2.1402. In Table B.4, the critical t value for 15 degree of freedom and probability of 0.05 is 2.1314 for the two sided test. Calculated t value, 2.1402, is larger than the critical t value, 2.1314. Therefore, it can be concluded with more than 95 % confidence that the strength of the stabilized fibers is higher when vibration is applied during stabilization as compared to the fiber stabilized without vibration. ***In this thesis, 95 % confidence limit is used as the criterion to judge if compared data sets are significantly different or not.***

B.4 Comparison of Data Serials in Minitab – Statistical Software [2]

The above *t* test calculations were done manually. Instead of manual calculations, another easy way to analyze and compared data sets is through Statistical software. Here the same data set is analyzed using the Minitab software.

The data values from two samples are input into Minitab. ANOVA function in Minitab was used. By calling the ANOVA function, the comparison of two data sets can be done quickly, and results are shown below.

Difference of Means	Adjusted T-Value	P-Value
0.0627	2.040	0.050

The P-value is the probability that the two data sets come from the same sample. These results show that the probability of the strength values of Sample 1 and Sample 2 coming from the same sample is only 5 %. Therefore, the probability that the two data sets come from different samples is 95 %.

B.5 References

[1] http://amchang.net/StatTools/tTest_Exp.php

[2]http://www.minitab.com/support/documentation/answers/PowerCalculationsforTwoSamplettest.pdf